INVESTIGATION OF SOME APPLICATIONS

OF PRIMITIVE FERROFLUIDS

by

A.I.A. Shobair, B.Sc., M.Sc.

An investigation conducted in the

Department of Electronic and Electrical Engineering

of the University of Sheffield

under the supervision of

Dr. R. Brown, B.Eng., Ph.D., C.Eng., M.I.E.E.

A thesis submitted to the
University of Sheffield
for the degree of
Doctor of Philosophy.

May, 1975.

IN THE NAME OF ALLAH THE BENEFICIENT

THE MERCIFUL

TO MY PARENTS

Acknowledgements

I wish to thank Dr. R. Brown for his continuous advice, encouragement and his invaluable suggestions and discussions throughout the course of the investigation and for giving me the opportunity to work with him.

I would like to express my gratitude to Professor F.A. Benson for the facilities afforded in the Department of Electronic and Electrical Engineering.

Thanks are also due to Dr. E. Rothwell of the Department of Chemical Engineering and Fuel Technology for his advice regarding the milling process and the use of his departmental milling facilities.

I would also like to thank Mr. R. Cousin and his team of technicians for their assistance throughout the project. Special thanks must go to Mr. J. Fouldes, Mr. B.G. Shelley, and Mr. D. Cocker for their help with the test equipment, and to Mr. M.B. Proctor and Mr. A. Sanby for making the glassware used in the course of the research.

I am also grateful to Mr. H. Flower and the workshop staff for constructing much of the test equipment.

Thanks are also extended to the Warren Spring Laboratory of the Department of Industry for their financial support for the investigation of the use of ferrofluids in mineral separation processes.

A.I.A. Shobair

A. I. Shobair

May, 1975.

Contents

Summary

The investigation covers two possible areas of application of magnetic fluids, one involving the production of torque by means of rotating magnetic fields and the other the use of magnetic fluids in the separation of non-magnetic ores on a density basis. The emphasis was upon the use of cheap, primitive ferrofluids i.e. non-colloidal suspension of relatively large particles.

Moskowitz and Rosensweig were the first to report electromechanical energy conversion with a rotating magnetic field. Their theory is not confirmed by their experimental results, however, nor the fact that the fluid can rotate in the opposite direction to the field. This phenomenon has been investigated experimentally for a range of field intensities, wave velocities, particle sizes, volume loading and fluid viscosities. The torque per unit volume has been found to be related linearly to the volume loading but nonlinearly to the frequency of the supply, field intensity and viscosity. For the primitive ferrofluids the results clearly indicate a combination of saliency and hysteresis torques. No satisfactory explanation for the reverse motion of the fluid has been produced and attempts to quantify the energy transfer have not been successful. Due to the inherently low permeability of the fluid, the torque per unit volume is much smaller than for conventional a.c. machines.

Primitive magnetic fluids have also been shown to have potential in the separation of ores according to their densities. The novelty of this work is that the particles, which flocculate in the presence of stationary fields, are kept in suspension by agitation caused by a

rotating wave. This agitation also serves to reduce the effective viscosity which at high volume loading can be high at zero field conditions. An effective specific gravity of about 12 has been obtained. The experimental results confirm the theory that the magnetic force in the linear condition is proportional to the magnetic energy - density gradient (in space) but with saturation the force is proportional to the field gradient and independent of body shape. A practical system seems to be feasible.

List of Principal Symbols

Symbol	Units	
A_c	m^2	area if the search coil used in section 1.
A_f	m^2	area of the fluid sample used in section 1.
A_a	m^2	difference between the area of the fluid and the area of the search coil.
a	m	radius of a magnetic particle.
B_f	T	flux density in a fluid sample = μ_o [M(H) + H]
C_f } C_ℓ } C_s }	$J.Kg^{-1}.{}^oC^{-1}$	respective specific heat of ferrofluid, carrier fluid and magnetic material.
E_m	N.m	magnetic energy.
f_o	sec^{-1}	supply frequency.
g	$m.s.^{-2}$	gravitational constant.
I	A	electric current in a stator or solenoid.
J_z	A/m	linear current density in the z-direction.
J_{max}	A/m	maximum linear current density in the z-direction.
K_p		volume loading of a ferrofluid.
K_z		depolarizing factor depends on the aspect ratio of a body.
L	m	length of a stator or a solenoid.
μ_o M or μ_o M(H)	T	magnetization of a magnetic fluid.
$\mu_o M_i$	T	intrinsic magnetization of magnetic material.
$\mu_o M_{sat}$	T	saturation magnetization of magnetic fluid.
m	$A.m^2$	dipole moment of a magnetic particle.
N	m^{-3}	number of particles per unit volume of a ferrofluid.
n_p	m^{-3}	actual number of particles participating in the process of torque generation.
p		number of pairs of poles.
R_o	m	outer radius of a fluid cylindrical containing vessel.
T	N.m.	generated torque from a magnetic fluid.

Symbol	Units	
T_h	N.m.	generated torque by hysteresis from a group of particles.
T_m or T_{max}	N.m.	maximum torque that can be generated by a particle.
T_p	N.m.	torque per particle.
T_s	N.m.	generated torque by saliency from a group of particles.
T_v	N.m.	torque generated within a unit volume of ferrofluid - Moskowitz and Rosensweig approach.
T_{vm}	N.m.	modified torque per unit volume of ferrofluid - our approach.
t	s	time.
$\tau(r)$	$N.m.^{-2}$	shear stress in a rotating fluid.
ω or) $\omega(r)$)	s^{-1}	angular velocity of a ferrofluid.
ω_o	s^{-1}	2 π . supply frequency.
ω_s	s^{-1}	spinning velocity of a magnetic particle.
X	-	figure of merit = $\dfrac{\mu_e (1 - \mu_e)}{K_z + (1 - K_z)\,\mu_e}$
η) η_s)	$N.S.m^{-2}$	respective viscosity of carrier fluid and magnetic material.
χ	-	the susceptibility of the linear part of ferrofluid magnetization curve.
μ_e) or) μ_f)	-	relative permeability of ferrofluid.
μ_o	$H.m.^{-1}$	permeability of free space = $4 \pi \cdot 10^{-7}$
μ_p	-	relative permeability of a magnetic particle.
ρ_m	$N.m.^{-3}$	magnetic force density or magnetic force per unit volume.
Ω	-	vorticity.

INTRODUCTION

I.1 History of the Project.

Laithwaite[1] reported that metal cylinders unexpectedly rolled in a direction opposite to that of the travelling field produced by a linear induction stator. In his article Laithwaite explained the reverse motion in terms of "levitation forces", although this approach failed to explain why steel cylinders also rolled in the opposite direction to that of the field travel.

Moskowitz and Rosensweig[3] in an earlier paper described the use of a travelling magnetic field to pump ferrofluids. They used the term "ferrofluid" to designate a magnetic colloid composed of a dispersed ferromagnetic or ferrimagnetic materials. Their ferrofluids contain submicron-size particles,in contrast to magnetic clutch fluids, which use large micron-sized particles in oil and are designed specifically to solidify[4] in a magnetic field. In their article Moskowitz and Rosensweig reported that the ferrofluids rotated in the same direction as the magnetic field when placed in a rotating magnetic field and they predicted that high rotation speed should be possible.

Experimental work within this department[28] had already shown that steel shot placed in the open bore of a cylindrical polyphase stator tended to travel around the stator surface in the opposite direction to the rotating magnetic wave, and Horsnell[2] noticed that similar reverse rotation occurred in the case of primitive magnetic fluids. An explanation for reverse rotation of Laithwaite's conducting cylinders, and of the steel shot was later given by Brown[6] when he showed that rotating and travelling magnetic waves can be expressed in terms of rotating field vectors.

The reverse rotation of the magnetic fluid was investigated further by Brown[5] et al who found there was a torque exerted upon the fluid container,

and that this always acted in the direction of the wave rotation. No explanation for the reverse rotation of the fluid was found, however.

It was an attempt to explain the reverse rotation of the fluid and to quantify the torque obtained that this work was started. The use of a rotating magnetic wave to simultaneously maintain primitive magnetic fluids in a fluid state and to produce magnetic forces which could be used to effect gravitational separation of non-magnetic ores was a logical extension.

I.2 Ferrofluids and their Preparation.

I.2.1 Colloidal ferrofluids.

These are a dispersion of stable colloidal subdomain magnetic particles, of the order of 100 Angstrons in dimension, in a carrier fluid. As with other colloidal solutions, a dispensing agent is needed to prevent agglomeration due to Van der Vaal's forces. These forces are caused by the attraction of a fluctuating electric dipole to a neighbouring induced dipole. Commercially available dispersions are produced in water, silicones, fluorocarbons and other solvents. These dispersions provide a wide choice of viscosities, wettability, density and other properties. Typical dispersing agents are oleic acid and 10-undecenoic acid. Thermal molecular agitation prevents particle settling.

Ferrofluid viscosity in the absence of an applied magnetic field exhibits ideal Newtonian behaviour with no dependence of viscosity on shear rate. In a uniform applied field, the viscosity tends to be non-Newtonian.

By controlling the number of particles in a unit volume of the ferrofluid, the magnetic properties may be varied over a wide range.

Papell was the first to prepare magnetic fluids with the forementioned properties. His technique[7] involved long-term grinding of magnetic powder in a ball mill with the dispersing agent and carrier fluid. This technique

has been expanded for the production of fluids with various dispersing agent-carrier fluid combinations[8]. The colloids prepared in this manner have some oversize material which will settle out on standing. Rosensweig et al[8] removed the oversize material by spinning in a high speed centrifuge. They claimed that the removal of all particles larger than about 500 Å will prevent the formation of a sediment.

More than 85% of the grinding time was saved[9] by grinding the room temperature metastable antiferromagnetic wustite instead of the ferrimagnetic oxide of iron. Disproportionation of colloidal wustite to yield stable colloidal particles of alpha-iron and magnetite, respectively, was accomplished rapidly at temperatures above 250° C but below 570° C (the eutectoidal stability point of the wustite phase).

Another method, called "Peptizing", was used by Reimers and Khalafalla[10]. A magnetic fluid was prepared from freshly precipitated hydrous iron oxides by spraying aqueous slurry of the precipitate into a heated mixture of kerosine and oleic acid.

I.2.2 Primitive ferrofluids.

We shall use the term "Primitive ferrofluid" to designate a magnetic fluid composed of dispersed magnetic material, (not in colloidal form) in a carrier fluid and dispersing agent. This fluid contains multidomain-size particles like that used by Brown and his colleagues[5]. Typical dispersing agents are oleic acid and a solution of sodium silicate. Primitive ferrofluid particles settle within 3 hours because of the large particle sizes.

The viscosity of such fluids in the absence of an applied field depends very much upon the volume loading of the magnetic material in the carrier fluid. A volume loading of about 11% of a typical primitive ferrofluid may result in a paste-form, rather than a liquid form, in the absence of the magnetic field. When placing these fluids in a d.c. field an aqueous slurry of the fluid is

attracted towards the pole faces and chains of the particles forming a short magnetic circuit between the poles are likely to occur. The viscosity can be so high that a pencil placed in the fluid will find a strong support. On the other hand if such fluids are placed in a rotating magnetic field, each particle tends to behave like a small permanent magnet that tries to align itself with the applied field and therefore to spin. The spinning particles drag the carrier fluid resulting in the rotation of the bulk of the fluid. The effect is that the viscosity of the fluid is reduced and the paste-form fluid acquires the properties of a normal fluid in the sense of its ability to move and change shape.

It appears that the effective viscosity decreases with increasing values of H, and with increasing values of supply frequency. The value of H necessary to make the medium reasonably fluid increases with increasing volume concentration. As in the case of proper ferrofluids the magnetic properties of primitive ferrofluids can be varied by varying their volume loadings.

In the present investigation primitive ferrofluids were prepared by grinding the magnetic powder in a ball mill with the dispersing agent and carrier fluid. The dispersing agents were oleic acid when paraffin was the carrier fluid and a 10% solution of sodium silicate when the carrier fluid was water.

Most of the investigation was carried out using two types of iron oxides, MO-2035 and MO-9853 supplied by Pfizer. Their particulars are summarized in table I.1.

Table I.1.

Property	MO-2035	MO-9853
Colour	Brown	Brown
Particle size	0.2	0.05 micron
Specific gravity	4.6	4.67
Coercive force	4.2×10^4	4.2×10^4 A/m
Flux density at saturation	.35	0.26 Tesla
Particle shape	acicular	cubic

A sample of fluid was also prepared by "Borohydride reduction"[11], described later in section 2.6. The authors claimed that this method yields particle sizes ranging from 0.1 to 1 micron. Some tests were also carried out on fluids containing either magnetite or ferrosilicon and on a true colloical suspension fluid.

I.3 Possible Applications of Ferrofluids.

The ferrofluids can produce torque, and so a motor is one possible application, and they can be transported i.e. pumped by rotating magnetic fields. The latter suggests a ferrofluid pump as another application.

Brown, Birch and McCormick[12] described the possibility of designing a ferrofluid valve. It consists mainly of a small air gap through which the fluid passes. Complete shut-off could be obtained with primitive ferrofluids, the action being similar to that of the magnetic clutch in that the particles build up in chains which eventually bridge the pole faces.

Moskowitz and Rosensweig suggested many other applications for single-domain colloidal suspension ferrofluids. One of these applications is the direct conversion of heat energy[13] based on the well known Curie phenomenon in which iron or almost any other magnetic material experiences a change of its magnetization when its temperature is changed.

Among other applications are magnetic levitation, utilizing spatially inhomogeneous magnetic fluid, and the magnetic seal. The latter is a commercial success. The magnetic fluid is trapped in the magnetic field between stationary and rotating surfaces, and it can resist differential pressures from 10^{-9} Torr up to about 100 lbf/in^2 per axial inch of shaft length. It can be used to seal off rotating shafts in vacuum systems. The same idea is used to seal off air thrust bearings.

The principles of ferrohydrodynamics have been applied[14] to develop accelerometers, altitude control devices. Concentrated magnetic fluids may also be sprayed on oil slicks[15] to give the oil magnetic properties such that it can be collected by means of strong magnetic field.

I.4. Layout of Thesis.

This thesis is divided into three main divisions. Section 1 describes measurements of the magnetic properties of the fluids. The two main properties are the average value of the unsaturated static susciptibility, χ and the saturation magnetization, $\mu_o M_{sat}$, both of which feature in the other two sections.

Section 2 contains an account of experimental work on a ferrofluid motor, and develops theories which attempt to explain the experimental results. The investigation of the mineral separation application is described in Section 3.

Some conclusions are drawn at the end of each section, but the main conclusions are given in section 4.

SECTION 1.

MEASUREMENTS OF THE MAGNETIC CHARACTERISTICS OF THE FLUIDS.

1.1 Variable Mutual Inductance Method.

This is a null method using switched direct currents. The circuit is as shown in Fig.1.1 and a photograph of the equipment is shown in Fig.1.2. The standard solenoid and search coil have a mutual inductance which is dependent upon their known dimensions and numbers of turns and upon the ferrofluid. The last is contained in a glass tube positioned inside the search coil, shown in Fig.1.3, and can be inserted or removed without disturbing the coil. The circuit allows the mutual inductance to be determined by comparison with the previously calibrated variable mutual inductance. The calibration curve of the latter approximates very closely to the form $M_{max} \cos \theta$, where M_{max} is 5.01×10^{-4} H, and θ is the angular position of the pointer linked to the secondary coil.

The demagnetizing factor of a prolate spheroid becomes smaller as the ratio of the major to minor axes becomes greater, where the major axis is in the direction of the magnetic field[26]. For that reason it was decided to make the length to diameter ratio of the sample 8 which corresponds to a demagnetizing factor of .02, assuming the sample to approximate to a prolate spheroid.

With no sample in the search coil, the variable mutual inductance was adjusted to give no reading on the galvanometer when the magnetizing current was switched on. The specimen was then inserted, and for each field strength, the variable inductance was readjusted to give no galvanometer reading upon switching on the current. The difference between the two adjustments will be d to the ferric induction of the specimen at the particular field intensity.

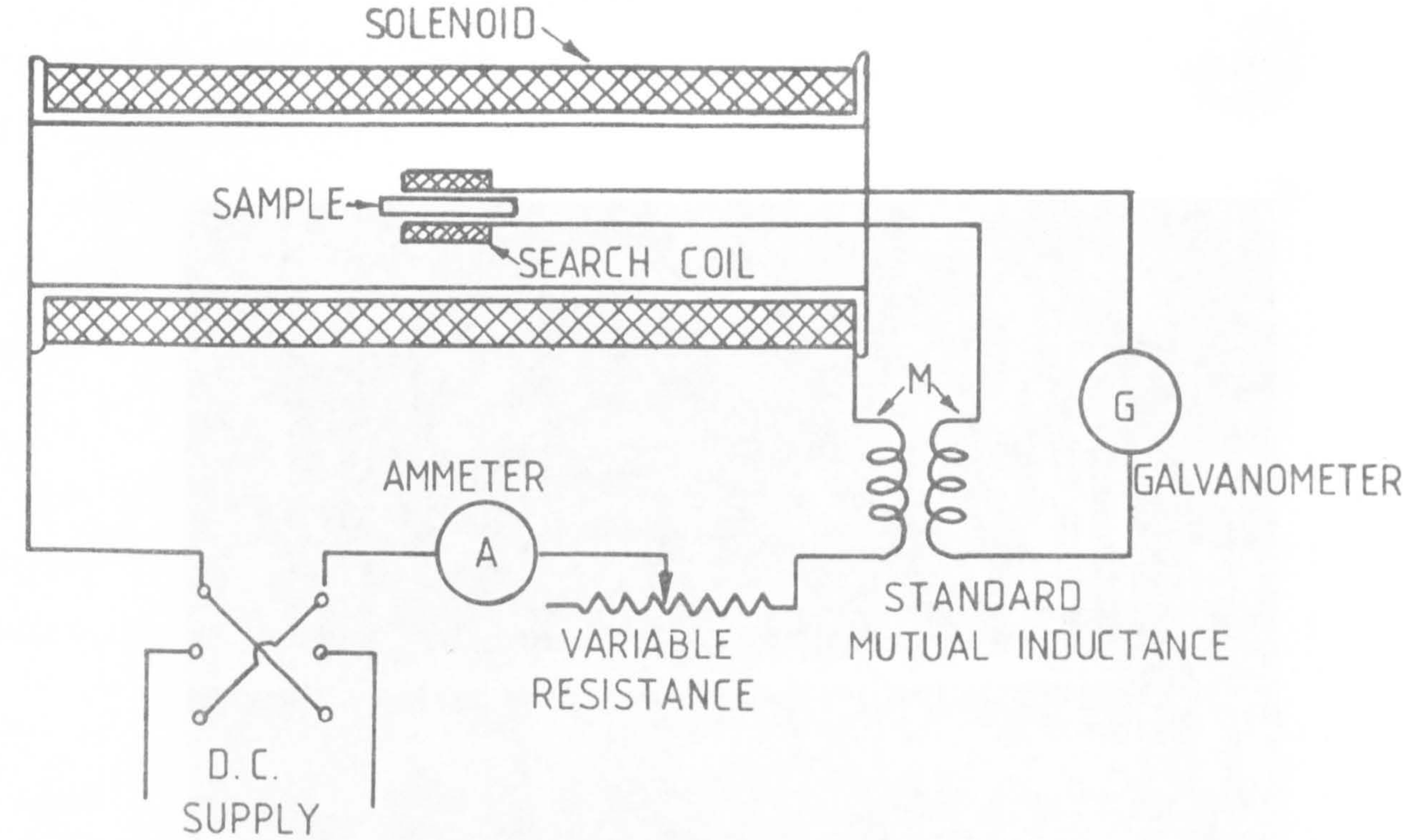

FIG. 1.1 CONNECTION DIAGRAM

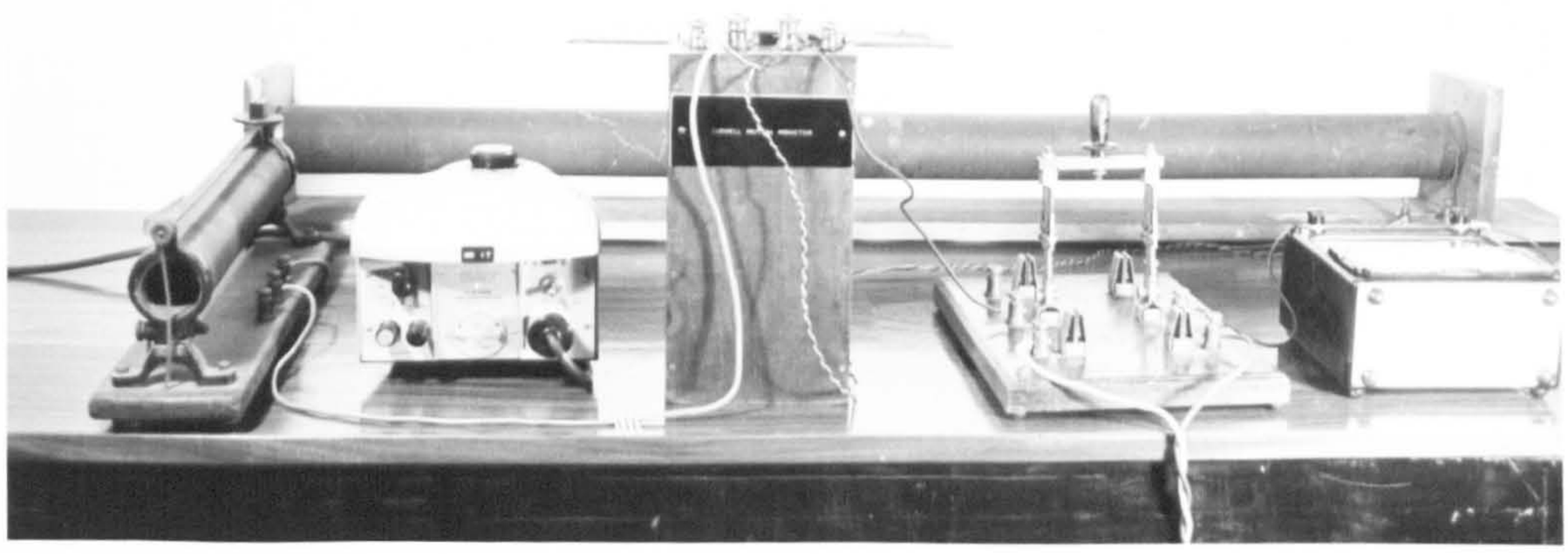

FIG. 1.2 EQUIPMENT FOR FIG. 1.1

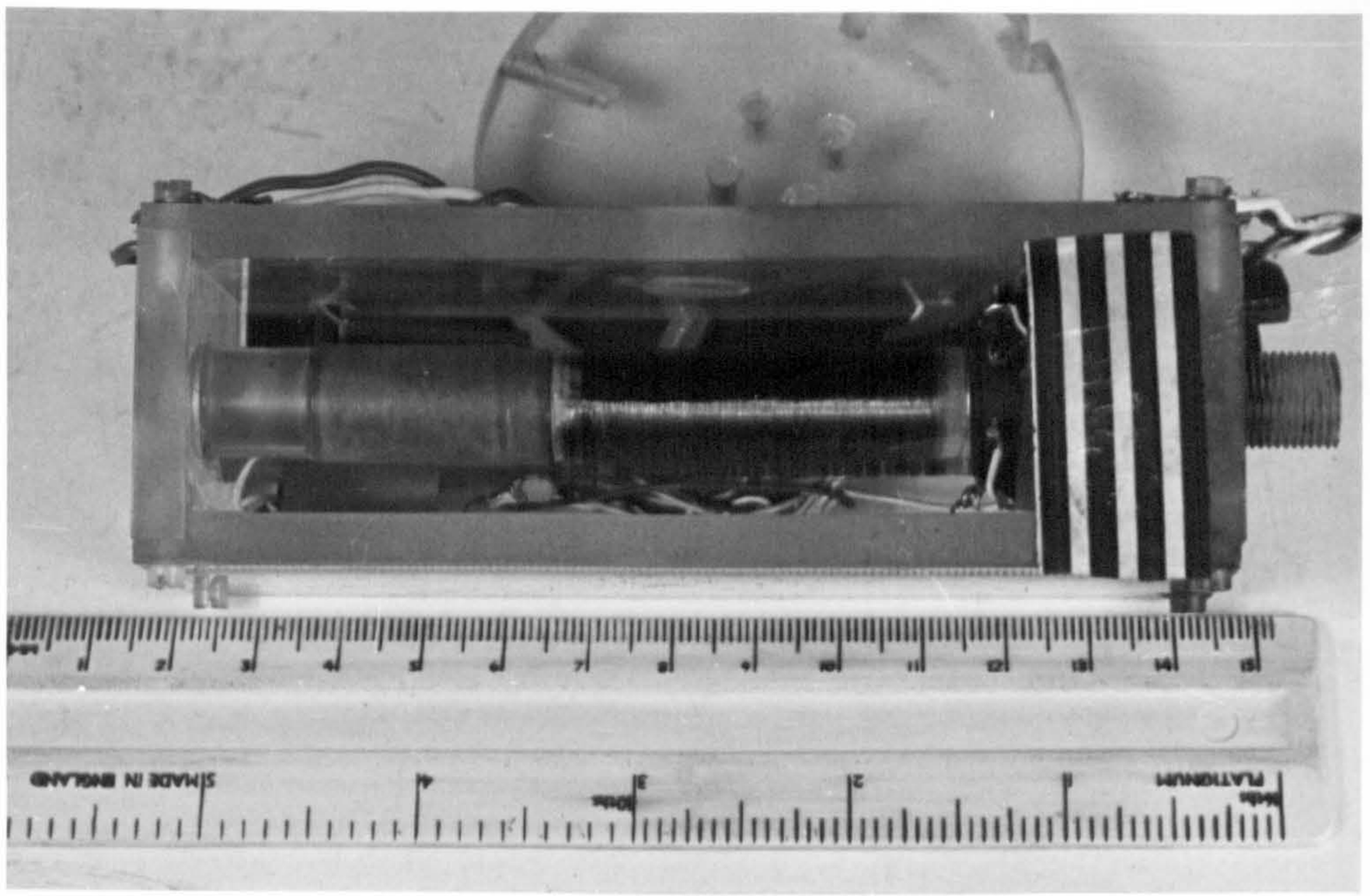

FIG. 1.3 - THE SEARCH COIL

A few samples of MO-2035 in paraffin were tested and showed no sign of saturation over the allowable current range of the solenoid. Line 'a' of Fig.1.4 shows variation of the calculated values of $(\mu_f - 1)$ with the percentage volume of magnetic material, K_p. The relationship was expected to be linear, see equation A2.5 of Appendix 2, and in view of the lack of linearity, the accuracy of the system was investigated.

1.1.1 Calculation of the error.

The standard solenoid was one which had been used for many years in the department, and was known to produce a very uniform axial field intensity. The relationship between field intensity, H, and current I, is

$$H = \frac{\omega_1 \, I}{L} = 1540 \quad I \text{ A/m}$$

where ω_1/L is the turns per unit length of the solenoid.

The search coil, a photograph of which is shown in Fig.1.3, had 1800 turns on a former of diameter 12.2 mm over a length of 45 mm.

In the presence of a magnetic field, part of the flux linking the search coil will pass through the fluid while the rest will pass through air. Let these be represented by ψ_f and ψ_a respectively, and let ϕ_f and ϕ_a be the corresponding linkages per turn.

Then $\psi_f = \omega_2 \, \phi_f$

and $\psi_a = \omega_2 \, \phi_a$

Where ω_2 is the number of turns of the search coil.

Upon switching the current in the solenoid, the e.m.f. induced in the search coil will be the sum of e_f due to ψ_f and e_a due to ψ_a.

Therefore, $$e_f = \frac{\partial \psi_f}{\partial t} = \omega_2 \frac{\partial \phi_f}{\partial t} = \omega_2 \, A_f \frac{\partial B_f}{\partial t} \quad \ldots\ldots \quad 1.1.1$$

and $$e_a = \frac{\partial \psi_a}{\partial t} = \omega_2 \frac{\partial \phi_a}{\partial t} = \omega_2 \, A_a \frac{\partial B_a}{\partial t}$$

$$= \omega_2 \, (A_c - A_f) \frac{\partial B_a}{\partial t} \quad \ldots\ldots \quad 1.1.2$$

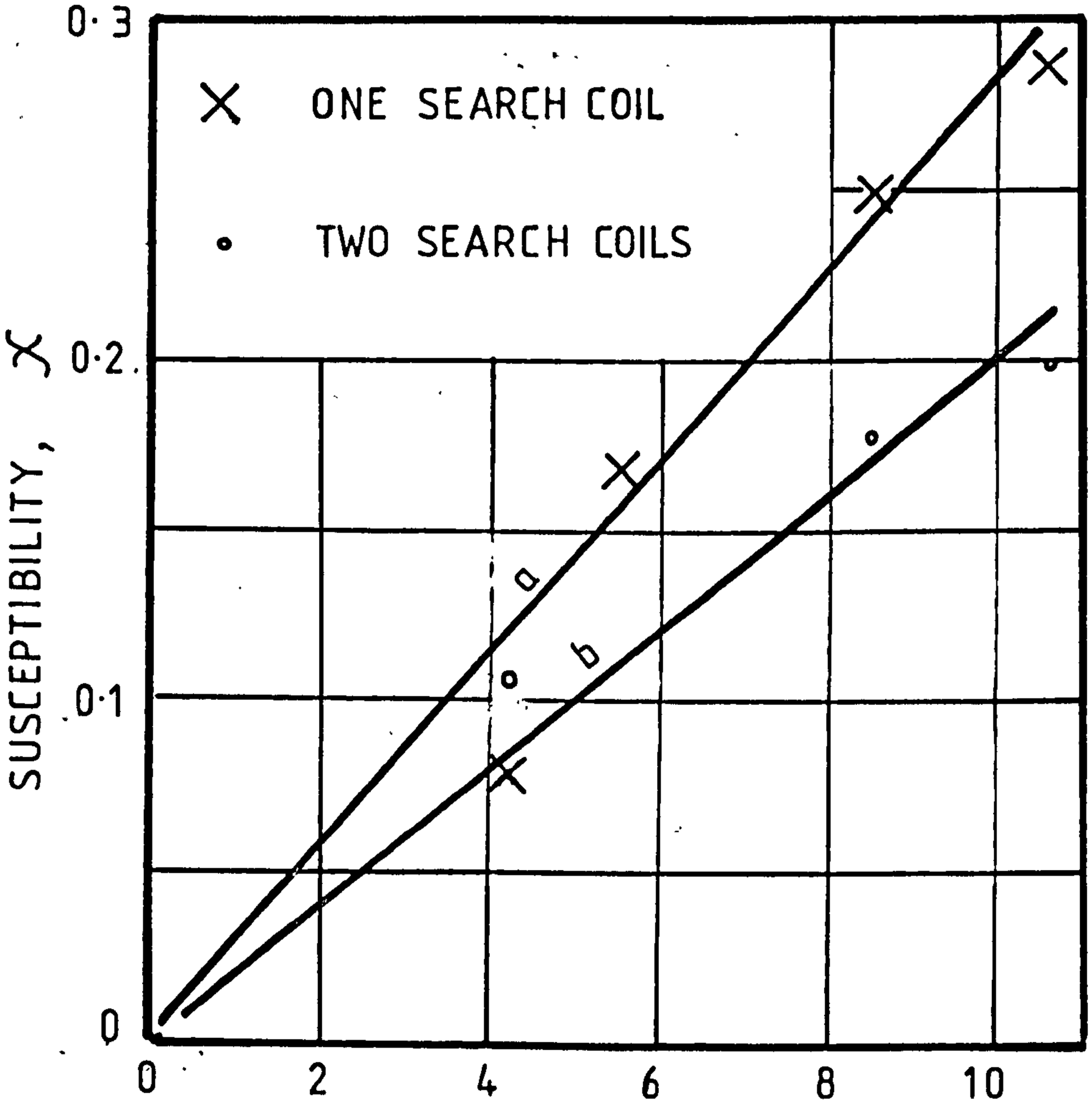

FIG. 1. 4 RESULTS OBTAINED FROM THE VARIABLE MUTUAL INDUCTANCE METHOD

Upon switching the current I through both the solenoid and the primary of the variable mutual inductor, the change of flux in the air, fluid and the mutual inductance will be respectively (assuming H in air and fluid to be the same):

$$\psi_f = \omega_2 A_f \mu_o \mu_f \left(\frac{\omega_1}{L}\right) I$$

$$\psi_a = \omega_2 (A_c - A_f) \mu_o \left(\frac{\omega_1}{L}\right) . I$$

$$\psi_d = M \cos \theta . I$$

where ψ_d is the flux linking the secondary coil of the variable mutual inductor.

ψ_f and ψ_a will oppose ψ_d, and at balance

$$\omega_2 A_f \mu_o \mu_f \frac{\omega_1}{L} I + \omega_2 (A_c - A_f) \mu_o \frac{\omega_1 I}{L} = M \cos \theta . I$$

from which

$$(\mu_f - 1) = \frac{M \cos \theta . L}{\omega_2 \omega_1 \mu_o A_f} - \frac{A_c}{A_f} \quad \ldots\ldots \quad 1.1.3$$

From which

$$\frac{\delta(\mu_f - 1)}{(\mu_f - 1)} = \frac{\delta \left(\frac{M \cos \theta . L}{\omega_2 \omega_1 \mu_o A_f}\right) - \delta \left(\frac{A_c}{A_f}\right)}{\left(\frac{M \cos \theta . L}{\omega_2 \omega_1 \mu_o A_f}\right) - \left(\frac{A_c}{A_f}\right)} \quad \ldots\ldots \quad 1.1.4$$

Now $\frac{A_c}{A_f}$ must be greater than unity, and allowing for the thickness of the search coil former and of the glass tube it is about 2 for our case. If $\mu_f - 1 \gg 1$ then the percentage error in the value of $\mu_f - 1$ will be of the same order as that of the quantity $\left(\frac{M \cos \theta . L}{\omega_2 \omega_1 \mu_o A_f}\right)$, assuming that the error in A_c is not very large. If, however, $(\mu_f - 1) \ll 1$, then $\frac{M \cos \theta . L}{\omega_2 \omega_1 \mu_o A_f} \simeq \frac{A_c}{A_f}$ and equation 1.1.4 approximates to:

$$\frac{\delta(\mu_f - 1)}{(\mu_f - 1)} \simeq \left[\frac{\delta x}{x} - \frac{\delta y}{y}\right] \cdot \frac{y}{(\mu_f - 1)} \quad \ldots\ldots \quad 1.1.5$$

where $x = \dfrac{M \cos\theta \cdot L}{\omega_2 \omega_1 \mu_o A_f}$ and $y = \dfrac{A_c}{A_f}$

From equation 1.1.5, the percentage error in $(\mu_f - 1)$ will be equal to the percentage errors in the quantities x and y multiplied by $\frac{y}{(\mu_f - 1)}$. Since y could be equal to 2, then for $\mu_f - 1 = 0.1$, say, the multiplying factor could be equal to 20.

The maximum percentage errors in A_c/A_f, and in $L/\omega_2\omega_1\mu_o A_f$ are likely to be of the order of 4% (mainly due to errors in estimation A_f). Now for $y = 2$ the value of $M \cos\theta$ is about 4.4×10^{-4} for $\mu_f - 1 = 0.1$. From the calibration curve an error of 0.3 in the value of θ corresponds to an error of 0.29% in the value of $M \cos\theta$. In addition to the above there is the error due to the insensitivity of the galvanometer. This error will be worst at low values of current. A test was carried out and at a current of 8 A, the change in the value of $M \cos\theta$ required to produce an appreciable deflection of the galvanometer was 1.52×10^{-4} H. For $\mu_f - 1 = 0.1$ again this corresponds to an error in the value of $M \cos\theta = 34.5\%$.

Presumable the percentage error in $\mu_f - 1$ could then be as high as

$$20 \left[(34.5 + 4) + 4\right]$$

$$\text{i.e.} \simeq 840\%$$

Within this possible extreme magnitude of percentage error it is perhaps not surprising that the curves of Fig.1.4 were not linear as expected.

It was thought that by putting another similar search coil of the same dimensions and turns side by side with the original one and connecting them in opposition one could achieve more sensitivity. A photograph of the two coils is shown in Fig.1.5. They were balanced so that with no fluid their e.m.f.'s

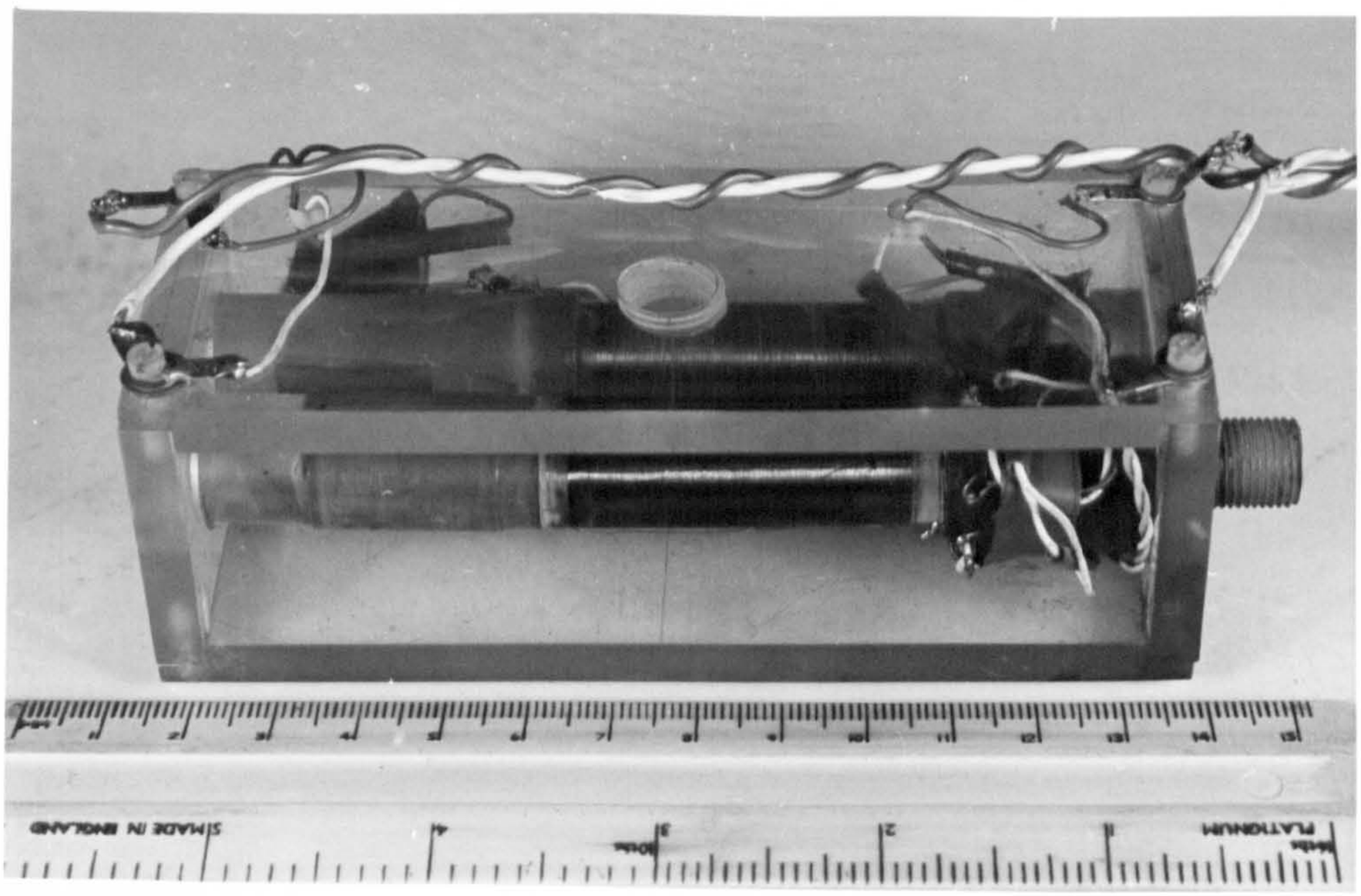

FIG. 1.5 THE TWO SEARCH COILS

cancelled. In effect this method will eliminate the term A_c/A_f from equation 1.1.3, to give

$$\mu_f - 1 = \frac{M \cos \theta . L}{\omega_2 \omega_1 \mu_o A_f} \quad \ldots\ldots \quad 1.1.6$$

$$\text{This time } \Delta(\mu_f - 1) = \frac{-M \sin \theta . L . \Delta\theta}{\omega_2 \omega_1 \mu_o A_f} + \frac{\Delta\psi_G}{I}$$

Where $\Delta\psi_G$ is a term to account for the galvanometer sensitivity which is unchanged. The percentage error due to the $\Delta\theta$ term is now given by:

$$\frac{\Delta(\mu_f - 1)}{(\mu_f - 1)} = -100 \tan \theta . \Delta\theta$$

and where θ was about 30° before, it is of the order of 85° in this case. For $(\mu_f - 1) = 0.1$, $\theta = 87.6^\circ$ and $\tan \theta = 23.86$.

Thus the error multiplier can, in fact, be large. Measurements were made but the curve of $(\mu_f - 1)$ against K_p, shown with the line 'b' in Fig.1.4 was again found to be non-linear and not in agreement with the single search-coil curve. Due to the lack of sensitivity of the variable mutual inductance and the galvanometer an A.C. magnetic field method was tried.

1.2 Alternating Magnetic Field Method.

In this method, the two similar coils mentioned before were used. The two coils were connected in opposition and were placed inside a solenoid which gave 2490 A/m per ampere.

The measuring circuit is shown in Fig.1.6a. and a photograph of the equipment is shown in Fig.1.6b. With no fluid in the sample coil the potentiometer labelled α was adjusted to give zero a.c. output signal from the integrator. The potentiometer, β, across the integrating amplifiers B and D were also adjusted to give a suitable compromise between true integration and d.c. drift of the system - typically β was about .002.

With no sample in, the zero error was not more than 0.03 m.v. per ampere passing through the solenoid, while the peak voltage output from the integrator due to one coil, with no sample, was 110 m.v. per ampere.

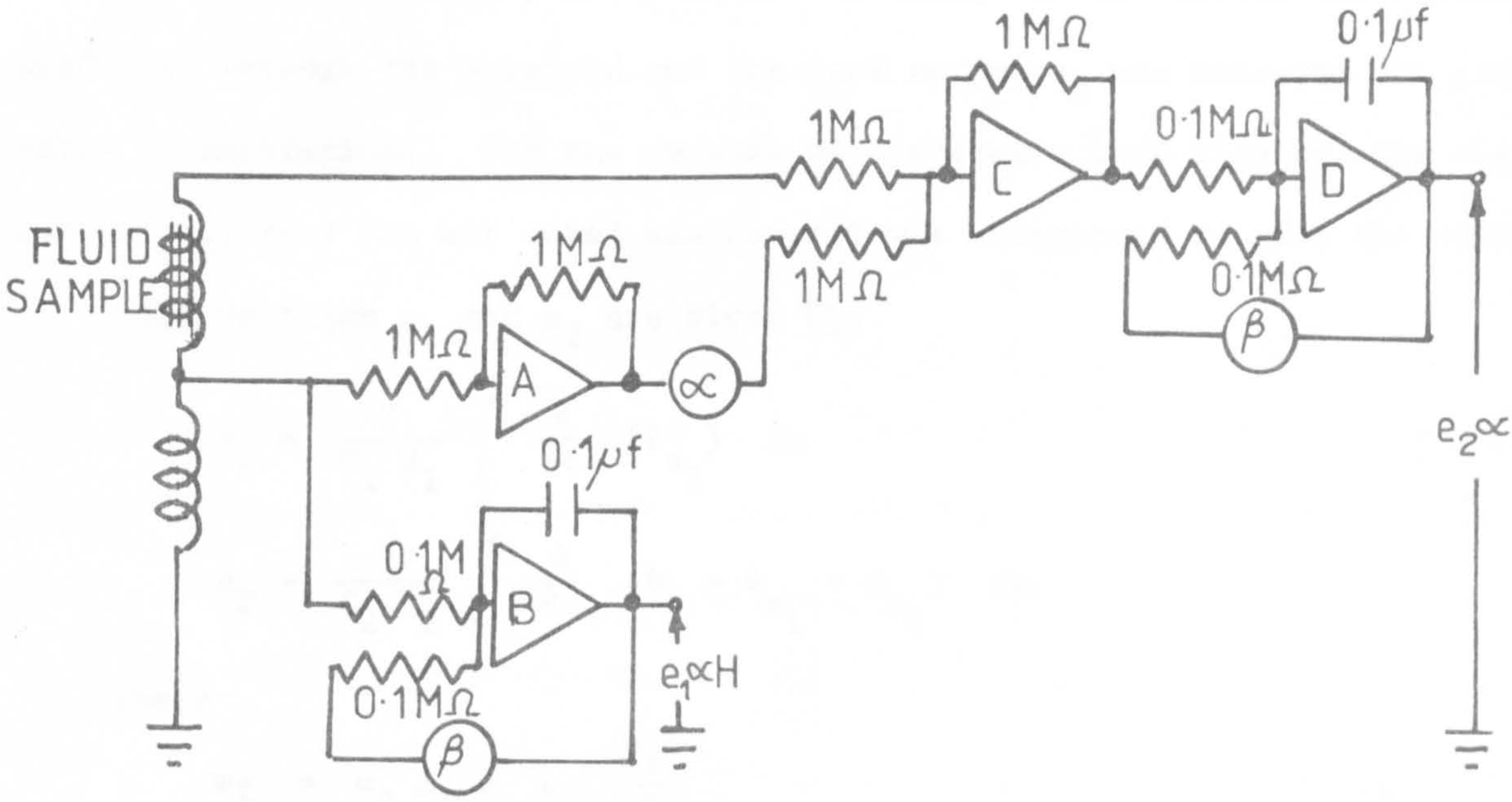

FIG.1.6.a ANALOGUE COMPUTER CIRCUIT FOR PERMEABILITY MEASUREMENT

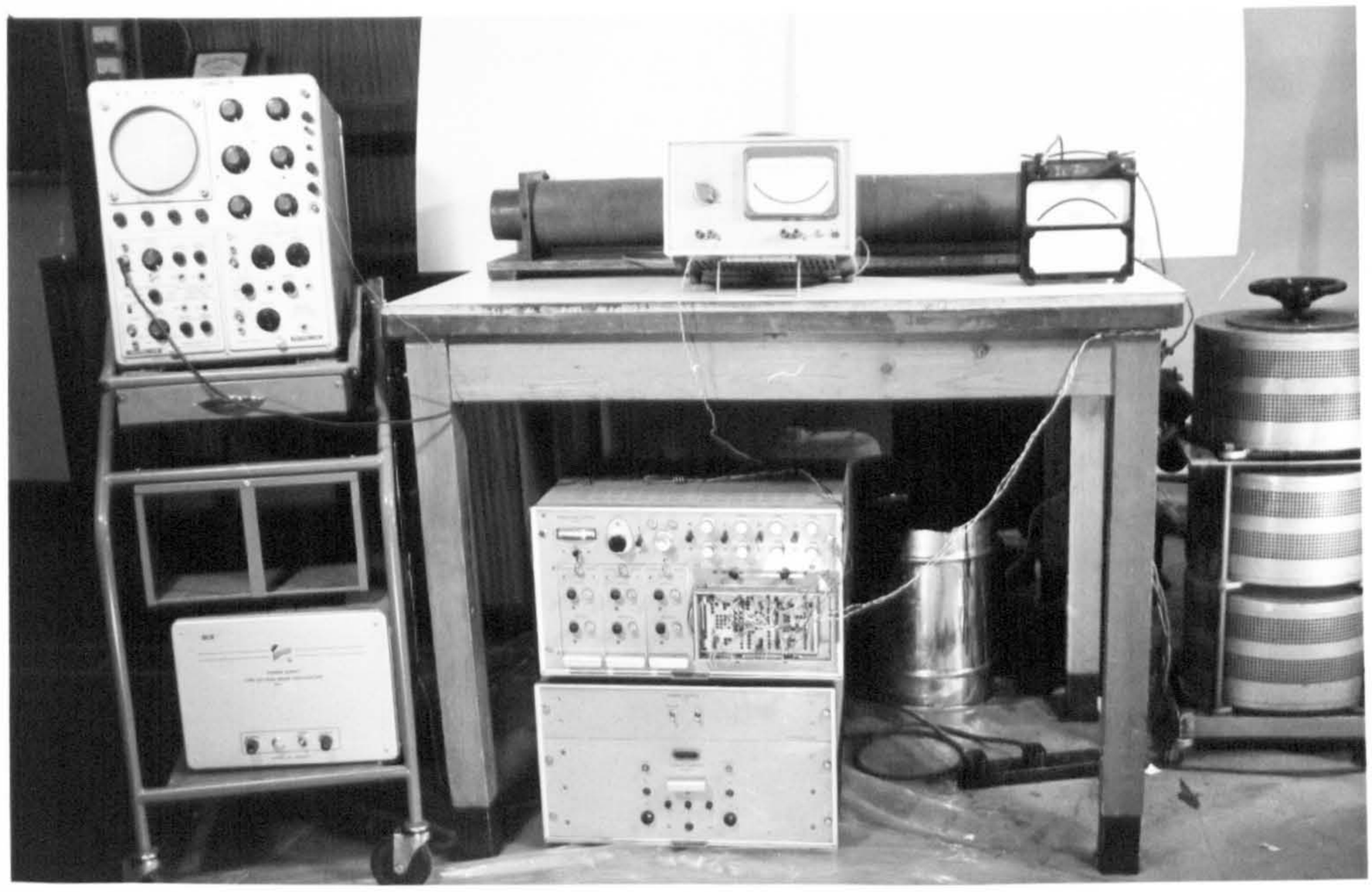

FIG.1.6.b EQUIPMENT FOR CIRCUIT 1.6.a

The sample was then placed inside the coil, the excitation was increased gradually through the solenoid and the peak output e_2 was measured for each value of excitation. For the purpose of hysteresis loop display, the signal output, e_1, from the air cored search coil was integrated to give the voltage, e_1. The voltages e_1 and e_2 are given by:

$$e_1 = \frac{2}{C_1 R_1} \int \frac{\partial}{\partial t} (\psi_{a_2}) \, dt$$

$$e_2 = \frac{2}{C_2 R_2} \int \frac{\partial}{\partial t} (\psi_f + \psi_{a_1} - \psi_{a_2}) \, dt$$

where

$$\psi_f = \omega_2 A_f \mu_o \mu_f \frac{\omega_1 I}{L}$$

$$\psi_{a_1} = \omega_2 (A_c - A_f) \mu_o \frac{\omega_1 I}{L}$$

$$\psi_{a_2} = \omega_2 A_c \mu_o \frac{\omega_1 I}{L}$$

C_1R_1 and C_2R_2 are time constants of the two integrators.

$$\therefore \quad e_1 = \frac{2}{C_1 R_1} \omega_1 \omega_2 \frac{\mu_o I}{L} A_c \quad \ldots\ldots \quad 1.2.1$$

and

$$e_2 = \frac{2}{C_2 R_2} \omega_1 \omega_2 \frac{\mu_o I}{L} (\mu_f - 1) A_f \quad \ldots\ldots \quad 1.2.2$$

$$\therefore \quad \chi = (\mu_f - 1) = \frac{C_2 R_2}{C_1 R_1} \cdot \frac{e_2}{e_1} \cdot \frac{A_c}{A_f}$$

If, as was the case for these measurements

$$C_2 R_2 = C_1 R_1,$$

$$\therefore \quad \chi = (\mu_f - 1) = \frac{e_2}{e_1} \cdot \frac{A_c}{A_f}$$

$$\therefore \quad \frac{\partial(\mu_f - 1)}{\mu_f - 1} = \frac{\partial e_2}{e_2} - \frac{\partial e_1}{e_1} + \frac{\partial(A_c/A_f)}{A_c/A_f}$$

The error in e_1 and e_2 is believed to be of the order of 3%. Therefore, the error in $(\mu_f - 1)$ could be as high as 10%, but of course this is considerably less than for the previous cases.

1.2.1 Experimental results and discussions.

The $\mu_o M$-H loops for a few samples of fluid are shown in Figs. 1.7 to 1.9. Fig.1.7 is for an 11.5% by volume of the iron oxide type MO-2035 in paraffin with no oleic acid. The paraffin was used more as a binder than as a Carrier fluid. In all figures the vertical axis is for $\mu_o M$ values in Tesla and the horizontal axis is for the H values, one large division represents 1.42×10^4 A/m.

1.2.1.a Variation of the size of the μ_oM-H Loop with the volume loading, size of the particles and material.

A plot of the areas of the $\mu_o M$-H loops against volume loading is shown in Fig.1.10 for the oxide-type MO-2035 in paraffin. The expected linearity between the areas and the volume loading of the fluid, K_p, is evident although two of the readings have errors of up to 7%.

Also, in Fig.1.10 are shown points for 11.5% volume concentration of magnetite and a 6.4% volume loading of ferrosilicon. The area of the magnetite fluid loop is about 30% smaller than that of MO-2035 of the same concentration, and comparing Figs. 1.7d and 1.9c, the magnetite has both a smaller saturation magnetization and coercive force.

The area of the ferrosilicon loop is extremely small, Fig.1.9a, also, as are its saturation magnetization and coercive force.

Bean[16] found that particles of single domain size have no remanence and no coercive force, which results in a zero area of $\mu_o M$-H loop. This is confirmed by experimental results since the magnetization curve of a magnetic colloid of kerosene base and of volume loading 4.7% did not exhibit the hysteresis loop expected for ferromagnetics or ferrimagnetics, but produced

$\mu_o M_{max}$ Tesla	H_{max} A/m×10^4	
·0134	1·35	a
·027	2·55	b
·035	3·80	c
·042	6·8	d

FIG. 1·7 HYSTERESIS LOOPS FOR 11·5% MO-2035 IN PARAFFIN

SCALE IS ·0336 T per LARGE VERTICAL DIVISION

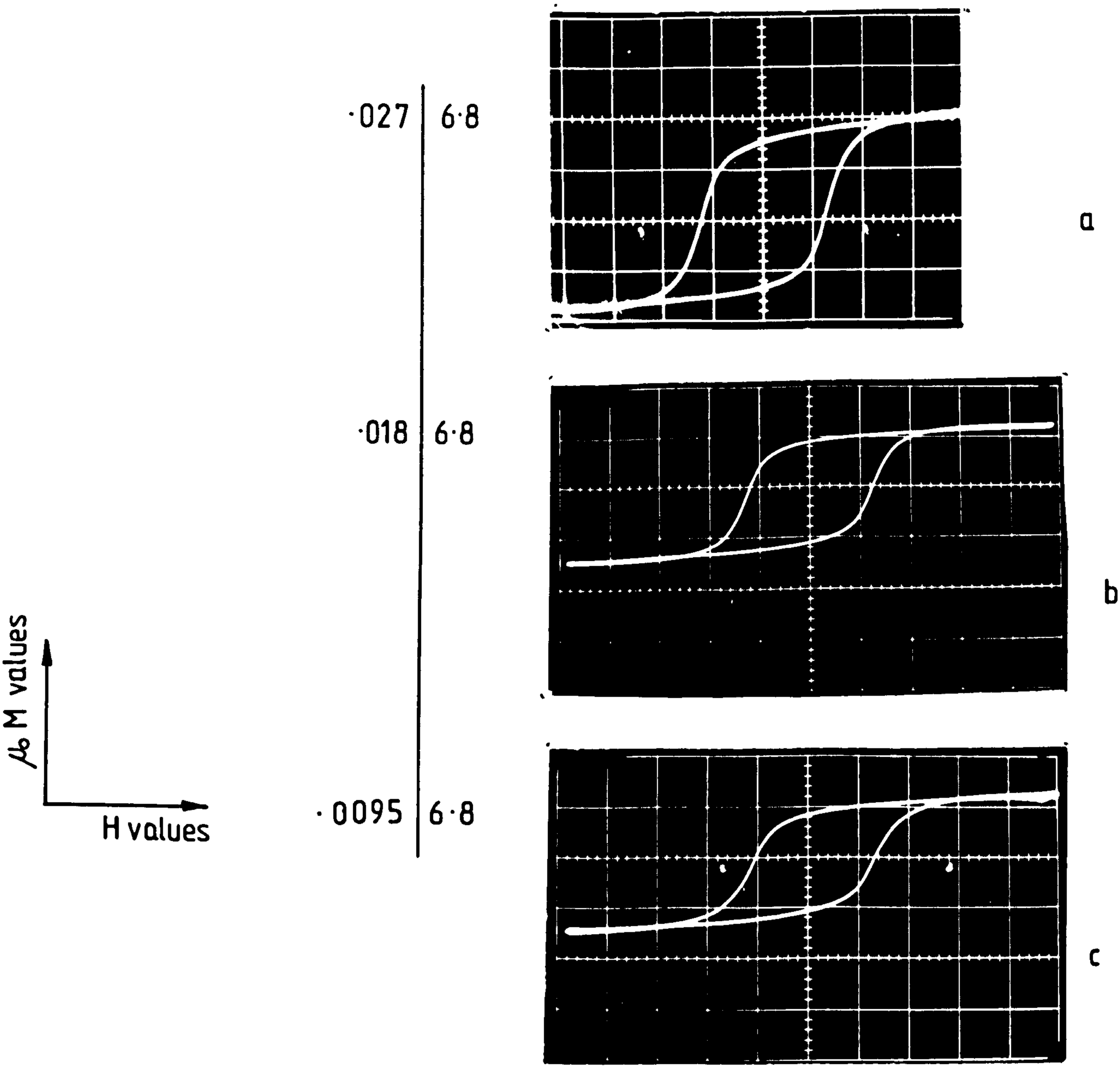

FIG. 1·8 HYSTERESIS LOOPS FOR TESLA per large vertical division

a. 8·17 % MO-2035 IN PARAFFIN ·0135

b. 5·36 % ——————"—————— ·0135

c. 2·64 % ——————"—————— ·0067

$\mu_o M_{max}$ Tesla	H_{max} A/m × 10^4
·032	6·8
·021	6·8
·0336	6·8

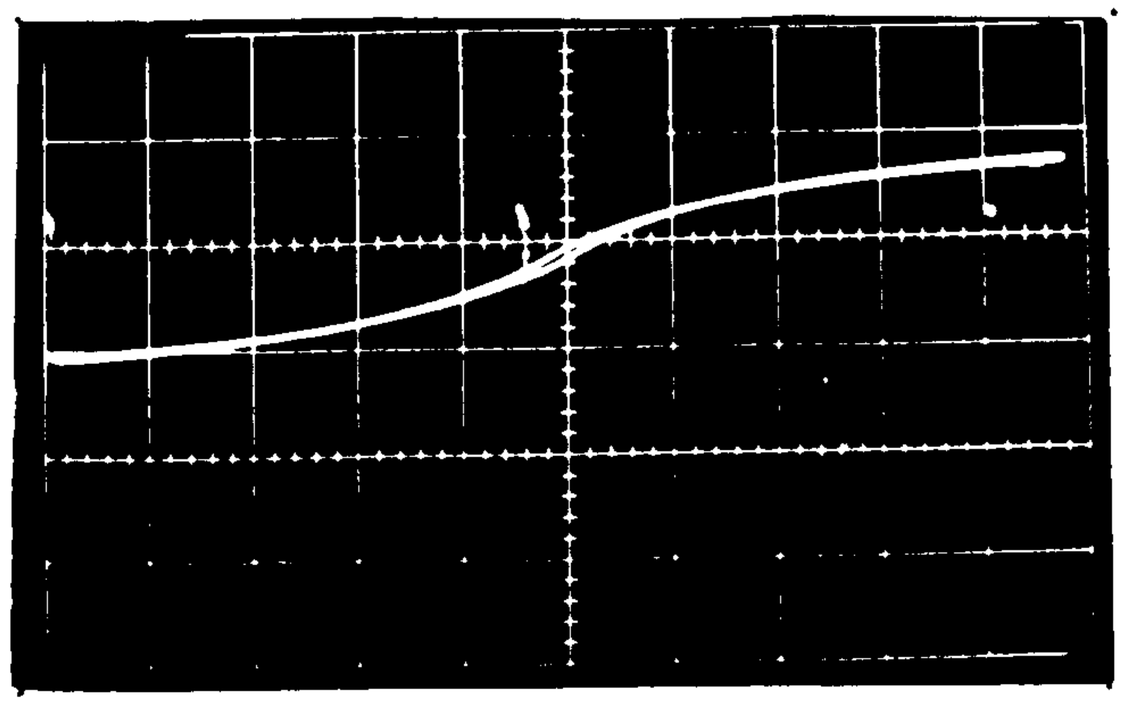

a.

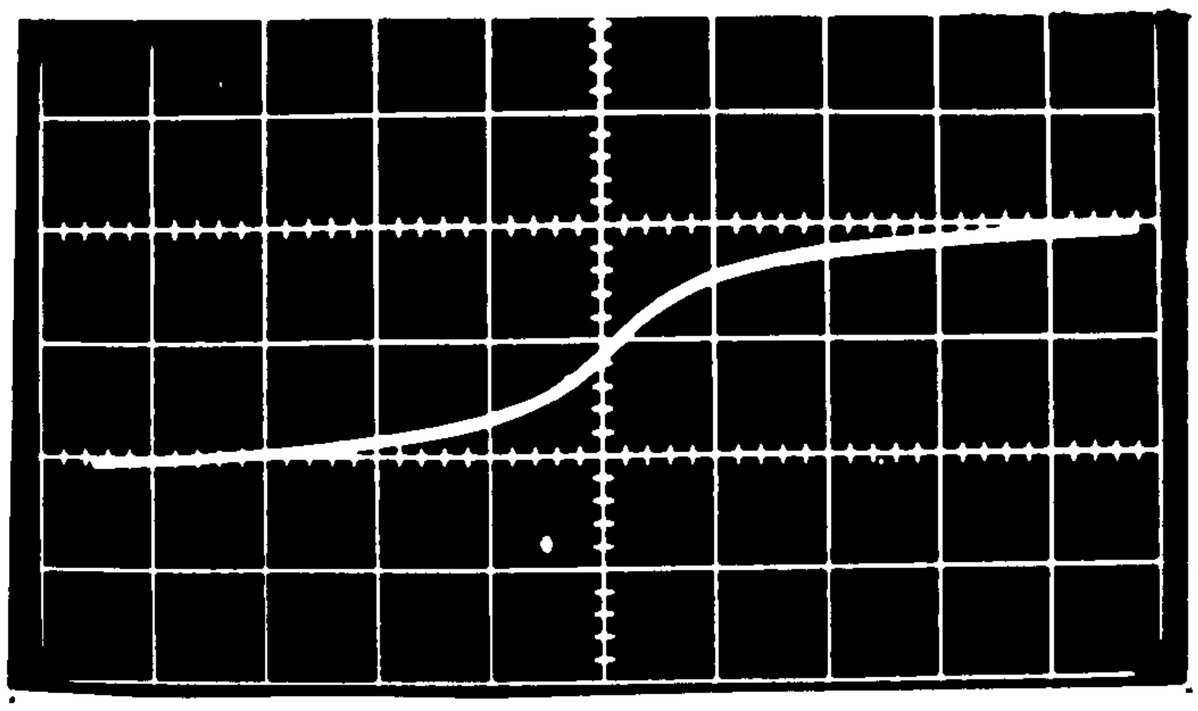

b.

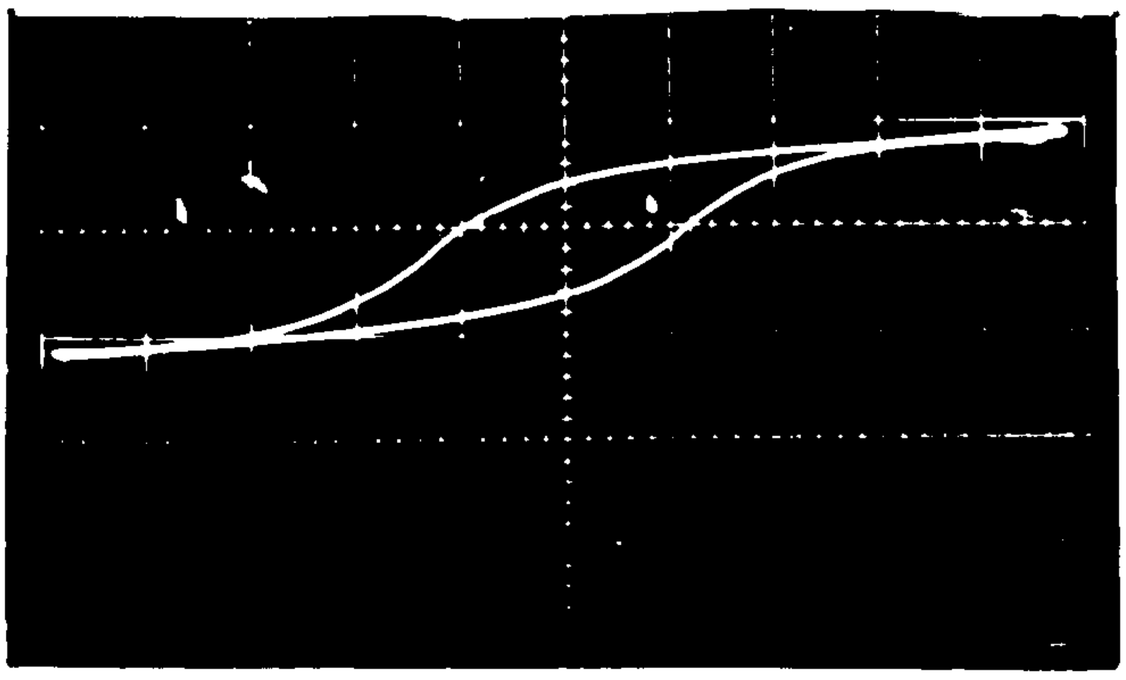

c.

$\mu_o M$ values

H values

TESLA per large vertical division

FIG. 1.9 HYSTERESIS LOOPS FOR -

a. 6·4 % FERROSILICON IN WATER ·0336

b. TRUE COLLOIDAL SUSPENSION FLUID WITH VOLUME LOADING 4·7 % ·0220

c. 11·5 % MAGNETITE IN WATER ·0336

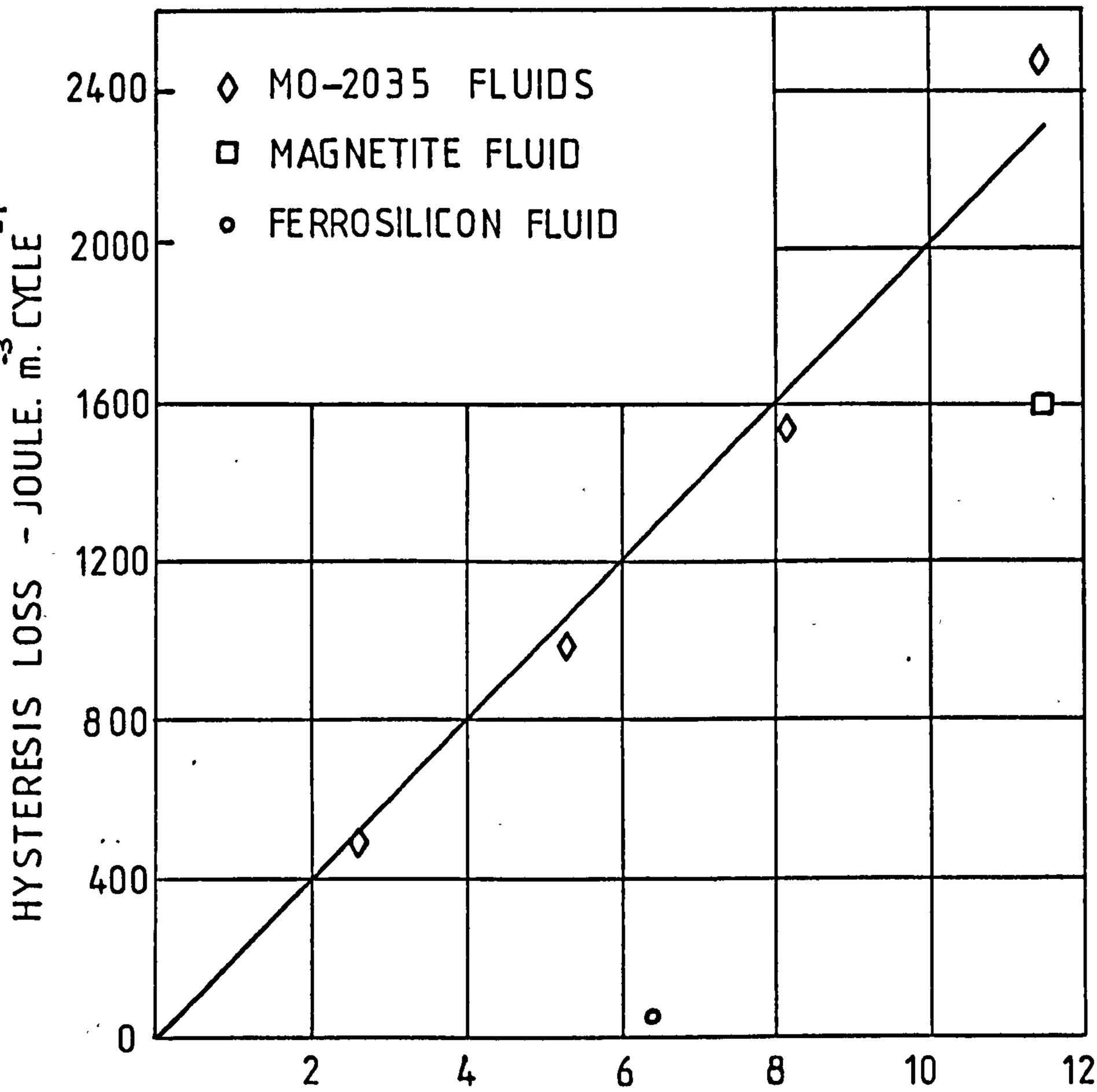

FIG. 1.10. VARIATION OF HYSTERESIS LOSS WITH VOLUME LOADING

instead a symmetrical curve about the origin, Fig.1.9b.

By contrast, the magnetization curves of the multidomain particle fluids mentioned above exhibited a well-defined hysteresis loop[5] as shown in Figs. 1.7 to 1.9. The remanent magnetization indicates the existence of randomly oriented, single-domain grains within the polycrystalline particles. The coercive force is primarily due to magnetostriction from strains introduced during grinding.

1.2.1.b Magnetization curves.

The magnetization curves, which are the relationship between the peak of $\mu_o M$ and the peak of the field strength, for some of the fluids investigated are shown by the curves,labelled a, in Figs. 1.11 to 1.14 and 1.16 to 1.18. The curves labelled b and c will be referred to later in section 3.4. For fixed field intensity, the magnetization curves of MO-2035 in paraffin show a linear variation of $\mu_o M$ with volume loading as expected, see Appendix 2. The magnetization expressed as a percentage of the saturation value is shown in Fig.1.15 for the fluids made up of MO-2035 in paraffin and this curve can be used as a general magnetization curve of such fluids. The saturation magnetization for 11.5% volume concentration of MO-2035 in paraffin is 0.042 corresponding to .365 T if the volume concentration is unity. This figure agrees very well with the manufacturers figure .35 T.

1.3 Conclusions.

As predicted, at a fixed field intensity, the magnetization, $\mu_o M$, was found to be proportional to the volume loading. The expected linearity between the areas of $\mu_o M$-H loops and the volume loading of the fluids is confirmed by the results of section 1.

The prediction of the effect of magnetic particle shape upon the magnetic properties of ferrofluid, (Appendix 2), has been supported by directly measured

values of fluid permeabilities in that acicular particles gave depolarizing factor of 0.15. The latter were confirmed by measurements of magnetic forces on non-magnetic bodies (section 3).

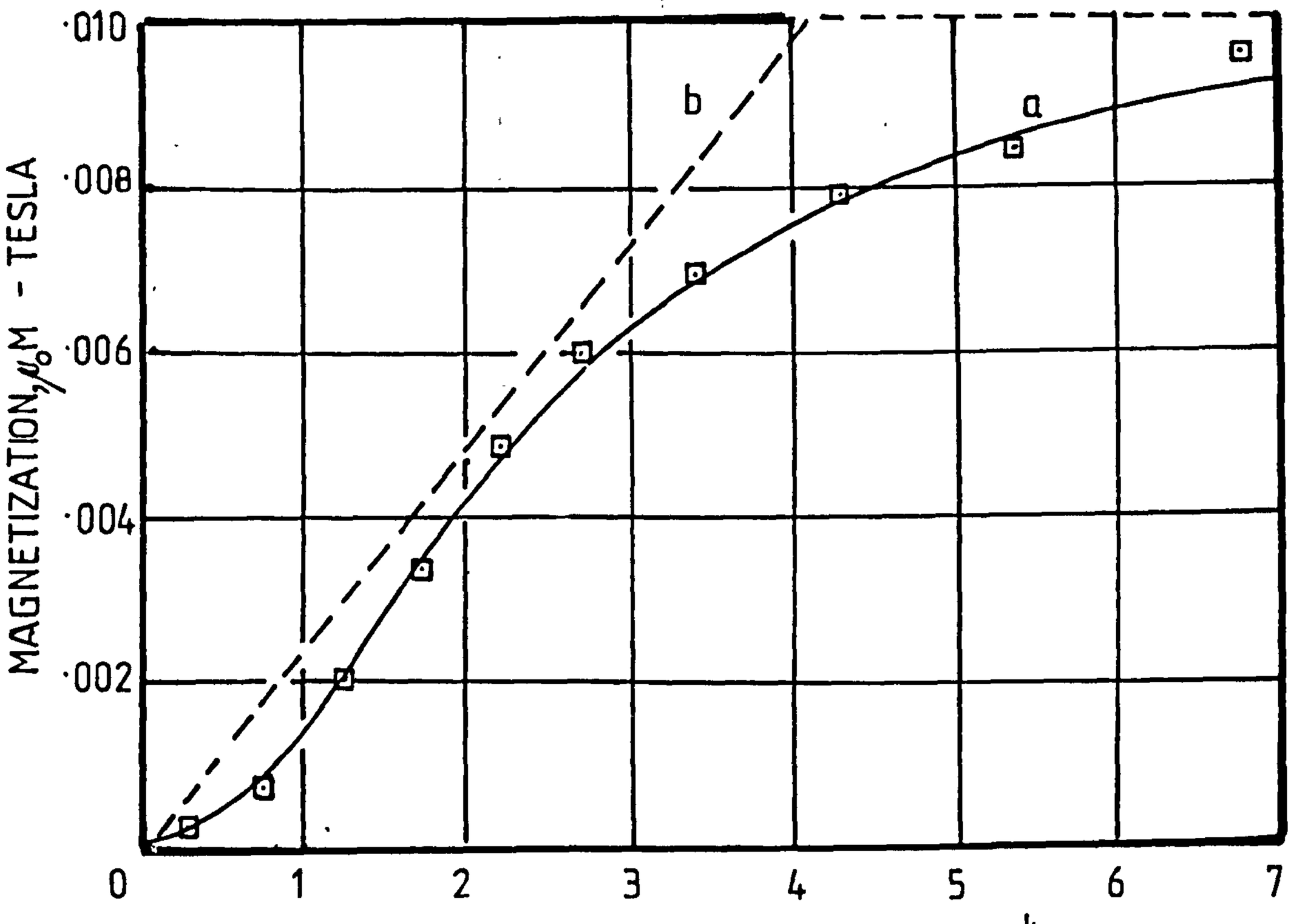

FIG.1.11 MAGNETIZATION CURVES OF 2·64% MO-2035 IN PARAFFIN.

(a) FROM PERMEABILITY MEASUREMENTS

(b) FROM FORCE MEASUREMENTS ON THE 118 mm DIAMETER 2-POLE STATOR

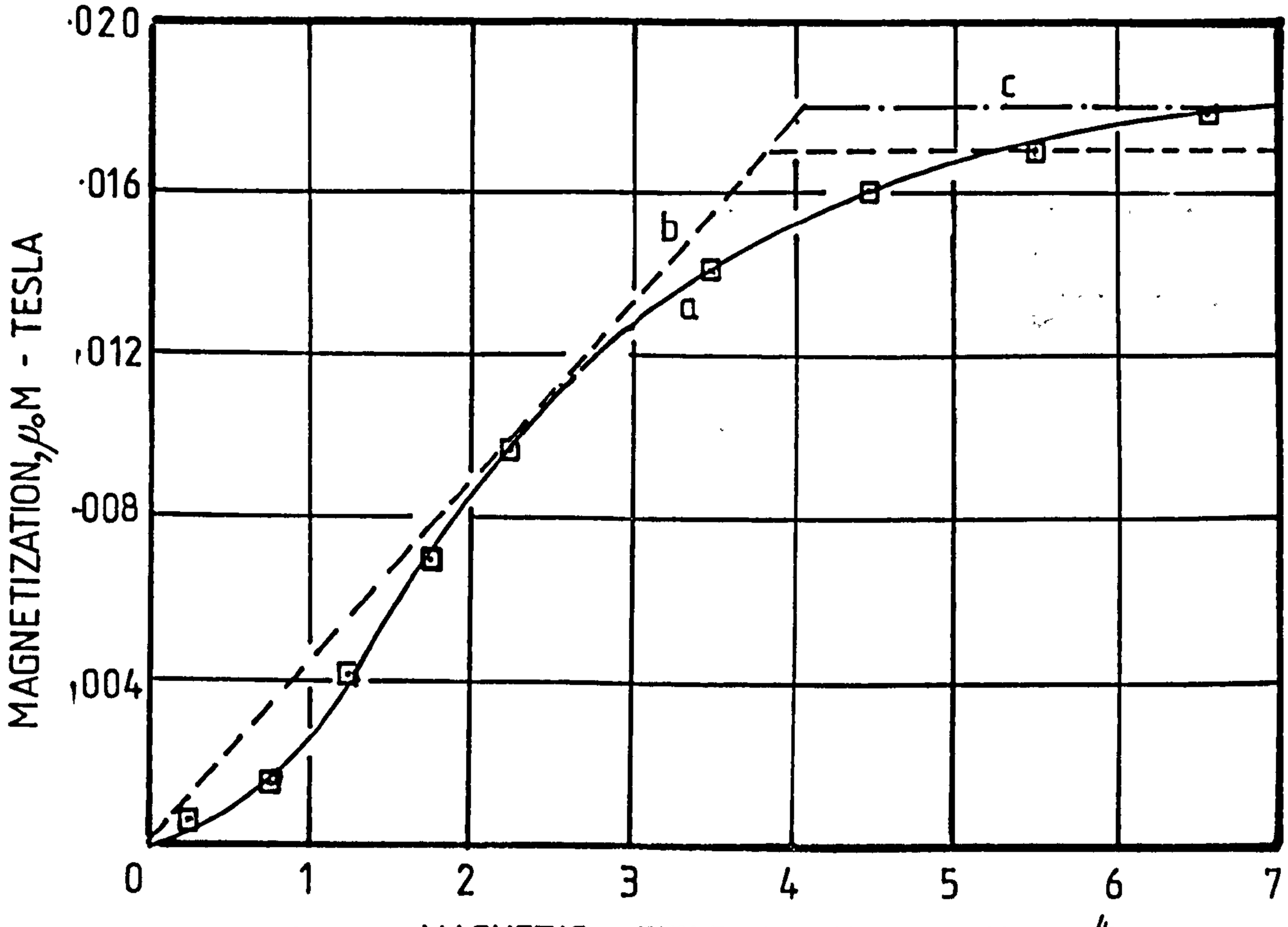

FIG. 1.12 MAGNETIZATION CURVES OF 5·35% MO-2035 IN PARAFFIN.

(a) FROM PERMEABILITY MEASUREMENTS

(b) FROM FORCE MEASUREMENTS ON THE 118mm DIAMETER TWO POLE STATOR

(c) FROM FORCE MEASUREMENTS ON THE 140mm DIAMETER TWO POLE STATOR

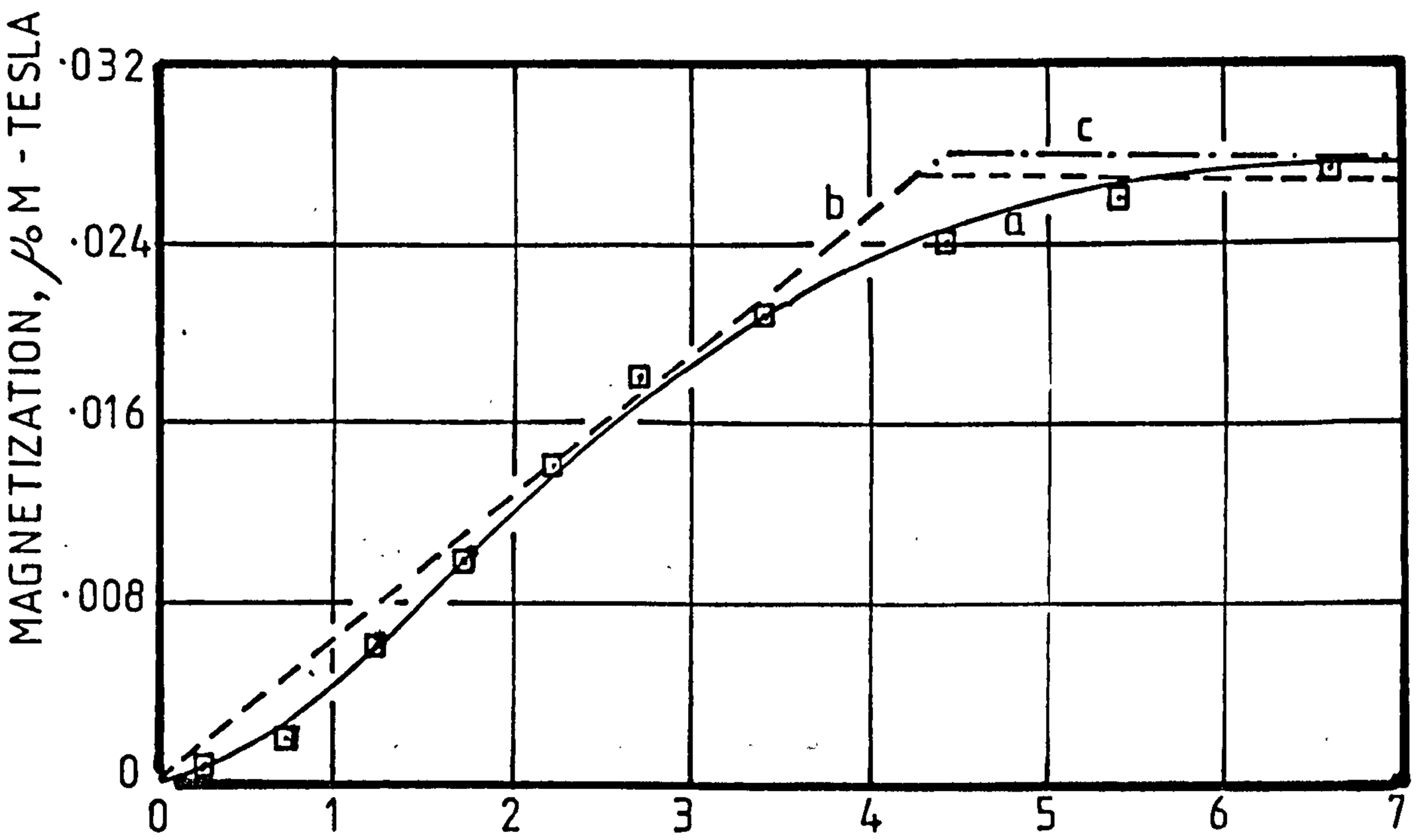

FIG.1.13 MAGNETIZATION CURVES OF 8·17 % MO-2035 IN PARAFFIN

(a) FROM PERMEABILITY MEASUREMENTS

(b) FROM FORCE MEASUREMENTS ON THE 118 mm DIAMETER TWO POLE STATOR

(c) FROM FORCE MEASUREMENTS ON THE 140 mm DIAMETER TWO POLE STATOR

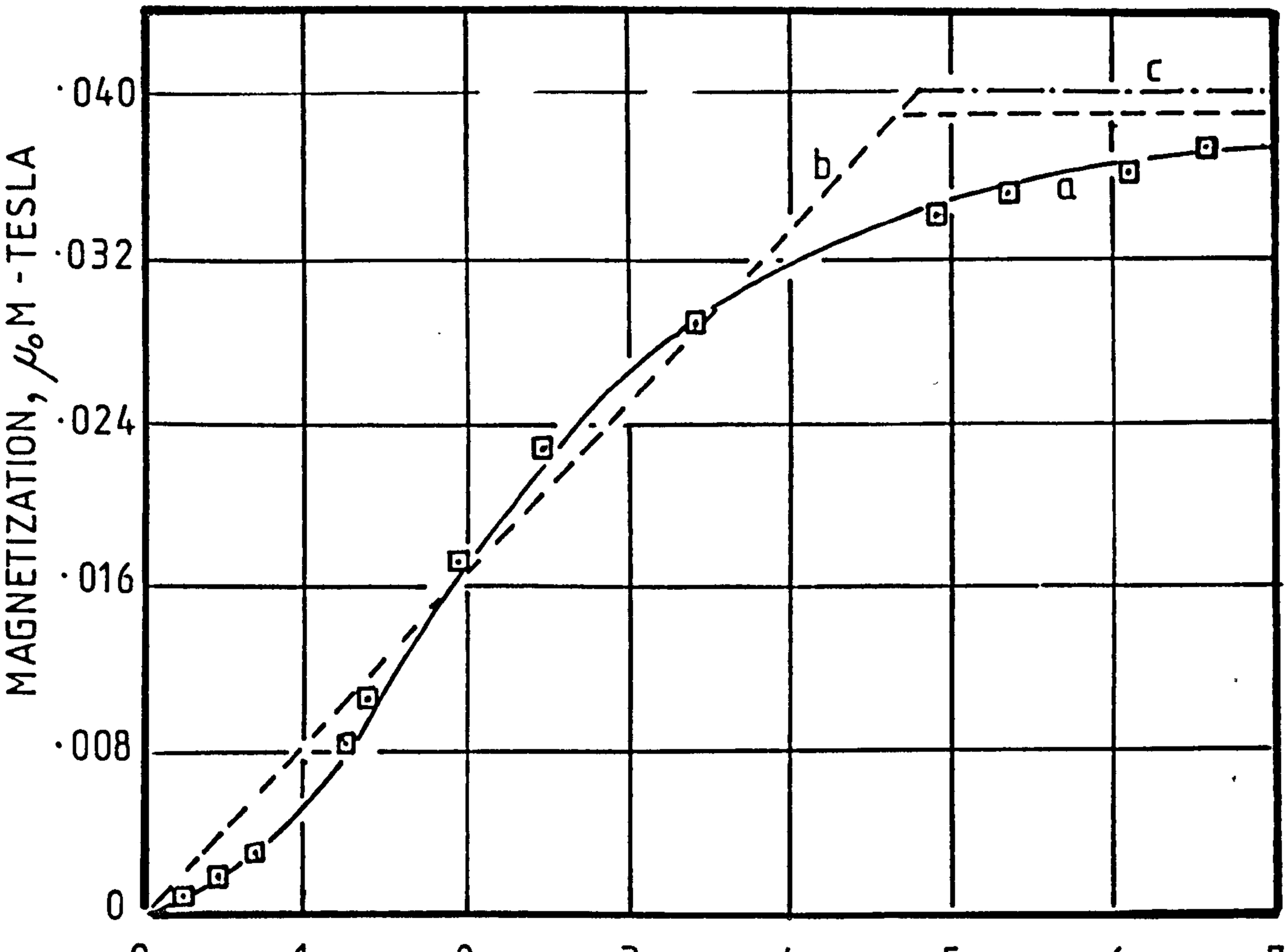

FIG. 1.14 MAGNETIZATION CURVES OF 11% MO-2035 IN PARAFFIN

(a) FROM PERMEABILITY MEASUREMENTS

(b) FROM FORCE MEASUREMENTS ON THE 118mm DIAMETER TWO POLE STATOR

(c) FROM FORCE MEASUREMENTS ON THE 140mm DIAMETER TWO POLE STATOR

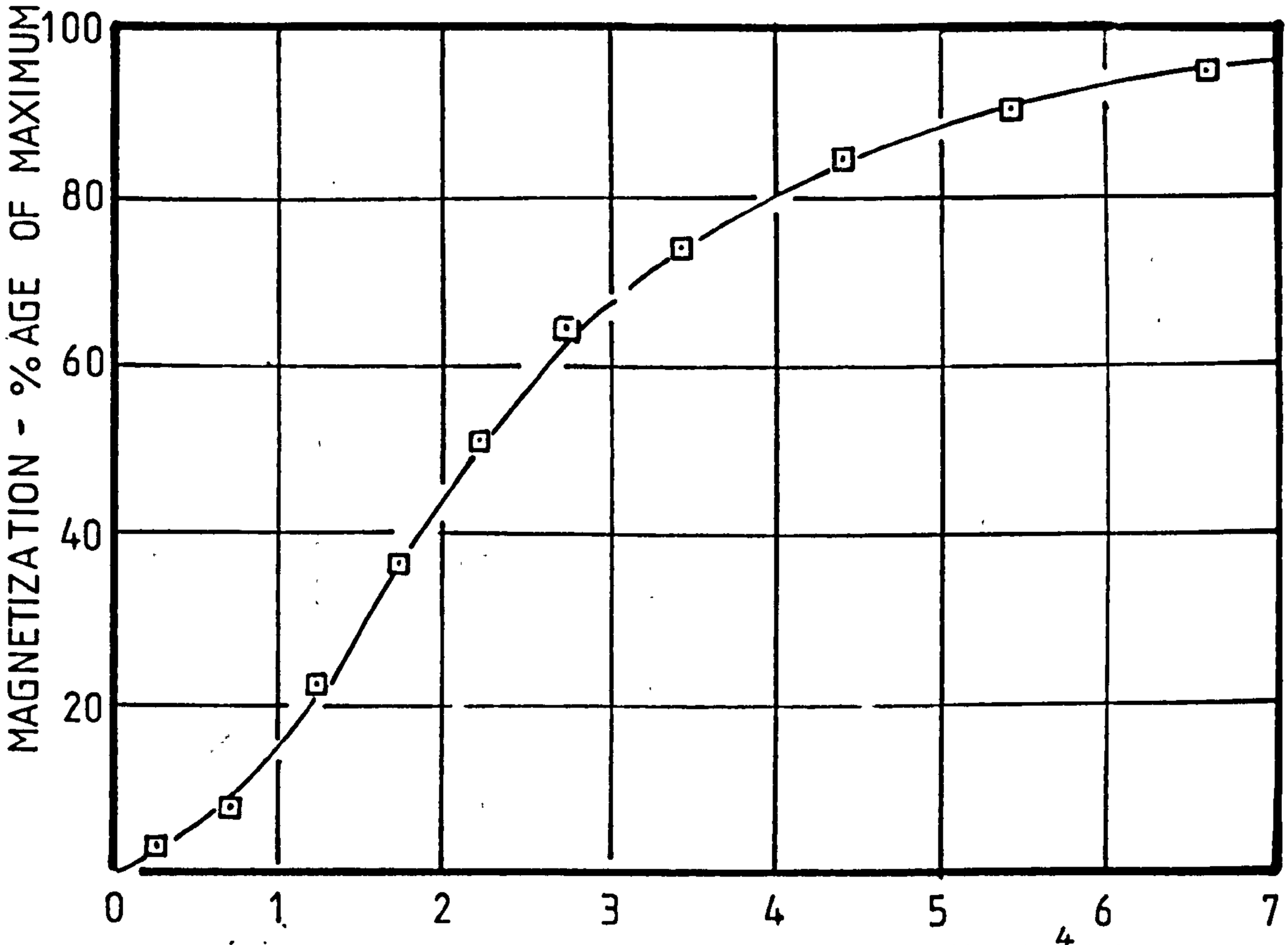

FIG. 1.15 MAGNETIZATION CURVE OF FLUID MADE FROM MO-2035 IN PARAFFIN–FROM PERMEABILITY MEASUREMENTS

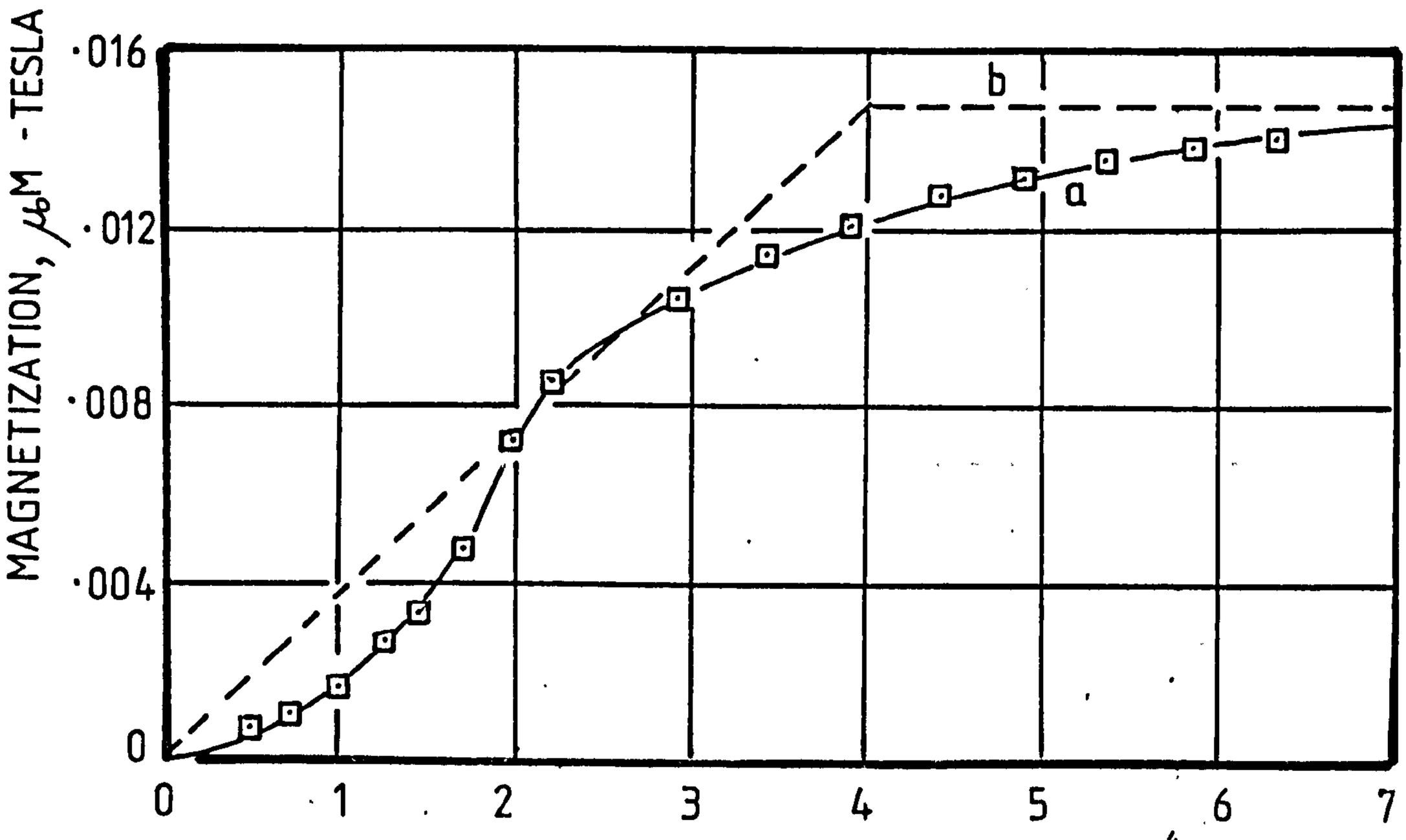

FIG. 1.16 MAGNETIZATION CURVES OF 4·4% MO-2035 IN WATER

(a) FROM PERMEABILITY MEASUREMENTS

(b) FROM FORCE MEASUREMENTS ON THE 118mm DIAMETER TWO POLE STATOR

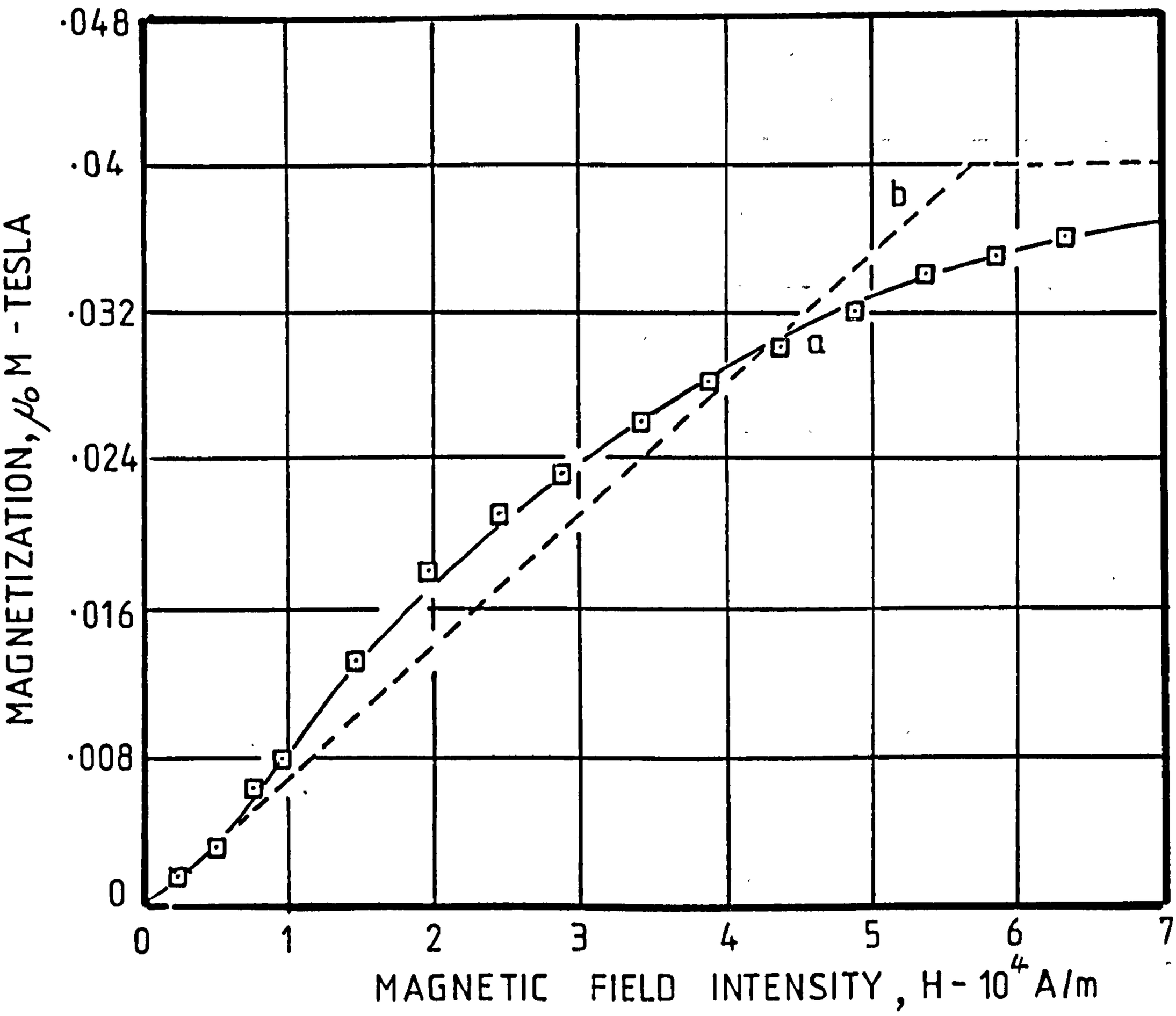

FIG. 1.17 MAGNETIZATION CURVES OF 6·4 % FERROSILICON IN WATER

(a) FROM PERMEABILITY MEASUREMENTS

(b) FROM FORCE MEASUREMENTS ON THE 118 mm DIAMETER TWO POLE STATOR

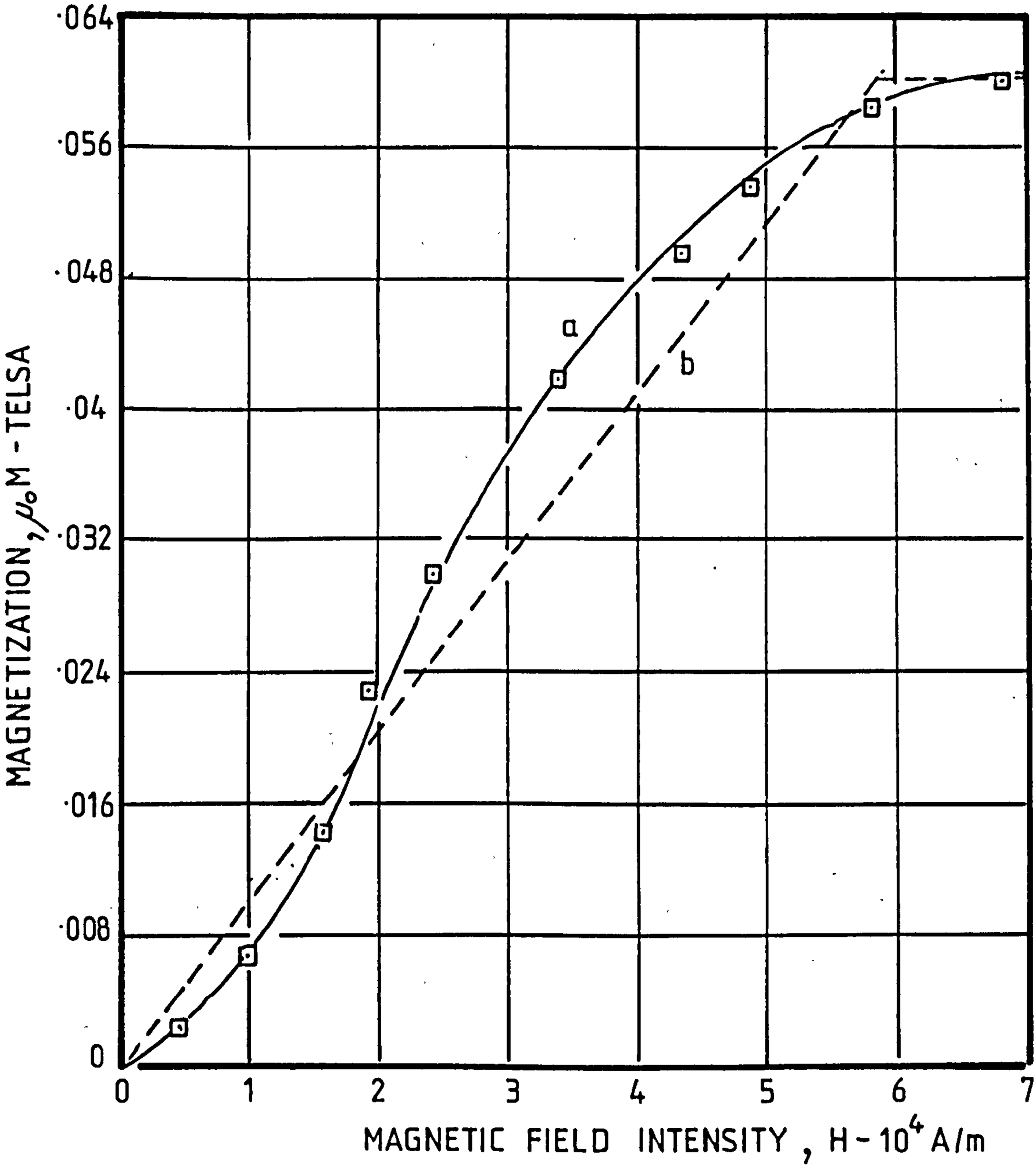

FIG.1.18 MAGNETIZATION CURVES OF 21 % MAGNETITE IN WATER

(a) FROM PERMEABILITY MEASUREMENTS

(b) FROM FORCE MEASUREMENTS ON THE 118mm DIAMETER TWO POLE STATOR

SECTION 2.

THE FERROFLUID MOTOR APPLICATION

2.1 Introduction.

Simple experiments were carried out using magnetic crack-detection fluid (suspension of finely-divided magnetic oxides in paraffin, with oleic acid as a surfactant to keep the particles apart from each other) in a beaker placed inside the bore of a conventional three phase stator. It was found that the fluids moved in the reverse direction at higher magnetic field, although at very low field intensities the rotation might be in the same direction as that of the field. The relative values of higher and lower field was dependent on the volume loading of magnetic material in fluids, size of the particles, and viscosity of parent fluid. Sometimes the fluid might oscillate and occasionally various eddies in the fluid were observed.

To add further to this confusion it was found that the torque exerted by the fluid on its containing vessel was not, as might have been expected, a simple drag torque in the direction of fluid motion, but it was actually in the opposite direction to that, i.e. always in the same direction as the rotating magnetic field. These observations were observed with both the two and four-pole stators.

2.2 Basic Principle.

2.2.1 Contrarotating vector approach.

Rotating magnetic fields can be represented locally by pairs of contra-rotating vectors[6].

For a cylindrical polyphase machine, neglecting harmonics and axial field variation, the field vectors are of magnitude $A\ r^{p-1}$ and $B\ r^{-(p+1)}$, A and B being constants and p the number of pairs of poles. They spin at angular velocities $+\ \omega_o$ and $-\ \omega_o$ respectively (not at wave velocity, ω_o/p). In the absence of any inner boundary the constant B must be zero.

For p > 1 the magnitude of the remaining vector, Ar^{p-1}, is greatest at the stator surface and thus there will be forces tending to draw particles radially outwards. In the 2-pole case, however, i.e. p = 1, the field is everywhere of constant magnitude and unless particles are very close to the stator surface, where "image" forces can become appreciable, there is no radial force. This could be confirmed by the behaviour of fine iron powder when placed in a beaker within the bore of an induction motor stator[6]. With the right balance between the peak magnitude of the rotating field and the amount of powder, a cloud of apparently violently agitated particles can be obtained. When illuminated with a stroboflash operating at near mains frequency, a slow rotating pattern corresponding to the expected field distribution can be distinguished (parallel lines in the case of a 2-pole stator). When the bore was subdivided into sectors the pattern still persists, indicating that the particles are simply spinning and not rotating about the stator axis. Field patterns can similarly be observed for p > 1 but due to the radial drift these quickly disappear.

The magnetic particles can presumably spin in media other than air provided that the viscosity is not too great for them to attain synchronization. There will be energy transfer by viscous torques from each particle to the fluid, the aggregate effect of individual transfers producing fluid rotation.

If the particles are brought into contact with the surface the magnetic vector, $A\ r^{p-1}$, launches "reverse" rolling action. This can be demonstrated by putting two drops of fluid at two adjacent points on the outside and the inside surface of a beaker and placing it inside an open a.c. stator. The effect of the rotating vector on the two points was to produce two streams of fluid running in opposite directions. The inside one was opposite to the wave direction. A diagram illustrating particles spinning in the middle of the fluid and folling at the beaker boundary is shown in Fig.2.1.

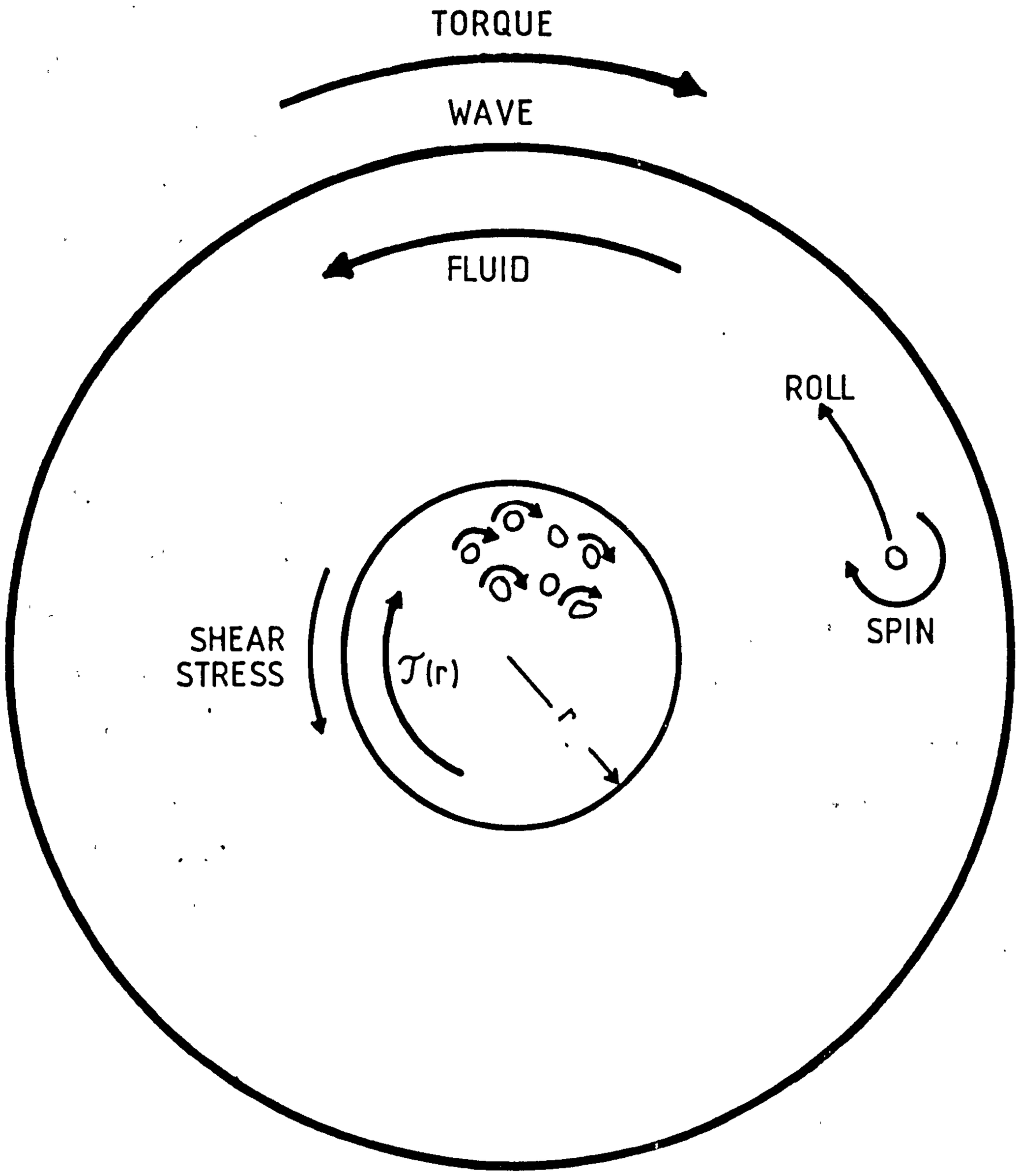

FIG. 2.1 ILLUSTRATIVE DIAGRAM FOR THE BEHAVIOUR OF PRIMITIVE FERROFLUIDS IN ROTATING FIELDS

2.2.2 Moskowitz and Rosensweig's approach[3].

Assuming a uniform field distribution, each single-domain particle behaves as a miniature synchronous motor with the load angle adjusting itself to equalize the generated and demanded torque.

The generated torque, T_p, which is exerted on each particle to align it with the field is given, in N.m, by:

$$T_p = \mu_o m H \sin \theta \quad \ldots\ldots \quad 2.2.1$$

where m is the dipole moment of a given suspended particle in A/m^2.

H is the applied magnetic field intensity in A/m and

θ is the angle between the dipole axis and the magnetic field, H.

If the magnetic field is rotating at angular velocity ω_o in a fluid, the torque T_p causes the particle to spin with the same angular velocity as the field, but the particle is subjected to a viscous drag rogque which causes the fluid to rotate.This viscous drag torque is the load torque or in other words, the demanded torque from each particle and if there is no interaction between the particles, it is given by[18]

$$T_p = 8 \pi \eta a^3 \omega_o \quad \ldots\ldots \quad 2.2.2$$

Where η, is the viscosity of the carrier fluid in $N.sec.m^{-2}$

a, is the radius of the particle, in metres, assumed spherical.

Assuming a uniform particle distribution and that all of them are spinning with the same angular velocity, ω_o, relative to the fluid, the summation of the individual particle torques per unit volume, T_v, should be constant throughout the fluid. The torque acting on the containing vessel is then given by the volume of the fluid multiplied by T_v. The latter is itself given by T_p multiplied by the number of particles, n_p, per unit volume participating in the process. If N is the actual number of particles per unit volume, $\mu_o M(H)$ is the magnetization of the ferrofluid with applied field H and $\mu_o M_{sat}$ is the saturation magnetization of ferrofluid,

then $\frac{n_p}{N} = \frac{M(H)}{M_{sat}}$

$$\therefore \quad T_v = 8 \pi \eta a^3 \omega_o N \frac{M(H)}{M_{sat}} \qquad \ldots\ldots \qquad 2.2.3$$

Now the volume loading of the ferrofluid can be expressed as

$$K_p = \frac{4}{3} \pi a^3 . N,$$

and its saturation magnetization by

$$M_{sat} = K_p M_i$$

where M_i is the intrinsic magnetization of the magnetic material.

Replacing ω_o by $2 \pi f_o$, where f_o is the rotation rate of the magnetic field in revolutions per second, equation 2.2.3 can be written as

$$T_v = 12 \pi \eta f_o . \frac{M(H)}{M_i}$$

It is desirable to operate on the linear portion of the magnetization curve where $M = \chi H$. This yields

$$T_v = 12 \pi \eta f_o \frac{\chi H}{M_i} \qquad \ldots\ldots \qquad 2.2.4$$

For a cylindrically symmetric flow, the shear stress, $\tau(r)$, on the inner and outer radii of an infinitesimal fluid annulus of thickness Δr must balance the torque per unit volume, T_v, in the annulus, thus

$$2 \pi r \Delta r T_v + \frac{\partial}{\partial r} \left[2 \pi r^2 \tau(r) \right] \Delta r = 0 \qquad \ldots\ldots \qquad 2.2.5$$

Integrating with respect to r

$$T_v + 2 \tau(r) = 0$$

Now $\tau(r) = \eta_s r \frac{\partial}{\partial r} \left(\frac{U_\theta}{r}\right)$ $\qquad \ldots\ldots \qquad 2.2.6$

Where U_θ is the tangential velocity and η_s is the viscosity of the colloidal suspension.

$$\therefore \quad \frac{\partial}{\partial r}\left(\frac{U_\theta}{r}\right) + \frac{T_v}{2\eta_s r} = 0 \qquad \ldots\ldots \qquad 2.2.7$$

Now the fluid velocity $\omega(r) = 0$ at $r = R_o$, the container surface, therefore

$$U_\theta\ (r) = \frac{T_v}{2\eta_s}\, r\, \ell n\, \frac{R_o}{r} \qquad \ldots\ldots \qquad 2.2.8$$

From equation 2.2.8 it was found that U_θ has a maximum, U_{max} at $r_m = R_o/e$, where e is the Naperian base, thus

$$U_{max} = \frac{R_o\ T_v}{2\ \eta_s\ e} \qquad \ldots\ldots \qquad 2.2.9$$

$$\text{Now } \omega_{max} = \frac{U_{max}}{r_m}$$

$$= 6\ \pi\ .\ \frac{\chi}{M_i}\ .\ \frac{\eta}{\eta_s}\ .\ f_o.H \qquad \ldots\ldots \qquad 2.2.10$$

$$\text{or} \quad \omega_{max} = 6\ \pi\ .\ F.\ f_o\ .\ H \qquad \ldots\ldots \qquad 2.2.11$$

$$\text{where } F = \frac{\chi}{M_i}\ \frac{\eta}{\eta_s} \qquad \ldots\ldots \qquad 2.2.12$$

Obtaining maximum rotation rate, means maximization of the figure of merit F.

Fig. 2.2, shows a plot of their results of maximum fluid rotation rate versus the magnitude of the applied magnetic field intensity, H, with field frequency as a parameter. The results are for a particular water base ferrofluid. The experimental data shows a linear increase of ω with the applied field in agreement with equation 2.2.10, but the nonlinear increase of ω with f_o has not been explained by the authors.

2.2.3 Comments on Moskowitz and Rosensweig's approach.

(a) The assumption that there is negligible interactions between the particles is only valid if $K_p << 1$.

(b) The approach assumed that the spinning velocity is ω_o, but it must be $\omega_o - p\omega(r)$ since the particles have to spin faster than ω_o, if the fluid is carrying them against the field, in order to attain synchronization and vice-versa.

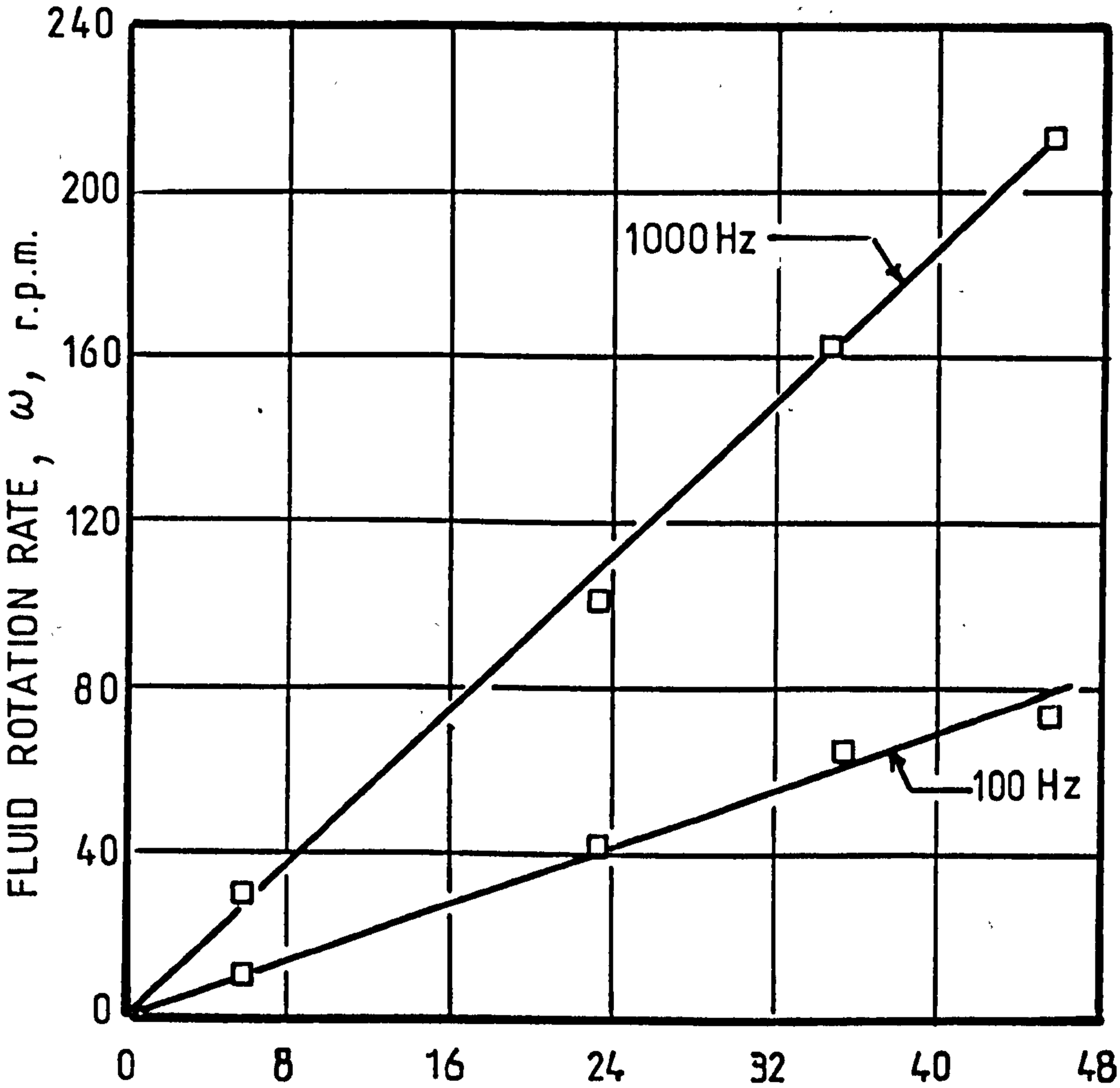

FIG. 2.2 A MACROSCOPIC FLUID ROTATION RATE AS A FUNCTION OF APPLIED MAGNETIC FIELD - RESULTS OF ROSENSWEIG AND MOSKOWITZ.

This assumption that the rate of spin is not affected by the fluid rotation implies that the particles are not transported by the fluid, in which case there must be a drag force due to the motion of the carrier fluid relative to a spinning particle.

(c) The approach ignores the constant of integration of equation 2.2.5.

(d) Equation 2.2.8 suggests that the fluid velocity is infinity at r = 0 which cannot be.

2.3 A Modification of Moskowitz and Rosensweig's Approach.

The basic assumptions are:

(i) Negligible particles interactions i.e. $K_p << 1$.

(ii) The field is uniform everywhere throughout the fluid i.e. end effects are ignored.

(iii) The particles distribution is uniform throughout the fluid.

(iv) At the boundary, some of the particles are rolling on the surface with a velocity which would be in the extreme case equal to $\frac{a}{R_o}\omega_o$, which is very small. As an approximation $\omega(r)$ will be taken equal to zero at $r=R_o$.

(v) The spinning particles are spinning with $\omega_s = \omega_o - p\omega$ ... 2.3.1

(vi) NO velocity gradient in the axial direction.

(vii) The fluid velocity is constant over an infinitesimal fluid annulus, such that expression 2.2.3 of the torque per unit volume could be used after replacing ω_o by ω_s, thus

Modified, $T_v = T_{v_m} = 8\ \pi\ \eta\ a^3\ \omega_o (1-p\ \frac{\omega}{\omega_o})\ N\ \frac{M(H)}{M_{sat}}$ 2.3.2

and since uniform field is assumed, p will be taken equal to 1 throughout the analysis.

$$\therefore\ T_{v_m} = T_v\ (1 - \frac{\omega}{\omega_o}) \qquad \text{.....} \qquad 2.3.3$$

Equation 2.2.5 still applies and by differentiating its second term, it becomes:

$$T_{v_m} + r\ \frac{\partial \tau(r)}{\partial r} + 2\ \tau(r) = 0. \qquad \text{.....} \qquad 2.3.4$$

Inserting the laminar relationship for shear, given by equation 2.2.6, into equation 2.3.4 yields

$$\frac{\partial^2(\omega/\omega_o)}{\partial r^2} + \frac{3}{r}\frac{\partial(\omega/\omega_o)}{\partial r} + \frac{T_v}{\eta_s \omega_o r^2}\left(1 - \frac{\omega}{\omega_o}\right) = 0 \quad \ldots\ldots \quad 2.3.5$$

The solution of this equation is

$$\frac{\omega}{\omega_o} = 1 + \left(\frac{r}{R_o}\right)^{-1}\left[A\left(\frac{r}{R_o}\right)^{K'} + B\left(\frac{r}{R_o}\right)^{-K'}\right] \quad \ldots\ldots \quad 2.3.6$$

where

$$K' = \sqrt{1 + \frac{T_v}{\eta_s \omega_o}} \quad \ldots\ldots \quad 2.3.7$$

i.e. $K' > 1$

and A and B are arbitrary constants.

If the boundary condition $\omega = 0$ at $r = R_o$ is to be satisfied then

$$A + B = -1 \quad \ldots\ldots \quad 2.3.8$$

Consider the gradient of ω with respect to r

$$\frac{\partial(\omega/\omega_o)}{\partial(r/R_o)} = (K'-1)\,A\left(\frac{r}{R_o}\right)^{K'-2} - (K'+1)\,B\left(\frac{r}{R_o}\right)^{-(K'+2)} \quad \ldots\ldots \quad 2.3.9$$

To get the correct sign of the torque exerted on the beaker the gradient must be negative at $r = R_o$. Because of condition 2.3.8 if A is positive, B is negative and the gradient will be positive at $r = R_o$ i.e. 'A' cannot be positive if the beaker torque is to be positive.

At very small values of $\frac{r}{R_o}$ the B term of equation 2.3.6 will be predominant and hence will dictate the sign of ω. Because of condition 2.3.8, if B is positive then ω will be positive for all $r < R_o$.

The range of B values not covered by the above is $-1 < B < 0$.

In this range $\frac{\omega}{\omega_o}$ will be negative at values of $\frac{r}{R_o} \ll 1$ but positive at some intermediate value.

In this range where both A and B are negative (and $|A| < 1$, $|B| < 1$), equation 2.3.9 can be written as:

$$\frac{\partial(\omega/\omega_o)}{\partial(r/R_o)} = \left(\frac{r}{R_o}\right)^{-2} \left[-(K'-1) \; |A| \; \left(\frac{r}{R_o}\right)^{K'} + (K'+1) \; |B| \; \left(\frac{r}{R_o}\right)^{-K'} \right]$$

Inevitably the gradient must be positive at small values of $\left(\frac{r}{R_o}\right)$, and it can only become negative if

$$(K' - 1) \; |A| > (K' + 1) \; |B|$$

or $$(K' - 1) \; |A| > (K' + 1) \; |1 + A|$$

i.e. if $$\frac{|A|}{|1 + A|} > \frac{K' + 1}{K' - 1} \qquad \ldots\ldots \qquad 2.3.10$$

If this approach is to completely satisfy the signs of (ω/ω_o) and of torque observed in some of our experiments, we are interested in condition 2.3.10. Fig.2.3.a. shows a possible velocity profile.

There are then the following points to consider:

(1) What factors govern the direction of rotation of the fluid, i.e. the values of A and B? Is it a case of maximum kinetic energy, and does this include thermal energy?

(2) Since it is not practical that the fluid velocity approaches infinity as $r \to 0$, what governs the inner boundary condition? Is it a case of the demanded torque being greater than the magnetic torque, i.e. in the case of negative fluid velocity, or that there is no particle spin relative to the fluid, i.e. in the case of positive fluid velocity?

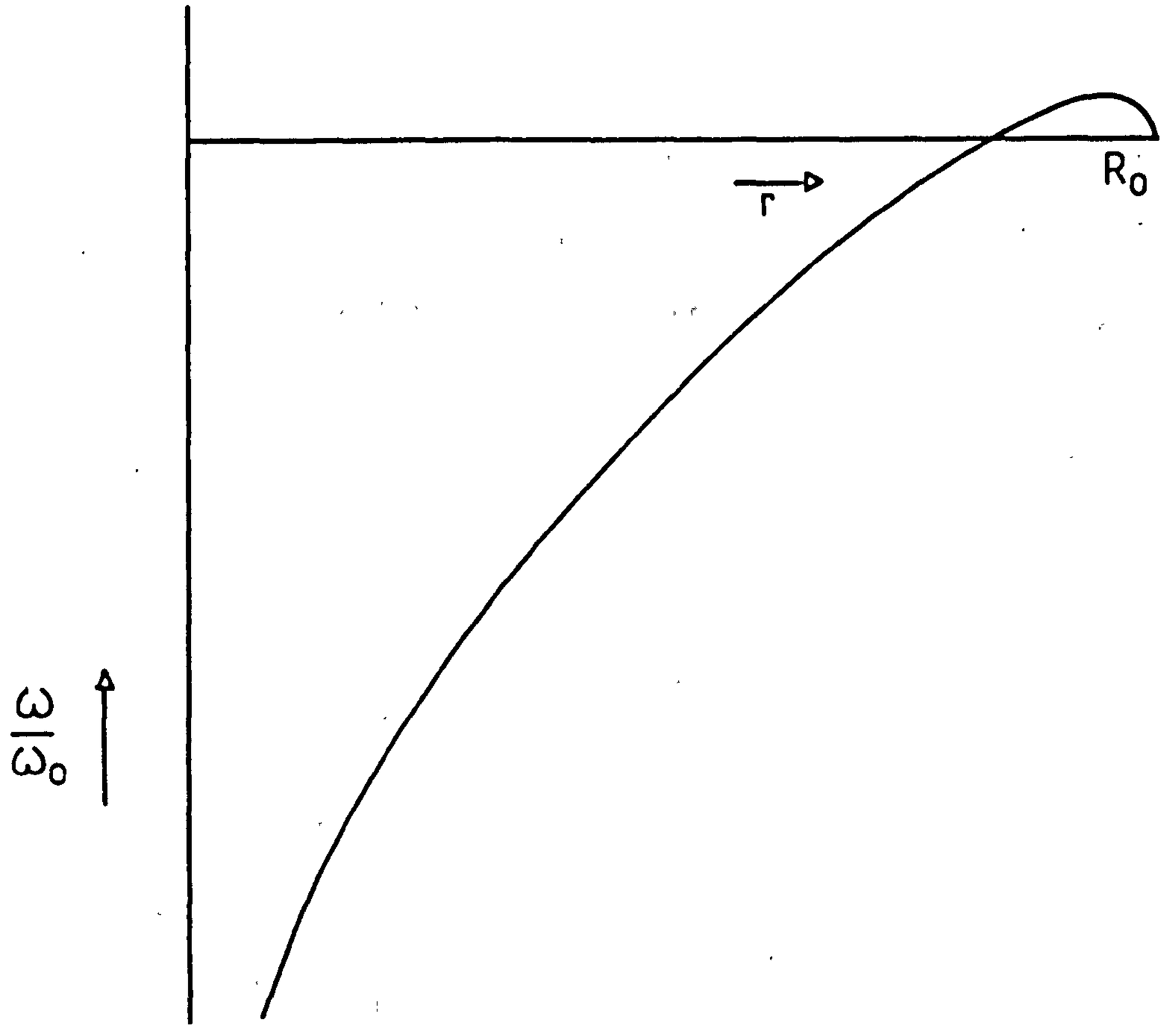

(a) ALL PARTICLES ARE SPINNING

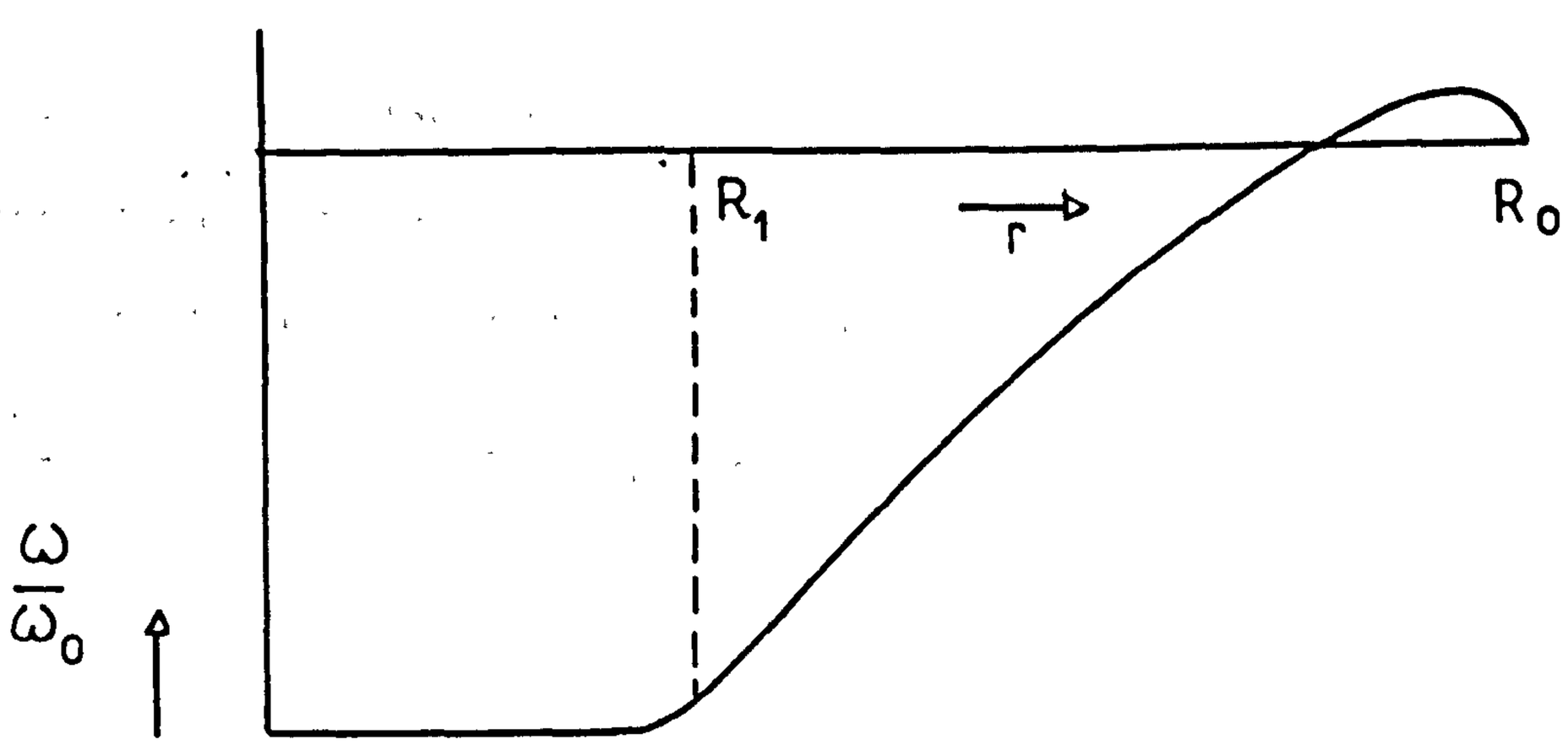

(b) NO SPINNING IN THE REGION $0 < r < R_1$

FIG. 2.3 VELOCITY PROFILE - MODIFIED MOSKOWITZ AND ROSENSWEIG'S APPROACH

(3) If this approach is to satisfy the magnitude of the total torque exerted on the beaker there must be another condition that the sum of all the particle torques must be related to the velocity gradient at $r = R_o$. This may supply the answer to points (1) and (2).

Taking point (3) first the equation for torque in terms of shear stress at the outer surface is:

$$T = -\eta_s \omega_o R_o \left[\frac{\partial(\omega/\omega_o)}{\partial r}\right]_{r=R_o} \cdot 2\pi R_o^2 L_f$$

where L_f is the height of the fluid.

$$\therefore \quad T = -2 \eta_s \omega_o \left[\frac{\partial(\omega/\omega_o)}{\partial(r/R_o)}\right]_{r=R_o} \cdot V_f$$

$$= -2 \eta_s \omega_o \left[(K' - 1) A - (K' + 1) B\right] \cdot V_f \quad \ldots\ldots \quad 2.3.11$$

where V_f is the volume of the fluid.

In terms of summing the particle torques, the torque generated in a cylindrical elemental of thickness δr, is given by:

$$\delta T = \eta_s \omega_o \left(1 - \frac{\omega}{\omega_o}\right) \cdot 2\pi r \cdot \delta r \cdot L_f \cdot K$$

$$= \eta_s \omega_o \left(1 - \frac{\omega}{\omega_o}\right) \cdot 2\pi r \cdot \delta r \cdot L_f (K'^2 - 1)$$

Substituting for $\frac{\omega}{\omega_o}$ from equation 2.3.6 and integrating, the integral will be infinite unless the limits are R_1 to R_o, where $R_1 > 0$.

Assuming that for $r < R_1$ the particles generate no torque because the demanded torque is greater than the particles can produce (and that they cannot generate any hysteresis torque) or because the fluid is rotating at synchronous speed ω_o/p, the total torque is given by:

$$T = -2\eta_s \omega_o \pi L_f R_o^2 (K'^2-1) \int_{R_1}^{R_o} \left[A \left(\frac{r}{R_o}\right)^{K'} + B \left(\frac{r}{R_o}\right)^{-K'} \right] d\left(\frac{r}{R_o}\right)$$

$$\text{or } T = -2\eta_s \omega_o \left[(K'-1)A-(K'+1)B-(K'-1)A\left(\frac{R_1}{R_o}\right)^{(K'+1)} + (K'+1)B\left(\frac{R_1}{R_o}\right)^{-(K'-1)} \right] . V_f \quad \ldots\ldots \quad 2.3.12$$

The velocity profile in this case is sketched in Fig.2.3.b.

From equations 2.3.11 and 2.3.12 we get

$$B = \frac{(K'-1)}{(K'+1)} A \left(\frac{R_1}{R_o}\right)^{2K'} \quad \ldots\ldots \quad 2.3.13$$

If now we try to supply the condition that $\omega = \omega_o$ at $r = R_1$, then from 2.3.6 this requires that

$$B = -A \left(\frac{R_1}{R_o}\right)^{2K'} \quad \ldots\ldots \quad 2.3.14$$

Obviously conditions 2.3.13 and 2.3.14 cannot be satisfied simultaneously, and so it must be concluded that $\omega \neq \omega_o$ at $r = R_1$, i.e. equation 2.3.14 is wrong.

Considering the alternative condition that at $r = R_1$ the viscous drag torque on each particle is equal to the maximum magnetic torque generated, T_{max}, we have:

$$T_{max} = -8\pi\eta a^3 \omega_o \left[A\left(\frac{R_1}{R_o}\right)^{K'-1} + B\left(\frac{R_1}{R_o}\right)^{-(K'+1)} \right] \ldots\ldots \quad 2.3.15$$

2.3.13 and 2.3.15 are not mutually exclusive and we are left with a third condition required if we are to solve for the three unknowns A, B and R_1. We have not yet made use of the possible boundary condition that at $r = R_o$, $\omega = 0$, which gave the relationship 2.3.8, i.e. $A + B = -1$.

From equations 2.3.8 and 2.3.13 we find that

$$A = \frac{-1}{\left[1 + \frac{(K'-1)}{(K'+1)}\left(\frac{R_1}{R_o}\right)^{2K'}\right]}$$

and

$$B = \frac{-1}{\left[1 + \frac{(K'+1)}{(K'-1)}\left(\frac{R_1}{R_o}\right)^{-2K'}\right]} \qquad \text{..... 2.3.16}$$

An important point to note is that from 2.3.16, A and B are of the same sign, in fact negative, and both are in the range

$$-1 < \frac{A}{B} \text{ (or) } < 0$$

Thus we appear to have satisfied part of the condition for ω to be negative at small values of (r/R_o) and the torque still positive.

The value of R_1 can presumably be obtained by substituting from 2.3.16 into 2.3.15, which leads to

$$\therefore \quad T_{max} = 8 \pi \eta a^3 \omega_o \frac{2K' \left(\frac{R_1}{R_o}\right)^{K'}}{(K'-1)\left(\frac{R_1}{R_o}\right)^{K'} + (K'+1)\left(\frac{R_1}{R_o}\right)^{-K'}} \qquad \text{..... 2.3.17}$$

This equation will govern the value of $\left(\frac{R_1}{R_o}\right)$.

As a further check that the velocity gradient may be negative as $r \to R_o$, from 2.3.16

$$\frac{|A|}{|1 + A|} = \frac{|A|}{|B|} = \frac{(K'+1)}{(K'-1)}\left(\frac{R_1}{R_o}\right)^{-2K'}$$

which is greater than $\frac{(K'+1)}{(K'-1)}$ viz 2.3.10

From equation 2.3.9 the velocity gradient is zero if

$$|B| = \frac{(K'-1)}{(K'+1)} |A| \left(\frac{r}{R_o}\right)^{2K'}$$

which is the same condition as 2.3.13 for $r = R_1$. This means that there must be zero torque transferred across the surface $r = R_1$, and hence justifies the neglect of the torque between $r = 0$ and $r = R_1$.

There is a possibility that there is a radius $R_2 < R_1$, in the region of negative velocity, at which the demanded torque on each particle is equal to T_{max} and that the torque contribution from the region $R_2 < r < R_1$ is zero. By applying this possibility it was found that $R_2 = R_1$ and so it does not provide a new useful condition.

Another possibility seems to be that there might be two distinct curves each one having different values of the constants A and B from the other and the two curves intercept at $r = R_1$. However, by applying the conditions that at $r = R_1$ not only must the values of ω be the same, but also the values of $\frac{\partial \omega}{\partial r}$, it was found that the constants A and B must be the same for both curves and so we finish up with only one continuous curve.

Summing up for this modified approach it is not possible to satisfy positive torque and negative fluid velocity, at least not with the boundary condition that $\omega = 0$ at $r = R_o$. Rolling of the particles around the surface could strictly lead to a non-zero surface velocity, but the actual magnitude resulting from the very small particles used must be so small as still to be negligible.

2.4 Vorticity Approach.

Vorticity Ω is defined as[19]

$$\Omega = \nabla \times U_\theta = 2\,\omega_i \qquad \text{.....} \qquad 2.4.1$$

where ω_i is the angular velocity of an infinitesimal fluid element and U_θ is the linear velocity.

Also the circulation Γ is defined as

$$\Gamma = \oint_C U_\theta \cdot d\ell = \int_A \Omega \cdot dA \qquad \text{.....} \qquad 2.4.2$$

Applying 2.4.2 and choosing a cylindrical path, radius r, such that the fluid velocity is constant

$$U_\theta \cdot 2\pi r = \int_A \Omega \cdot dA \qquad \ldots\ldots \qquad 2.4.3$$

By the analogy with $\oint H.d = \int J\, dA$, if the current flows in isolated filaments, then $\int J.dA = \int J \times$ area of one filament X area packing factor X dA $\equiv \int_A$ current of filament X K_A . dA, equation 2.4.3 could be written as

$$U_\theta \cdot 2\pi r = \int_A \Omega \cdot dA \equiv \int_A 2\omega_i \cdot K_A \cdot dA \qquad \ldots\ldots \qquad 2.4.4$$

where K_A is an area packing factor in number of vortices per unit sectional area.

$\omega_s = \omega_o - \omega$, if we take the case of p = 1. $\qquad \ldots\ldots \qquad 2.4.5$

where $\omega_o = 2\pi$ X supply frequency and $\omega_s = \omega_i$ is the spinning velocity of a particle.

$$\therefore \int_A 2\omega_i . K_A . dA$$

$$= 2K_A \int_o^r (\omega_o - \omega) \cdot 2\pi r\, dr \qquad \ldots\ldots \qquad 2.4.6$$

From equations 2.4.4 and 2.4.6

$$\frac{\partial}{\partial r}(\omega . 2\pi r^2) = 4\pi K_A (\omega_o - \omega) \cdot r$$

or $$2\pi r^2 \frac{\partial \omega}{\partial r} + 4\pi r \omega = 4\pi K_A (\omega_o - \omega) \cdot r$$

$$\therefore r\frac{\partial \omega}{\partial r} + 2(1 + K_A)\omega = 2K_A \omega_o$$

$$\therefore \frac{\omega}{\omega_o} = \frac{K_A}{(1 + K_A)} + A.r^{-2(1+K_A)}$$

If $\omega = 0$ at $r = R_o$, then

$$A = -\frac{K_A}{(1 + K_A)} R_o^{2(1+K_A)}$$

$$\therefore \quad \frac{\omega}{\omega_o} = \frac{K_A}{(1 + K_A)} \left[1 - \left(\frac{R_o}{r}\right)^{2(1+K_A)}\right] \quad \ldots\ldots \qquad 2.4.7$$

Thus ω will be negative for $r < R_o$.

The velocity profile is sketched in Fig.2.4.a. The laminar relationship for the shear stress $\tau(r)$ is that

$$\tau(r) = - \eta_s \, r \frac{\partial (U_\theta / r)}{\partial r} = - \eta_s \, r \frac{\partial \omega}{\partial r}$$

But

$$r \frac{\partial (\omega/\omega_o)}{\partial r} = 2 K_A \left(\frac{R_o}{r}\right)^{2(1+K_A)}$$

$$\therefore \tau(r) = - 2 \omega_o \eta_s K_A \left(\frac{R_o}{r}\right)^{2(1+K_A)}$$

and at $r = R_o$

$$\tau(R_o) = - 2 \eta_s K_A \omega_o$$

The torque on the containing vessel, per unit axial length, is given by

$$T = - 4 \pi \eta_s K_A \cdot R_o^2 \cdot \omega_o$$

This obviously does not fit in with the experimental, and theoretical, fact that the torque is in the direction of magnetic wave motion.

On the other hand the torque approach used by Moskowitz and Rosensweig leads to positive torque but also positive fluid motion.

Thus neither the vorticity approach nor the torque approach completely satisfy the constants. The most likely reason for this is that the boundary conditions are not being correctly applied, i.e. the equations are probably satisfactory throughout the bulk of the fluid, but do not satisfy the boundary conditions at $r = 0$ and $r = R_o$ because of the discontinuous nature of the fluid.

One way of substantially avoiding the boundary problem is to use the vorticity approach to find the fluid velocity and then use this expression for

the velocity to find the total torque in terms of the summation of the individual particle torques. Admittedly to find the fluid velocity one needs to apply one boundary condition. If we assume that the velocity is zero at $r = R_o$, we are likely to be in error in that it may actually be zero at $r = R_o - 2a$, (a = particle radius), but the error due to this will be negligible.

Thus we have

$$\frac{\omega}{\omega_o} = \frac{K_A}{1 + K_A} \left[1 - \left(\frac{R_o}{r}\right)^{2(1+K_A)} \right] \quad \ldots\ldots \quad 2.4.7$$

But now the torque per unit axial length is given by: $\int_o^{R_o}$ N X viscous drag torque on a particle X element of volume

$$= \int_o^{R_o} N \cdot 8 \pi \eta a^3 \omega_o \left(1 - \frac{\omega}{\omega_o}\right) 2 \pi r \cdot dr$$

$$= 16 \pi^2 N \eta a^3 \omega_o \left\{ \frac{r^2 - R_o^2 \cdot \left(\frac{R_o}{r}\right)^{2K_A}}{2 (1 + K_A)} \right\}_o^{R_o} \quad \ldots\ldots \quad 2.4.8$$

This approaches infinity (positive), so something must be corrected. Obviously the infinite term arises because from 2.4.7 the spin velocity must approach infinity as $r \to 0$, and thus the particles near the centre are assumed to generate very large values of torque. One possibility is again to limit the torque integration to some inner radius R_1 at which the drag torque exerted on the spinning particle is the maximum torque the particle can generate in the magnetic field, T_{max}.

This should not affect the velocity equation except for $r < R_1$. The velocity profile in this case is sketched in Fig.2.4.b.

Then the torque on the containing vessel is

$$T = \frac{16 \pi^2 N \eta a^3 \omega_o R_o^2}{2 (1 + K_A)} \left\{ \left(\frac{R_o}{R_1}\right)^{2K_A} - \left(\frac{R_1}{R_o}\right)^2 \right\} \quad \ldots\ldots \quad 2.4.9$$

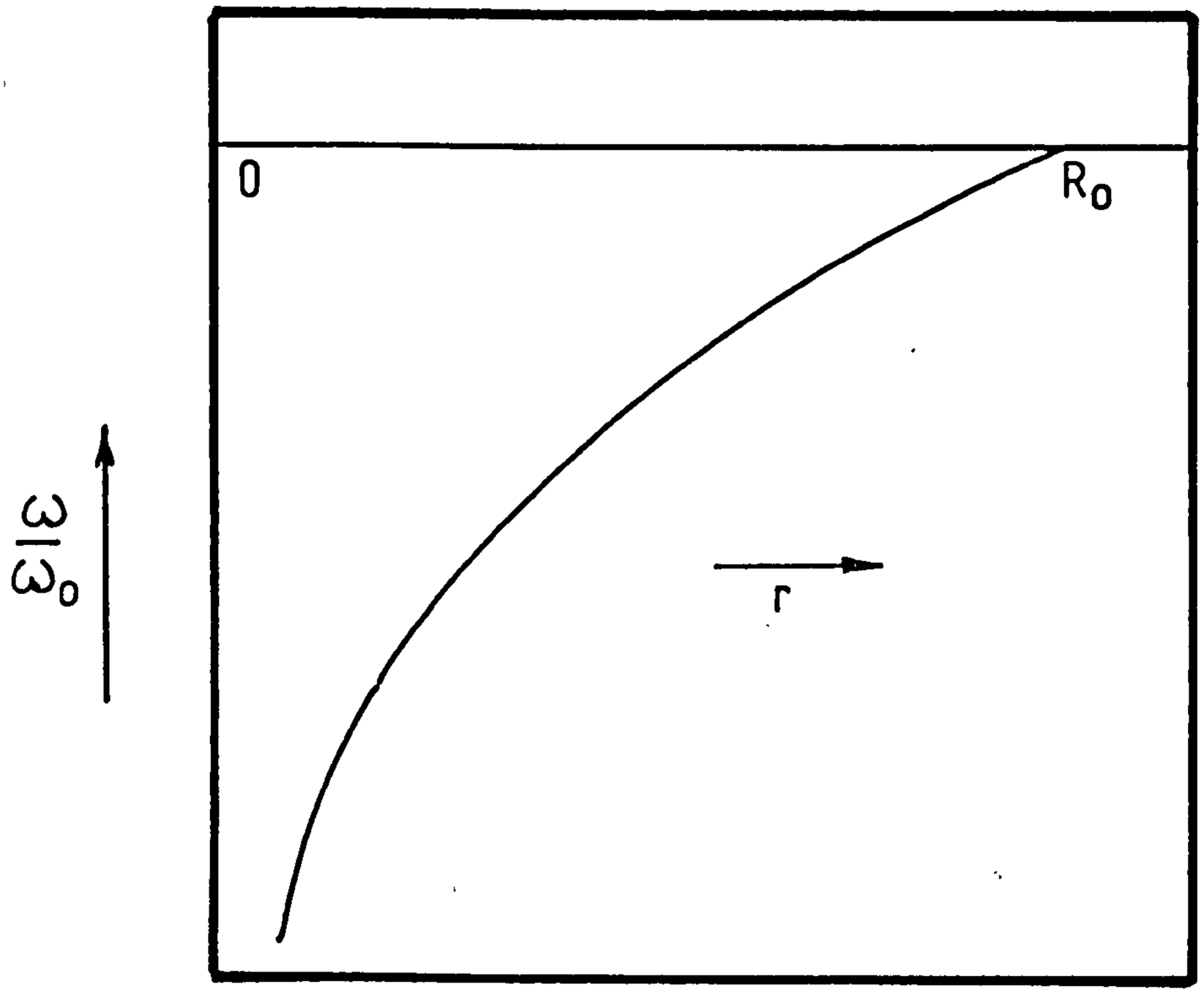

(a) ALL PARTICLES ARE SPINNING

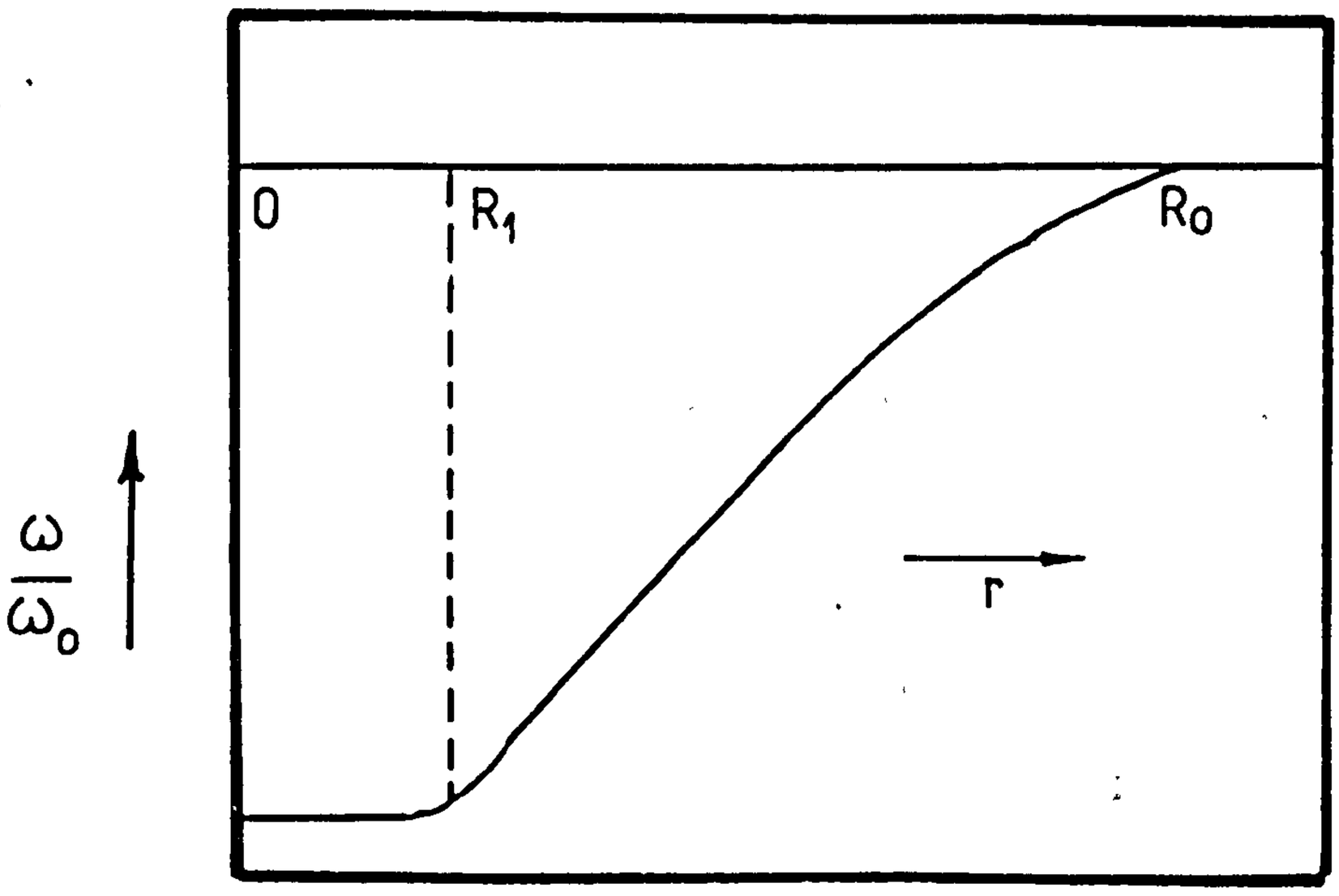

(b) NO SPINNING IN THE REGION $0 < r < R_1$

FIG. 2.4 VELOCITY PROFILE - VORTICITY APPROACH

where $T_{max} = 8 \pi \eta a^3 \omega_o \left[1 - \frac{\omega(R_1)}{\omega_o}\right]$

or $T_{max} = 8 \pi \eta a^3 \omega_o \left\{1 - \frac{K_A}{1 + K_A}\left[1 - \left(\frac{R_o}{R_1}\right)^{2(1+K_A)}\right]\right\}$ 2.4.10

or $\left(\frac{R_o}{R_1}\right)^{2(1+K_A)} = \frac{1}{K_A}\left[\frac{T_{max}(1 + K_A)}{8 \pi \eta a^3 \omega_o} - 1\right]$

$$\therefore \quad T = \frac{16 \pi^2 N \eta a^3 \omega_o R_o^2}{2 (1 + K_A)} \left\{ \begin{array}{l} \left\{\frac{1}{K_A}\left[\frac{T_{max}(1+K_A)}{8 \pi \eta a^3 \omega_o} - 1\right]\right\}^{\frac{K_A}{(1+K_A)}} \\ - \left\{\frac{1}{K_A}\left[\frac{T_{max}(1+K_A)}{8 \pi \eta a^3 \omega_o} - 1\right]\right\}^{\frac{-1}{(1+K_A)}} \end{array} \right\}$$

..... 2.4.11

Alternatively we can write

$$\frac{T}{2 \pi N T_{max} R_o^2} = \frac{1}{(T_{max}/8\pi\eta a^3 \omega_o)} \cdot \left(\frac{R_1}{R_o}\right)^2 \cdot \frac{1}{2K_A}\left[\frac{T_{max}}{8\pi\eta a^3 \omega_o} - 1\right] \quad ..... \quad 2.4.12$$

where, $\frac{R_1}{R_o} = \left[\frac{(1+K_A)}{K_A}\left(\frac{T_{max}}{8\pi\eta a^3 \omega_o} - 1\right) + 1\right]^{\frac{-1}{2(1+K_A)}}$ 2.4.13

If the particles can generate a continuous torque only at synchronous speed, there will be no torque contribution from those particles inside the surface R_1 and the total torque will be as given by 2.4.12. On the other hand if the particles can also produce hysteresis component of torque, those inside the surface R_1 can generate torque corresponding to T_{max} per particle, which is purely of hysteresis origin. The torque contribution per unit axial length from the particles inside the surface R_1, T_h, is given by

$$T_h = \pi R_1^2 \cdot N T_{max} \quad ..... \quad 2.4.14$$

In that case the total torque acting on the containing vessel, T, will be given by equation 2.4.12 plus equation 2.4.14. Plots of $\frac{T}{2\pi N\, T_{max}\, R_o^2}$ against $T_{max}/8\pi\eta a^3\omega_o$ for the cases of pure saliency and pure hysteresis, are shown in Figs. 2.5 and 2.6 respectively.

It is of interest to predict the value of K_A. Let us assume that the particles have been rearranged in a uniform array with b the distance between two particles as shown in Fig.2.7,

$$\therefore \quad b^3 N = 1 \qquad \text{or} \qquad b = N^{-\frac{1}{3}} \quad \ldots\ldots \quad 2.4.15$$

$$\text{and} \qquad K_p = \frac{\frac{4}{3}\pi a^3}{b^3} \quad \ldots\ldots \quad 2.4.16$$

If we cut through parallel planes to one side of the array by a plane of dimensions bXb and if the cutting region is from -b/2 to b/2 we will find that no particles exist in the region $0 \rightarrow (b/2 - a)$ and then one particle exists in the region $(b/2 - a)$ to $(b/2 + a)$ and no particle exists in the region $(b/2 + a)$ to b. The distribution of the existing particles over that region is shown in Fig.2.8. The average number of particles in an area of b^2 is 2a/b or the number of particles per unit area is $\frac{2a}{b^3}$

$$\therefore \quad K_A = 2a/b^3$$

$$\text{but} \qquad b^3 = \frac{4/3\ \pi\ a^3}{K_p}$$

$$\therefore \quad K_A = \frac{3}{2}\,\frac{K_p}{\pi\ a^2} \equiv 2aN \quad \ldots\ldots \quad 2.4.17$$

2.5 The Main Test Apparatus.

The motor consists of a rotor (perspex container filled with the fluid under investigation), placed vertically inside the bore of a conventional three phase cylindrical stator for the production of a rotating magnetic field. Two stators were used; one a 2-pole and the other 4-pole.

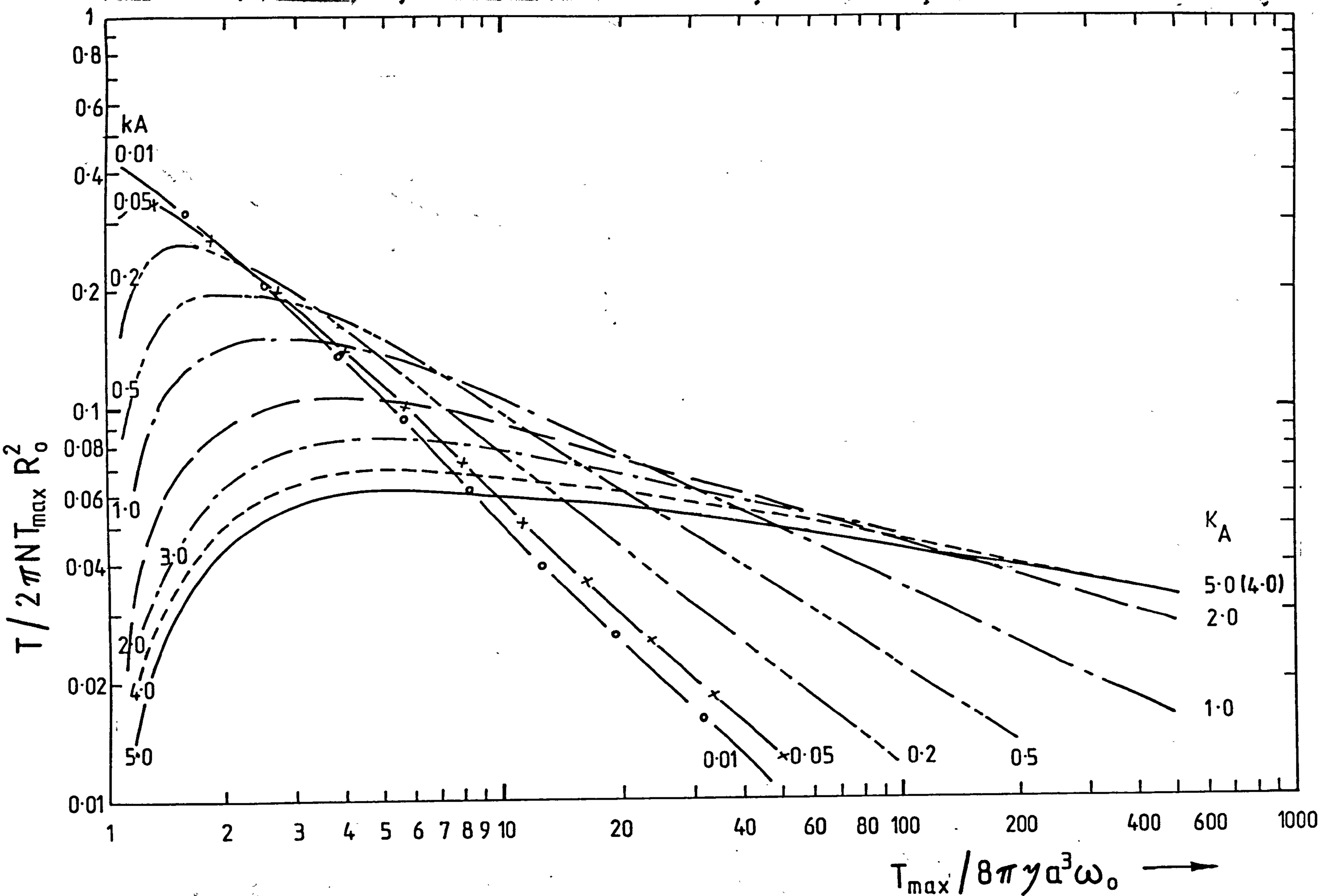

FIG. 2.5. TORQUE BY SALIENCY ONLY

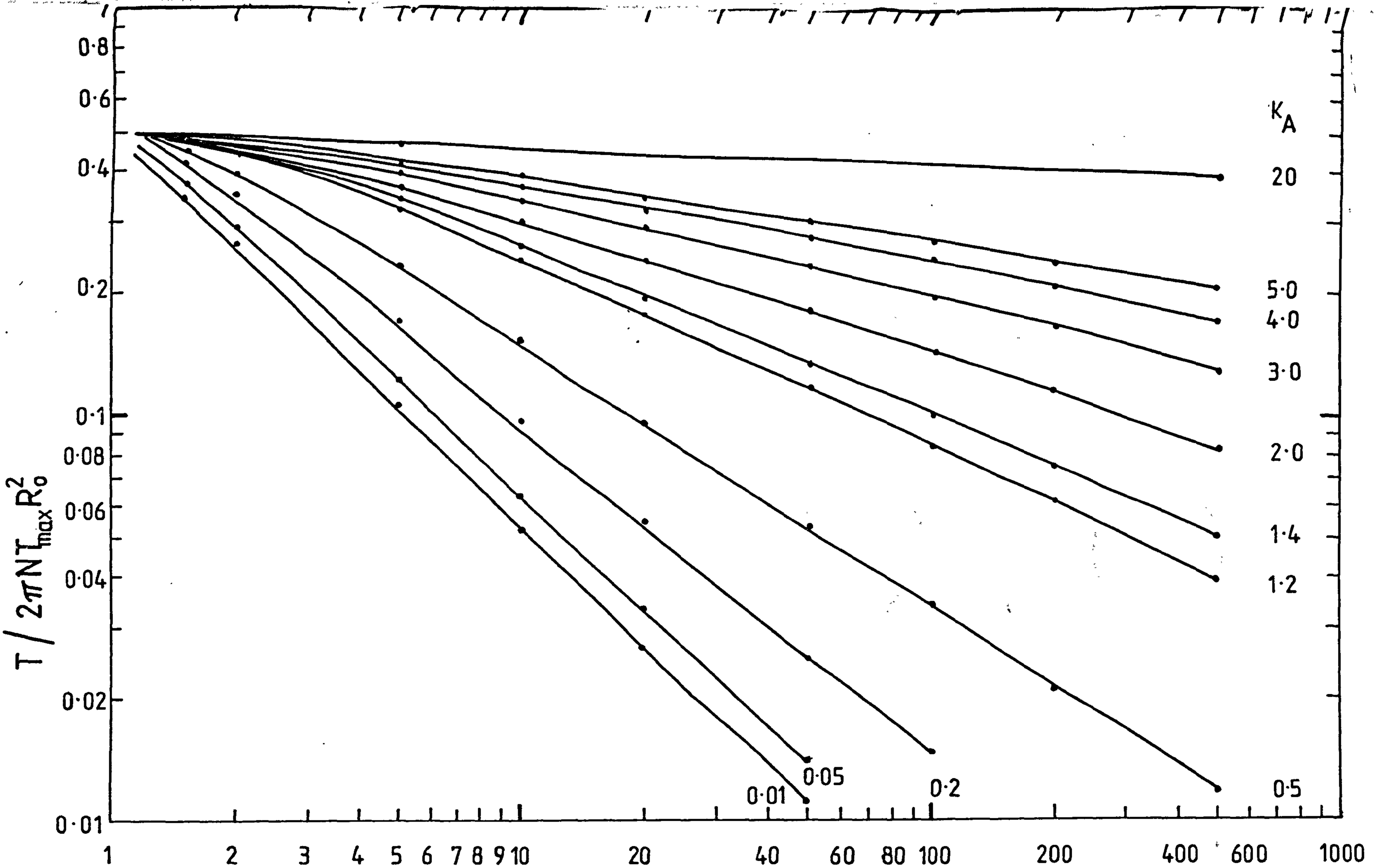

FIG. 2.6. TORQUE BY HYSTERESIS ONLY

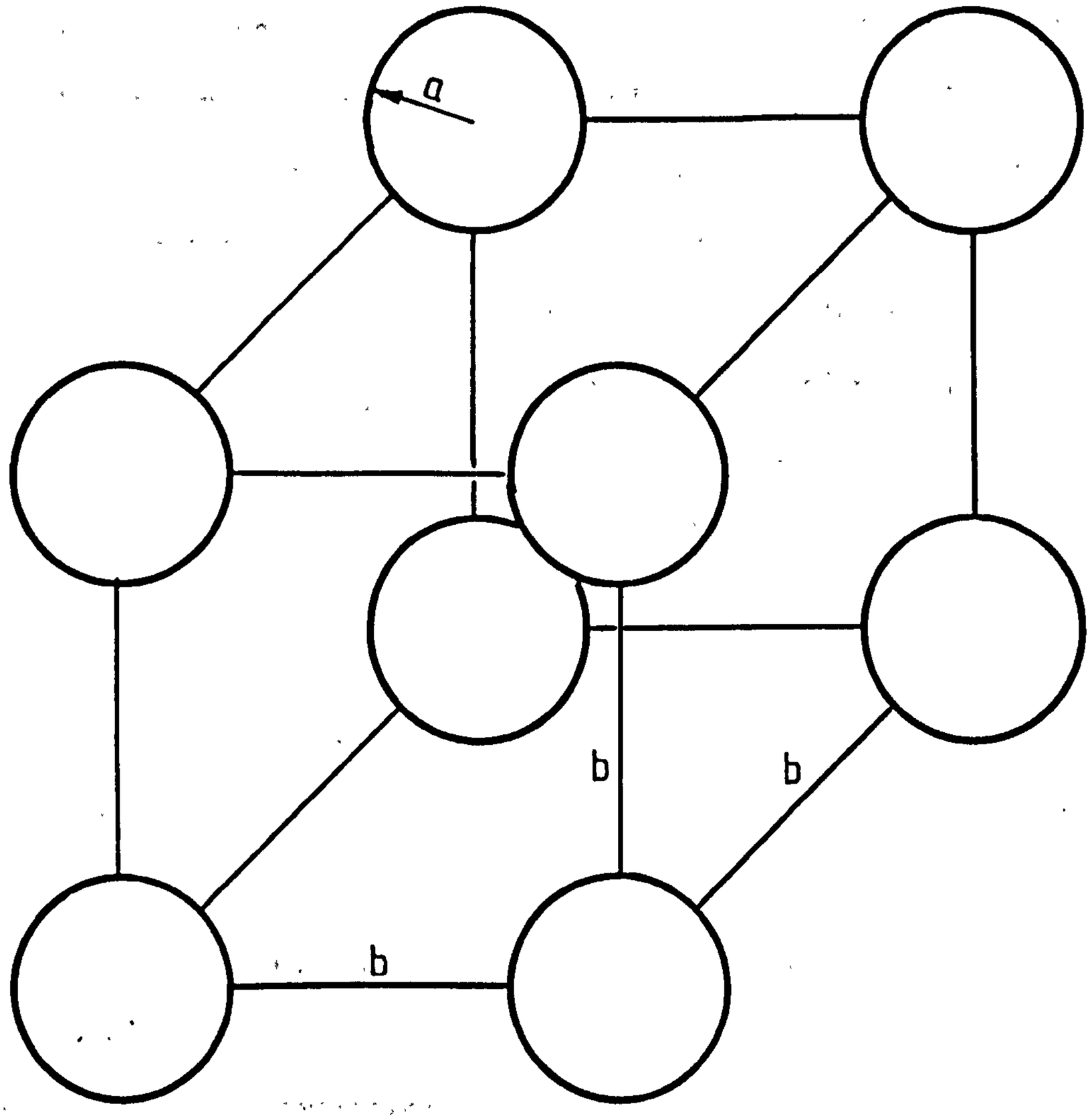

FIG. 2.7 PARTICLES ARRANGED IN UNIFORM ARRAY

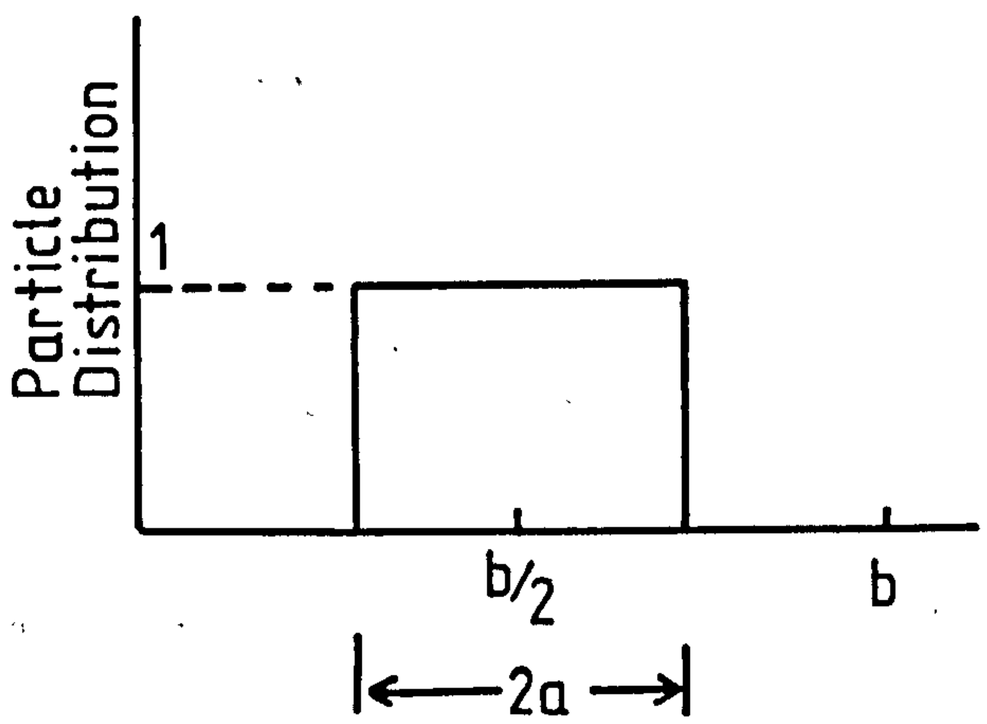

FIG. 2.8 PARTICLE DISTRIBUTION

The investigation started using an already existing system for static torque measurements. A nylon cord was wrapped around the rotor shaft, and a weight was attached to one end and a spring fixed to the other. This system suffered from the fact that it was difficult to separate the generated torque from the friction torque in the bearing of the rotor. Furthermore, the performance of the motor under variable running speed could not conveniently be measured by means of that system. Another system was designed, the idea of which was to measure the reaction torque on the stator of a dynamometer coupled to the rotor mechanically. The reaction torque was measured by means of strain gauges

2.5.1 The rotor.

Fig. 2.9 shows a photograph of the rotor and Fig.2.10 shows a detailed sketch of it. The rotating part of the rotor was supported by means of a two roller bearings. The top roller bearing was shielded from the rotating magnetic field by a steel plate. Also, a nonmagnetic cap was fixed to the shaft to prevent any magnetic material from getting inside the bearings. In order to measure the fluid temperature, a hole was drilled to allow a thermometer to be inserted through the rotor lid.

2.5.2 The stators.

The two-pole stator has a stack length of 70 mm and bore diameter of 118 mm. It had 24 slots each containing a coil side. It produced a reasonably uniform magnetic field, at least within the bore, the pattern of which rotates at the frequency of the supply.

The four-pole stator had 36 slots. The stack length was 42 mm and the bore diameter was 90 mm. The lines of force start from a north-pole to an adjacent south-pole leaving zero field in the middle of the stator. The field pattern rotates at half the supply frequency.

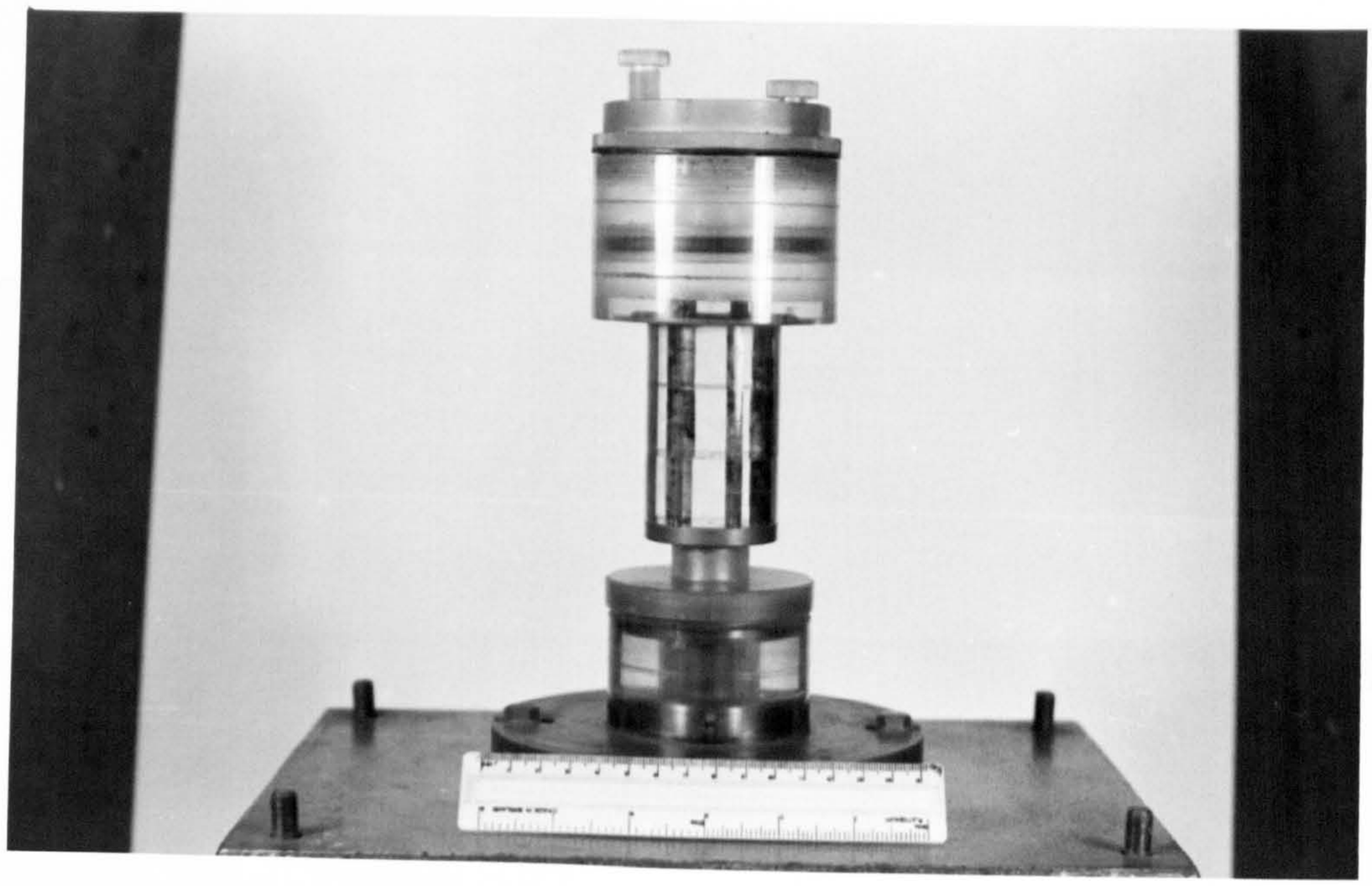

FIG. 2.9 THE ROTOR

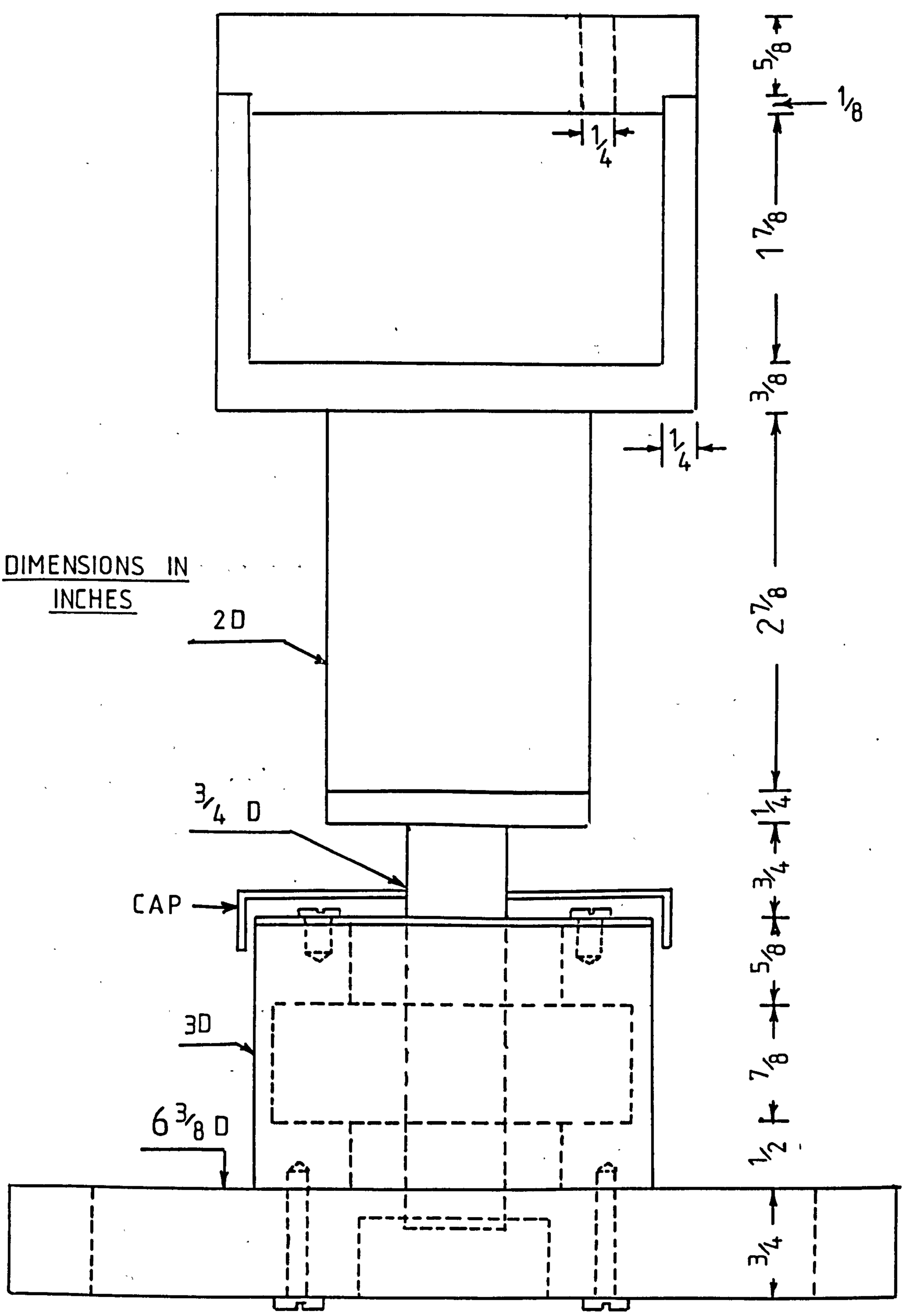

FIG. 2.10 DIAGRAM OF ROTOR CONSTRUCTION

2.5.3 The power supply.

For 50 Hz supply, the motor was supplied via a 415 volts three phase variac.

A 10-Kw three phase alternator driven by a d.c. motor was used to supply frequencies less than 50 Hz. The output voltage and frequency of the alternator were varied by varying both its d.c. field excitation and the motor speed.

A 100 Hz supply was obtained from the stator of an induction motor whose rotor was connected to a three phase supply and driven by a d.c. motor in the same direction as the rotating field.

The frequency was measured by a digital frequency meter which was calibrated against a calibrated oscillator.

2.5.4 Dynamometer and strain gauges.

The rotor of the ferrofluid motor was coupled to the rotor of a dynamometer of the printed circuit type. The dynamometer stator was fixed to one flange of the torque reaction tube, the other flange being screwed to a stationary frame. The ferrofluid rotor shaft passed through the hollow tube and coupled to the dynamometer rotor. Fig.2.11 shows a schematic diagram of the system. The strain on the tube due to reaction torque, was measured using two pairs of gauges cemented on the outer surface of the tube and coated with a protective layer of paint. Fig.2.12 shows a photograph of the tube with gauges attached while Fig.2.13 shows a photograph of the assembly of the ferrofluid rotor, the dynamometer and the frame to which the tube is fixed as well as the amplifier and voltmeter used for measuring the torque.

The design of the torque reaction tube is discussed in Appendix 3. Referring to Fig.2.14, the shear stress, f_s, is equivalent to a tensile stress, f_t and a compressive one, f_c. To measure the strain, two strain gauges of

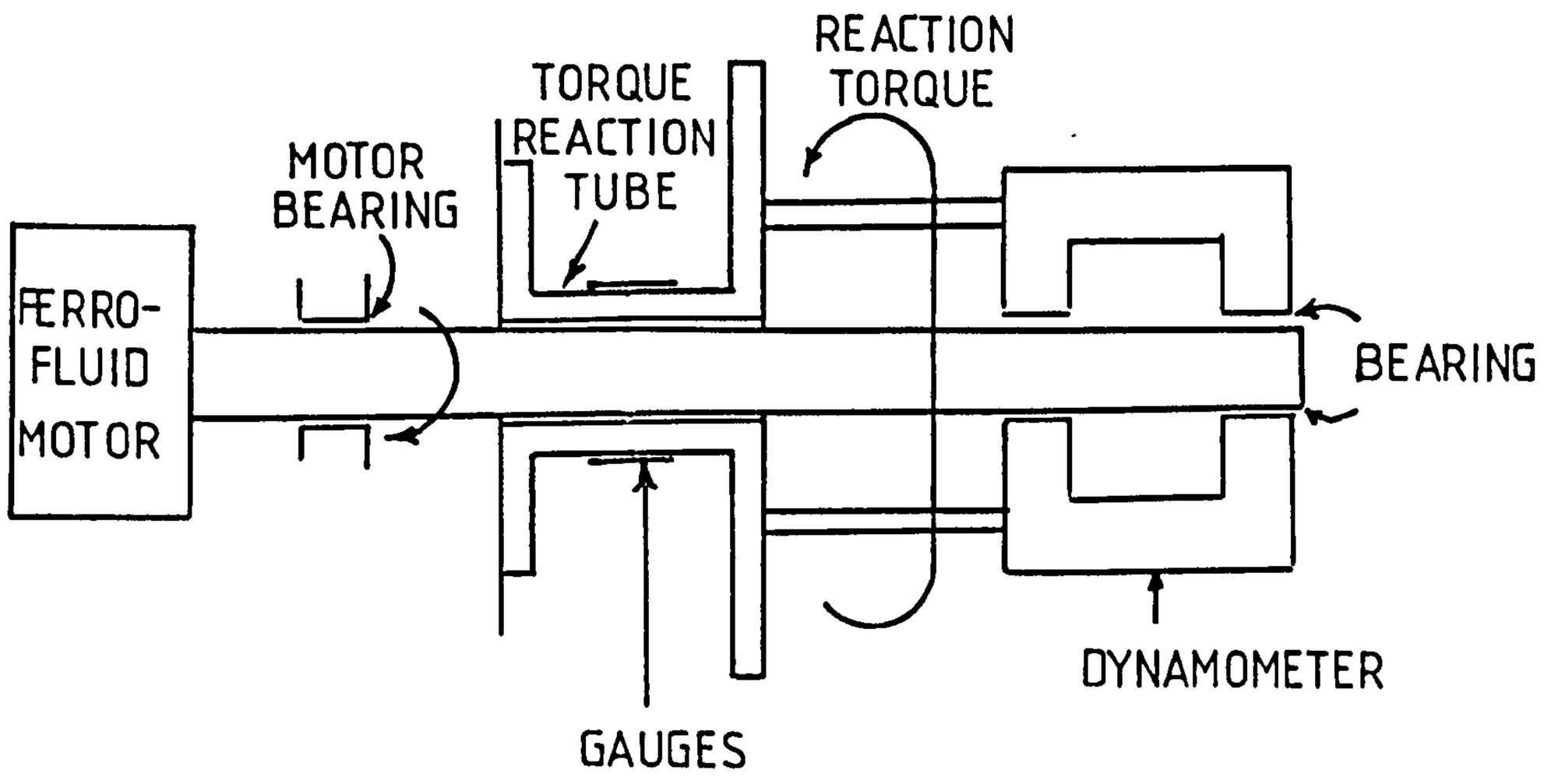

FIG. 2.11 SCHEMATIC DIAGRAM OF THE GAUGES SYSTEM

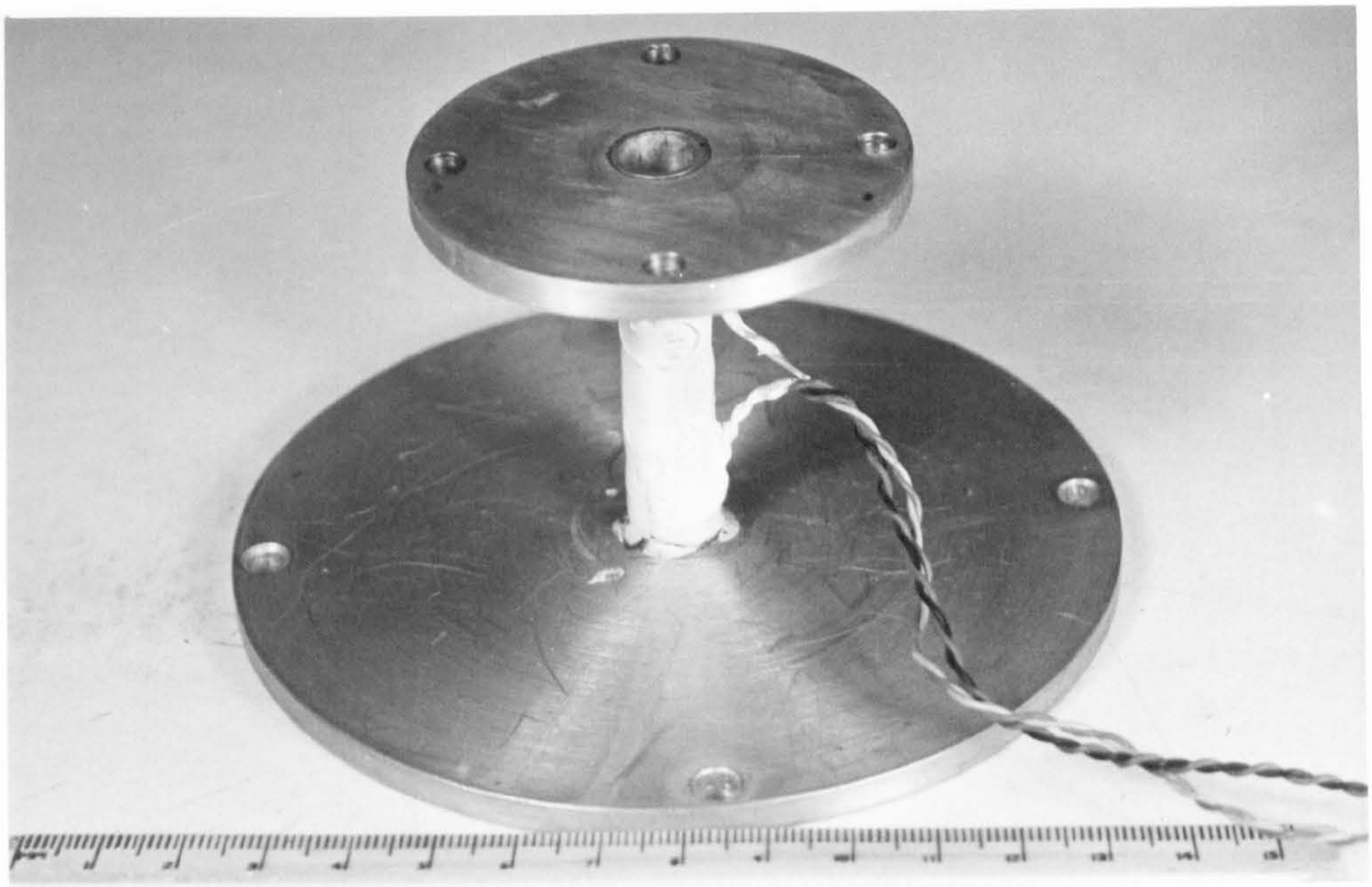

FIG. 2.12 THE TORQUE REACTION TUBE WITH GAUGES IN PLACE

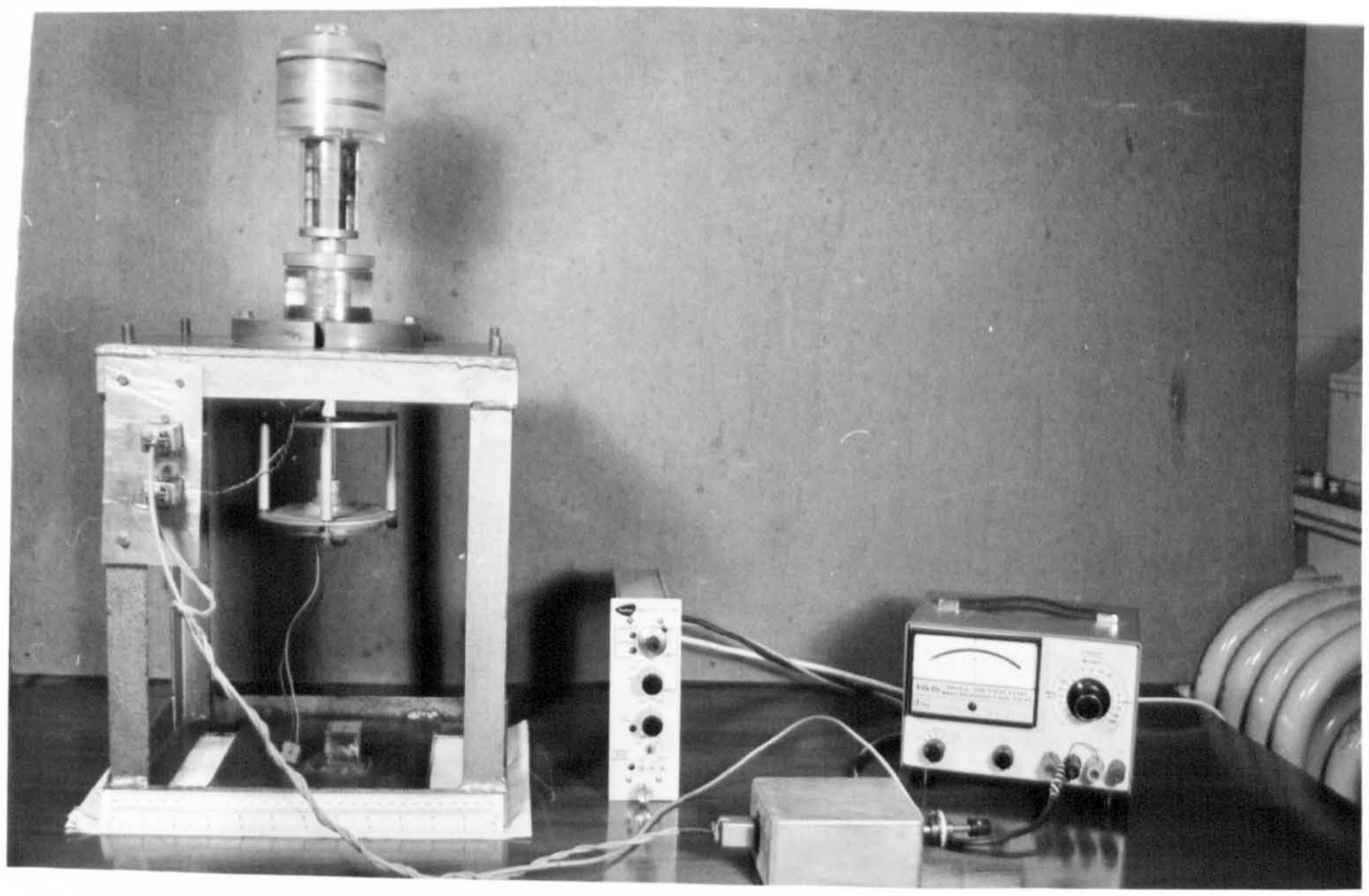

FIG. 2.13 ASSEMBLY FRAME AND EQUIPMENT FOR TORQUE MEASUREMENTS

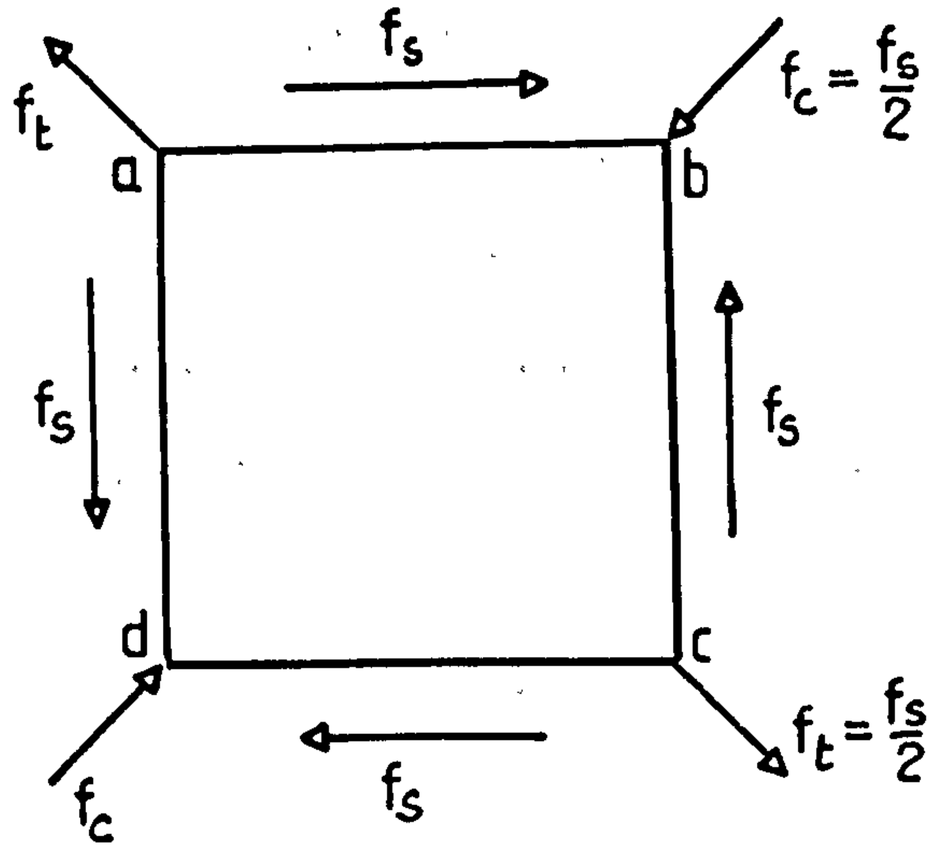

FIG. 2.14 SHEAR STRESS IS EQUIVALENT TO TENSILE AND COMPRESSIVE STRESSES

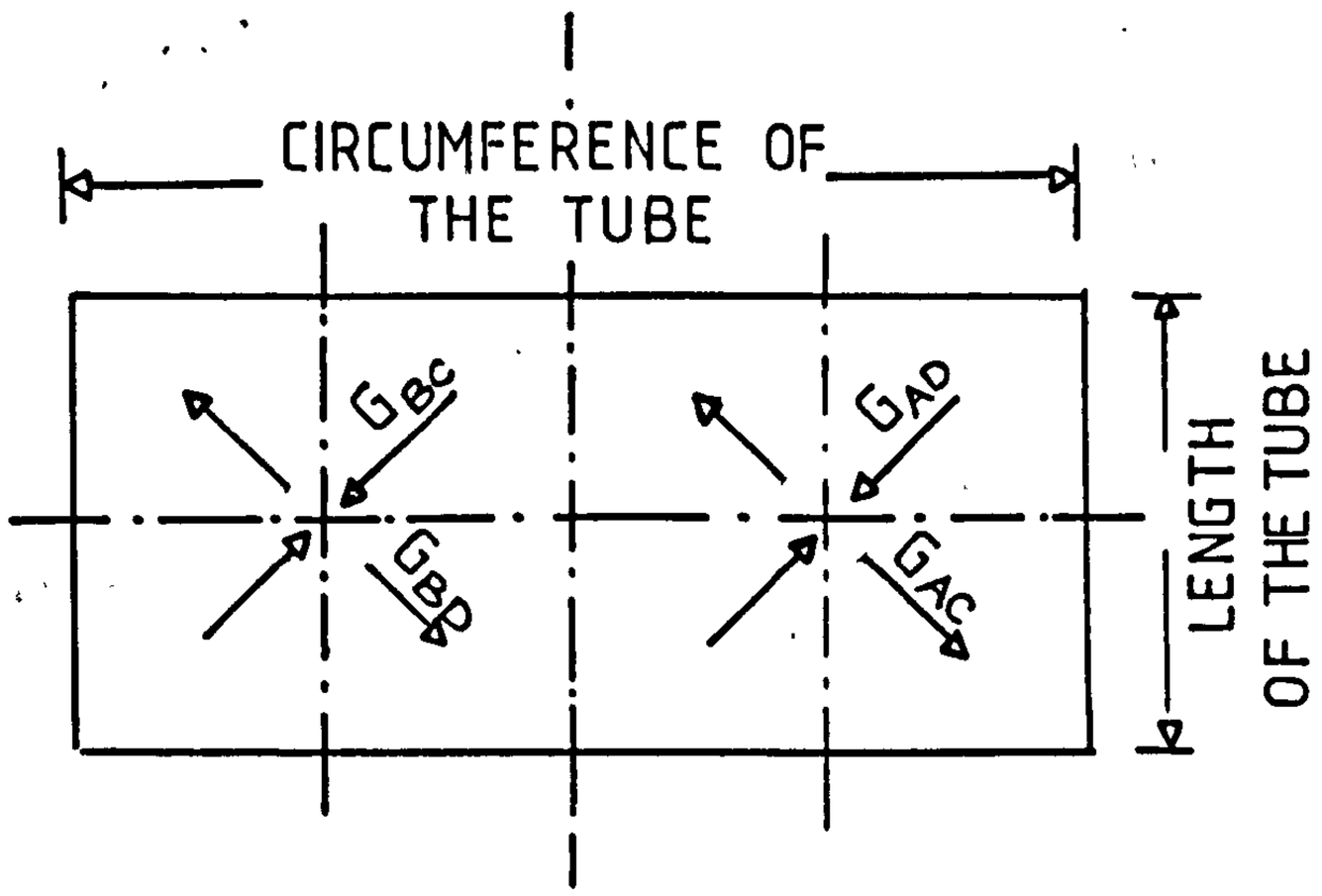

$G_{AD}, G_{AC}, G_{BC}, G_{BD}$ ARE GAUGES IN BRANCHES AD, AC, BC, BD OF BRIDGE SHOWN IN FIG. 2.16

FIG. 2.15 ILLUSTRATION OF THE POSITIONS OF THE GAUGES

nominal resistance R were cemented on the outer surface of the tube, one had its centre in the direction ac and the other had its centre in the direction bd. When the first was under tension and its nominal resistance changed to $R + \Delta R$, the other was under compression and its resistance changed to , $R - \Delta R$, where ΔR is the change in the gauge resistance due to strain ϕ. Two similar gauges were cemented at 180^{o} from the two gauges mentioned before. Fig.2.15 illustrates the positioning of the gauges. The four gauges form the four arms of the wheatstone bridge shown in Fig.2.16.

To allow for maximum current in the gauges to be about 200 mA, the d.c. voltage U should not exceed 5 volts. The maximum relative variation in gauge resistance, $\frac{\Delta R}{R}$, is equal to the gauge factor times the maximum strain

$$= \quad 2.05 \times (20 \times 10^{-6})$$

$$= \quad 40.1 \times 10^{-6}$$

The maximum output voltage, V_o, from the bridge is $U. \frac{\Delta R}{R}$

$$= \quad 5 \times 40.1 \times 10^{-6} \quad \simeq 200 \ \mu V.$$

The voltage, V_o, was amplified 800 times and then measured by a micro-voltmeter whose input resistance was 10 MΩ at the range used which was high enough compared to the bridge impedance between C and D. The voltmeter manufacturers claim an accuracy of $\pm$ 2% of full scale and 0.5 microvolt zero drift per 24 hours.

2.6 Experimental Results and Discussion.

2.6.1 Introduction.

The variables investigated were volume concentration, carrier fluid viscosity, field strength, supply frequency and size of the particles. Static torque measurements were carried out over a wide combination of variables and some dynamic torque speed measurements were also carried out. Most of the measurements were carried out using a two-pole stator, however, in some tests

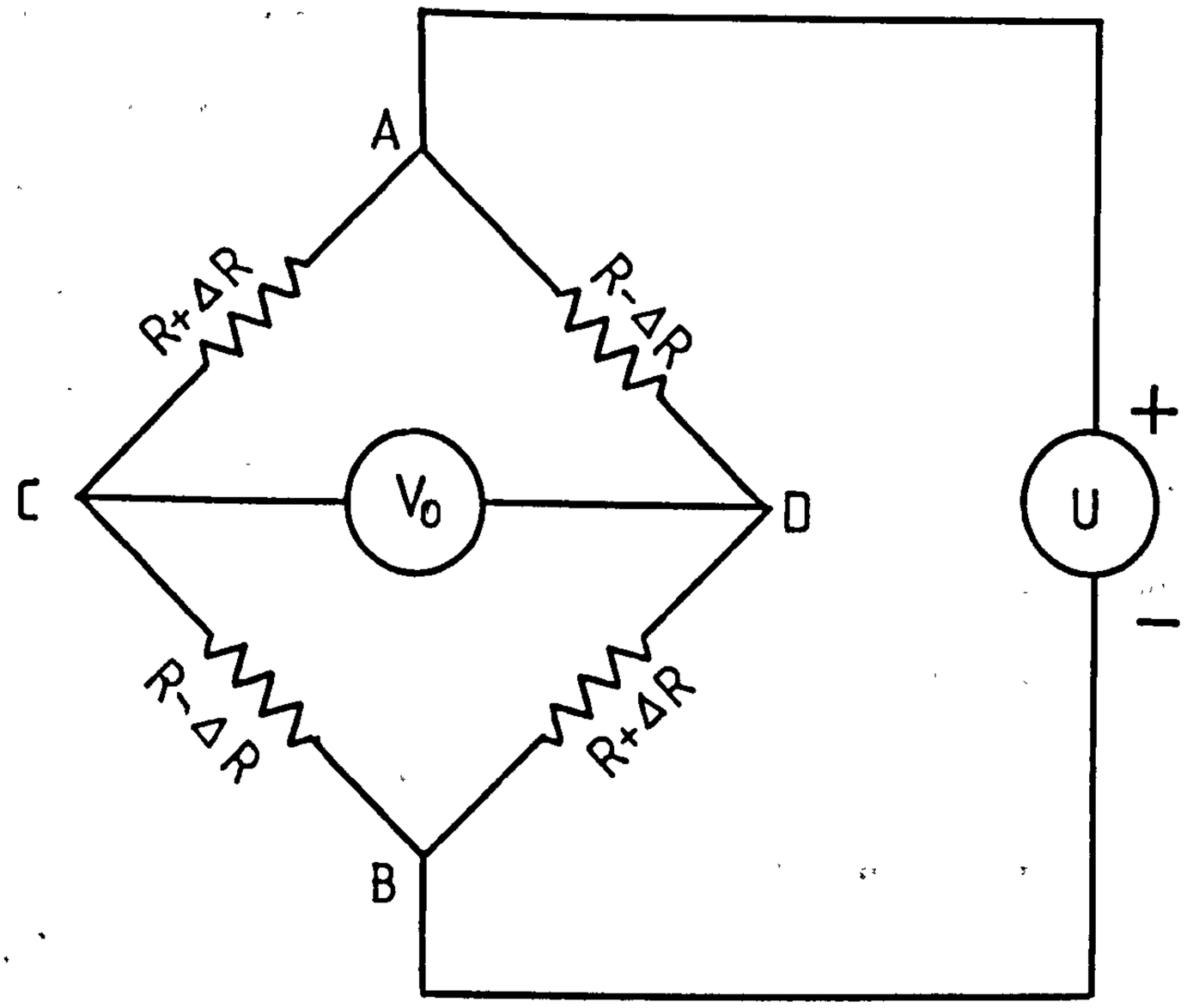

FIG. 2.16 BRIDGE FOR MEASUREMENT OF STRAINS

a four-pole stator was used. Some measurements of the thermal energy generated in the ferrofluid were also carried out in the hope that these might lead to an understanding of the nature of the torque production mechanism. In addition, however, they are of relevance to the variable-density-fluid work described later in section 3.

2.6.2 Static measurements.

A wide range of viscosities of carrier media varying from a thick viscous oil to air were considered. In some tests a mixture of oil and paraffin was used as a carrier fluid. In the tests where the paraffin only was used as a carrier fluid, the paraffin volume was varied to give a range of volume loading between 8.42% and 4.26%. The results for both the 2-pole stator and the 4-pole were similar and only the two-pole results are given. In all cases 40 gms of γFe_2O_3 with 9 ml of oleic acid as wetting agent were used. Figs.2.17 to 2.22 show the variation of torque with field intensity, H, for different supply frequencies, f_o. The results show that the torque does not vary much with frequency. The curve marked "solid" which is common to all these figures. is for the same mass of powder in solid form (produced by centrifuging and then drying to produce a cylindrical tube of solid material).

Another test was started with a fluid made up of 40 gms of γFe_2O_4 with 9 ml of oleic acid as wetting agent and 60 ml of oil as a parent fluid. To this, various amounts of paraffin were added sequentially in order to modify the viscosity of the carrier fluid. For each fluid, the torque was measured for three values of frequency at the same field intensity, ($H_{max} = 4 \times 10^4$ A/m). A plot of the measured torques against volumes of paraffin is shown in Fig.2.24.

The behaviour of small iron particles is of considerable interest and acicular or elongated particles, in which shape anisotropy can contribute greatly to improved magnetic properties, are of particular interest.

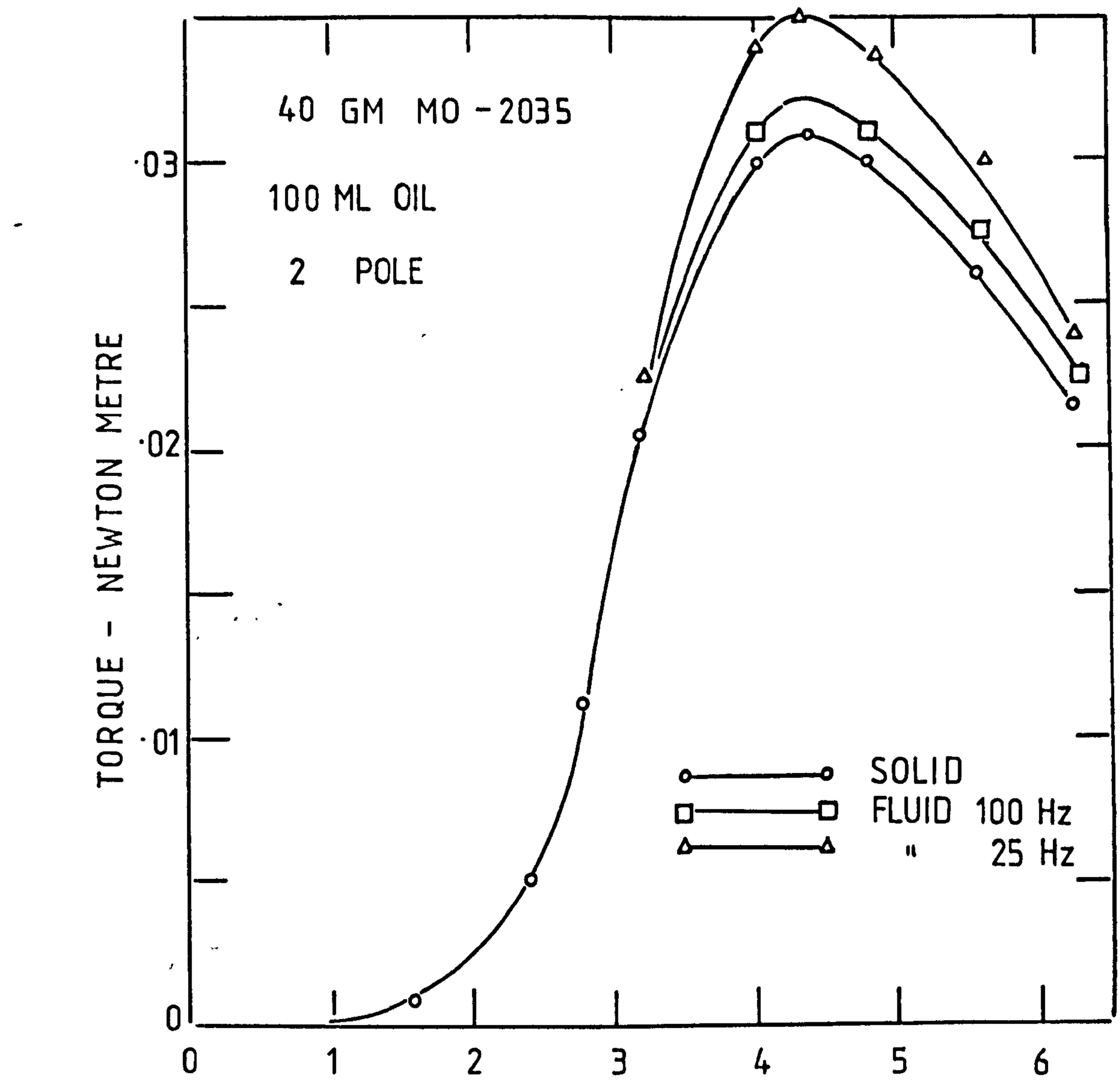
40 GM MO - 2035
100 ML OIL
2 POLE
TORQUE - NEWTON METRE
·03
·02
·01
0
SOLID
FLUID 100 Hz
" 25 Hz
0
1
2
3
4
5
6
FIELD INTENSITY - 10^4 A/m

FIG. 2.17

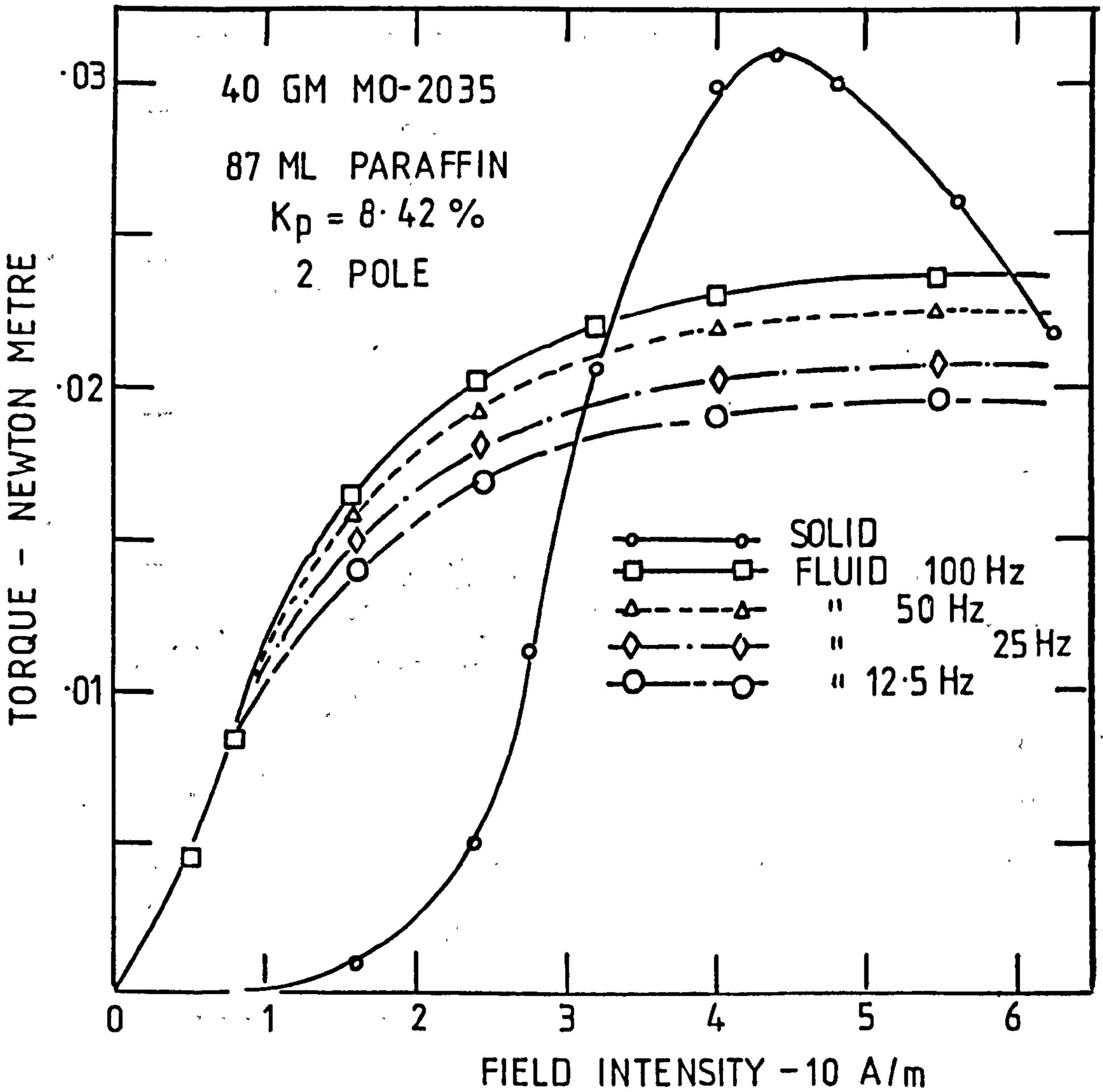
40 GM MO-2035
87 ML PARAFFIN
Kp = 8·42 %
2 POLE
SOLID
FLUID 100 Hz
" 50 Hz
" 25 Hz
" 12·5 Hz
TORQUE - NEWTON METRE
·03
·02
·01
0
1
2
3
4
5
6
FIELD INTENSITY - 10 A/m

FIG. 2.18

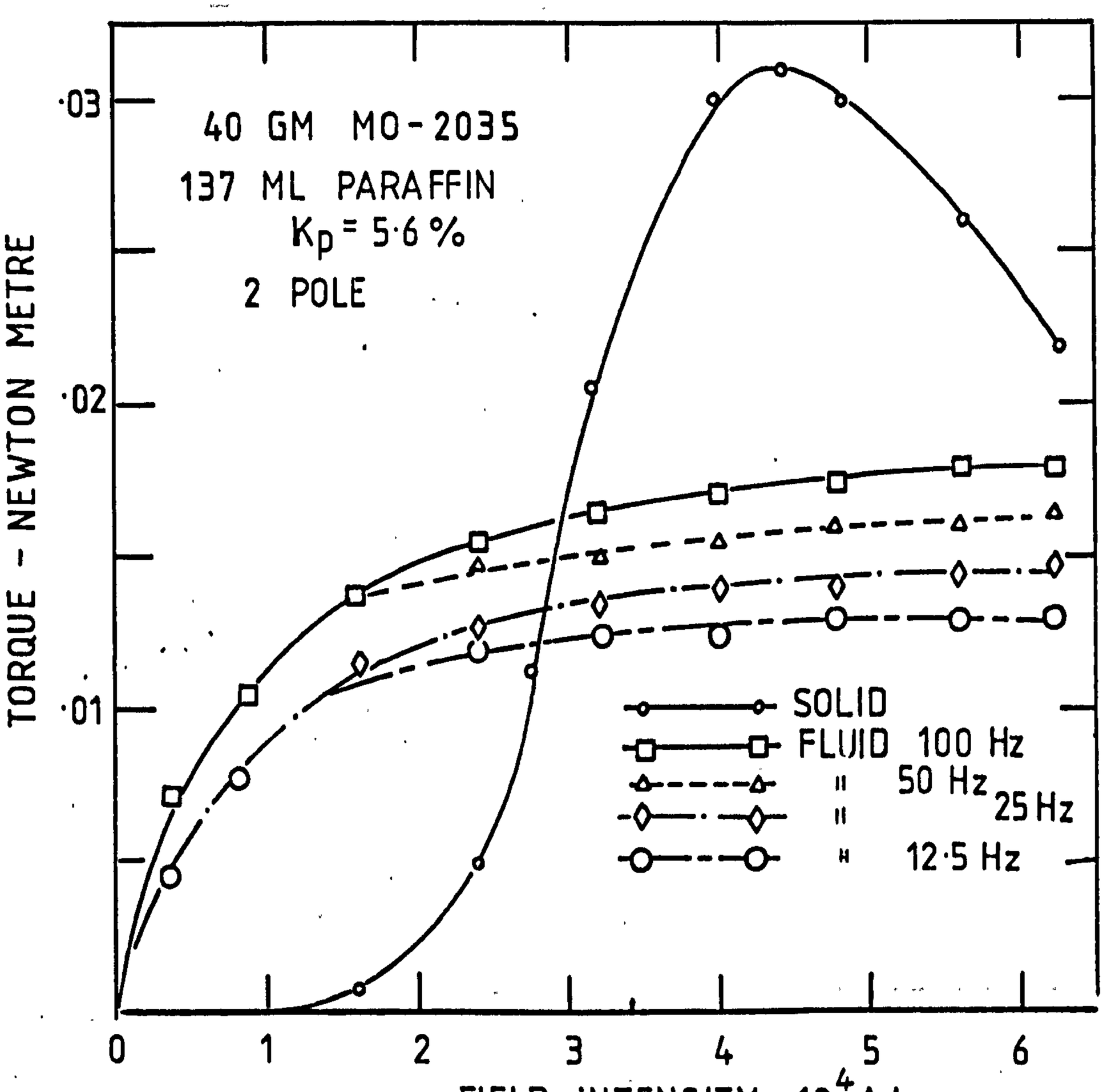
40 GM MO-2035
137 ML PARAFFIN
K_p = 5·6 %
2 POLE
TORQUE - NEWTON METRE
·03
·02
·01
SOLID
FLUID 100 Hz
" 50 Hz
" 25 Hz
" 12·5 Hz
0
1
2
3
4
5
6
FIELD INTENSITY - 10^4 A/m

FIG. 2.19

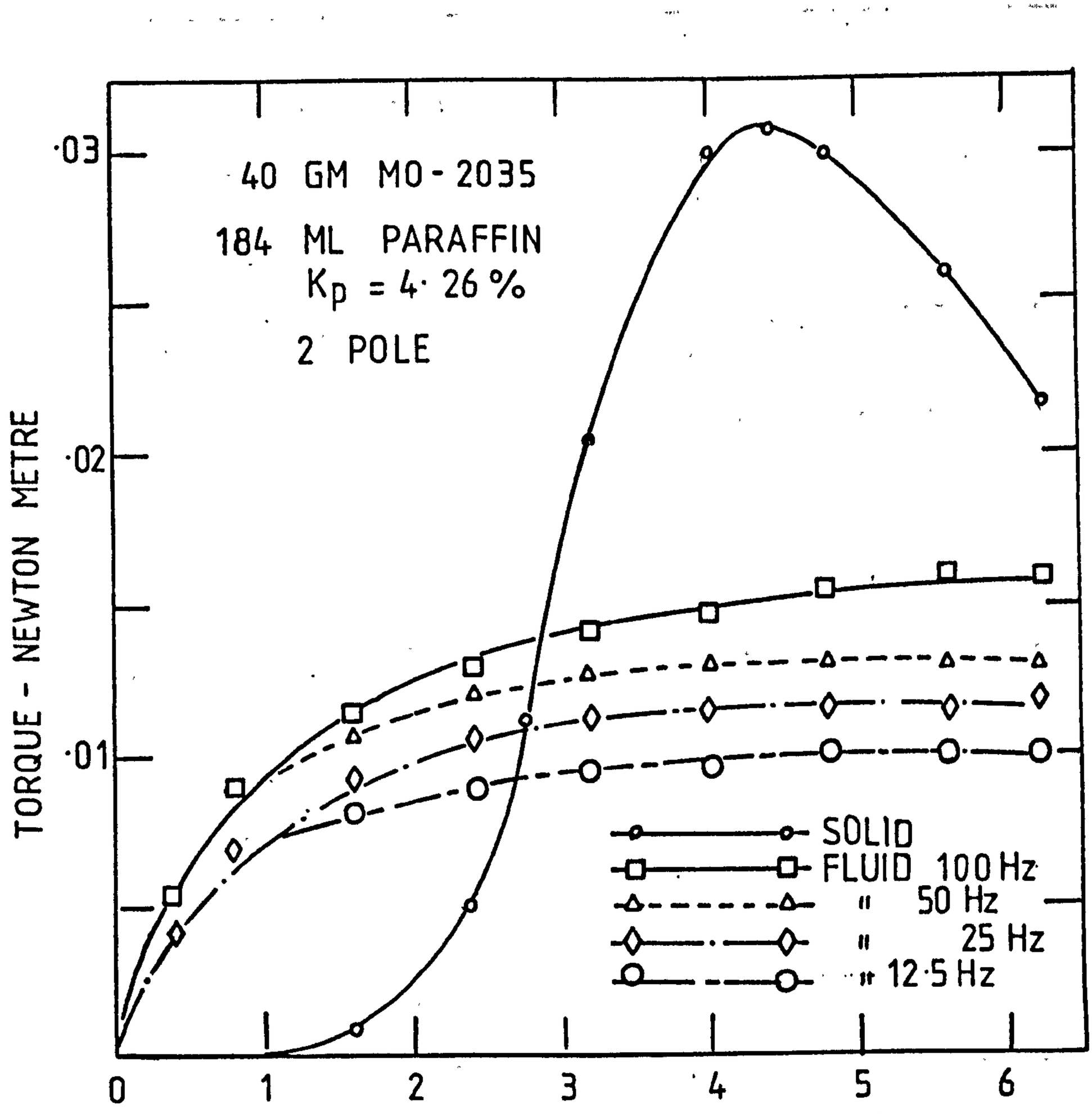
40 GM MO-2035
184 ML PARAFFIN
K_p = 4·26 %
2 POLE
TORQUE - NEWTON METRE
·03
·02
·01
0
1
2
3
4
5
6
SOLID
FLUID 100 Hz
" 50 Hz
" 25 Hz
" 12·5 Hz
FIELD INTENSITY - 10^4 A/m

FIG. 2.20

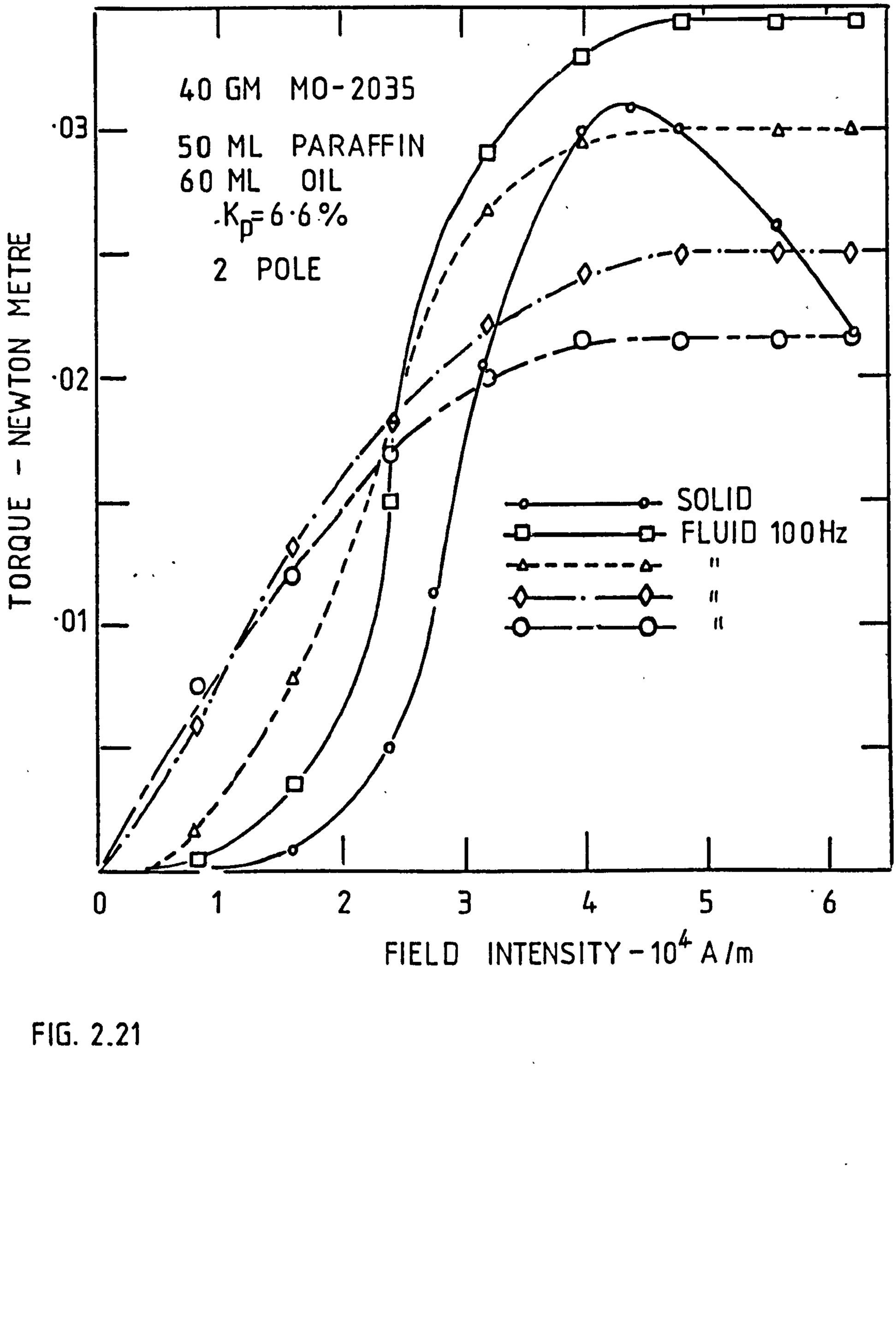
40 GM MO-2035
50 ML PARAFFIN
60 ML OIL
K_p= 6·6 %
2 POLE
SOLID
FLUID 100Hz
"
"
"
TORQUE - NEWTON METRE
·03
·02
·01
0
1
2
3
4
5
6
FIELD INTENSITY - 10^4 A/m

FIG. 2.21

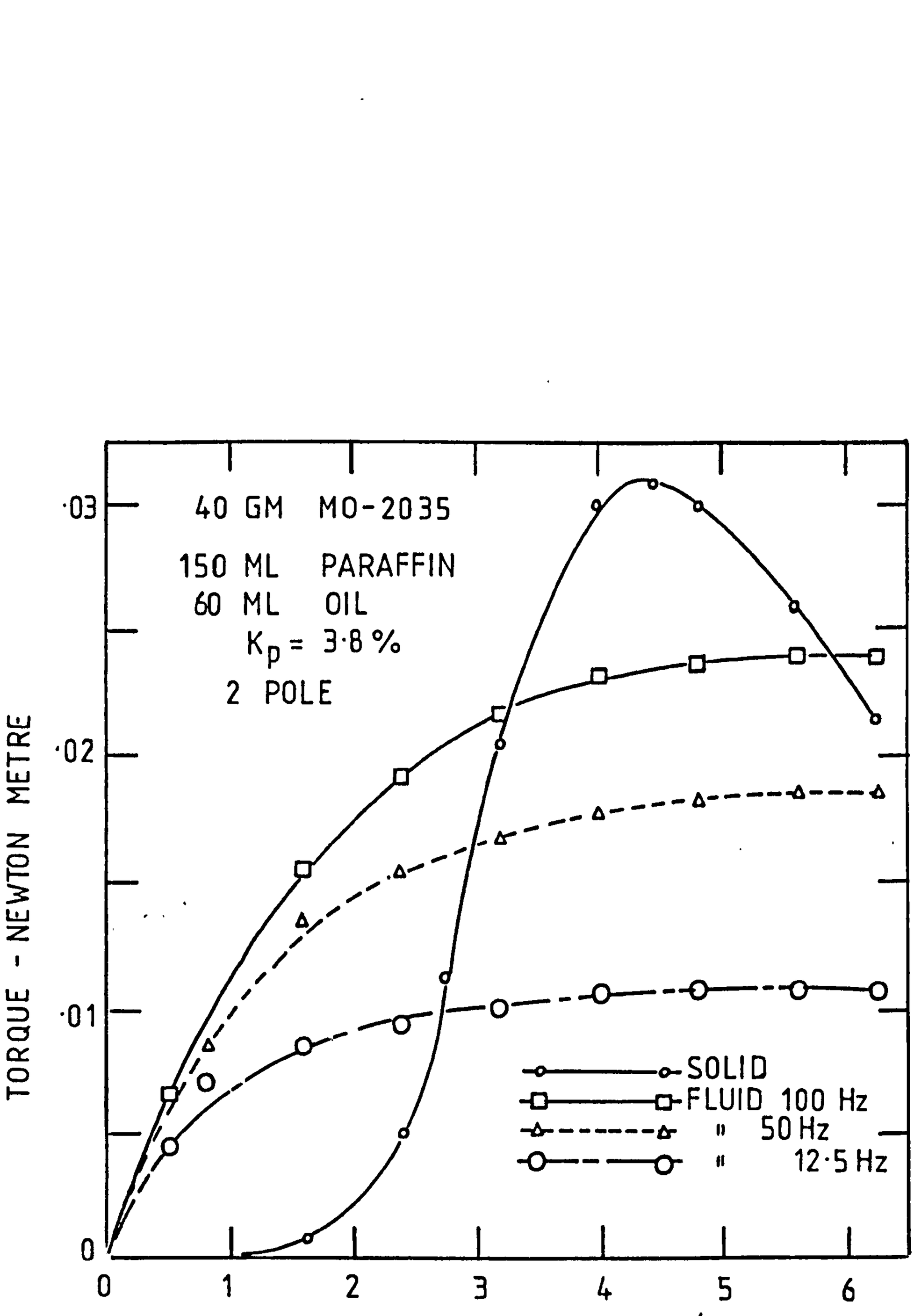
40 GM MO-2035
150 ML PARAFFIN
60 ML OIL
K_p = 3·8 %
2 POLE
·03
·02
·01
0
TORQUE - NEWTON METRE
SOLID
FLUID 100 Hz
" 50 Hz
" 12·5 Hz
0
1
2
3
4
5
6
FIELD INTENSITY - 10^4 A/m

FIG. 2.22

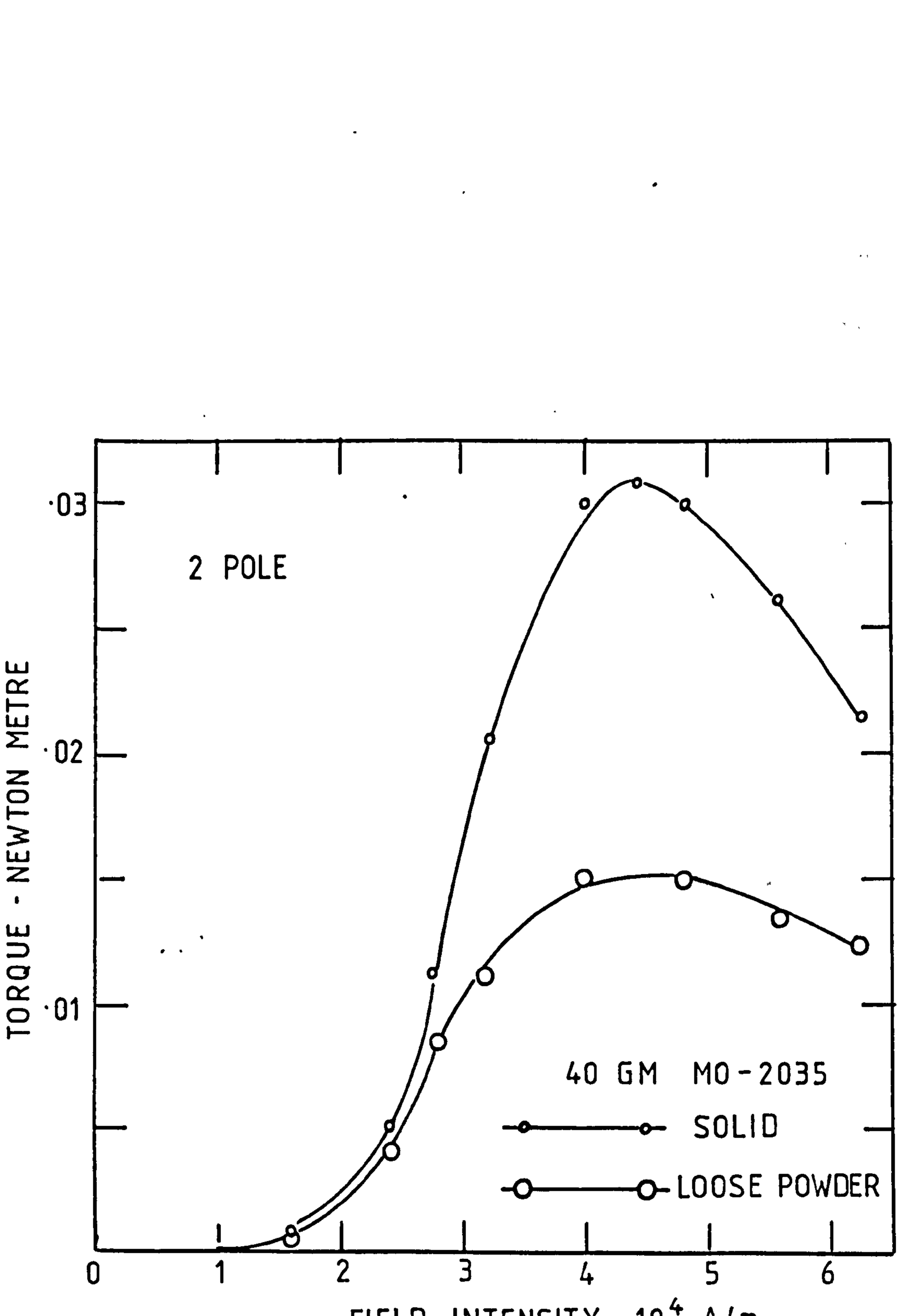
2 POLE
·03
·02
·01
TORQUE - NEWTON METRE
40 GM MO-2035
SOLID
LOOSE POWDER
0
1
2
3
4
5
6
FIELD INTENSITY -10⁴ A/m

FIG. 2.23

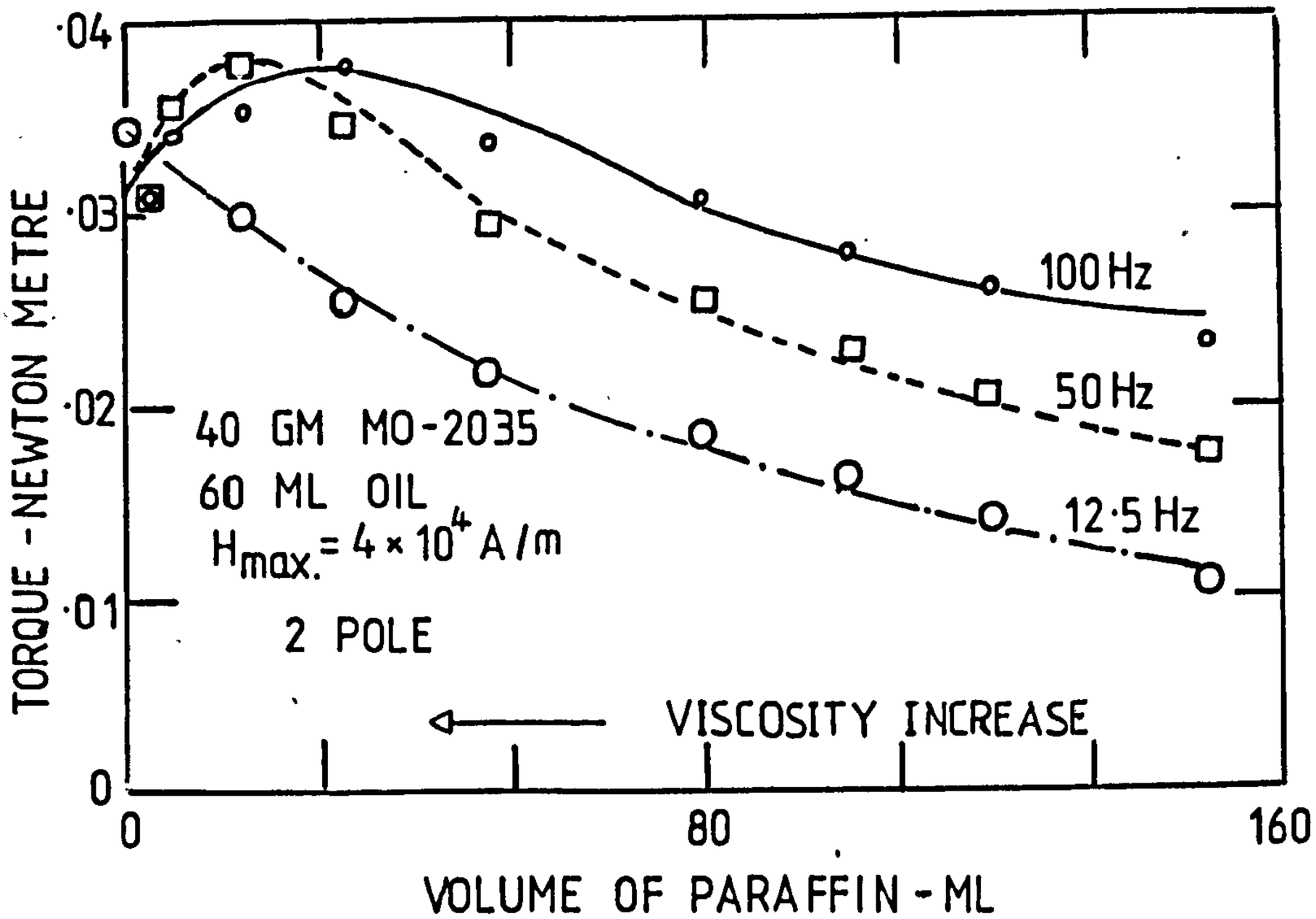

FIG.2.24 INFLUENCE OF VISCOSITY OF CARRIER FLUID ON TORQUE

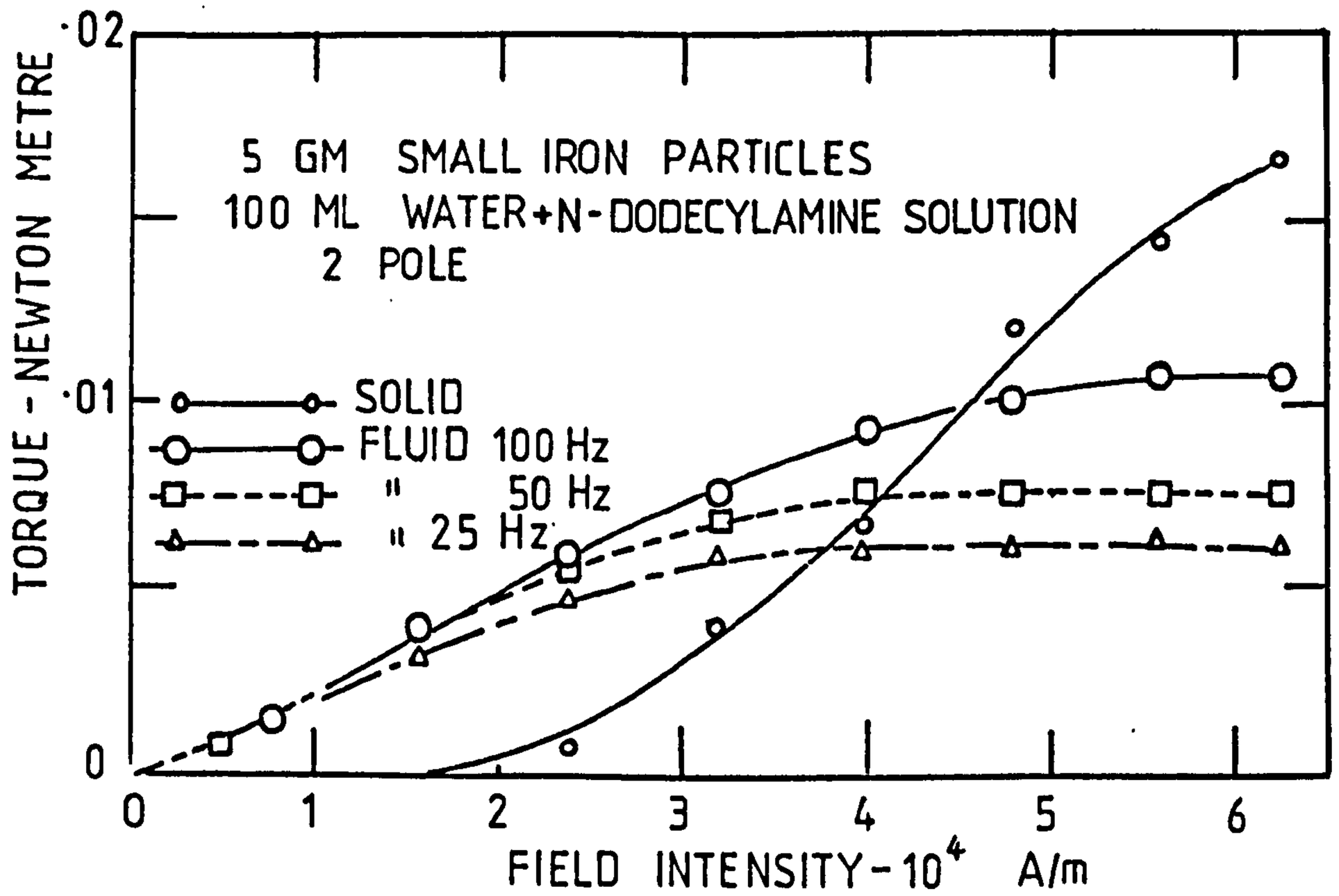

FIG. 2.25 GENERATED TORQUE FROM SMALL IRON PARTICLES

The particles were prepared by "Borohydride reduction" which yields single domain particles and more acicular particles were formed in the presence of magnetic fields[11].

In a typical procedure 100 ml of 1 M KBH_4 was added over a period of three minutes, the mixture being continuously stirred, to 100 ml of 1 M Fe SO_4. The mixture was contained in a 500-ml. beaker resting on the poles of a 5000-gauss U-shaped magnetron magnet. The black product was immediately collected on a filter and washed quickly with copious amounts of water, followed by an acetone rinse. After removal of the solvent in a slow stream of dry air 5 gm of fluffy, strongly magnetic material remained. The authors[11] claim that the particles should be only 0.1 to 1 μ long.

The surfactant used for these particles was a solution of n-dodecylamine prepared by dissolving dodecylamine in 10 mls of N-HCl until a pH value of 7 was obtained. Water was used as the carrier fluid, and this was added to the solution, bringing its volume to 100 ml before mixing in the prepared particles. The torque was measured for three values of frequency at various values of field intensity. The results are shown in Fig.2.25.

2.6.3 Discussion of the results of static measurements.

The two theories presented in section 2.3 and 2.4 assumed negligible particles interaction, which can be shown is unlikely to be true for some of the fluids investigated. Assuming the array shown in Fig.2.7 the gap, ℓg, between particles is related to particle diameter, d, by

$$\ell g = \left[\left(\frac{\pi}{6}\right)^{\frac{1}{3}} \cdot \frac{1}{K_p^{1/3}} - 1 \right] d$$

A plot of $\ell g/d$ against K_p is shown in Fig.2.26, and it will be seen that for a volume loading K_p of 6.4% ℓg is almost equal to d. If there is interaction

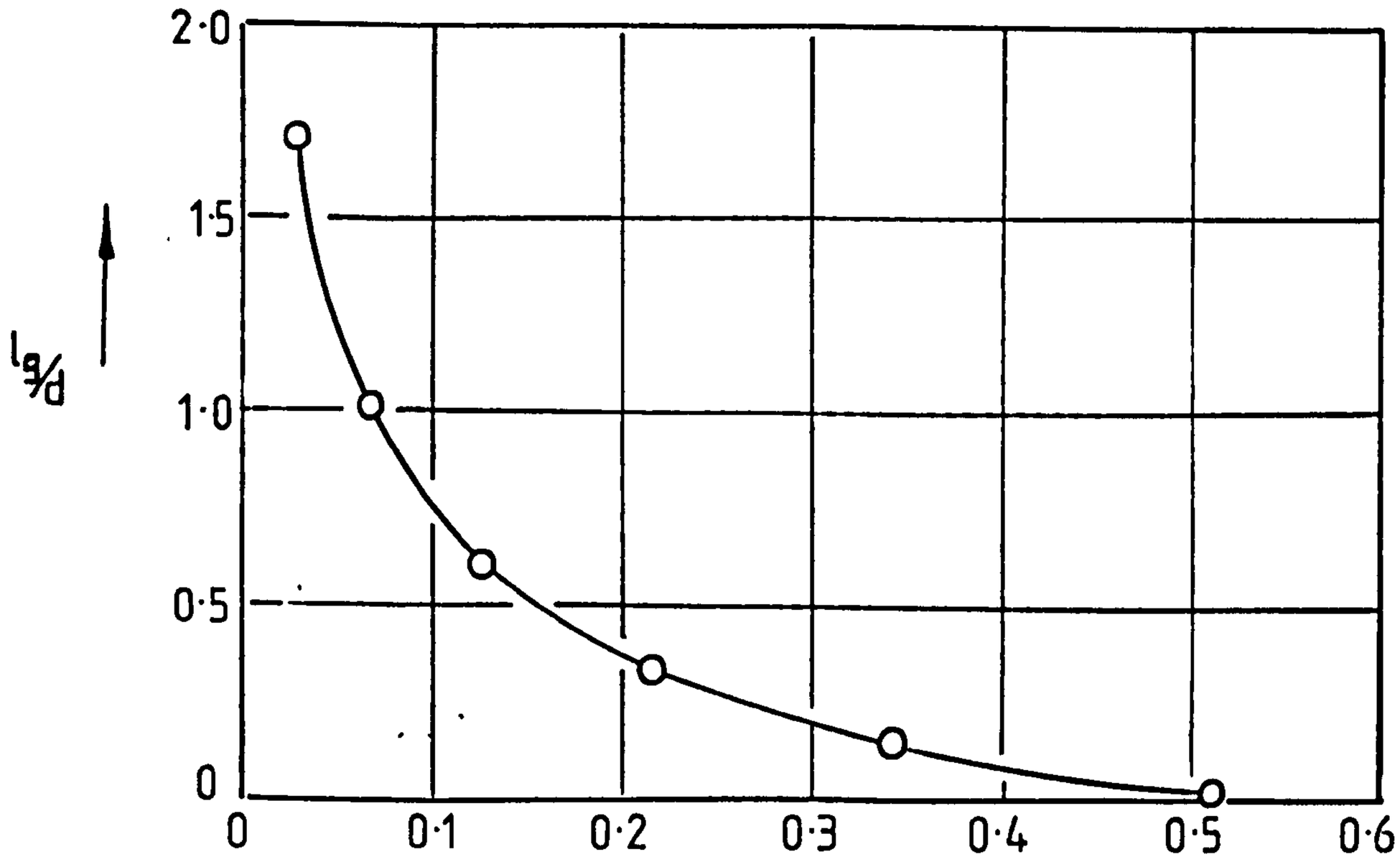

FIG. 2.26 THE GAP BETWEEN PARTICLES AGAINST VOLUME LOADING

between the vortices associated with the spinning particles the demanded torque on each particle will be greater than that given by equation 2.2.2 which means effectively an increase in the value of η, which will no longer be simply the viscosity of the carrier fluid. Thus we must use an "effective viscosity", which will be a function of the volume loading of the fluid, the size of the particles, and the viscosity of the carrier fluid.

As has been pointed out the torque variation with frequency is not very great, and from the modified Moskowitz and Rosensweig theory discussed in section 2.3, this could be due to one of the following possibilities:

(a) At all frequencies the fluid reverse angular velocity could be very high compared to the wave velocity. This would mean that the spinning velocity does not increase much with frequency.

(b) Most of the torque generated by the particles could be due to hysteresis, in which case the fluid velocity in the backward direction adjusts itself until the viscous drag torque is equal to the hysteresis torque that can be generated by each particle. Since the hysteresis torque tends to be independent of frequency this would give little variation of overall torque with frequency. This is unlikely to be so, however, since the torque generated can be higher than the hysteresis torque, as shown in Figs. 2.18 to 2.22.

(c) Not all the particles are synchronized but only some of them and these could generate a saliency torque.

From equation 2.3.3 $\frac{T_{vm}}{\omega_o}$ is independent of ω_o unless the number of particles spinning is a function of ω_o. It would seem that the higher the frequency the less will be the number of particles spinning and therefore the smaller $\frac{T_{vm}}{\omega_o}$. With the near solid mixture, the torque was independent of frequency and it must have been purely due to hysteresis. The hysteresis torque, T_h, is related to the area of the hysteresis loop S_H and the volume of material, V_r, by[17]:

$$T_h = \frac{1}{2\pi} S_H \cdot V_r \qquad \ldots\ldots \qquad 2.6.1$$

An assessment of the possible order of value of the hysteresis torque of the oxide MO-2035 for various field intensities was made and the results are compared with measured hysteresis torque generated by the same material in solid form. The comparison is shown in Fig.2.27 and it will be seen that the maximum torque predicted from the area of the alternating hysteresis loop is of the same order as the maximum torque measured. However, the measured torque rises more rapidly with field intensity and shows the distinct fall off at high field intensity which is a characteristic of rotational magnetization, and was first found by Graetz[24].

As more carrier fluid is added the effective viscosity is reduced and presumably more particles are able to synchronize and contribute saliency torque rather than hysteresis torque. The number of particles taking part in the process would be expected to increase as the field strength is increased[3] but the highest torque which could be reached at a particular frequency will be governed by the torque demanded at that particular frequency. This levelling off of torque is evident in Figs. 2.18 to 2.22.

On the other hand, if the effective viscosity is such that the demanded torque is equal to the peak saliency torque at a particular supply frequency and field intensity, the torque will be maximum and any reduction or increase of the viscosity will be accompanied by a reduction in the torque. An optimum value of torque is shown in Fig.2.24 and it can be seen from the curves that the value may be independent of frequency. This ought to be so since the peak saliency torque that can be generated should be independent of the spinning velocity. Since the demanded torque is proportional to the product of the effective viscosity of the fluid and the spinning velocity, the viscosity at which the maximum torque occurs should be small for high frequency and this is evident from Fig.2.24.

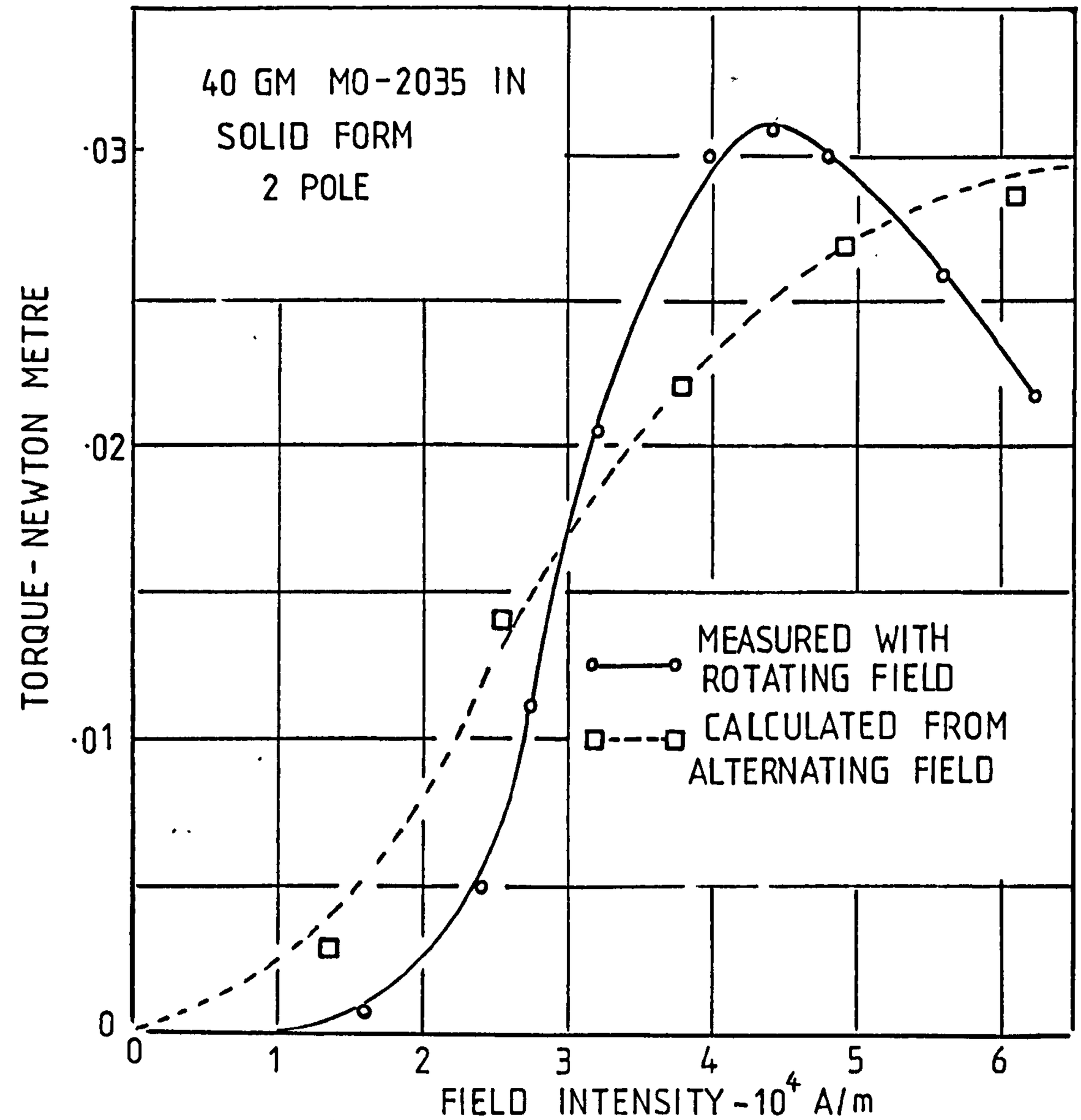

FIG. 2.27 COMPARISON BETWEEN HYSTERISIS TORQUE DUE TO ROTATING AND ALTERNATING FIELD

In the test of the air medium fluid it was noticed that the moisture content in the loose powder caused the agglomeration of the particles into large spheres while the particles were spinning. The pattern is shown in Fig.2.28. The spheres have no saliency and so they should not contribute to saliency torques. This might be the reason why the generated torque, Fig.2.23 for loose powder, is almost equal to the hysteresis value at low field intensities. At higher intensities the torque is less than the hysteresis value and this could be because the demanded torque is less than the hysteresis torque.

In Figs. 2.17 and 2.21, at low field intensity, and 2.24, with no paraffin added, the torque at small frequencies was higher than that at high frequency. It might be that the fluid was so viscous that more particles were able to synchronize at smaller than at higher frequency.

In Fig.2.17 the fluid curves are similar to the hysteresis curve which suggests that the hysteresis torque was predominant.

Fig.2.29 shows a linear variation between the torque generated, at a fixed field intensity of 6×10^4 A/m, and the volume loading of the fluids of paraffin base for different supply frequency, f_o.

The predicted curves, shown in Figs. 2.5 and 2.6, emphasize the fact that the torque varies nonlinearly with the wave velocity which was found experimentally.

For fixed excitation, these graphs represent the variation of generated torque within the fluid to some scale with $1/\omega_o$. For a given fluid if we plot the measured torque, for a fixed value of excitation, against $1/\omega_o$, we can find a predicted curve of constant K_A (an area packing factor) which fits with the experimental. When the two curves are fitted together as best as they can be the ordinate scale will be in the ratio $2\pi N\ T_{max}\ R_o^2$ and the abscissae in the ratio $8\pi\eta a^3/T_{max}$. These two ratios can be read-off and

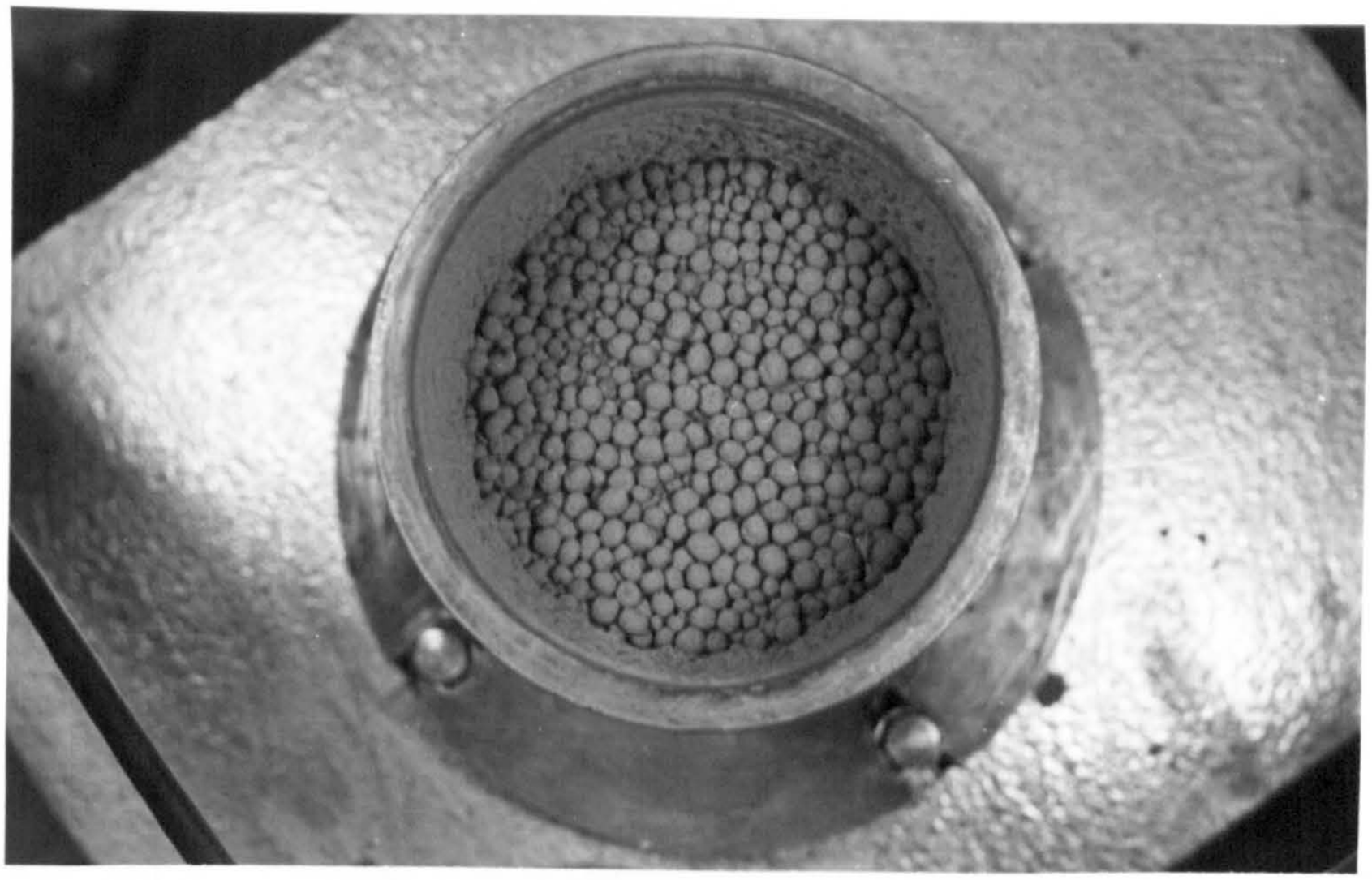

FIG. 2.28 THE PATTERN OF AGGLOMERATING PARTICLES

knowing R_o, NT_{max} can be found. Now $\frac{4\pi a^3}{3}$. N is equal to the volume loading factor K_p, and if this is known, the value of η can also be obtained. Table 2.1 gives the estimated values of effective viscosity of some ferrofluids referred to by the number of figure. The viscosity values were obtained by fitting curves of Fig.2.5 with the experimental results of torque - frequency variation.

Table 2.1

Referred Fig.	Fluid Ingredients	K_p	Field Intensity -10^4 A/m	K_A	Estimated value of viscosity - MKS units
2.18	40 gm MO-2035 + 87 ml Paraffin + 9 ml oleic acid.	.084	6 4 2.4	5 5 5	0.74 1.03 0.98
2.19	40 gm MO-2035 + 137 ml Paraffin + 9 ml oleic acid.	.056	6 4 2.4	4 4 4	0.44 0.51 0.475
2.20	40 gm MO-2035 + 184 ml Paraffin + 9 ml oleic acid.	.043	6 4 2.4	3 3 3	0.32 0.314 0.333
2.21	40 gm MO-2035 + 50 ml Paraffin + 60 ml oil + 9 ml oleic acid.	.066	6 4	2 2	0.992 0.98
2.22	40 gm MO-2035 + 150 ml Paraffin + 60 ml oil+ 9 ml oleic acid.	.038	6 4 2.4	2 2 2	0.38 0.38 0.32
2.25	5 gm small iron particles in water.	.006	6 4 2.4	1 1 1	0.22 0.31 0.27

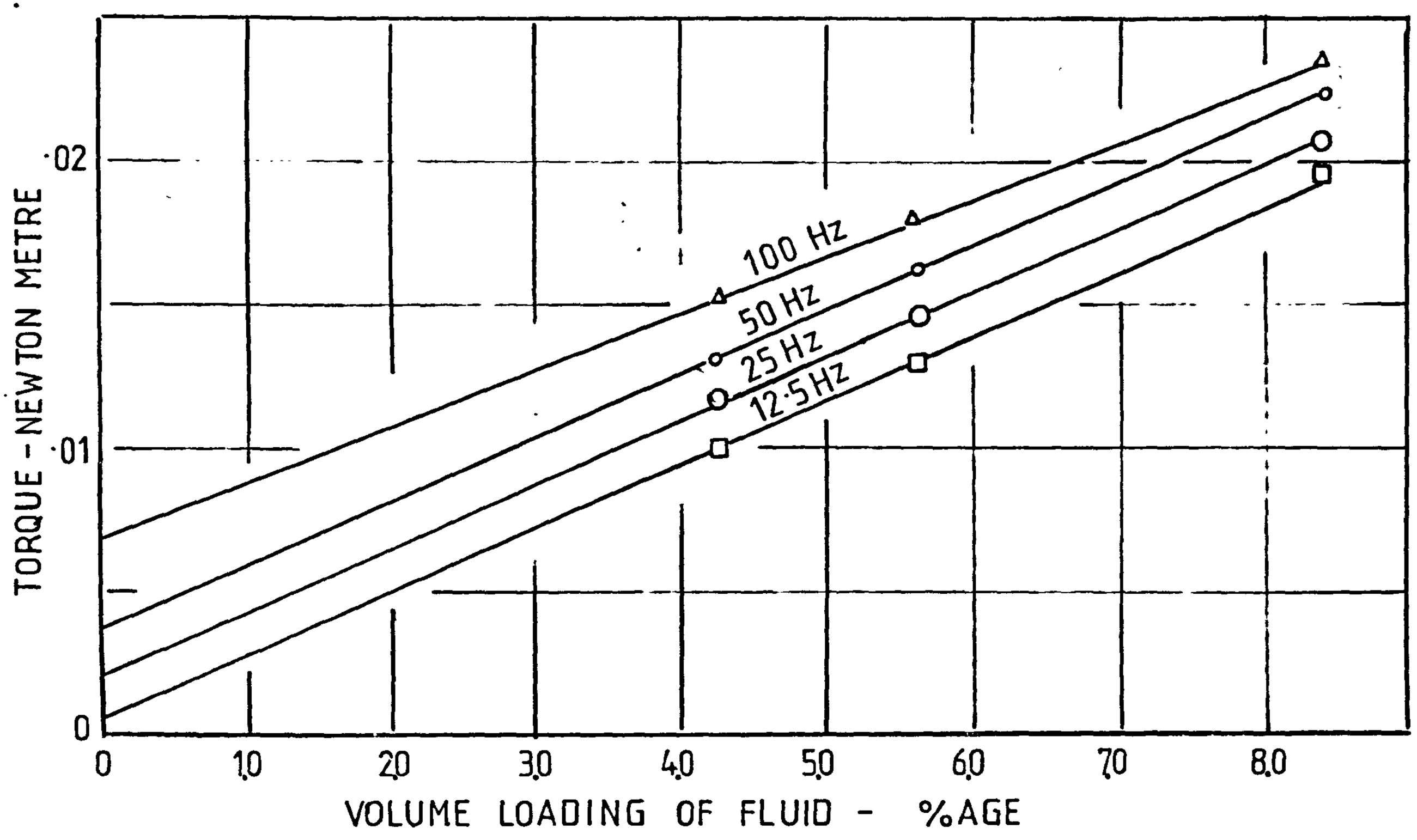

FIG. 2.29 EFFECT OF VOLUME LOADING UPON SATURATION TORQUE

The results of table 2.1 show some consistency of the way the viscosity varies with the volume loading and field intensity. Moreover the various values of effective viscosity obtained for each fluid by varying the field intensity are of the same order of magnitude although they are very much higher than the viscosity of the carrier fluid which is of the order of 0.001 MKS unit.

The overall viscosity could be much higher than the actual viscosity of the carrier fluid due to interaction between the vortices associated with the particles, but it is doubtful whether it will be 1000 times as high.

The values of K_A do not agree at all with the predicted one, equation 2.4.17 e.g. for $K_A = 5$, $K_p = 0.1$, $a = 0.1$ m, but in practice more like 10^{-7} m.

The curves of Fig.2.25 are similar to those of 2.18 to 2.20. Now replacing the dipole moment, m, of one particle by the dipole moment, M(H), per unit volume of fluid in equation 2.2.1 leads to an expression for the torque generated per unit volume of fluid,

$$T_v = \mu_o M(H) \cdot H \cdot \sin\theta \quad \ldots\ldots \quad 2.6.1$$

The maximum value of T_v, $T_{v_{max}}$ will be obtained when all the particles are participating in the process, i.e. $M(H) = M_{sat}$ and the demanded torque is such that $\sin\theta = 1$. In that case

$$T_{v_{max}} = \mu_o M_{sat} \cdot H \quad \ldots\ldots \quad 2.6.2$$

i.e. the maximum torque that can be generated per unit volume of fluid at a given field intensity is proportional to its saturation magnetisation, M_{sat}. Therefore for two fluids having different values of M_{sat}, the torques per unit volume must be proportional to their saturation magnetizations.

$$\therefore \quad \frac{T_{v_{max\ 1}}}{T_{v_{max\ 2}}} = \frac{M_{sat_1}}{M_{sat_2}} = \frac{\mu_o M_{i_1}}{\mu_o M_{i_2}} \times \frac{K_{p_1}}{K_{p_2}}$$

where suffix 1 and 2 refers to two fluids and $\mu_o M_i$ is the intrinsic magnetization of the magnetic material,

but $$\frac{K_{P_1}}{K_{P_2}} = \frac{V_{m_1}}{V_{m_2}} \cdot \frac{V_2}{V_1}$$

where V_m is the volume of magnetic material in a fluid of volume V.

Therefore $\frac{T_1}{T_2} = \frac{\mu_o M_{i_1}}{\mu_o M_{i_2}} \cdot \frac{V_{m_1}}{V_{m_2}}$ where T is torque generated.

Knowing that the intrinsic magnetization of the iron particles and the MO-2035 oxide are 2.02 and 0.35 T and that their volumes are 0.62 and 8.4 c.c. respectively, $\frac{T_1}{T_2}$ was found to be 0.43.

The measured values of T_1 (Fig.2.25) and T_2 (Fig.2.18) for H = 6 x 10^4 A/m and f_o = 100 Hz are found to have about the same ratio i.e. 0.42:1.

In short, it seems that the torque generated is due to a volume effect and that it is not only the rolling particles beside the boundary that are contributing to the torque.

Further experiments were carried out to see the effect of introducing other boundaries. Primitive ferrofluids made up of either the magnetic powder type MO-2035 or type MO-8853 in paraffin, both using oleic acid as a surfactant, were used for this investigation. For the establishment of various boundary conditions, a set of concentric cylinders, shown in Fig.2.30, were introduced inside the fluid containing vessel. The various zones and barriers are labelled.

The results shown in Fig.2.31 are the torque generated by the fluid made up of the powder type MO-9853 at various field intensities and 50 Hz. Curve I is for a 40 gms of the magnetic powder added to 60 ml paraffin and 30 ml oleic acid. Curve II is for half the amount of this same fluid, while curve III is for 40 gm of powder in solid form. Both curve I and II were plotted for the fluid placed in various zones.

The results for the MO-2035 fluid are shown in Fig.2.32. Curve I is for

DIMENSIONS IN mm

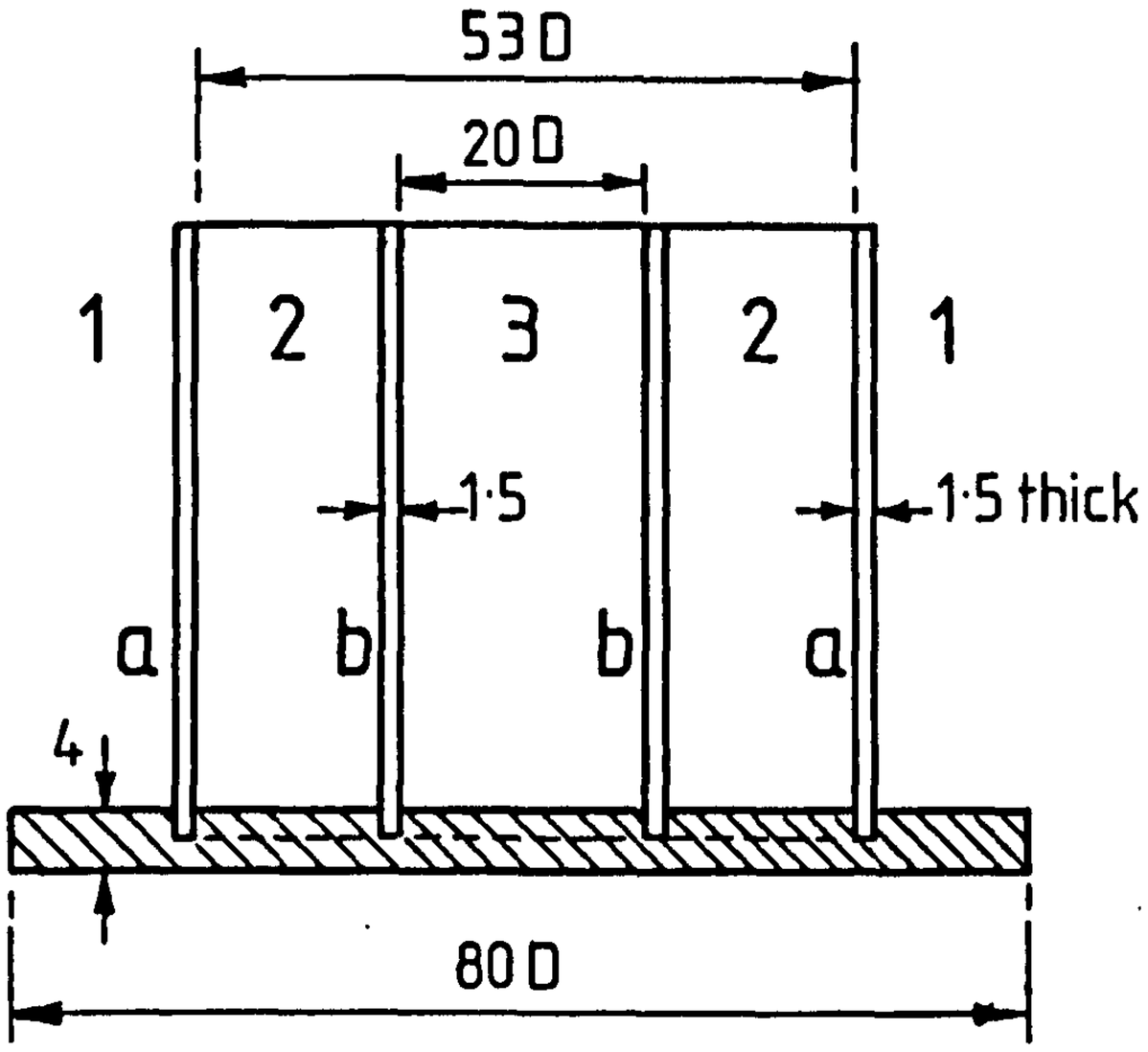

FIG. 2.30 THE CONCENTRIC CYLINDERS AND THEIR ZONES

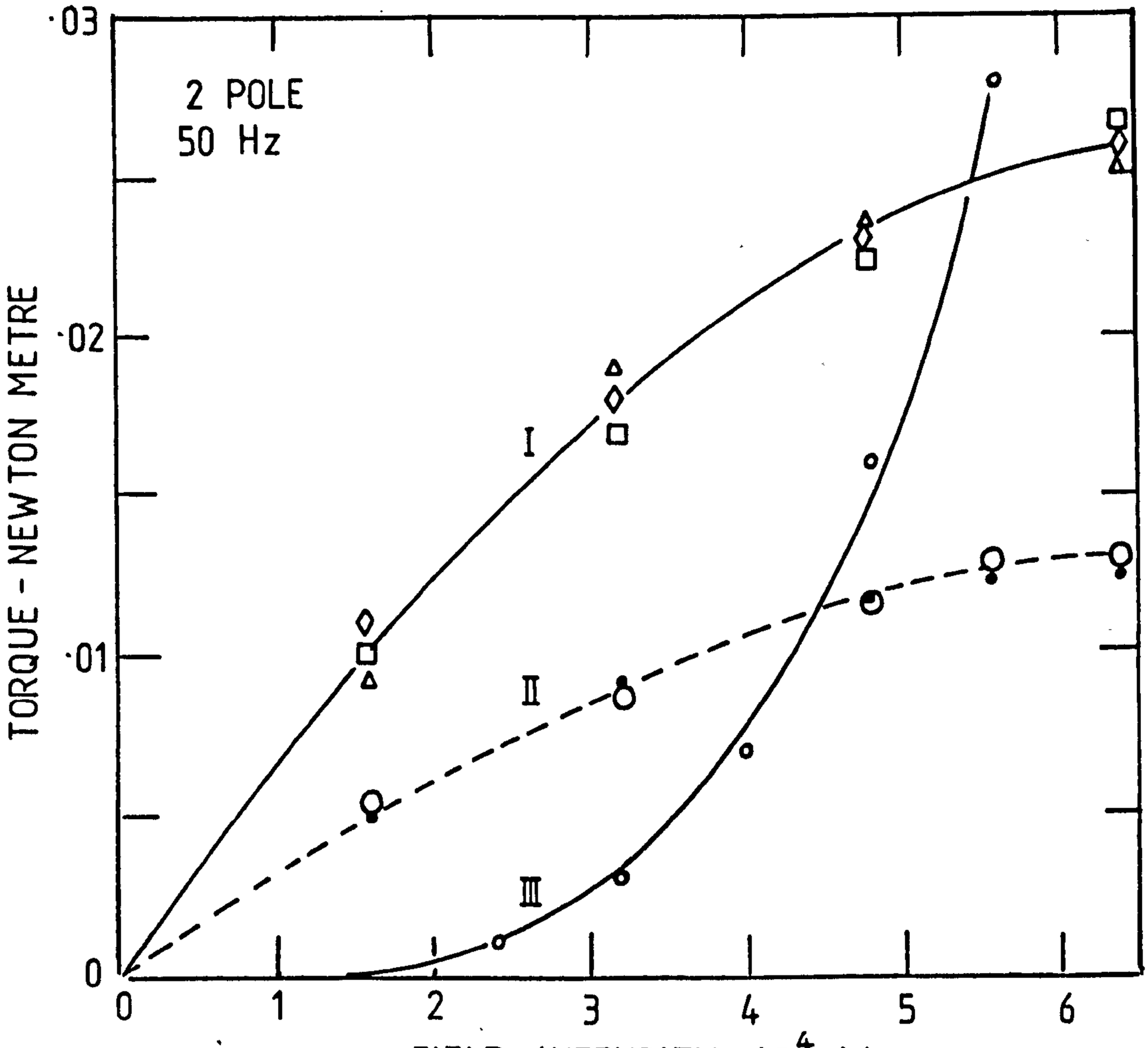

FIG. 2.31 EFFECT OF AREA OF CONTACT ON GENERATED TORQUE

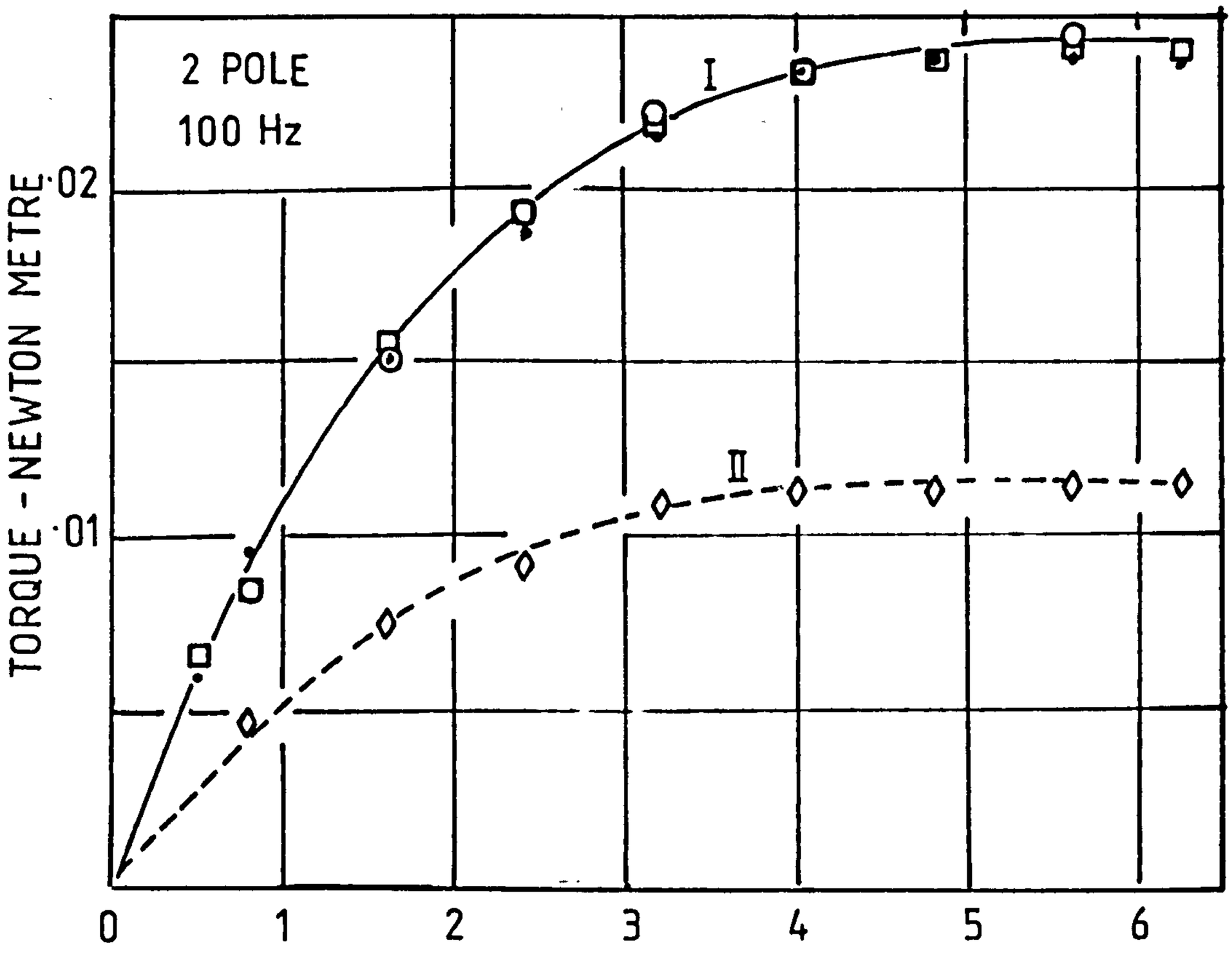

□ ZONES 1 2 & 3 ,

• " " BARRIERS a & b

○ " " BARRIER a

◇ ZONE 1 , " a

FIG. 2.32 EFFECT OF AREA OF CONTACT ON GENERATED TORQUE

40 gms of the magnetic powder added to 150 ml paraffin, 60 ml oil and 9 ml oleic acid. Curve II is for half the amount of this same fluid. In this test the frequency of the supply was 100 Hz.

The results suggest that the torque generated by a given fluid is proportional to its volume. The results also show that the presence of the barriers had no effect upon the torque. Certainly the introduction of these barriers must affect the velocity profile of the fluid, but as the fluid velocity is small in all cases perhaps particles simply adjust themselves to generate a certain amount of torque according to the effective viscosity of the fluid, supply frequency and field intensity.

2.6.4 Dynamic measurements.

When free to rotate the rotor containing ferrofluid was able to accelerate up to the synchronous speed of the wave, ω_o/p, and not to that of the spinning field vector, ω_o.[6] After the rotor had been running for some time, the magnetic particles centrifuged out from the carrier fluid, forming a thin layer adjacent to the wall.

At synchronous speed small load disturbances caused oscillations in rotor speed, suggesting anisotropy due to particle alignment. Larger disturbances caused a temporary loss of synchronism.

The magnetic powder type MO-2035 was used in the preparation of two fluids of different volume loadings. Both the two-pole and the four-pole stators were used in the tests. The torque, for different wave velocities, was measured for various values of rotor speed. In each test the field intensity was kept constant. The results are shown in Figs. 2.33 and 2.34.

In the near-solid condition of the particles which was obtained after the rotor had been running for a length of time, the particles tend to lock together rather than spin and the torque must be of hysteresis origin. Moreover if the fluid carried by the rotor also rotates at the wave velocity, the

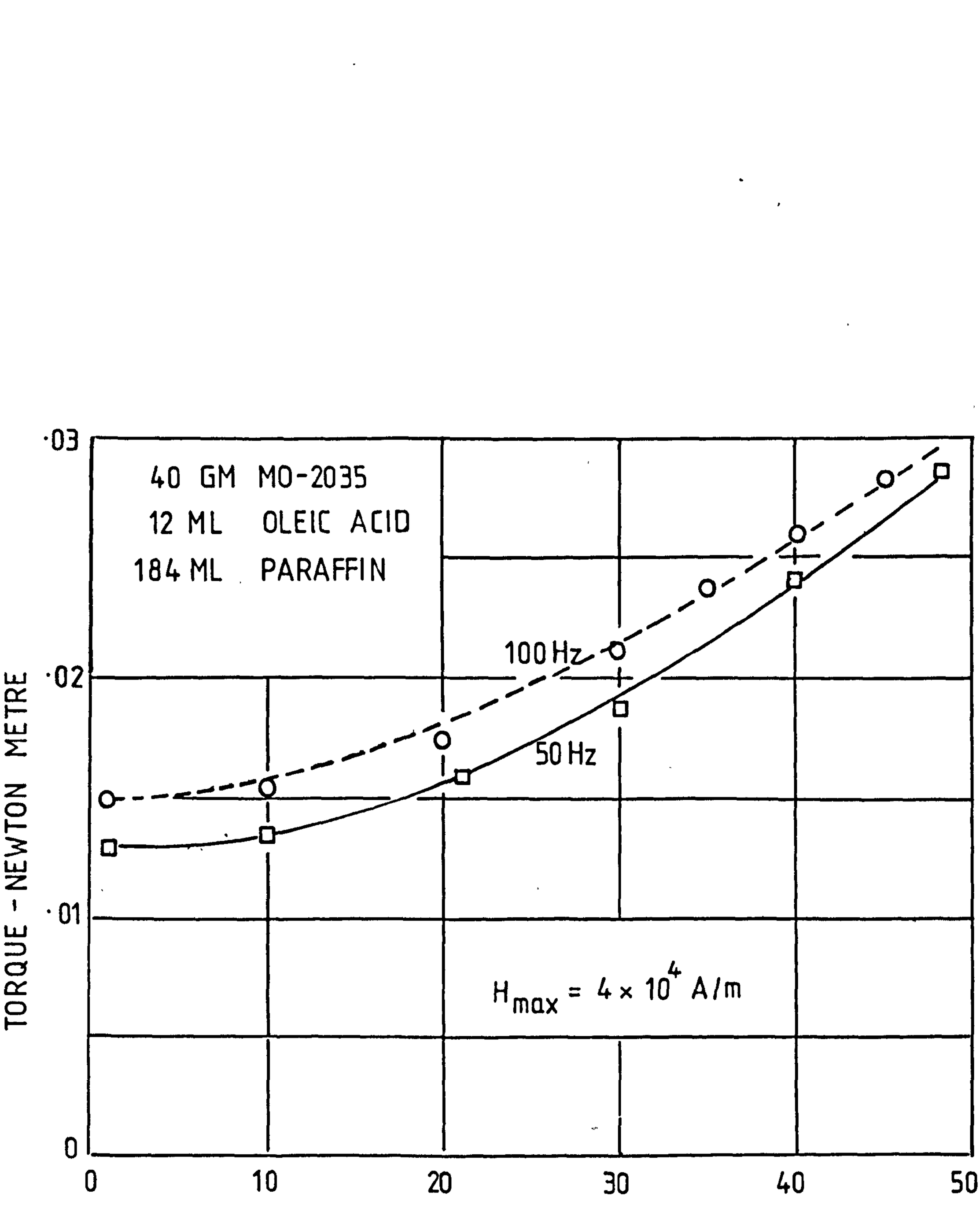

FIG. 2. 33 TORQUE SPEED CHARACTERISTIC – 2 POLE

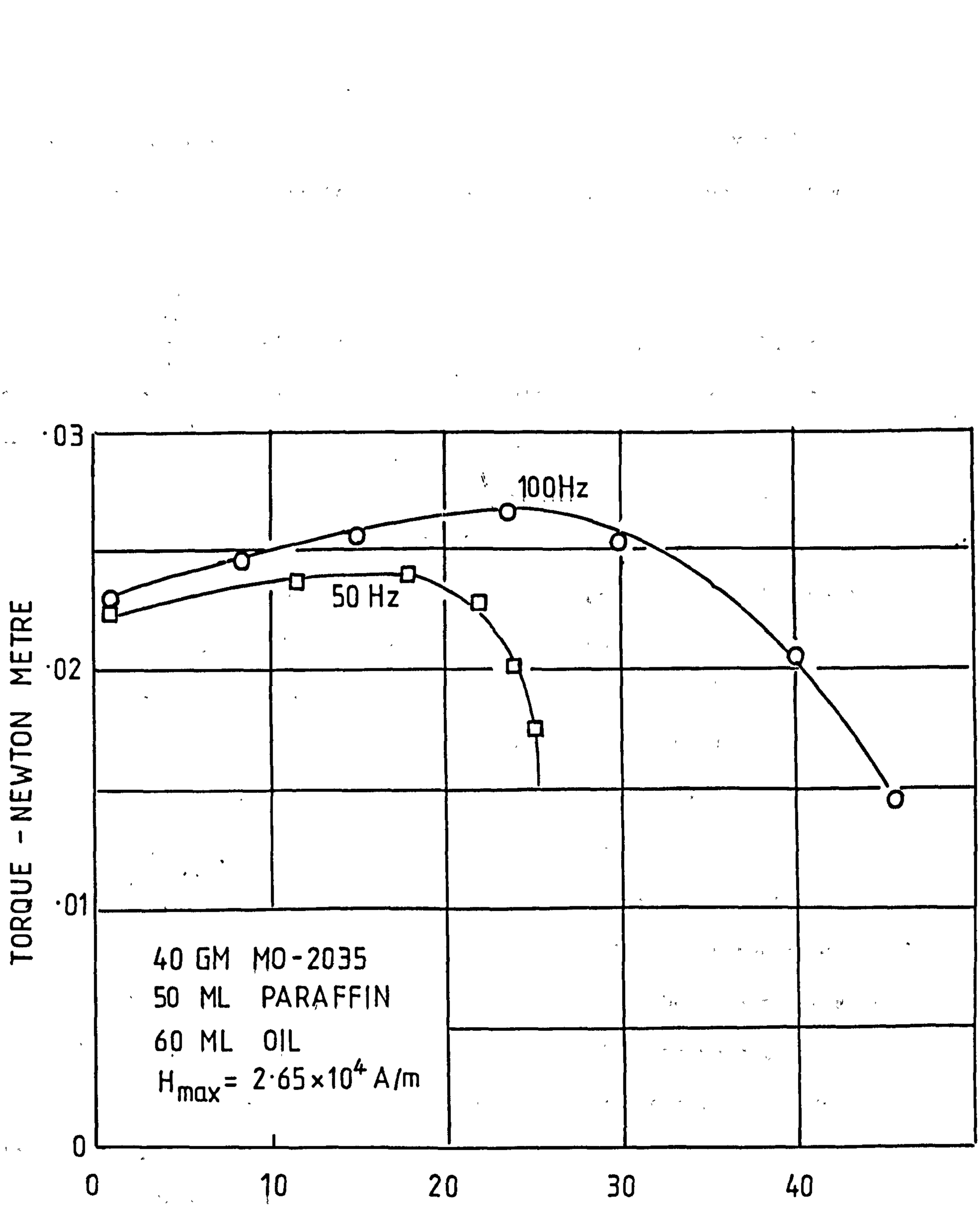

FIG. 2. 34 TORQUE - SPEED CHARACTERISTIC
4 POLE

particles do not need to spin in order to remain in synchronism with the field and no torque can be transmitted by viscous action. This suggests a solid transmission.

In Fig.2.33 the torque increases with speed and just below 50 rev./sec. approaches the value obtained for the solid tests (Fig.2.20). The rise in torque with speed is possibly due to the greater centrifuging effects leading to smaller particle spacings and a greater value of effective viscosity. This seems to be confirmed by the fact that at fixed speed there was a tendency for the torque to slowly increase with time.

In Fig.2.34, the torque at standstill is higher than the solid hysteresis torque (Fig.2.21), and as the rotor speeds up the torque initially increases - again this is believed to be due to an increase in the effective viscosity due to centrifuging. At a given speed it appears that the demanded torque must become equal to the maximum torque that can be generated. Above this speed, an increasing number of particles drop out of synchronism and produce only hysteresis component of torque and the overall torque generated decreases. One might expect the 100 Hz curve to fall off at the same speed, or even at a lower one, as the 50 Hz curve. However, the standstill measurements indicate that the torque does not vary much with frequency, and at 100 Hz the higher spinning energy of the particles may partly overcome the centrifuging effect.

2.6.5 Energy dissipation measurements.

Part of the thermal energy gained by the fluid may be radiated from the stator surface but most results from the viscous drag torque exerted by the parent fluid on the spinning particles. The thermal energy is a loss as far as the separation process, described in section 3, is concerned, and so should be kept as small as possible. The loss may vary with the intensity of the magnetic field, the supply frequency, the size, shape and magnetic

properties of the particles, the viscosity of the carrier fluid and with the volume loading.

Assuming that the rate of generation of thermal energy to be constant (which implies the viscosity of the fluid does not change) the fluid temperature will tend to rise exponentially. The temperature measurements were obtained simply from thermometer readings.

If the fluid is at ambient temperature at time t = 0, the initial rate of rise of temperature will be given by:

$$\frac{\partial \theta}{\partial t} = \frac{P}{C_f}$$

where P is the power generated in unit mass of the fluid and C_f is its specific heat. Thus knowing C_f the specific power loss can be determined from the initial gradient of the temperature rise/time curves.

The specific heat of the fluid can be estimated according to the proportions by weight of the magnetic material and the parent fluid. If the weight ratio is q and their specific heats are C_s and C_ℓ respectively, then

$$C_f = q\, C_s + (1 - q)\, C_\ell .$$

The 11.8 mm diameter two-pole stator was used throughout this investigation. For the 50 Hz tests two values of field intensity were considered i.e. 7×10^4 and 13.2×10^4 A/m, and the fluid tested had 11% by volume of the powder type MO-2035 in paraffin. The temperature rise/time curves are shown in Fig.2.35. The specific heat of this fluid was estimated to be 1620 Joule/Kg.^{o}C. The initial rate of rise of temperature was 0.072^{o}C/S. Therefore the power loss was estimated to be 116.5 watts/kg.

Further tests were carried out on the above 11% fluid at frequencies of 20 and 100 Hz, the field intensity being again 7×10^4 A/m. The power losses from the 20 Hz and 100 Hz tests are compared with the 50 Hz results in Table

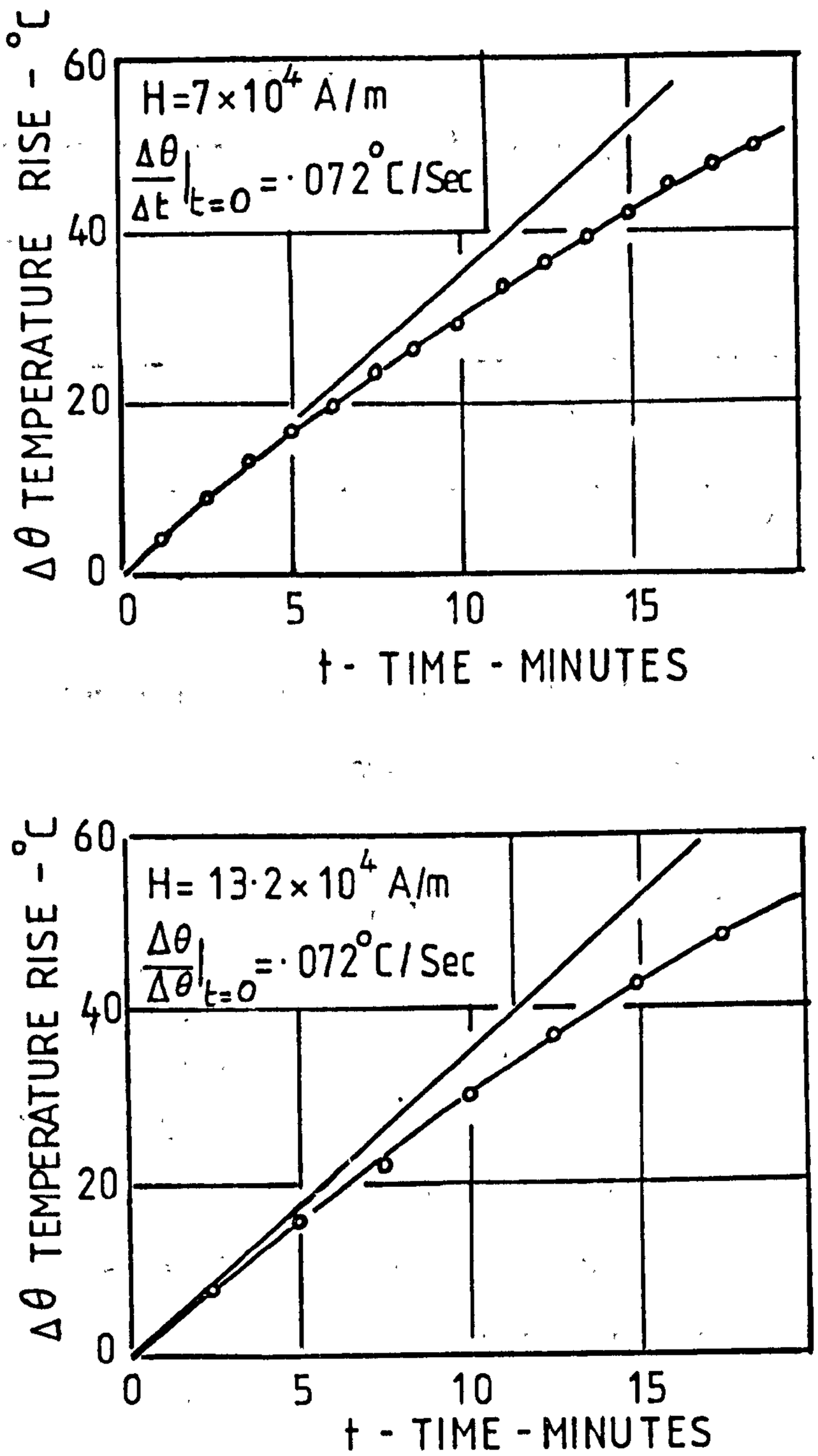

FIG. 2.35 EFFECT OF FIELD INTENSITY ON LOSSES. FREQUENCY = 50 Hz - 11% BY VOLUME OF MO-2035 IN PARAFFIN.

2.2 below. The temperature rise/time curves are shown in Fig.2.36.

Table 2.2

Variation of Power Loss with Frequency

Frequency, f_o, Hz	20	50	100
Power loss, P, Watts/Kg.	44.5	116.5	239
P/f_o	2.22	2.33	2.39

Measurements of the temperature rise/time were carried out on fluids made up from various volume loadings of the magnetic material type MO-2035 in paraffin, (2.64, 5.36, and 8.17%). The maximum field intensity in the two-pole stator was 7×10^4 A/m and the supply frequency was 50 Hz. The results are shown in Fig.2.37.

2.6.6 Discussion of the measurements of the thermal energy generated in the fluid.

It has been shown that the generated torque could be either of hysteresis or saliency origin. The demanded torque is proportional to the spinning velocity of the particles relative to the fluid which is proportional to the supply frequency since the fluid velocity is believed to be small. Since the power is the demanded torque times the spinning velocity, the power loss of the unsynchronized particles (hysteresis torque) should be proportional to the supply frequency. On the other hand those particles which are synchronized (saliency origin torque) should contribute to a power loss proportional to the square of the supply frequency. The results of table 2.2 suggests that the torque is of hysteresis origin. Yet the torque measurements suggest the torque is of saliency origin (at least at low field intensities) and if the particles are synchronized at low intensities of field strength why should they not be synchronized at higher intensities?

The results of Fig.2.37 and 2.38 show that the power loss is roughly proportional to the volume loading at low values. At higher values of volume loading the losses are roughly proportional to K_p^2. It is believed that this is due to the interactions between the eddies produced by adjacent particles.

2.7 Conclusions.

The use of ferrofluids to generate torque seems to be impractical unless for any particular reasons a motor is required which can operate at very low field intensities - at which the generated torque is higher than the hysteresis torque. The motor in this condition would have to run at low speeds so that the particles did not centrifuge to the outside - this would result in a solid outer layer and a smaller torque predominantly of hysteresis origin.

The experimental results confirm that if the fluid is saturated the maximum possible torque per unit volume is proportional to the saturation magnetization of the fluid and is independent of the size of the particles.

The power loss is roughly proportional to the volume loading, K_p, at low values but at high volume loadings the loss increases much more rapidly. The latter is believed to be due to interaction between the eddies produced by adjacent particles. For K_p = 11% of MO-2035, the power loss at 50 Hz is about 0.14 watt per cm^3.

The paradox remains that for the torque generated in the inner region of the fluid to be transmitted to the container the velocity gradient $\frac{\partial \omega}{\partial r}$ must be negative throughout the fluid, which means that the fluid velocity must be more positive near the centre than at the outside - yet the bulk velocity seems to be negative. A possible conclusion is that relative velocity at the container boundary is not zero, but negative - which is not the case for normal Newtonian flow.

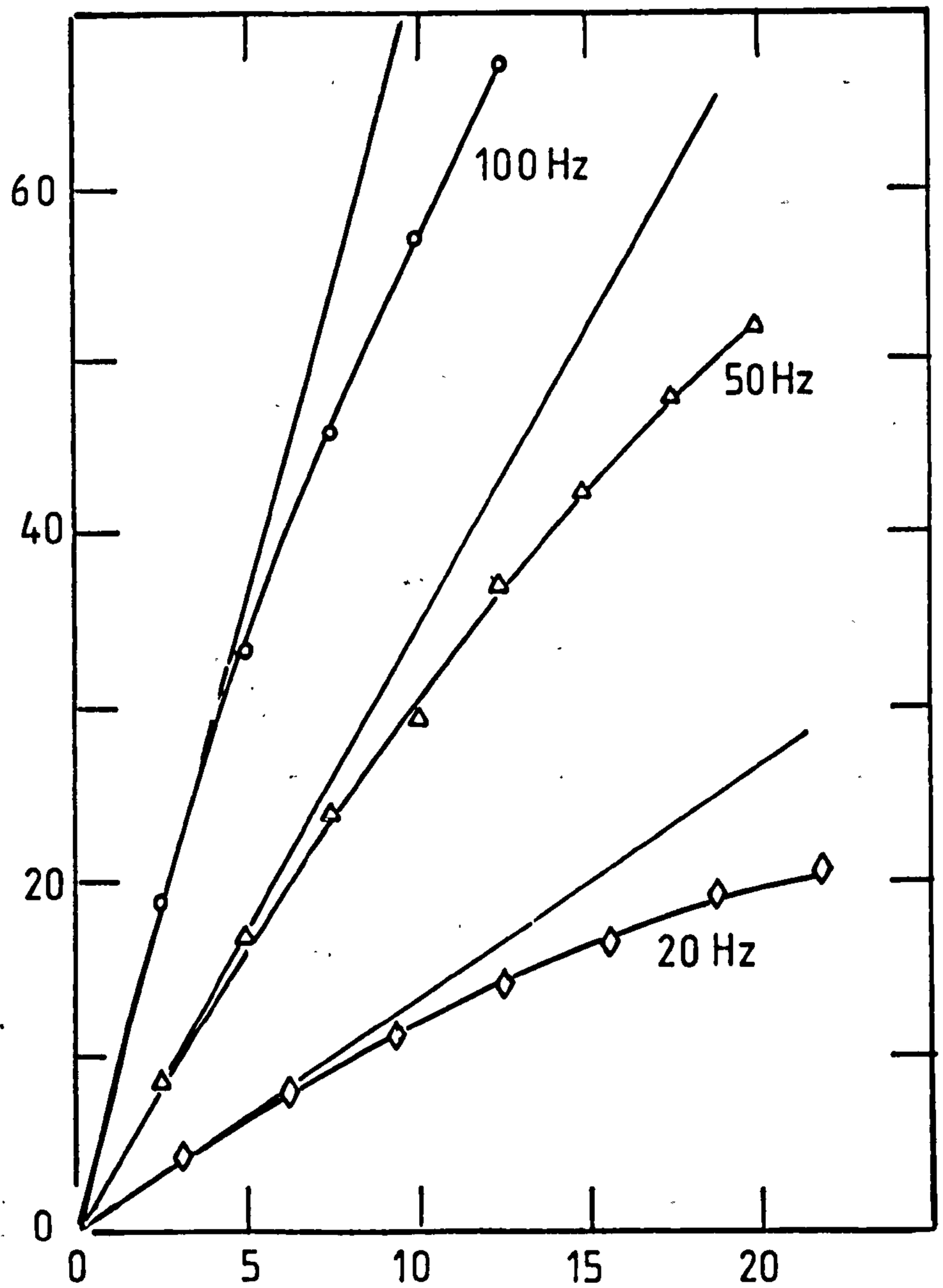

FIG. 2.36 EFFECT OF FREQUENCY ON LOSSES
FIELD INTENSITY = 7×10^4 A/m - 11% BY VOLUME
OF MO-2035 IN PARAFFIN

FIG. 2.37 EFFECT OF VOLUME LOADING ON LOSSES
FIELD INTENSITY = 7×10^4 A/m -
SUPPLY FREQUENCY = 50 Hz

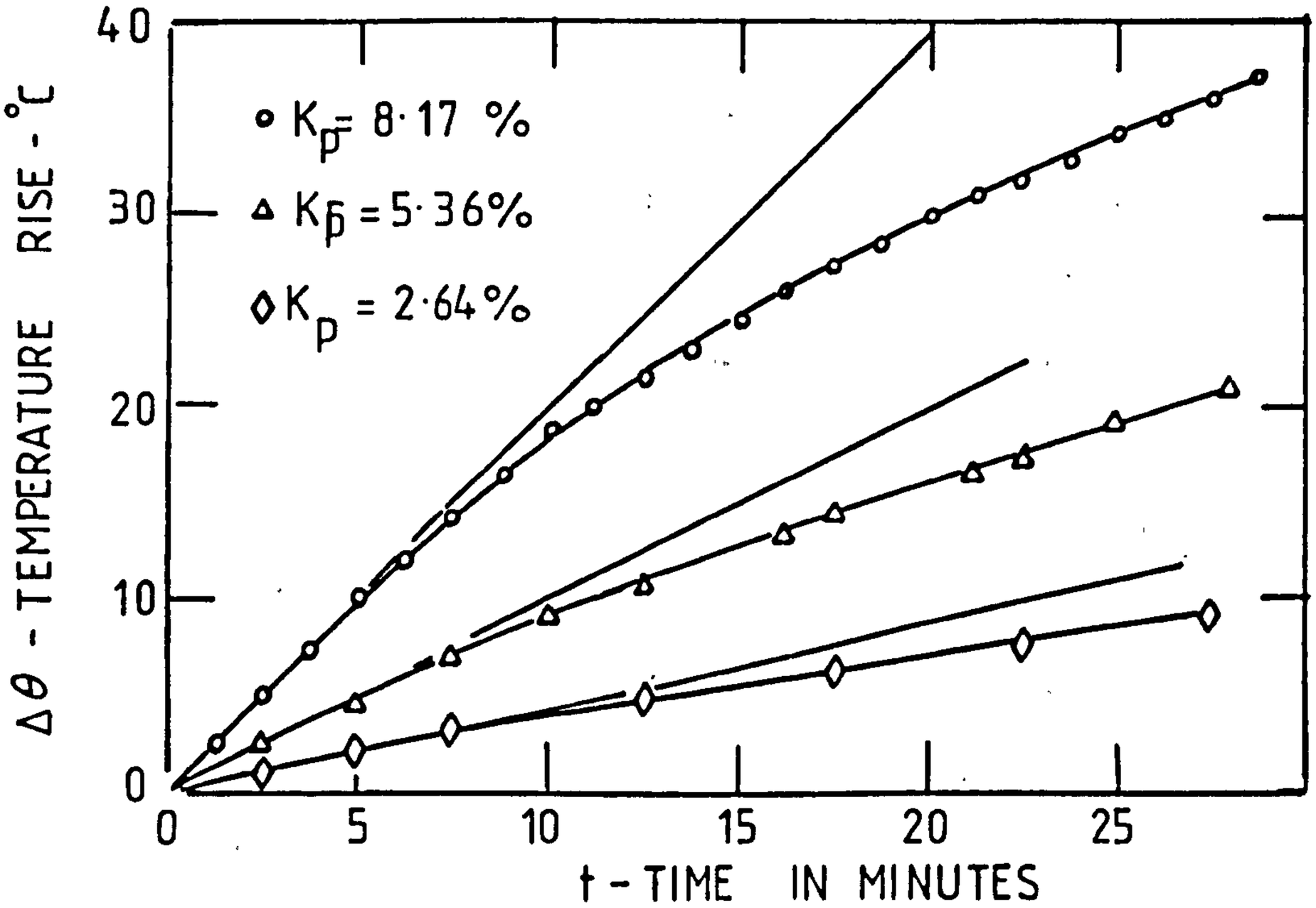

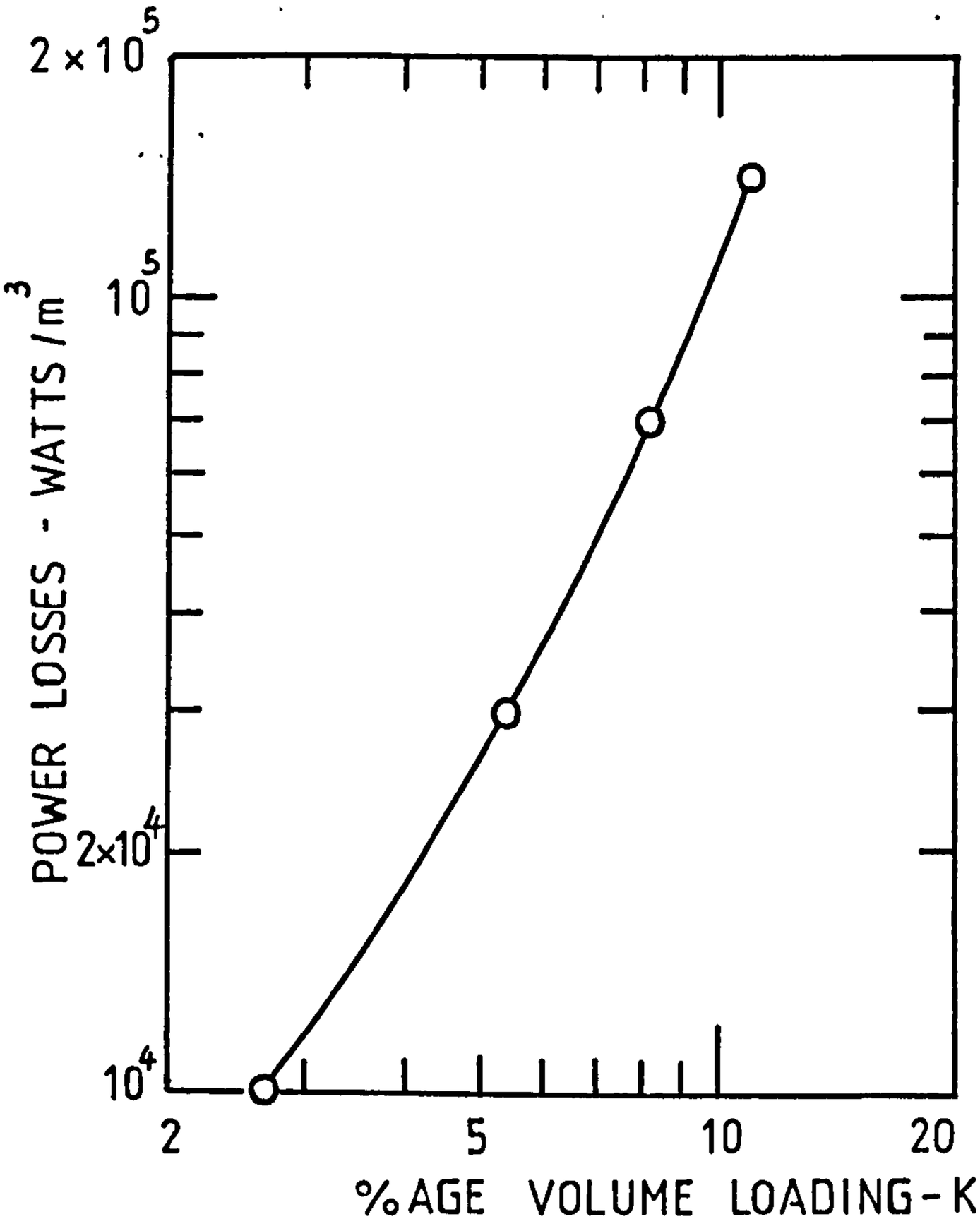

FIG. 2.38 EFFECT OF VOLUME LOADING ON POWER LOSSES

The modified Moskowitz and Rosensweig's approach appeared to satisfy part of the condition for ω to be negative at small radii and the torque still positive. Unfortunately, there is a contradiction between equation 2.3.10 and 2.3.13 since if 2.3.10 exists at outer radii, then 2.3.13 can only exist at radii equal or greater than that of the container boundary. Thus, no really satisfactory mathematical explanation for the fluid rotation being opposite to that of the wave has been found, although in physical terms this seems easy to explain (action and reaction).

The vorticity approach gives the wrong sign of torque. On the other hand, it gives a reasonable explanation for the nonlinear variation of torque with frequency. However, the predicted values of effective viscosity and the number of particles per unit volume obtained by this approach are wrong by several orders of magnitude.

The increase of area of contact between the fluid and its boundaries by introducing barriers inside the fluid did not affect the torque produced, which seems to confirm that the torque generated is a volume effect.

SECTION 3.

THE USE OF FERROFLUIDS, AS A VARIABLE DENSITY MEDIUM, IN MINERAL SEPARATION PROCESSES.

3.1 Introduction.

3.1.1 Some physical means of separation.

There are many bases for separation, some of which will be discussed here:

3.1.1.A On the basis of magnetic permeability.

Magnetic minerals may be separated from non-magnetic minerals by means of an ordinary electromagnet[20]. If the magnet is strong, minerals which are feebly magnetic may also be attracted. If the minerals are feebly magnetic, strong magnetic field is required, which requires a very high powerful magnet, which means high power consumption, or a shorter air gap which makes the throughput smaller resulting in a less efficient apparatus. Various vigorous mechanical means of handling the fractions have been developed.

3.1.1.B On the basis of dielectric properties.

This method of separation is based on the principle that two oppositely charged poles attract each other with a force that varies inversely as the square of the distance between them and depends on the medium. A mineral grain in a medium of a given dielectric constant will be attracted to the electric field between the electrode if it has a constant greater than that of the medium.

Berg[21] placed the mineral in a container and drew from burettes in proportion the desired proportions of furfural and benzene. Needles mounted on an isolated pencil-like handle immersed in the liquid and placed about 1 mm apart served as the electric field needed for separation after connecting them to an electrical source. He decided to use the mixture of furfural and benzene, which have dielectric constants of 42 and 2.28 respectively,

to obtain the desired permitivity of the medium. The grains with a dielectric constant higher than the liquid moved into the area between the needle-points, whereas those with lower constant were repelled. The grains attracted to the points are then transferred to a smaller dish placed in the larger container, the needle-points at all times held in the liquid, by moving the electrodes over the small dish and then withdrawing them from the liquid. When the needles are raised above the liquid, the grains fall off into the smaller dish.

3.1.1.C Electrostatic separation.

Crook[22] used two copper plates, which were separated a small distance by glass insulators. The lower plate was grounded and the upper plate had its lower side shellacked. An induced charge was put on the upper plate. The conductive minerals which were put on the lower plate become negatively charged and are attracted to the upper plate. The shellac keeps the charge from being neutralized. This method is applicable only for small size mineral grains so that the electrostatic force is enough to keep them stuck to the upper plate - for larger grains a higher field is needed. Moreover the grains and the atmosphere must be dry in order to make the method a success.

3.1.1.D Separation on the basis of shape.

By placing the grains on an inclined piece of blotting paper, the micas and fibrous minerals may be made to remain on the paper, while the rest will roll off.

3.1.1.E Separation on the basis of different specific gravities.

In general, this method preceeds the use of electromagnetic, electrostatic and dielectric methods of separation. By placing mineral fragments in a solution whose density is greater than that of one mineral and less than that of another, they may be separated by the floating of the lighter and the

sinking of the heavier material. This method needs a number of solutions some of which could be highly expensive to achieve perfect separation.

3.1.2 Causes introducing errors in separation.

(a) Grains may be made up of more than one mineral which easily influence magnetic and specific gravity separation.

(b) There is always a finite discrimination and minerals lying along the border line of separation may go into either group.

(c) In specific gravity methods and in magnetic separation the mass action effect causes certain minerals to be trapped among separates other than that to which they belong. This effect can usually be overcome by performing at least two operations.

The present investigation makes the change of the specific gravity of one medium, ferrofluid, much easier. By the control of the field intensity and its gradient it is hoped that good mineral separation will be achieved. The method could not be used with magnetic minerals, however.

3.1.3 The method of mineral separation under investigation.

The idea of the magnetic method for separation of nonmagnetic materials, according to their densities is based upon the principle that a magnetic body placed inside a magnetic field tends to move to the region of higher magnetic intensities - a magnetic force being exerted on the body to perform the work necessary to move it to the point of higher magnetic energy. If the field is uniform there will be no energy density gradient and hence no magnetic force. On the other hand if we have a nonmagnetic body placed inside a volume of magnetic material across which there is a field gradient, and if this volume of magnetic material is deformable, i.e. the body can move through it, the body will tend to move from the region of higher magnetic energy density to that of lower energy density. To obtain a deformable magnetic region we must have a magnetic fluid and to get a magnetic energy density gradient we must have a magnetic field gradient.

If the magnetic fluid is a true colloidal suspension, static magnetic fields can be used, but due to the very high costs of the colloidal fluids, at current prices about $1.2 per c.c. for material saturating at about 0.06 T, the process is uneconomic for most large scale applications. If cheaper, non-colloidal magnetic fluids are used the magnetic particles tend to flocculate under the influence of static magnetic fields, and the firm clusters of particles can completely block the passage of the material to be separated. Flocculation of the cheap fluid can be avoided, however, if the individual particles can be made to spin vigorously, and this can be achieved by the use of a suitable rotating magnetic wave[6]. The field distribution can then simultaneously produce spinning vectors and a large energy density gradient.

A conventional a.c. stator is one means of producing a system of spinning vectors, and if the rotor is absent only vectors with the same sense of rotation as the wave can exist, at least inside the stator and away from the ends. Towards the end there is a distinct energy density gradient, and so this was chosen as one configuration to investigate.

Similarly, a single sided linear stator can simultaneously produce vectors with only one sense of rotation and an energy density gradient. By placing two stators with their surfaces facing, but inclined away from each other, as shown in Fig.3.1, the energy density gradient can be made large. On the other hand, this system gives rise to two systems of rotating vectors, and near the plane midway between the two faces the magnitude of the two systems will be almost equal. The result is that there may be a tendency for the individual magnetic particles in this region to flocculate rather than spin and the effective viscosity may become very large. A low viscosity is necessary if the separation rate is to be large.

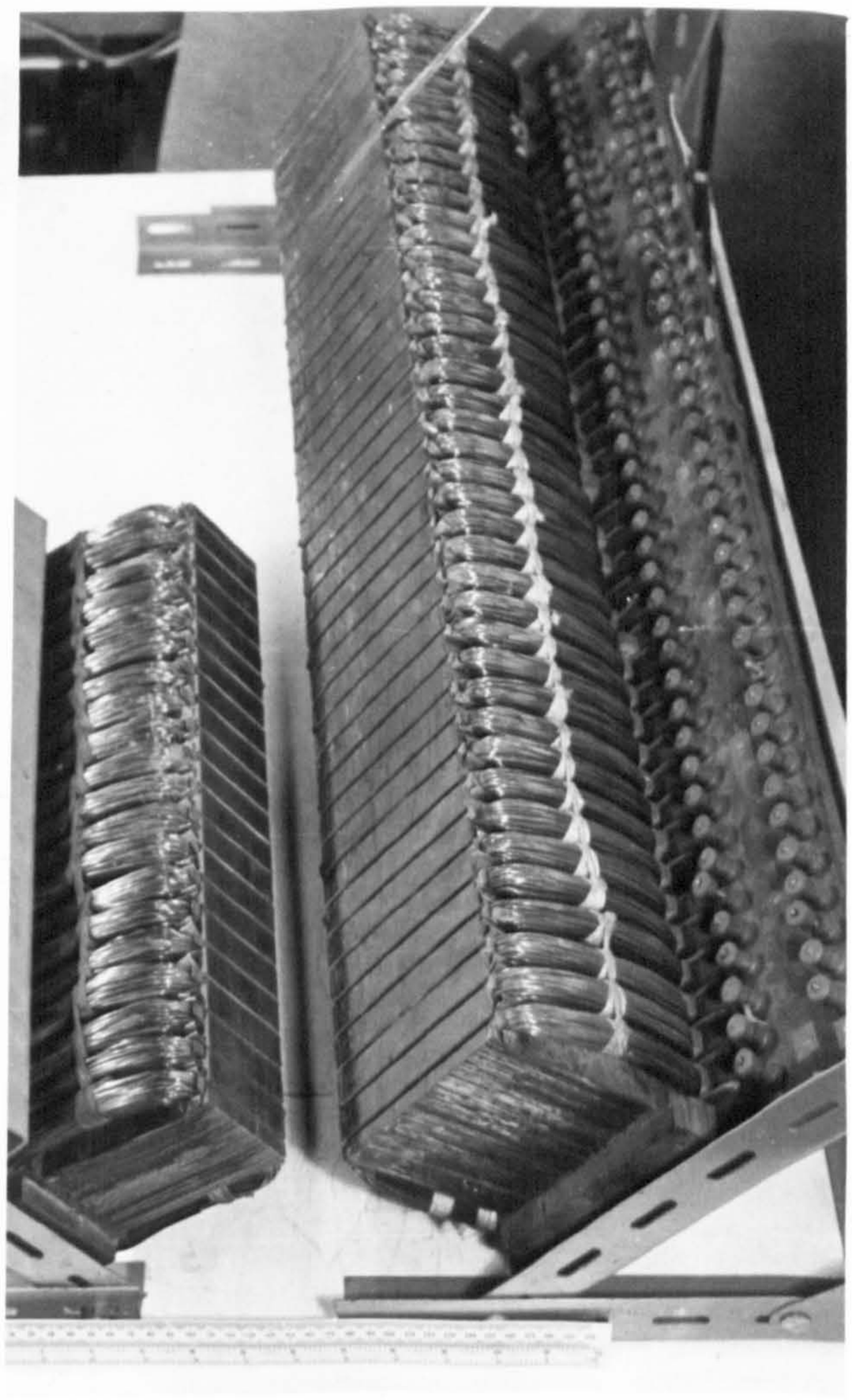

FIG. 3.1a. LINEAR ARRANGEMENT

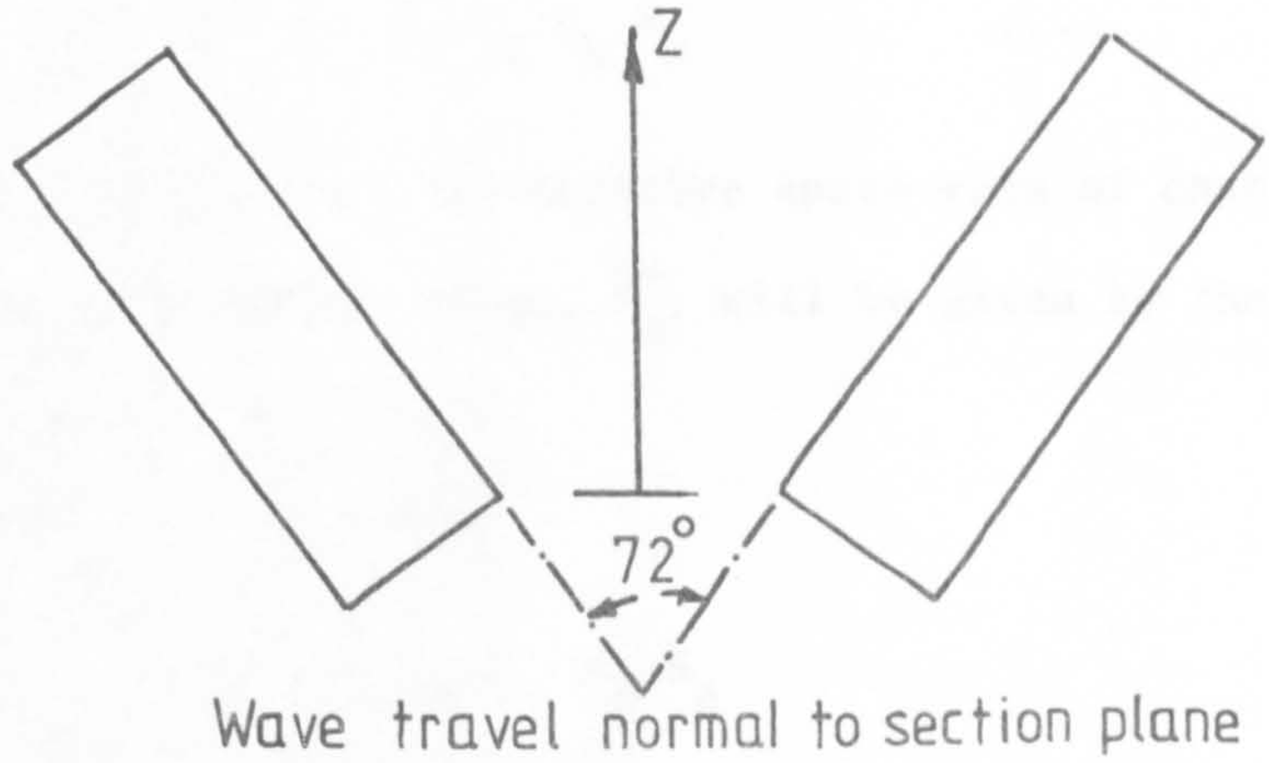

FIG. 3.1b. SECTION THROUGH LINEAR CONFIGURATION

3.2 Theory.

Equation A.1.16 of Appendix 1 shows that a body of permeability μ_i placed in a uniform field H_o in a medium of permeability μ_e will have a dipole moment m_b where

$$\overline{m_b} = \frac{(\text{Volume of body})\ (\mu_i - \mu_e)}{K_z\left[\mu_i + (1/K_z - 1)\ \mu_e\right]} \cdot \overline{H_o}$$

where K_z is a depolarizing factor depending upon the aspect ratio of the body. For a sphere $K_z = 1/3$.

The potential energy, E_m, of a magnetic dipole, $\overline{m_b}$, in a uniform field, $\overline{H_o}$, is given[23] by:

$$E_m = - \mu_o \mu_e \overline{m_b} \cdot \overline{H_o}$$

$$= - \mu_o \mu_e m_b \cdot H_o \cos\theta$$

where θ is the angle between the two vectors $\overline{m_b}$ and $\overline{H_o}$, m_b and H_o are their magnitudes respectively and μ_o is permeability of free space $= 4\pi \times 10^{-7}$. If a principal axis of the body is aligned with the field, θ will be zero and

$$E_m = - \mu_o \mu_e m_b H_o \qquad \ldots\ldots \qquad 3.2.1$$

The force is defined as the negative space rate of change of the potential function, hence the magnetic force, $\overline{F_m}$, will be given by the negative gradient of the scalar function E_m, thus,

$$\overline{F_m} = - \nabla E_m$$

$$= \mu_o \mu_e \nabla\ m_b H_o$$

$$= \frac{(\text{volume of the body})\ (\mu_i - \mu_e)}{K_z\left[\mu_i + (1/K_z - 1)\ \mu_e\right]}\ \nabla\ \left(\frac{\mu_o \mu_e}{2}\ H_o^2\right)$$

$\ldots\ldots$ 3.2.2

If the densities of the body and fluid are ρ_i and ρ_e, the net vertical ($\ddot{z}$) and horizontal ($\ddot{x}$) components of acceleration (neglecting viscosity) are given by:

$$\ddot{z} = \frac{(\mu_i - \mu_e)}{\rho_i K_z \left[\mu_i + (1/K_z - 1)\mu_e\right]} \frac{\partial}{\partial z} \left(\frac{\mu_o \mu_e}{2} H_o^2\right) - g\left(1 - \frac{\rho_e}{\rho_i}\right) \quad \ldots\ldots \quad 3.2.3$$

where g is the gravitational constant.

$$\text{and } \ddot{x} = \frac{(\mu_i - \mu_e)}{\rho_i K_z \left[\mu_i + (1/K_z - 1)\mu_e\right]} \frac{\partial}{\partial x} \left(\frac{\mu_o \mu_e}{2} H_o^2\right) \quad \ldots\ldots \quad 3.2.4$$

From equation 3.2.2, the magnetic force density ρ_m is given by:

$$\rho_m = \frac{(\mu_i - \mu_e)\ \mu_e}{K_z \left[\mu_i + (1/K_z - 1)\mu_e\right]} \nabla \left(\frac{\mu_o}{2} H_o^2\right) \quad \ldots\ldots \quad 3.2.5$$

Since $\mu_i = 1$ for a nonmagnetic body, for a given field and field gradient, the magnetic force density is proportional to the figure of merit X

where
$$X = \frac{\mu_e (1 - \mu_e)}{K_z + (1 - K_z)\mu_e} \quad \ldots\ldots \quad 3.2.6$$

The condition for a maximum X is that

$$\mu_e = \frac{-K_z \pm \sqrt{K_z}}{1 - K_z}$$

The negative sign of $\sqrt{K_z}$ does not fulfil the condition that μ_e must be positive, as $K_z < 1$, therefore

$$\mu_{e_{max}} = \frac{-K_z + \sqrt{K_z}}{1 - K_z} \quad \ldots\ldots \quad 3.2.7$$

Equation 3.2.7 gives a positive value of $\mu_{e_{max}}$ which is less than unity, i.e. the maximum would occur only for a diamagnetic fluid. However, it will be seen from Fig.3.2, plotted for a spherical body (i.e. $K_z = \frac{1}{3}$), that if a negative value of X is acceptable, which it is, then the positive maximum is exceeded by the magnitude of the negative value for μ_e greater than about 1.4. In this negative region, where $\mu_e > 1$, X is more or less linearly proportional to $(\mu_e - 1)$, so the higher $(\mu_e - 1)$, the higher the magnitude of X and of the effective magnetic density, ρ_m.

Fig.3.3 shows a curve of K_z for a prolate spheroid as the aspect ratio b/a is varied[26], and corresponding curves of $|X|$ for $\mu_e = 1.5$, 1.75 and 2.0. For the lower value of μ_e it will be seen that the aspect ratio has little effect upon the value of X, and thus of ρ_m. This suggests that at low values of μ_e, e.g. $\mu_e \leq 1.75$ the effective magnetic density as seen by a submerged body may be relatively independent of the shape of the body. This is, of course, a very desirable feature from the point of view of separation of materials according to their densities.

From equation 3.2.5, the magnetic force density ρ_m, for a spherical body, is given by:

$$\rho_m = \frac{3\,(\mu_i - \mu_e)\,\mu_e}{\mu_i + 2\,\mu_e} \nabla \left(\frac{\mu_o}{2} H_o^2\right)$$

where $\mu_i = 1$, for a non-magnetic body and μ_e is the permeability of fluid = 1 + the susceptibility χ.

Along the z - axis the magnitude of the magnetic force density $|\rho_m|$ is given by

$$\rho_m = \frac{3\,\mu_o\,\chi\,(1 + \chi)}{3 + 2\chi} H_o \cdot \frac{\partial H_o}{\partial z} \qquad \ldots\ldots\ldots \qquad 3.2.8$$

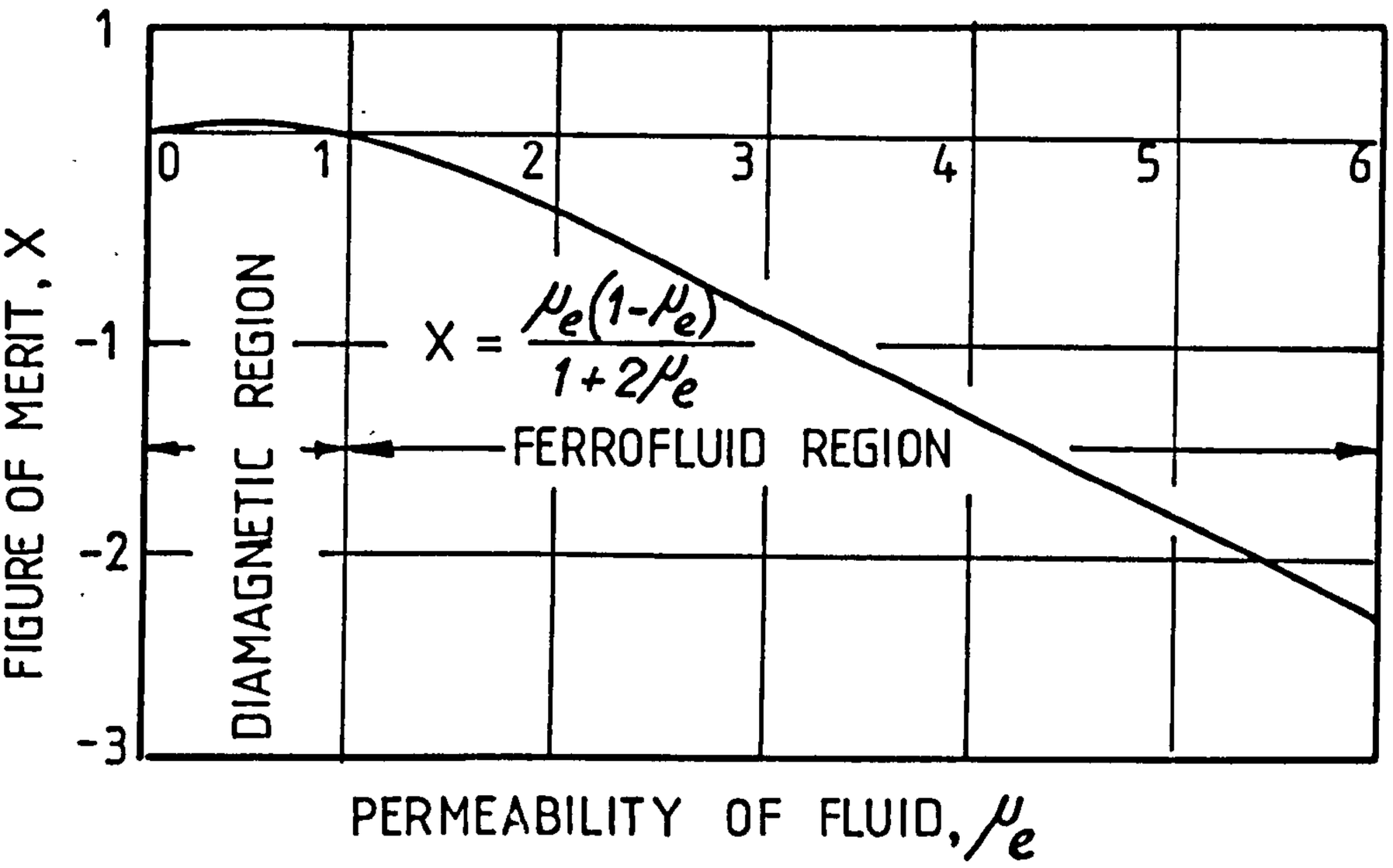

FIG. 3.2 VARIATION OF THE FIGURE OF MERIT X WITH THE PERMEABILITY OF FLUID FOR A SPHERICAL BODY.

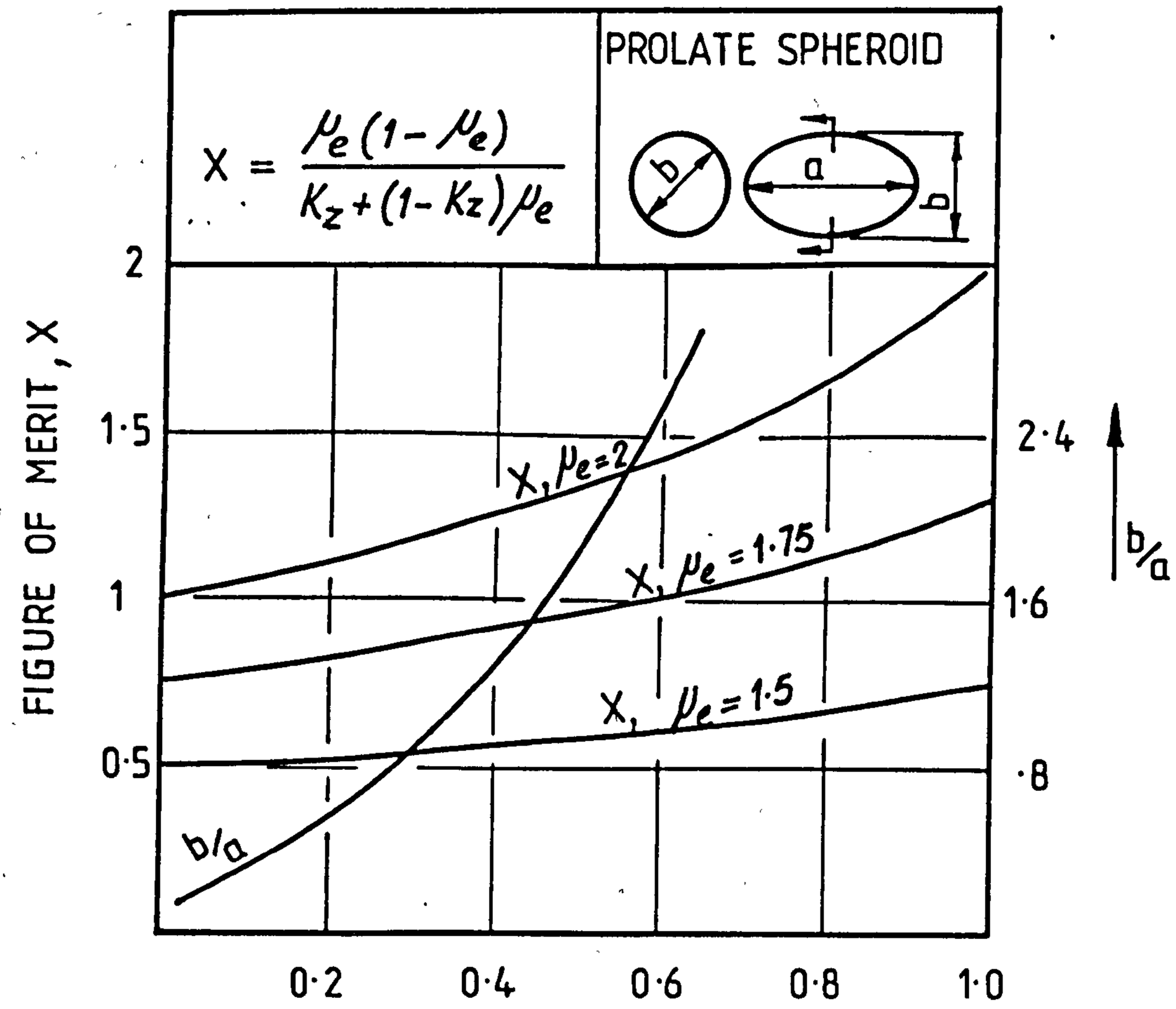

FIG. 3.3 VARIATION OF X WITH K_z AND μ_e & VARIATIONS OF K_z WITH ASPECT RATIO OF A PROLATE SPHEROID

This is valid only if the fluid is unsaturated.

If the fluid is saturated, the magnetization of the fluid is constant and equation 3.2.8 is no longer valid. In that case

$$\rho_m = \mu_o M_{sat} \frac{\partial H_o}{\partial z} \quad \ldots\ldots \quad 3.2.9$$

where $\mu_o M_{sat}$ is the saturation magnetization of the fluid.

3.3 Experimental Work.

3.3.1 Preliminary investigation.

In the preliminary investigation of the magnetic forces available for the separation process, the two pole a.c. stator used in the investigation of the ferrofluid motor was used. The nonmagnetic body was a plastic ball of diameter 20 mm filled with heavy material such as sand or powdered lead bromide. The fluid under investigation, which had a volume loading of 5.36% of MO-2035 in paraffin, was put in a jar which was positioned symmetrically inside the magnetic field.

To measure the force acting on the ball, it was simply suspended from the hook of a spring balance, as shown in Fig.3.4. Knowing the weight of the body, the force exerted by the fluid can be determined from the deflection of the balance. For the position at which the ball was just above the bottom of the fluid the position of the clamp with respect to the scale of the stand was marked. The clamp was then raised a distance X to adjust the position of the ball inside the fluid. Upon applying the magnetic field, the deflection of the balance changed and so the position of the centre of the ball was no longer X above the reference mark. The ball could be returned to the original position, however, by correcting for the amount of contraction or extension of the spring, and thus a series of measurements can be carried out with the ball in one fixed position. The magnetic force, and the magnetic force per unit volume (magnetic force density) can readily

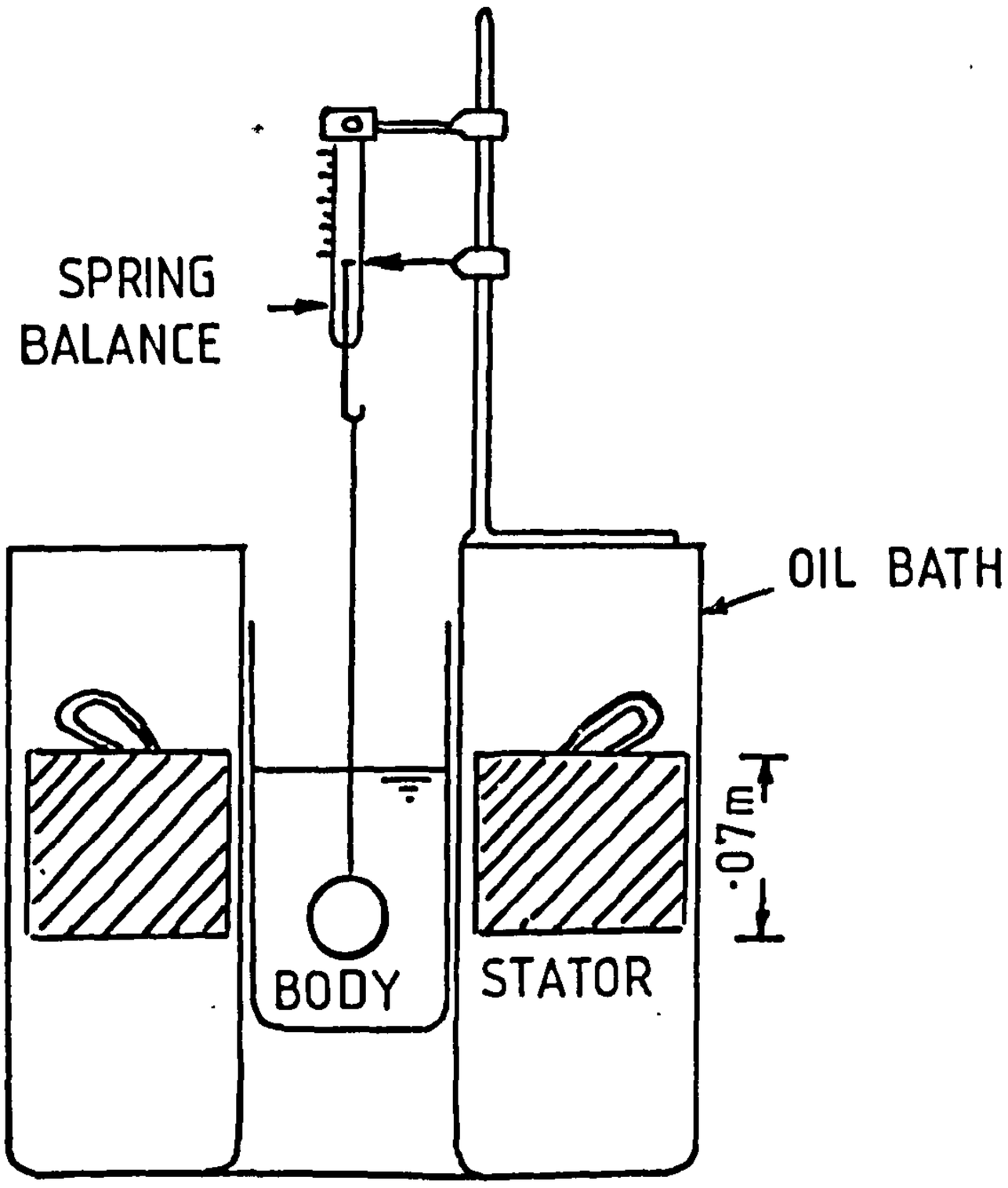

FIG. 3.4 SCHEMATIC DIAGRAM OF THE ARRANGEMENT FOR THE MEASUREMENT OF MAGNETIC FORCE.

be determined by allowing for the normal unmagnetised density of the fluid.

The field intensity was measured by measuring the radial component of the flux density, using a flat Hall probe, at various positions on the axis of the stator (on the axis $H_z = 0$ and H_r and H_θ are equal in magnitude).

From equation 3.2.5, the magnetic force should be proportional to $\frac{\partial(\frac{1}{2} H_o^2)}{\partial z}$ i.e. $H_o \frac{\partial H_o}{\partial z}$, if the medium is unsaturated. The values of $H_o \frac{\partial H_o}{\partial z}$ were estimated from the Hall probe measurements, shown in Fig.3.5 and are plotted against force per unit volume of the ball in Fig.3.6. This graph shows that the magnetic force is linearly proportional to $H_o \frac{\partial H_o}{\partial z}$, showing no sign of saturation over the test range

The maximum field intensity in the test was 4.2×10^4 A/m. There was a need for much higher field strength to obtain higher values of effective densities, possibly using less concentrated fluids. Unfortunately, the simple method of removing heat from the oil by means of passing cold water through coils of copper tubing immersed in it was not adequate and the winding insulation broke down. The cooling system was then redesigned, and to cope with a considerably increased power rating to the rewound stator a commercial heat exchanger was installed external to the oil bath. For a temperature difference of 40° C between water and oil inlet temperature and an extraction rate of 20 KW the oil flow was specified as 45 litres/minute, so an oil pump was incorporated in the system. The specified water flow rate of 26.6 litres/minute was obtained direct from the main water supply. A new oil-bath was also obtained and this had much greater space of oil flow past the stator windings than the previous one. The flow of oil was directed to penetrate the coil using flow guides. The level of the inlet pipe of oil

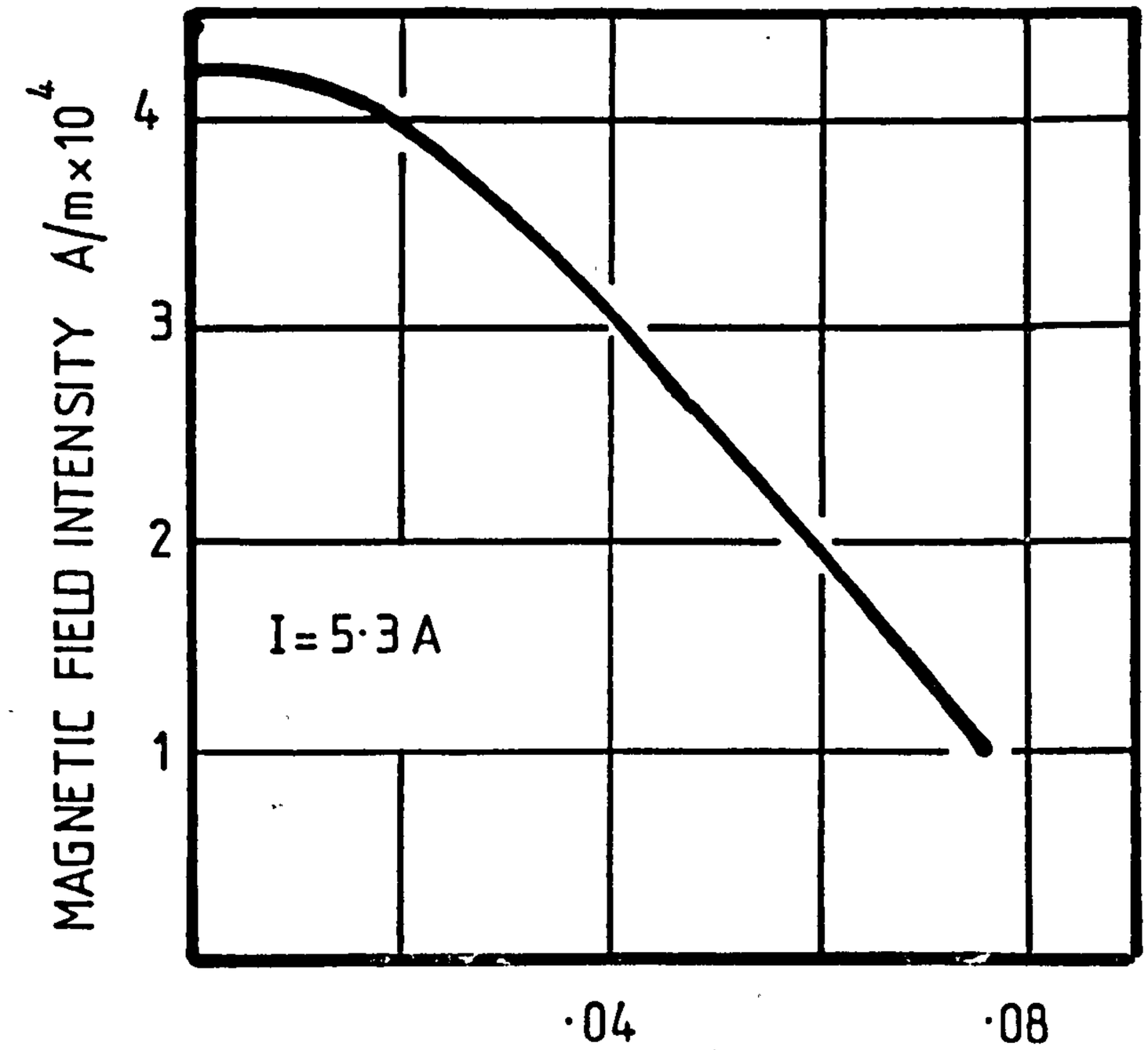

FIG. 3.5 FIELD DISTRIBUTION OF THE 118mm DIAMETER TWO POLE STATOR FOR PRELIMINARY INVESTIGATION.

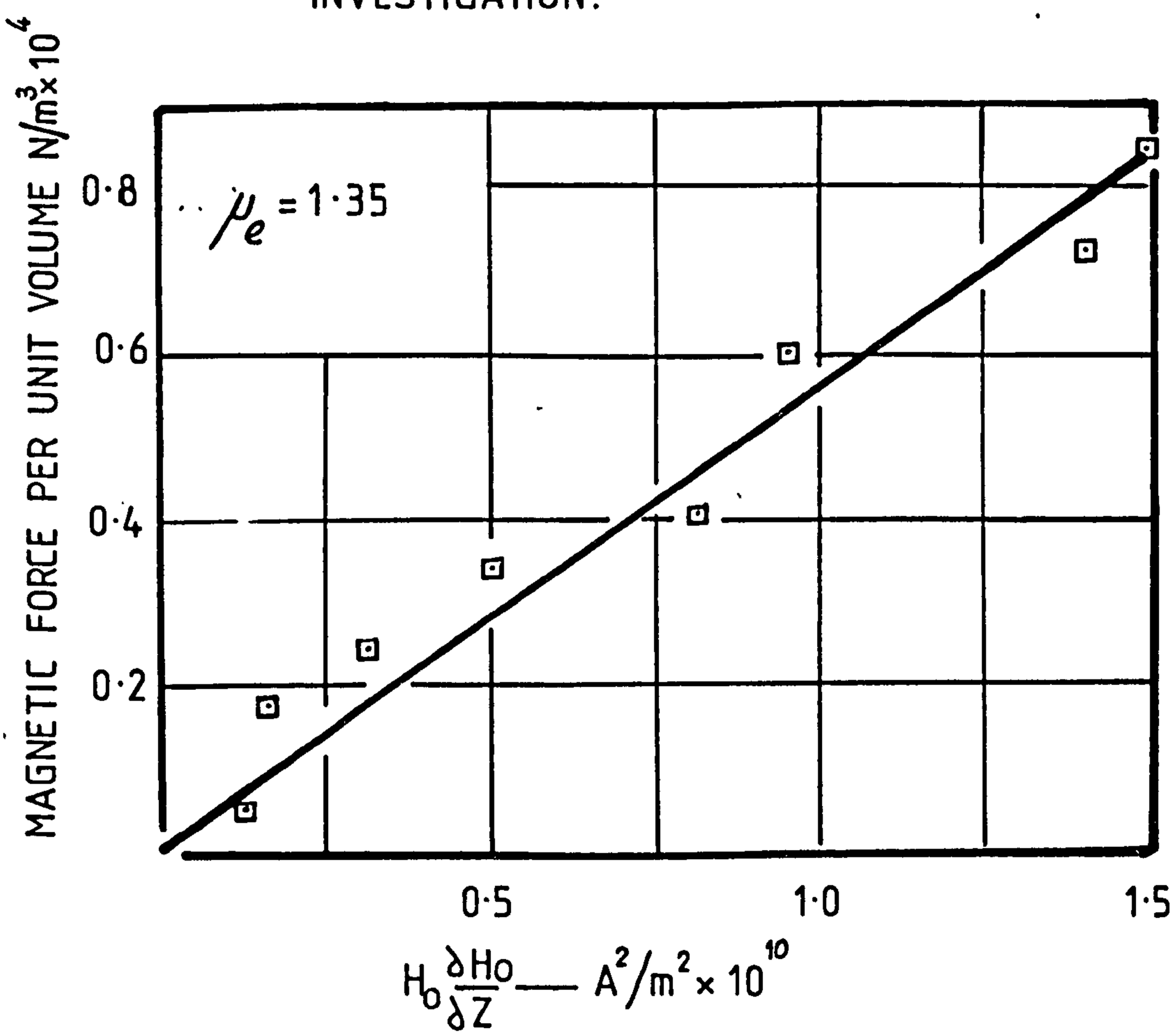

FIG. 3.6. VARIATION OF MAGNETIC FORCE DENSITY WITH $H_o \frac{\delta H_o}{\delta Z}$ — 118 mm DIAMETER TWO-POLE STATOR FLUID UNMAGNETIZED DENSITY = 0·98

to the tank was positioned to supply the cold oil at the bottom of the water stack while the outlet opening was just above the top of the winding, i.e., the forced flow was in the direction of normal convection. Fig.3.7 shows a schematic diagram of the new cooling system while a photograph of the equipment is shown in Fig.3.8.

Since the stator winding was twice damaged by overheating, with consequent delays in waiting for rewinding, another two-pole stator was acquired. This had a diameter of 140 mm and a stack length of 120 mm, compared to the original stator's 118 mm diameter and 70 mm stack length.

The average temperature of the winding was determined by comparing its resistance, at the temperature to be determined, with its resistance at a known temperature. Extreme care was taken to secure accurate resistance measurements because a small error will cause a comparatively larger error in the calculated temperature. The cold resistance was measured only after the motor had remained in a constant ambient long enough that the winding was at that ambient temperature. Resistance measurements were made as outlined in AIEE test code No. 550, May, 1949.

It was found that the steady state temperature of the 118 mm stator was 120^{o} at an excitation current of 19 A per phase and this brought the magnetic field intensity up to 15.3×10^{4} A/m in the middle of the stack. On the other hand the steady temperature of the 140 mm stator was 115^{o} C at an exciting current of 27 A per phase and this excitation brought the magnetic field intensity up to 12.66×10^{4} A/m in the middle of the iron stack.

3.3.2 The power supply.

In addition to 50 Hz measurements, using both stators, tests were carried out using the 118 mm stator, at 20 Hz and 100 Hz.

For 50 Hz excitation the power was obtained from the a.c. mains via a variac. To reduce the current loading of the variac the stators, connected in delta, had 50 μF, 500 V capacitors across each phase.

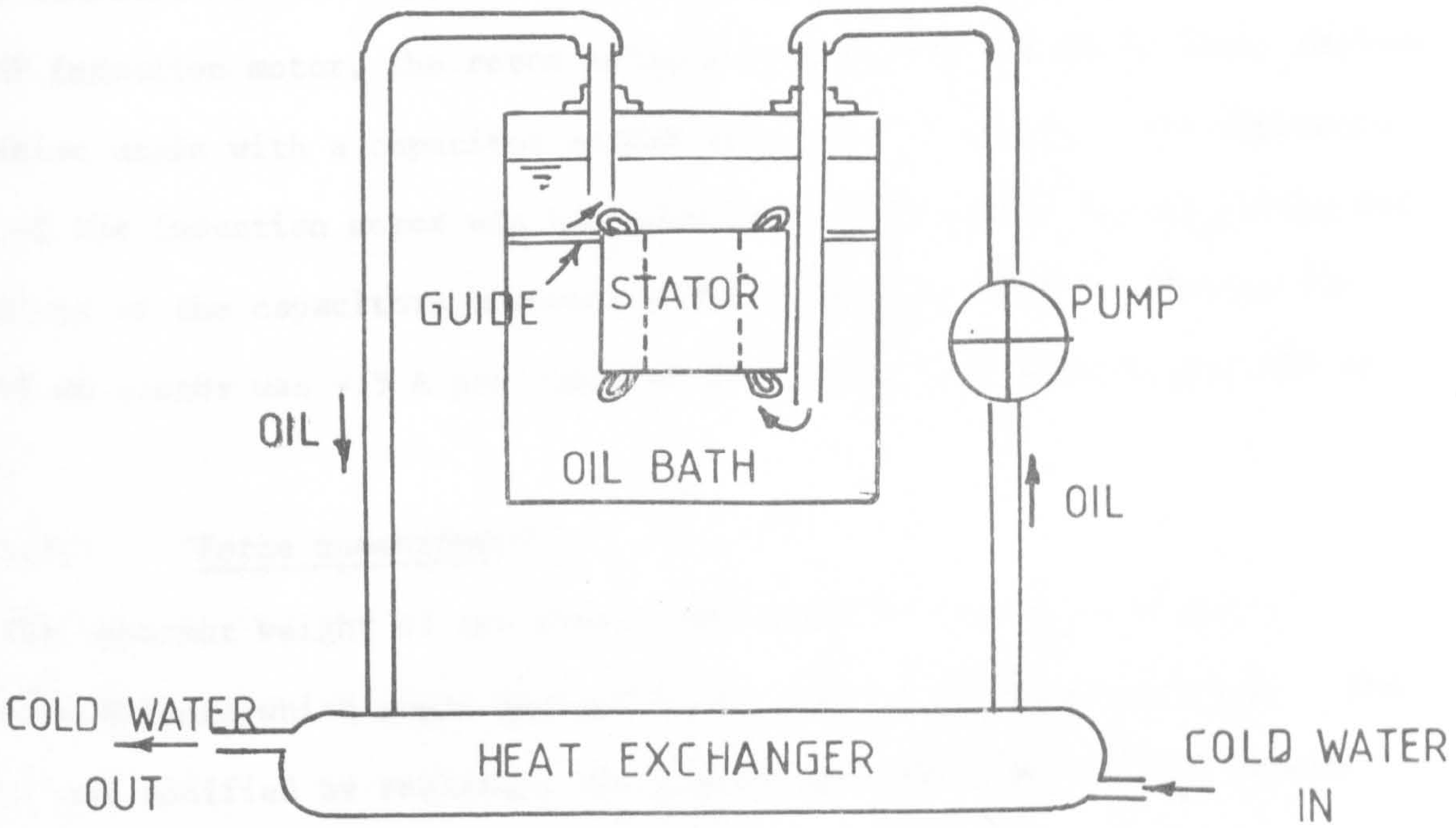

A FIG. 3.7 SCHEMATIC DIAGRAM OF NEW COOLING SYSTEM

FIG. 3.8 NEW COOLING RIG

For the 20 Hz and 100 Hz measurements, which were carried out on the 118 mm diameter stator only, the frequency changing was achieved by using a 25 HP induction motor, the rotor being supplied from the 50 Hz mains through the variac again with a capacitor across each pair of lines. The impedance level of the induction motor was not ideally matched to the variac rating and the values of the capacitors however, and the maximum value of current for the 118 mm stator was 9.5 A per phase at 20 and 100 Hz compared with 19A at 50 Hz.

3.3.3 Force measurements.

The apparent weight of the nonmagnetic body was measured with a sensitive balance which could measure up to 4.01 Kg and down to 0.1 g. The balance was modified by replacing the pan with an attachment whose length could be varied to suit the required position of the body. The body was hung from this attachment via a ball race to prevent the tangentional component of force, due to the spinning of the body, from affecting the balance lever.

3.3.4 The main factors to be investigated.

Among the factors that were to be investigated were the effect upon the magnetic force density of:-

(i) axial position of the body.

(ii) distribution and intensity of the magnetic field.

(iii) the volume concentration of the magnetic material in the fluid.

(iv) frequency of the supply.

(v) the shape of the body.

Equally important, however, was to compare the performance of different cheap magnetic powders, and of water compared with paraffin as a carrier fluid.

The greatest range of measurements were carried out on the 118 mm diameter stator, the tests on the 140 mm diameter stator being restricted to various concentrations of the Pfizer powder MO-2035 in paraffin and to 50 Hz.

3.3.5 Variation of magnetic force with axial position and field intensity.

With the exception of a few tests to determine the effect of body shape and the proportionality between magnetic force and the volume of the immersed body, for a given shape, (results not given), the nonmagnetic body was a hollow glass ball of volume 8.1 c.c. The apparent weights of the body submerged in the fluid under various magnetic field intensities and axial positions were measured and knowing the actual weight of the body and the nonmagnetized fluid density, the magnetic forces and from these the magnetic force densities (the magnetic forces divided by the volume of the body) were determined. Four fluids having volume concentrations of the magnetic material type MO-2035 in paraffin of 2.64, 5.36, 8.17 and 11% were investigated. The surfactant was oleic acid. The body was always on the axis of the stator. Figs. 3.9 and 3.10 show sample of results of the variation of the magnetic force density with the distance, z, along the axis from the middle of the machine for each fluid under the various field intensities.

3.3.6 Influence of frequency upon the magnetic force.

The magnetic force densities for a supply frequency of 50 Hz were compared with those for two other frequencies 20 and 100 Hz at the same value of field intensity 7.7×10^4 A/m. The fluid had a volume concentration of 11% of MO-2035 in paraffin. The results are shown in Fig.3.11.

3.3.7 Influence of body shape upon the magnetic force.

Measurements were also made of the magnetic forces exerted by a fluid made up of 11% volume loading of the Pfizer powder, type MO-2035, upon a nonmagnetic

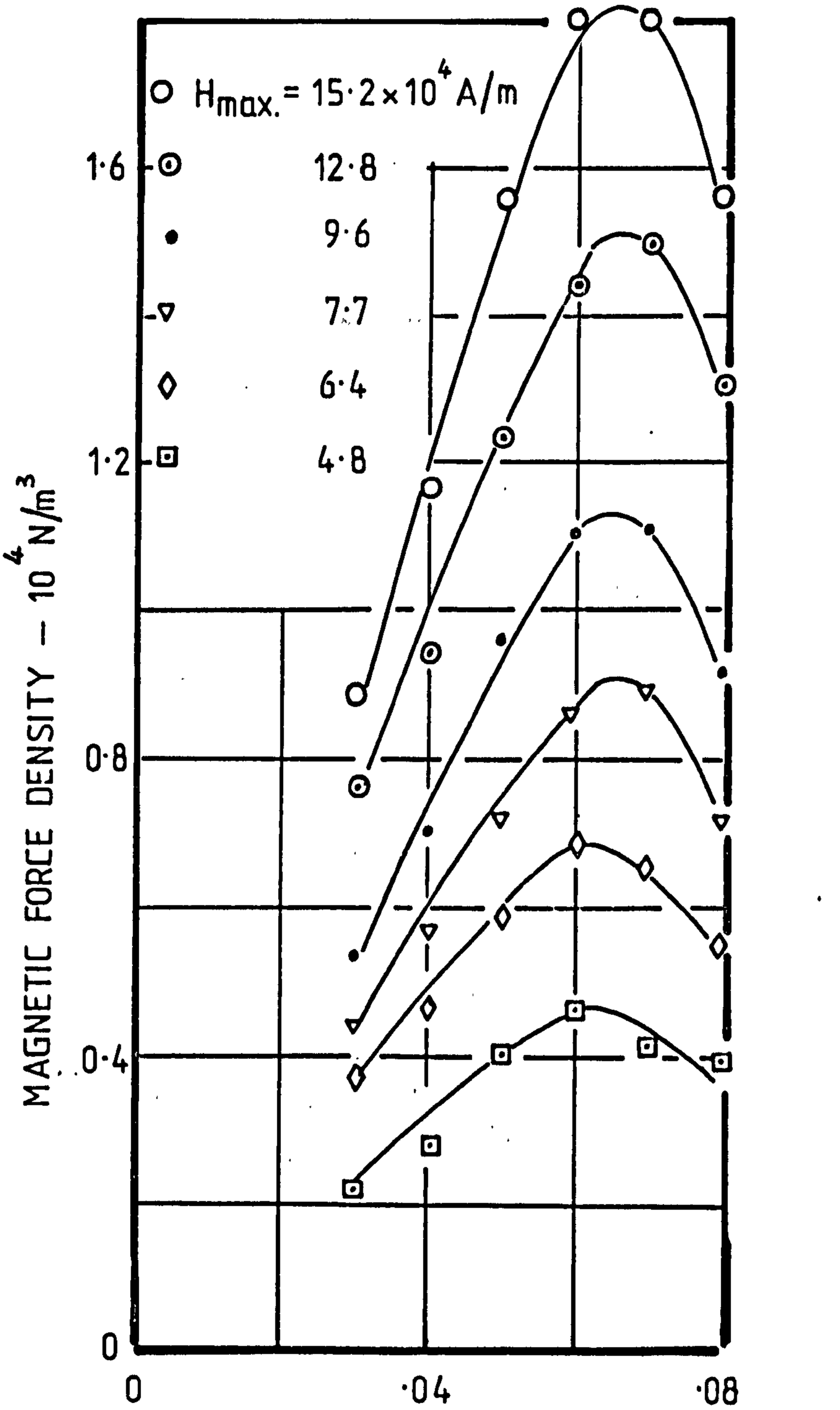

FIG. 3.9 2·64 % MO - 2035 IN PARAFFIN

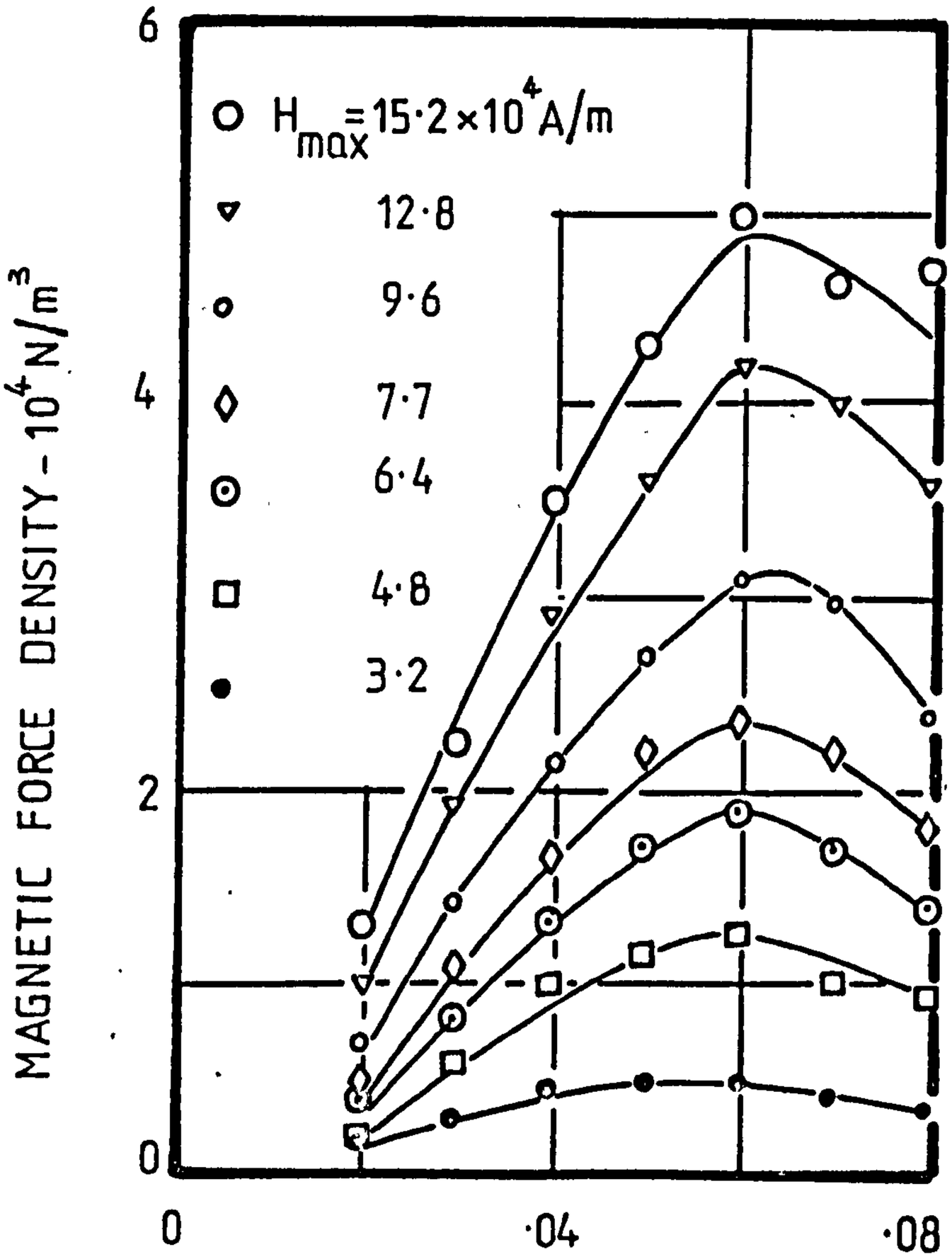

FIG.3.10 8·17 % MO-2035 IN PARAFFIN

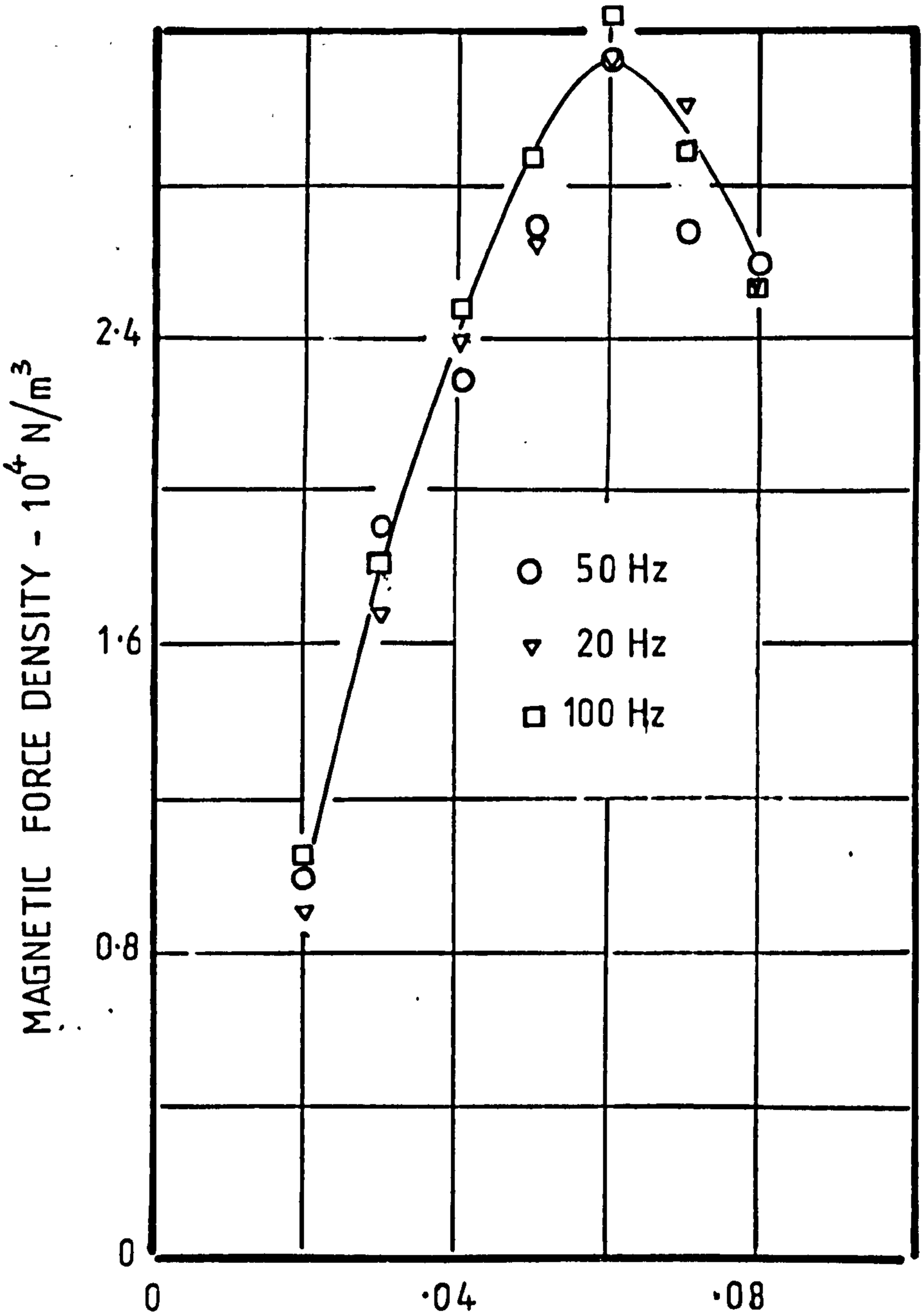

FIG. 3.11. EFFECT OF FREQUENCY ON MAGNETIC FORCE DENSITY – 11% MO 2035 IN PARAFFIN. $H_{max} = 7{\cdot}7 \times 10^4$ A/m

prolate spheroid 51 mm long x 27.5 mm diameter. A comparison of the magnetic force obtained, for two values of field, with that of a spherical body of a 25 mm diameter is shown in Fig.3.12.

3.3.8 Effect of carrier fluid upon the magnetic force.

It was thought that possible chemical or physical effects might take place during milling process and therefore it was decided to examine the effect of using a carrier fluid other than paraffin in the preparation of the fluid upon the magnetic force. A fluid made up of 4.4% of the powder type MO-2035 in water, using sodium silicate as the surfactant, was tested. The results for this fluid, shown in Fig.3.13, are in fact in close agreement with that of a fluid of the same volume concentration of MO-2035 in paraffin and there has been no fluid deterioration over a month.

3.3.9 Effect of magnetic material upon the magnetic force.

So far, the magnetic oxide MO-2035 has been used. It was decided to see whether other magnetic material, if used in the preparation of ferrofluid, would give similar results. Magnetite and ferrosilicon,both of which are cheap materials, were tried. The magnetite fluid had 21% by volume of magnetite and the other fluid had 6.4% by volume of ferrosilicon both in water as a carrier fluid. Appropriate volume of sodium silicate was added to both of the fluids as a surfactant. The magnetic force densities are plotted against exciting currents for the magnetite and ferrosilicon fluids in Figs. 3.14 and 3.15 respectively.

3.3.10 Test with 140 mm diameter stator.

Force measurements were carried out on three fluids made up from the Pfizer powder, type MO-2035. They have volume loading of magnetic powder in paraffin and oleic acid of 5.36, 8.17 and 11.0%. Sample of the results of magnetic force densities against exciting currents are presented in Fig.3.16.

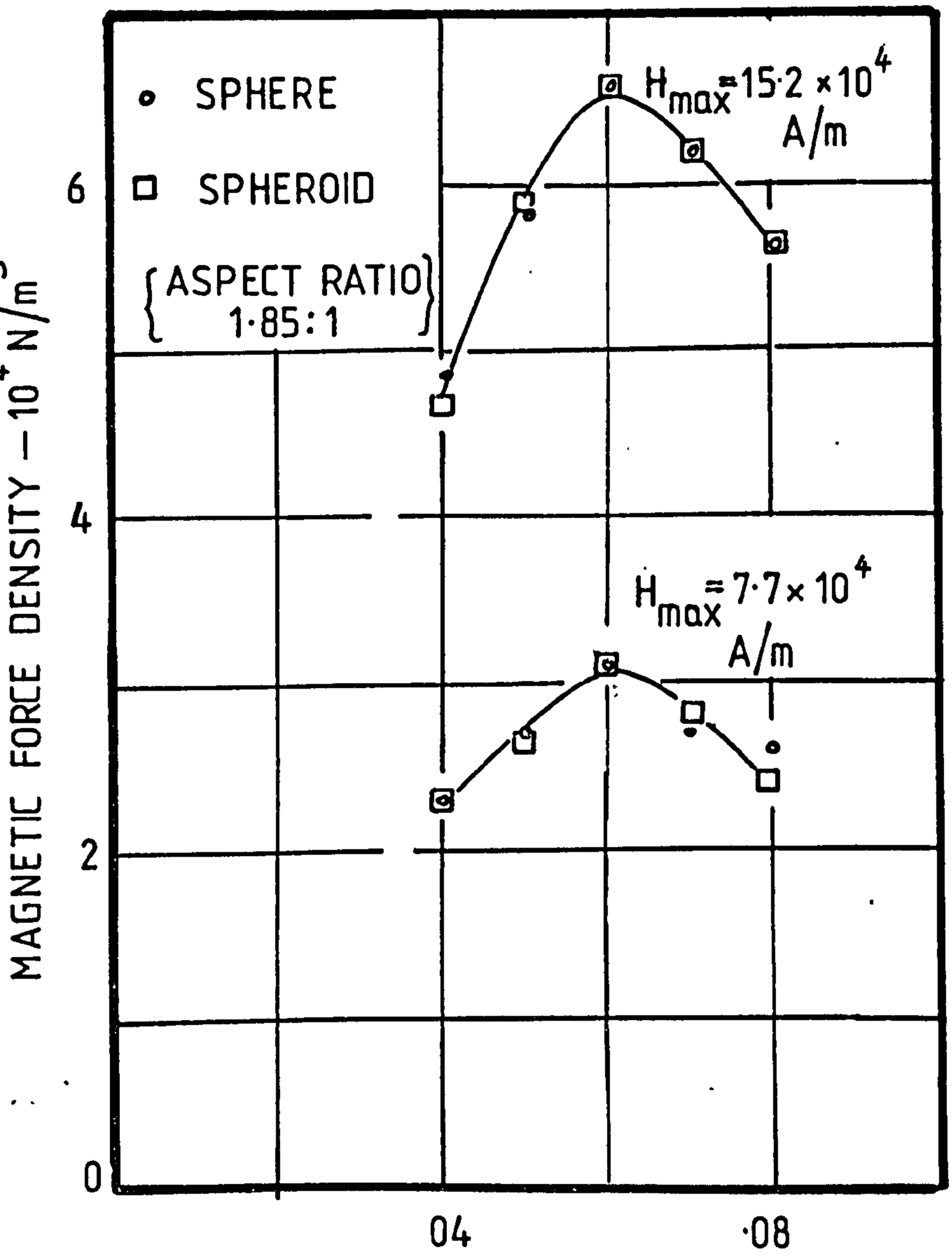

FIG. 3.12. EFFECT OF BODY SHAPE UPON MAGNETIC FORCE DENSITY −11% MO-2035 IN PARAFFIN.

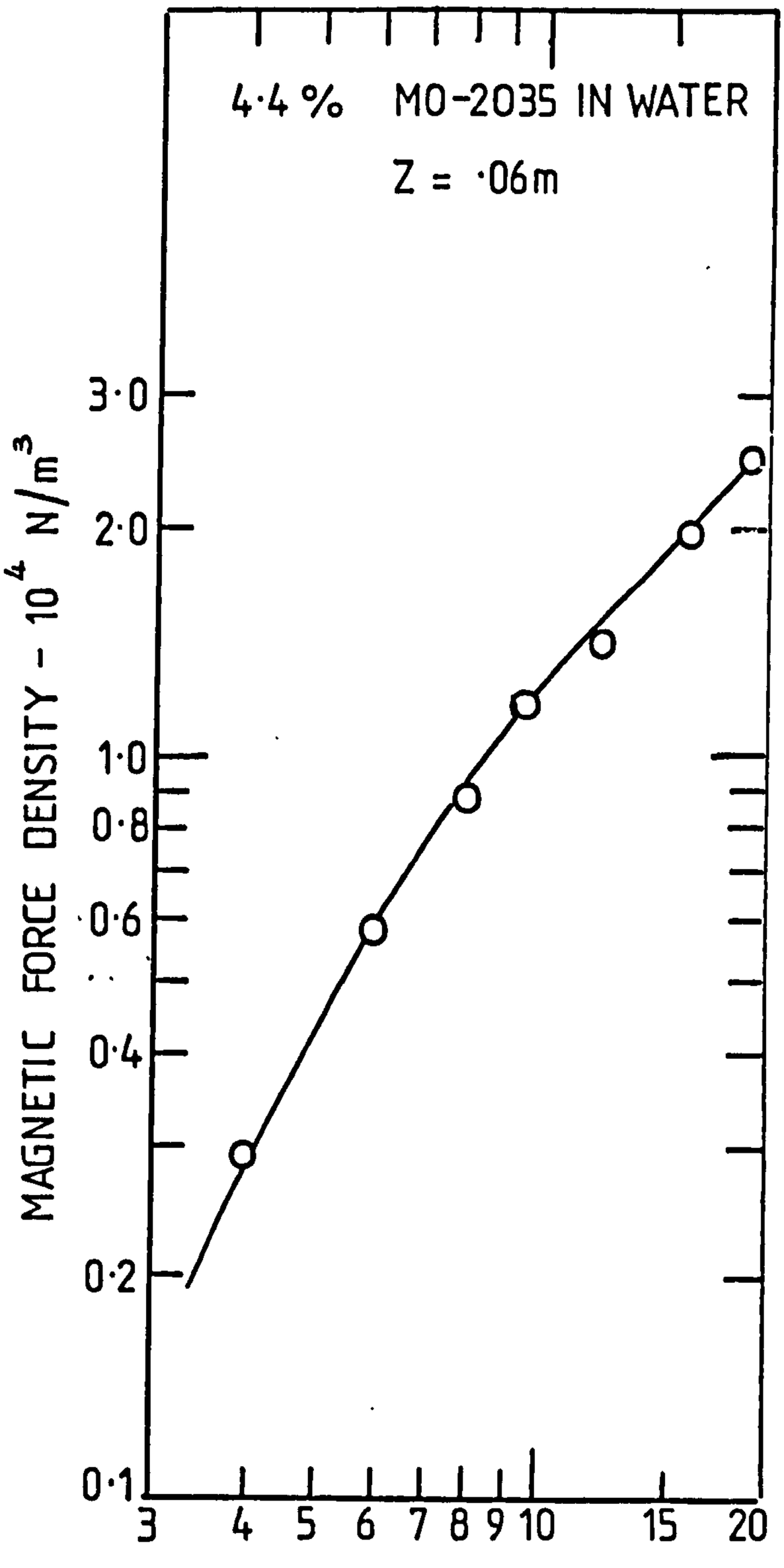

FIG. 3.13. VARIATION OF MAGNETIC FORCE DENSITY WITH SUPPLY CURRENT FOR WATER BASE FLUID.

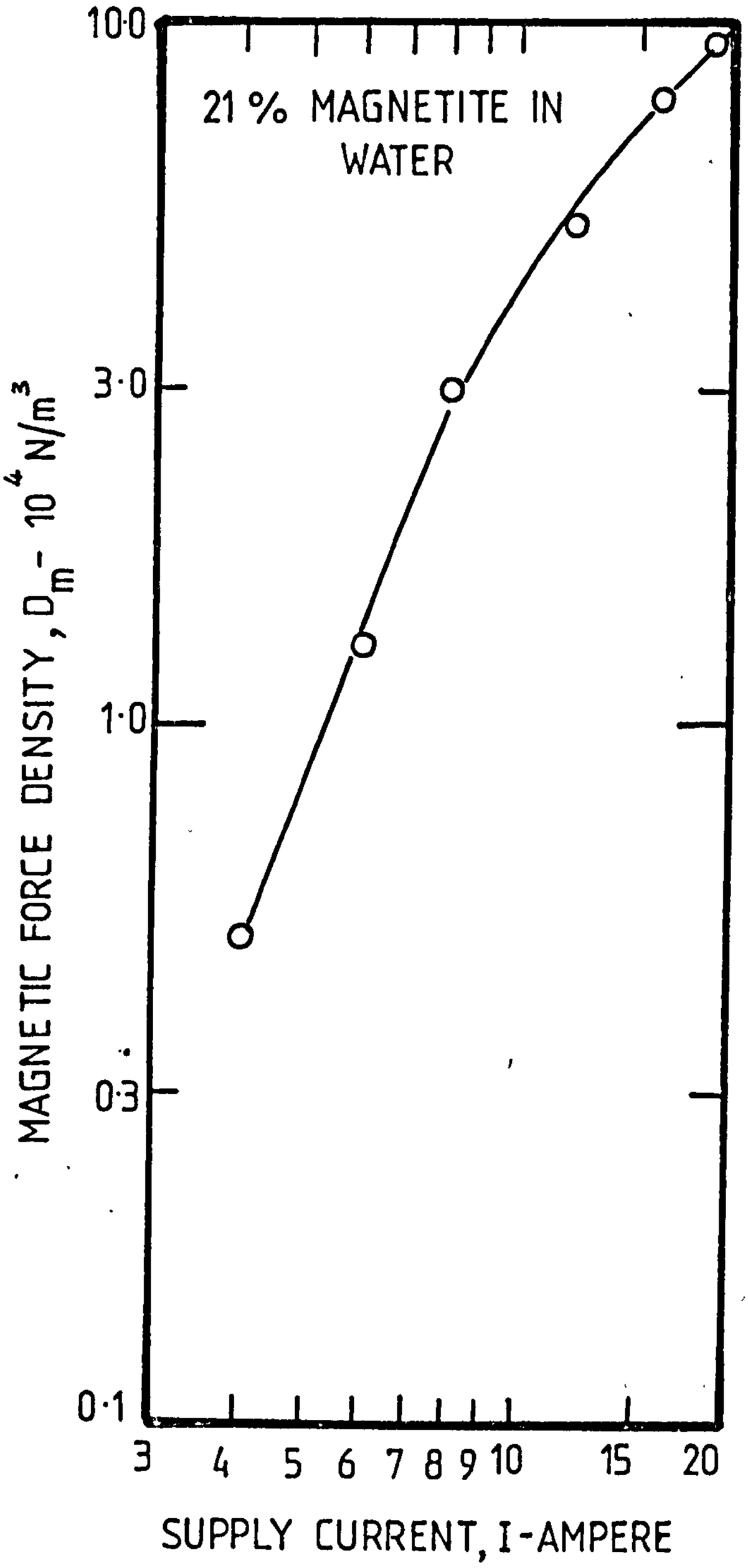

FIG. 3.14. VARIATION OF MAGNETIC FORCE DENSITY WITH SUPPLY CURRENT AT Z = .0 6m

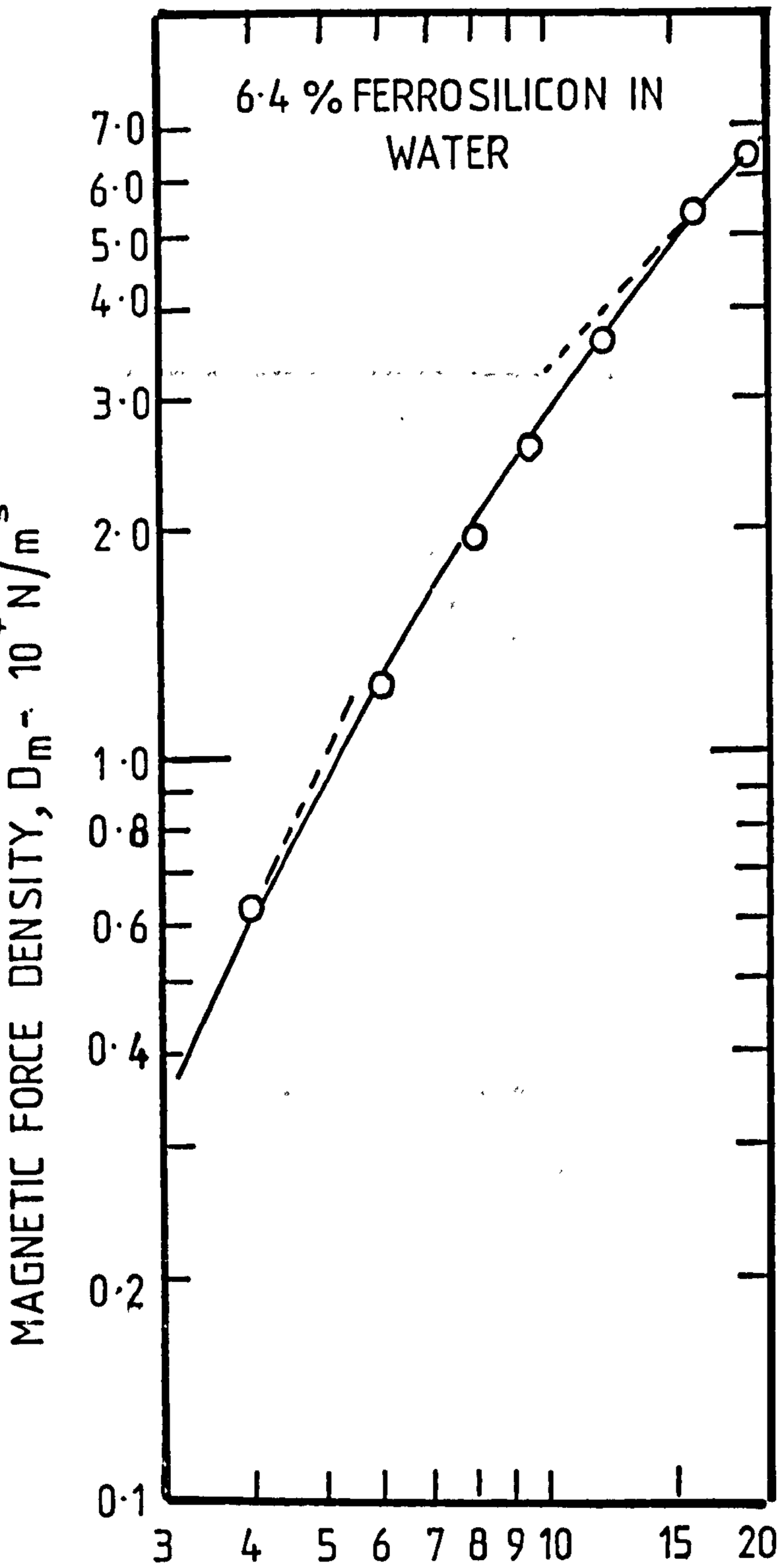

FIG. 3.15. VARIATION OF MAGNETIC FORCE DENSITY WITH SUPPLY CURRENT AT Z = ·05 m

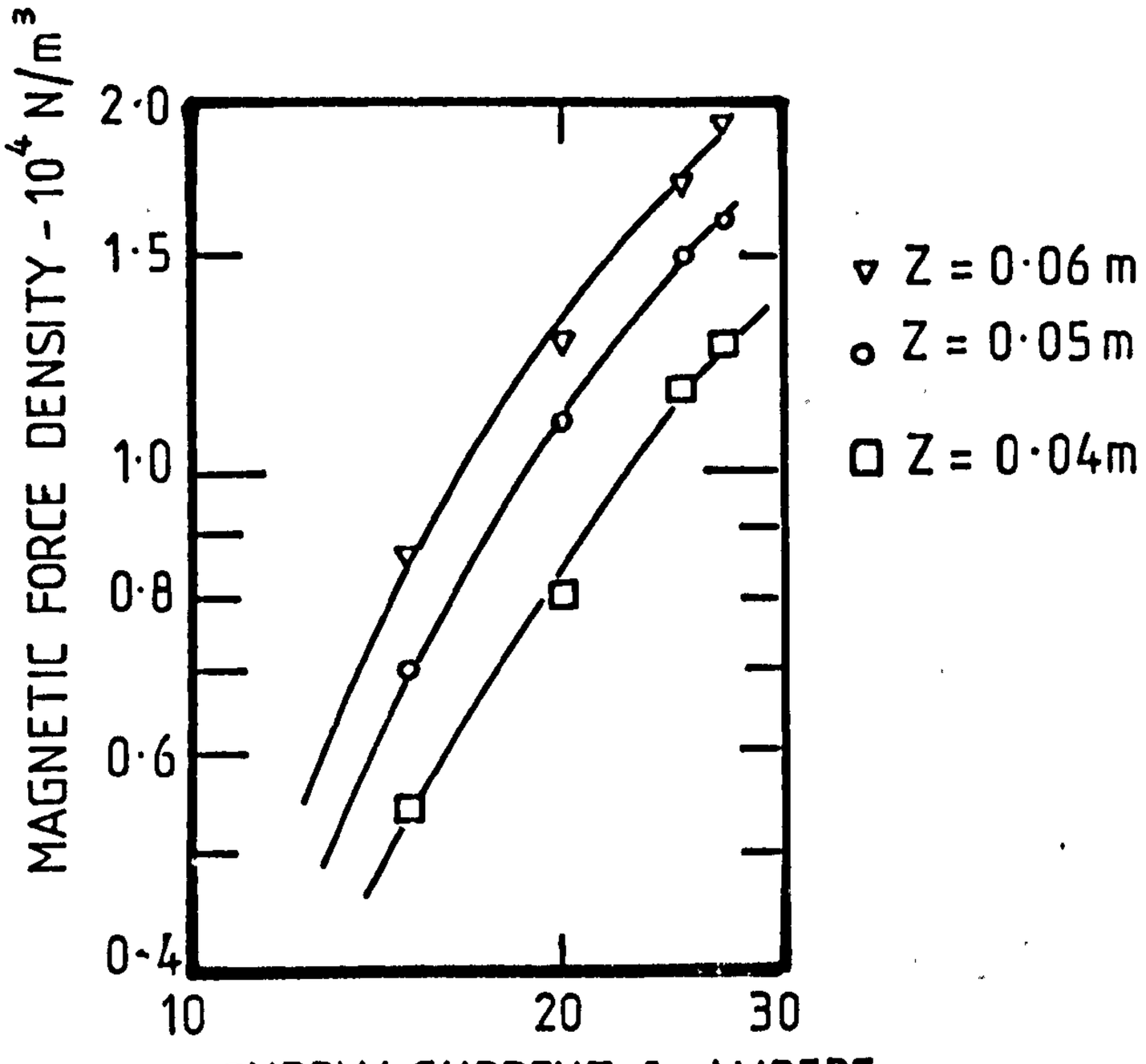

FIG. 3.16. SAMPLE OF THE RESULTS OF THE 140 mm DIAMETER TWO POLE STATOR - 8·17 % MO-2035 IN PARAFFIN.

3.3.11 Measurements of the field distributions of the 118 mm diameter and the 140 mm diameter stators.

The radial component of the field intensity was measured using a search coil whose axis was in the radial direction and its centre was along the axis of each stator. The coil was wound on a perspex former of 5 mm diameter and 5 mm length and it had 500 turns. The coil was fixed to a disc which is fixed to the wall of a hollow cylinder which can be moved up and down in order to vary the position of the search coil along the stator's axis. Fig.3.17 shows a photograph of the search coil. The coil was calibrated against a magnetic field produced by a standard solenoid. Fig.3.18 shows a photograph of the equipment used in the calibration. Figs.3.19 and 3.20 show the variation of the radial component of the magnetic field along the axis of the 118mm and the 140 mm diameter stators respectively. The axial component along the axis of the stators is zero.

3.3.12 Effect of the length and constant diameter upon the field distribution of a 2-pole stator.

When it was found that the measured force densities obtained were agreeing well with those predicted from magnetic characteristics of the stators and the fluids, it was decided that the most convenient way of investigating the effect of the length to diameter ratio of the stator was simply to concentrate upon measurements of the stator field distribution. Since all but a two-pole field distribution gives zero field intensity on the axis even a primitive two-pole winding can be used (the space harmonics giving zero field on the axis). Moreover, the winding can be single phase. The simplest possible form is a single coil with sides 180^{o} apart.

For this purpose two rigid single turn coils were threaded in a steel stack. Each coil was placed inside two slots, 180^{o} mechanical apart, in the steel stamping of bore diameter .066 m as shown in Fig.3.21.a. The length

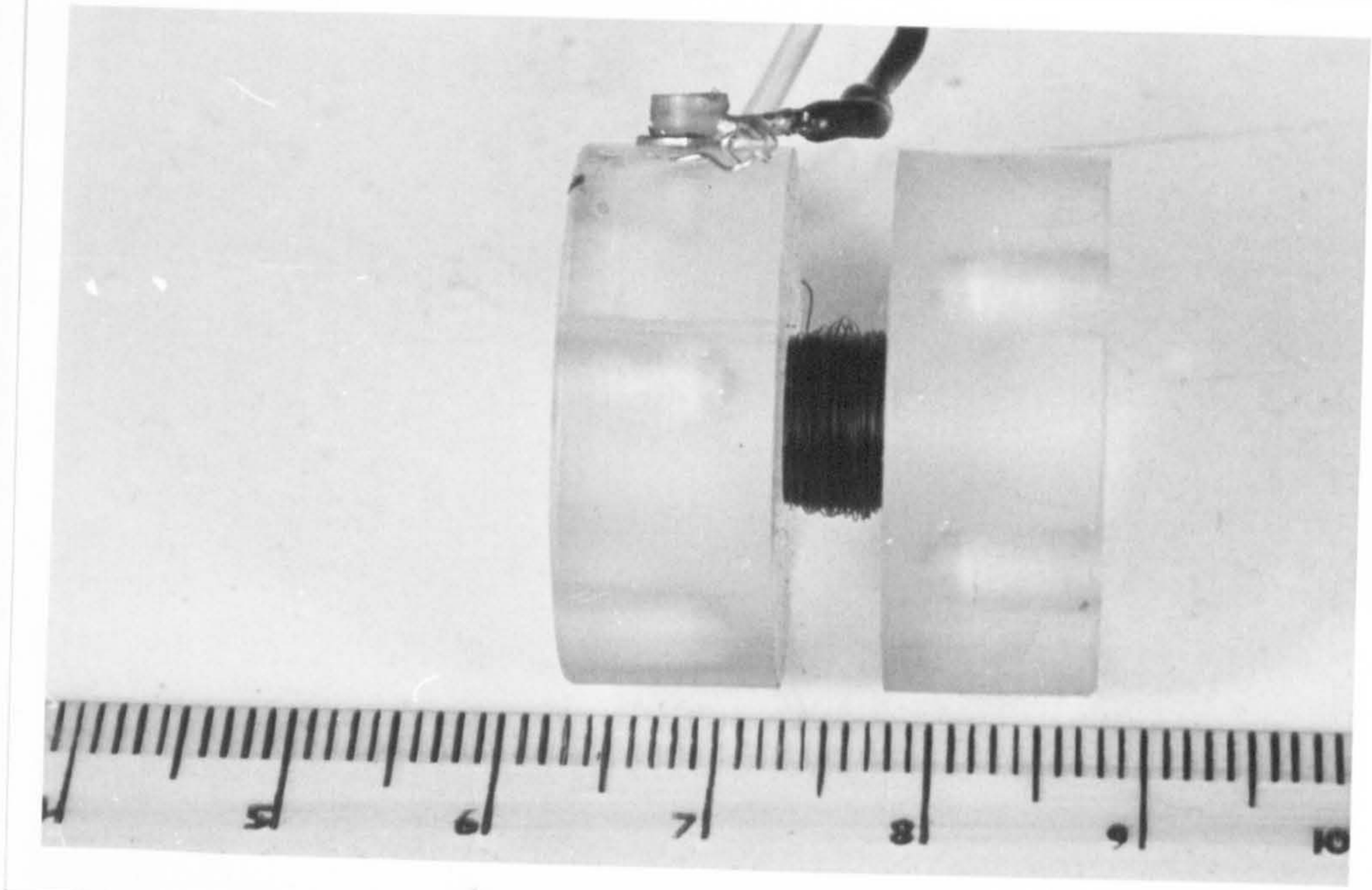

FIG. 3.17 THE SEARCH COIL

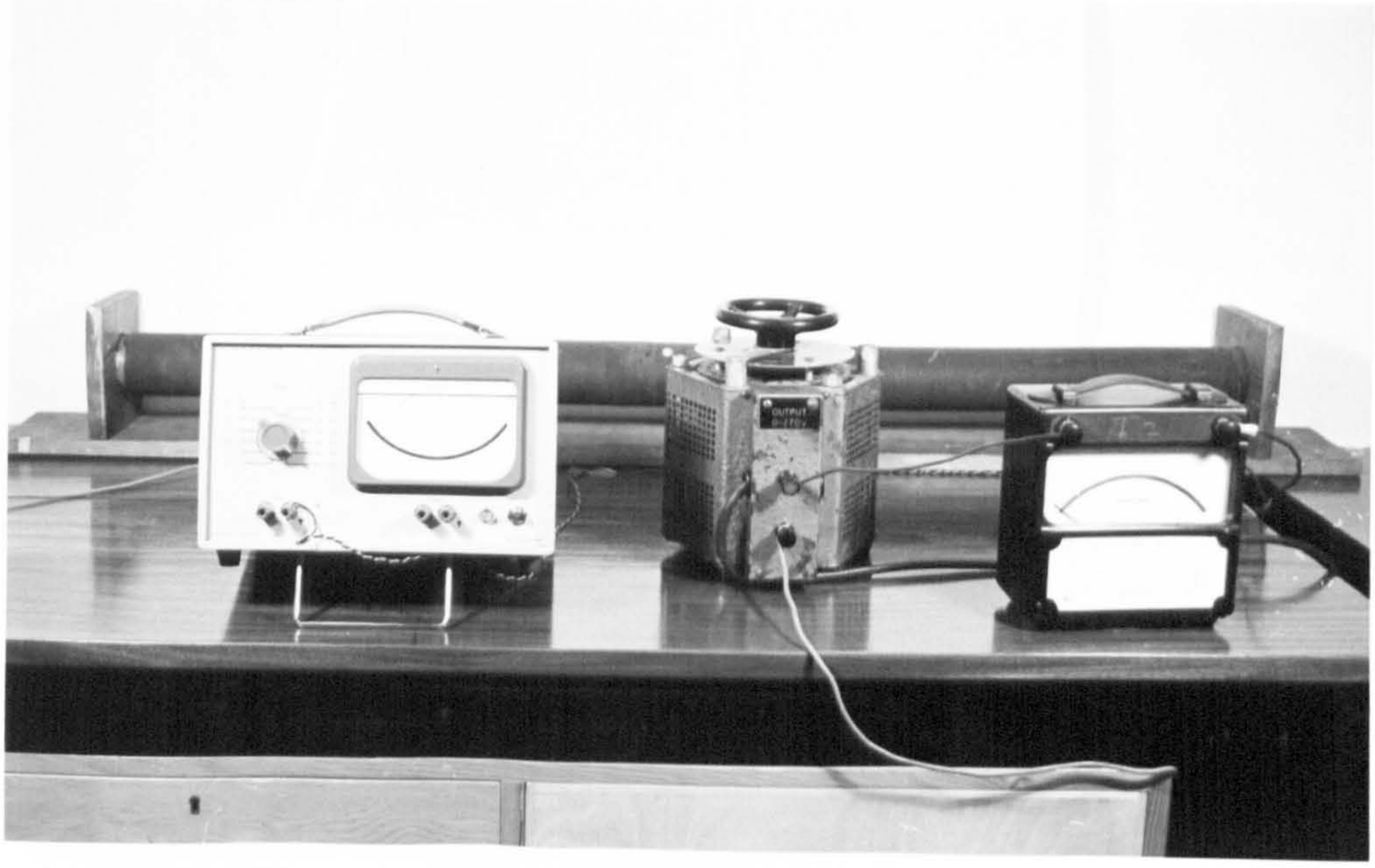

FIG. 3.18 PHOTOGRAPH OF THE EQUIPMENT USED IN CALIBRATION OF THE SEARCH COIL

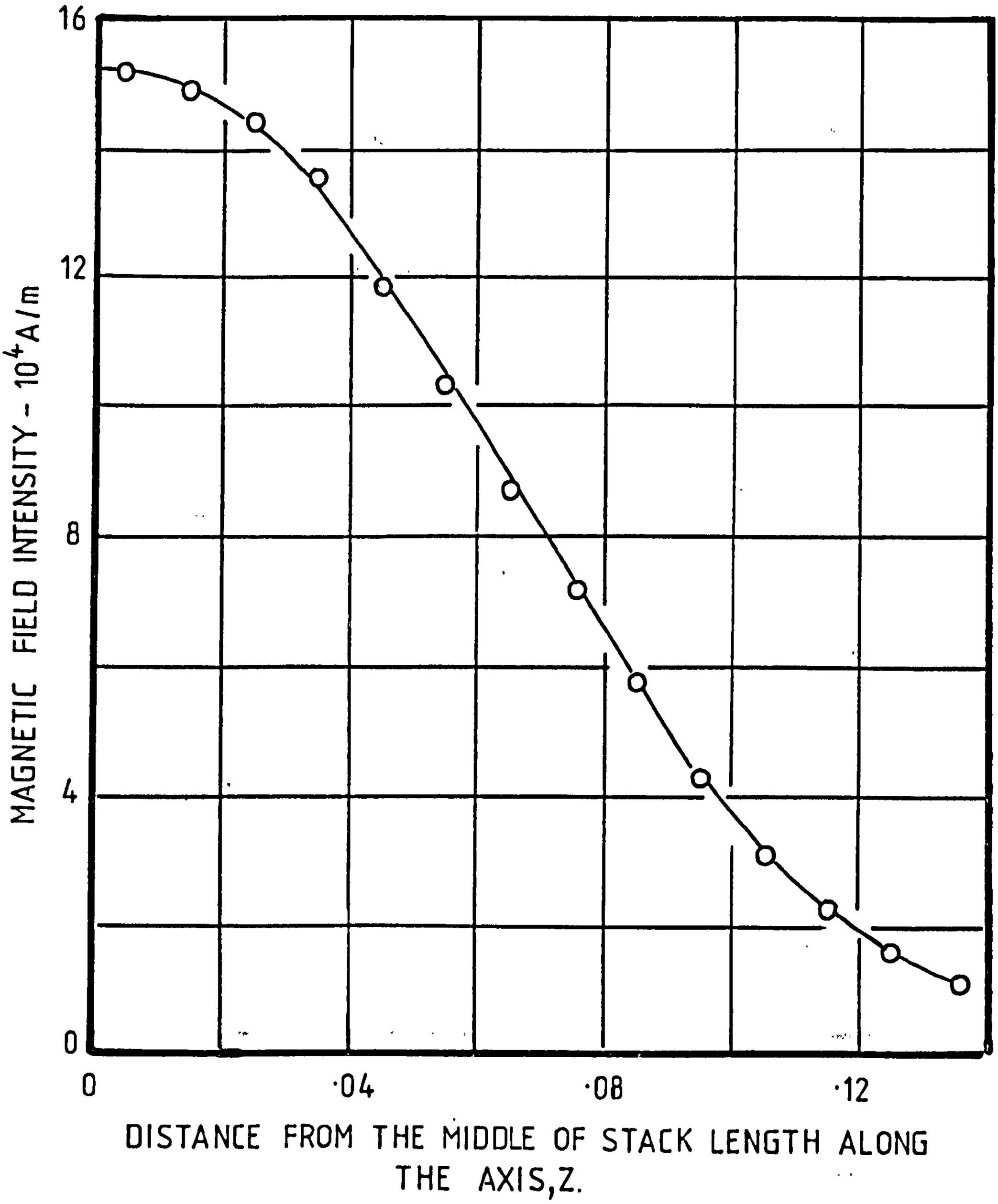

FIG. 3.19. DISTRIBUTION OF THE MAGNETIC FIELD ALONG THE AXIS OF THE 118 mm DIAMETER TWO POLE STATOR — PHASE CURRENT IS 19 A.

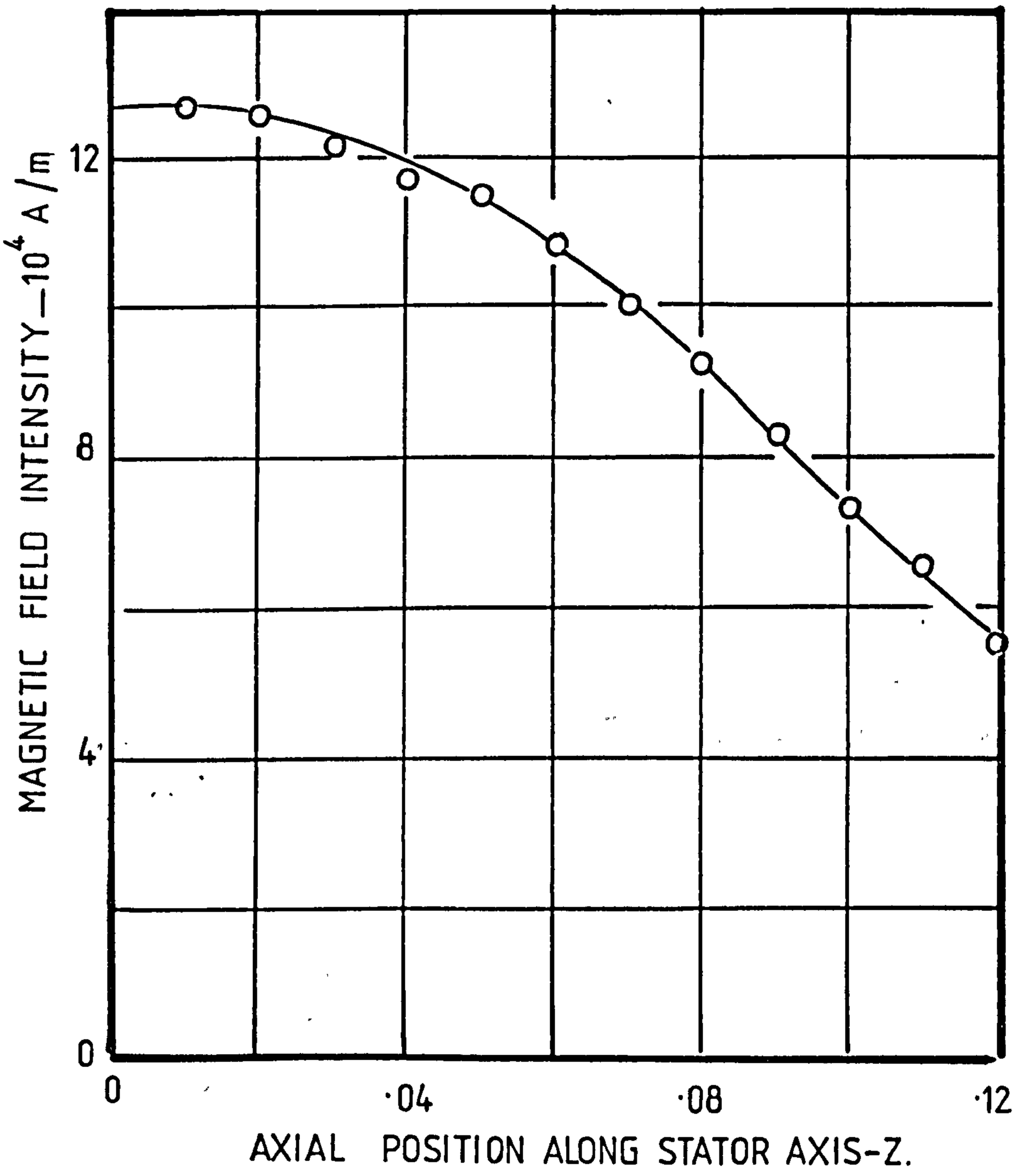

FIG. 3.20. DISTRIBUTION OF THE MAGNETIC FIELD ALONG THE AXIS OF THE 140 mm DIAMETER TWO-POLE STATOR — PHASE CURRENT IS 27 A.

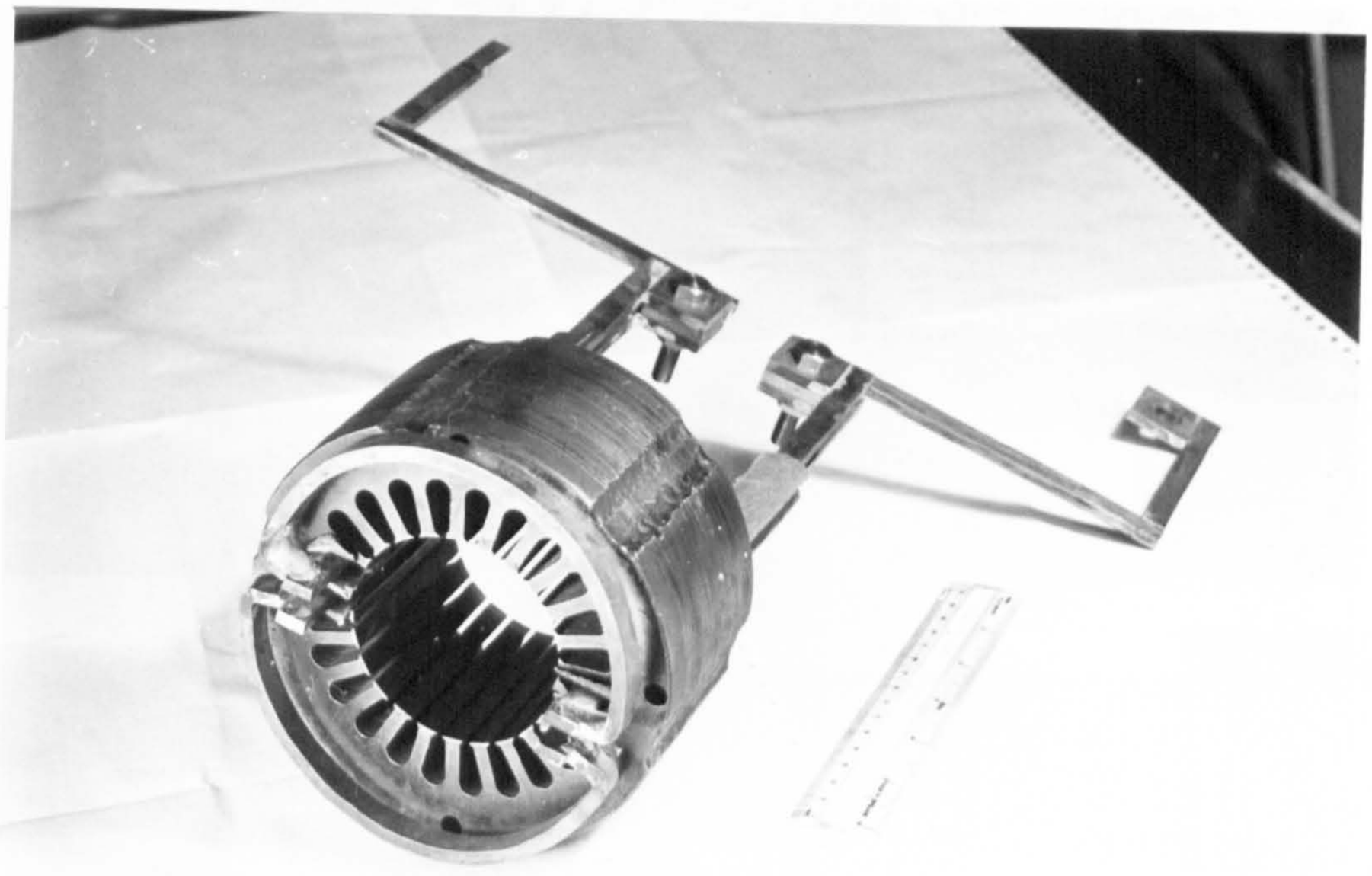

(a) NORMAL WINDING

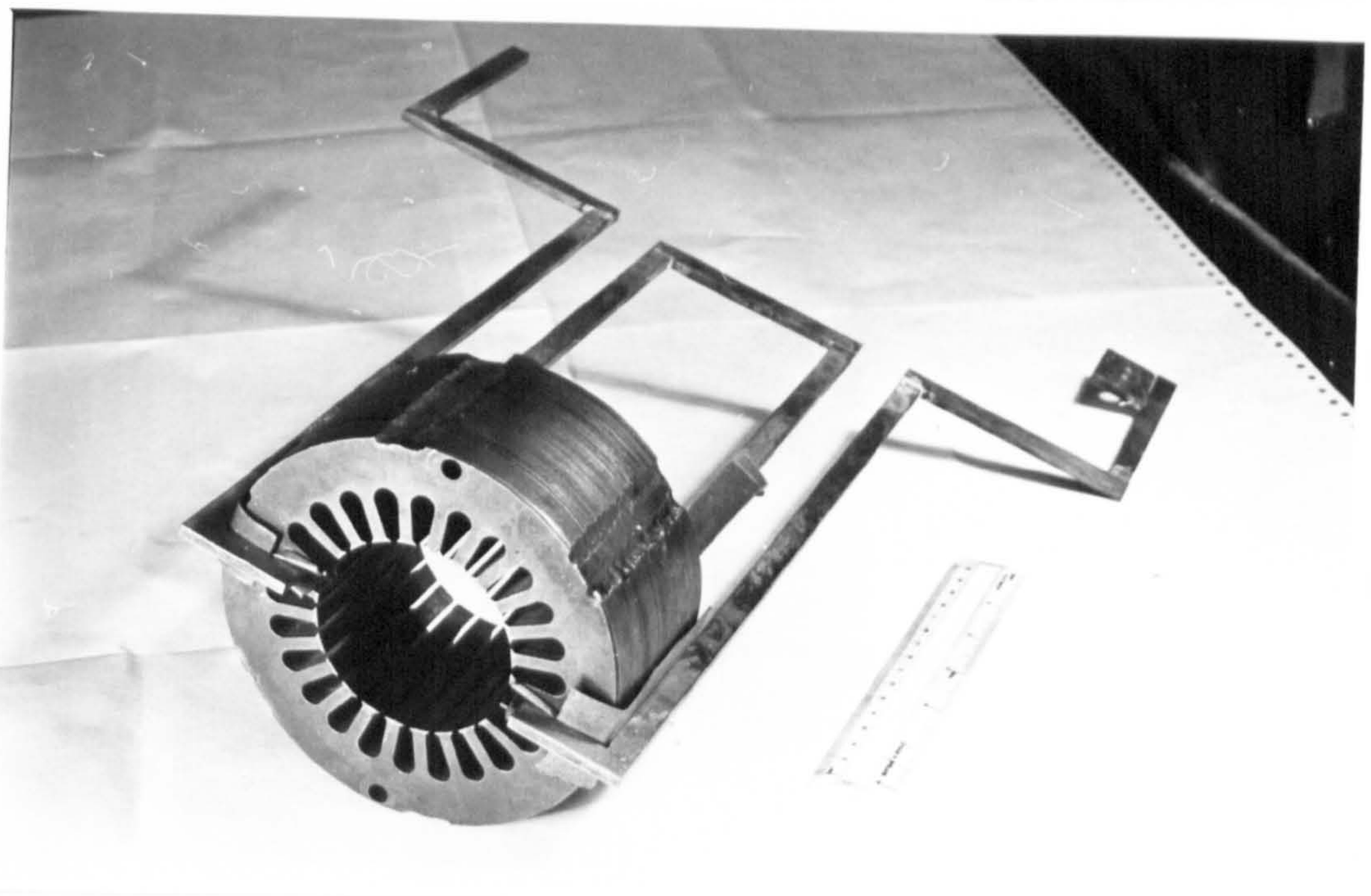

(b) GRAMME RING WINDING

FIG. 3.21 THE SINGLE TURN COILS

of the stack was varied by threading on more stampings and for each length the radial component of the field was measured at various points along the axis. The search coil shown in Fig.3.17 was used and its axis was kept normal to the plane of the single turn coil to record the maximum value.

The ends of the single turn coils were almost half circles lying on the plane of the top face of the iron stamping. At the other end the coil sides were long enough to avoid the effect of end winding on the field distribution.

For the same M.M.F. the output of the search coil, at various axial positions, was measured for different lengths of stamping.

These tests were further extended to investigate the effect of a Gramme-ring winding, using the preformed rigid conductor arrangement shown in Fig.3.21.b.

The results of these tests for the 'normal' and Gramme-ring windings are shown in Fig.3.22.

3.3.13 Test with the linear arrangement.

Magnetic force measurements were carried out on the linear arrangement, with two stator surfaces facing towards, but inclined away from each other as in Fig. 3.1. Motion of the ferrofluid along the stator surfaces led to difficulties in measuring the magnetic force initially, but the force measuring arrangement was redesigned to overcome these.

The angle of inclination was 72^{o}, and the shorter distance between edges .044 m. The direction of travelling wave was the same for both stators. The currents in each stator winding were equal. To overcome the problem of the motion of ferrofluid along the stator surfaces a measuring cylinder filled with a sample of the fluid under investigation, was placed in the air gap between the two stators. The volume of the sphere used throughout this investigation was 9.4 c.c. The position of the sphere in the air gap was adjusted as in the cylindrical arrangement and the force was measured.

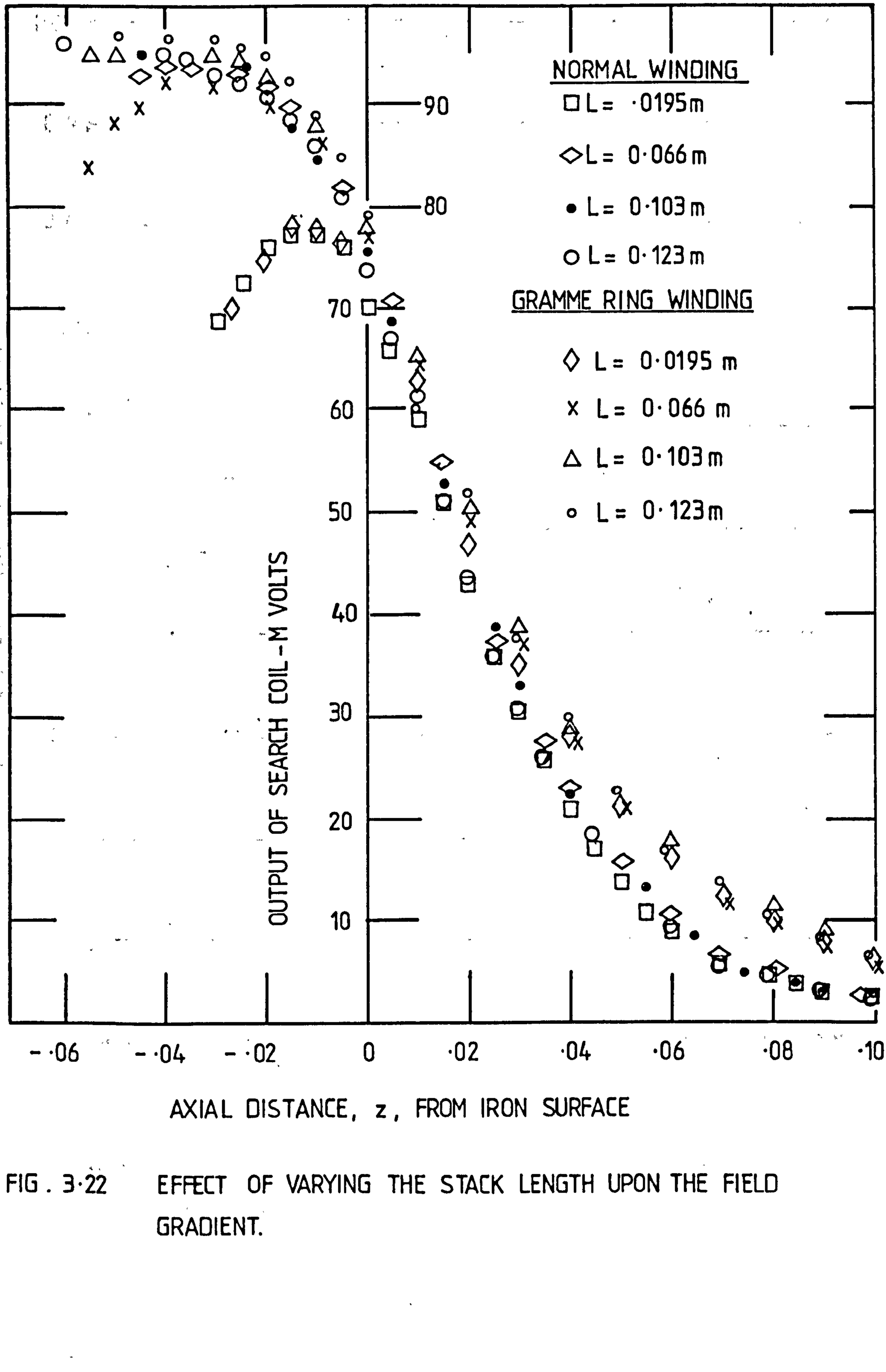

FIG. 3·22 EFFECT OF VARYING THE STACK LENGTH UPON THE FIELD GRADIENT.

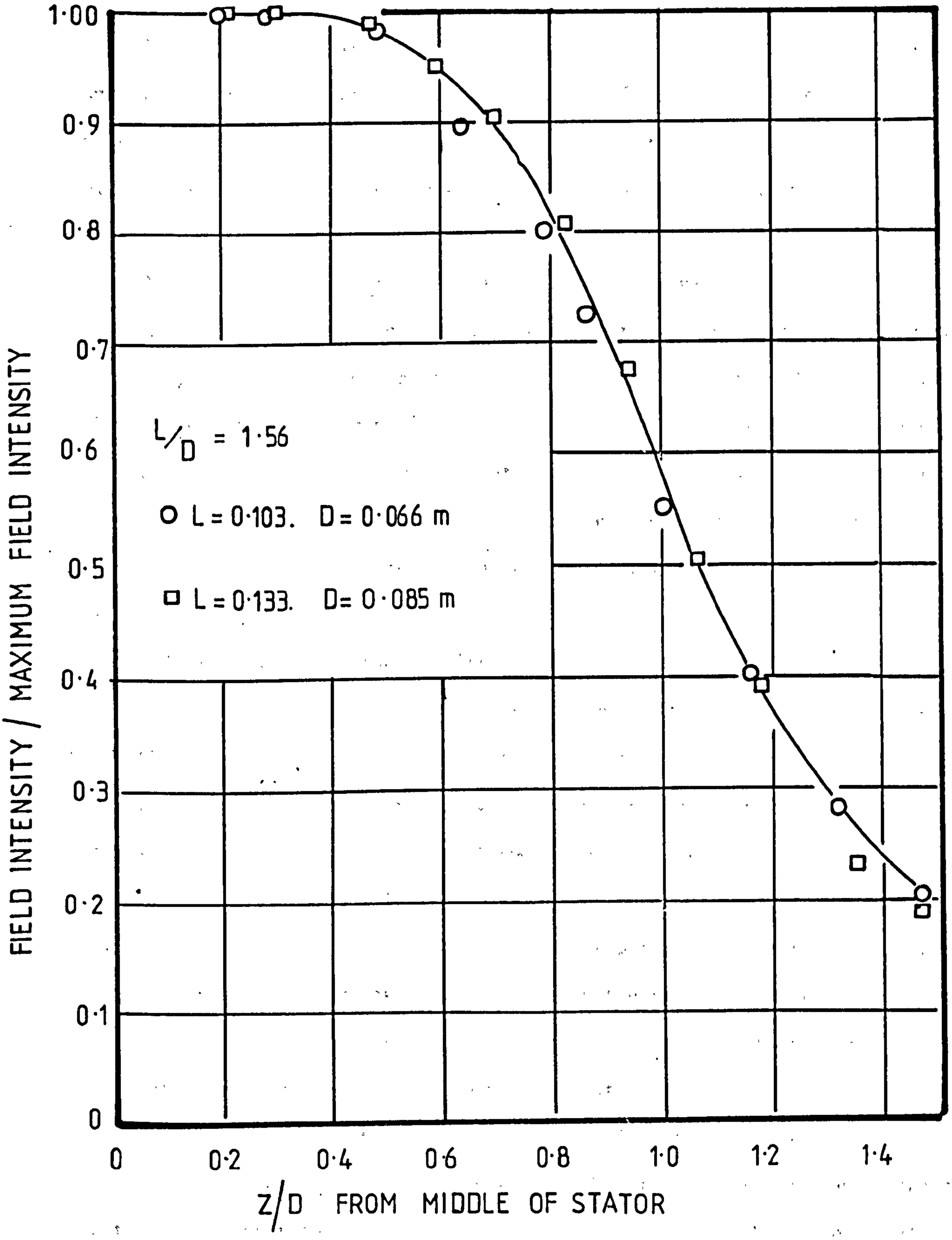

FIG. 3.23. NORMALIZED CURVE OF VARIATION OF FIELD INTENSITY WITH AXIAL POSITION.

The three fluids investigated had volume concentration of 4.29, 6.4 and 9.85% MO-2035 in paraffin. The magnetic force per unit volume (the magnetic force density) for different values of z, the height of the centre of the sphere above the bottom edges of the stators, are shown in Figs. 3.24 to 3.26.

3.3.14 Test with a colloidal suspension ferrofluid.

A sample of true colloidal suspension ferrofluid was supplied by Warren Spring Laboratory of the Department of Trade and Industry. The particles of this fluid did not sediment in the absence of magnetic field. The volume loading and the saturation magnetization were 4.67% and .021 t respectively. The density of this fluid at a fixed position, z, inside the 118 mm diameter two-pole stator was measured for variations of exciting current. The results are shown in Fig.3.27.

3.4 Discussion of the results.

3.4.1 Effect of field gradient and intensity upon the magnetic force.

The curves of Fig.3.9 and 3.10 are similar in shape. If they are extrapolated they pass through origin, which means that no magnetic force is produced at the centre of the stator where there is no field gradient.

Figs. 3.27 to 3.30 illustrate the variation of magnetic force density, ρ_m, with exciting current for three different positions of the body along the axis. These curves are again similar in that each seems to consist of three distinct parts: one is a straight line of slope two, the second is also a straight line of unity slope (although this area is not very well defined) and the last one is a transition region from one slope to the other.

The first region, actually represents the state where the fluid magnetization is unsaturated and hence the fluid magnetization is proportional to the exciting current. Since the field gradient is also proportional to the current from equation 3.2.8, the magnetic force density should be proportional to I^2, hence the slope of 2 on a log-log scale.

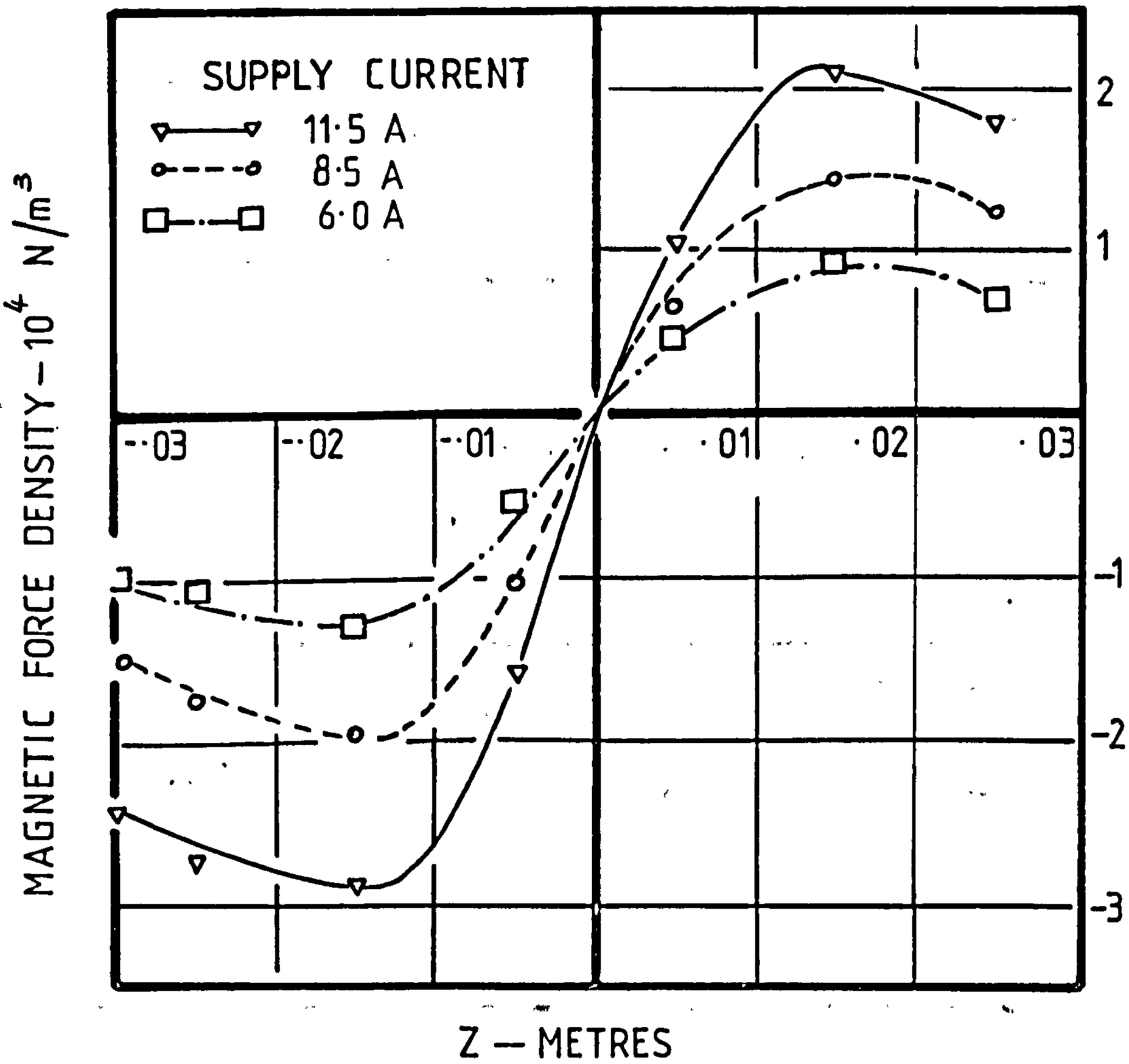

FIG. 3.24. VARIATION OF MAGNETIC FORCE DENSITY WITH Z— LINEAR CONFIGURATION–FLUID CONTAINS 4·29%, BY VOLUME, MO-2035 IN PARAFFIN.

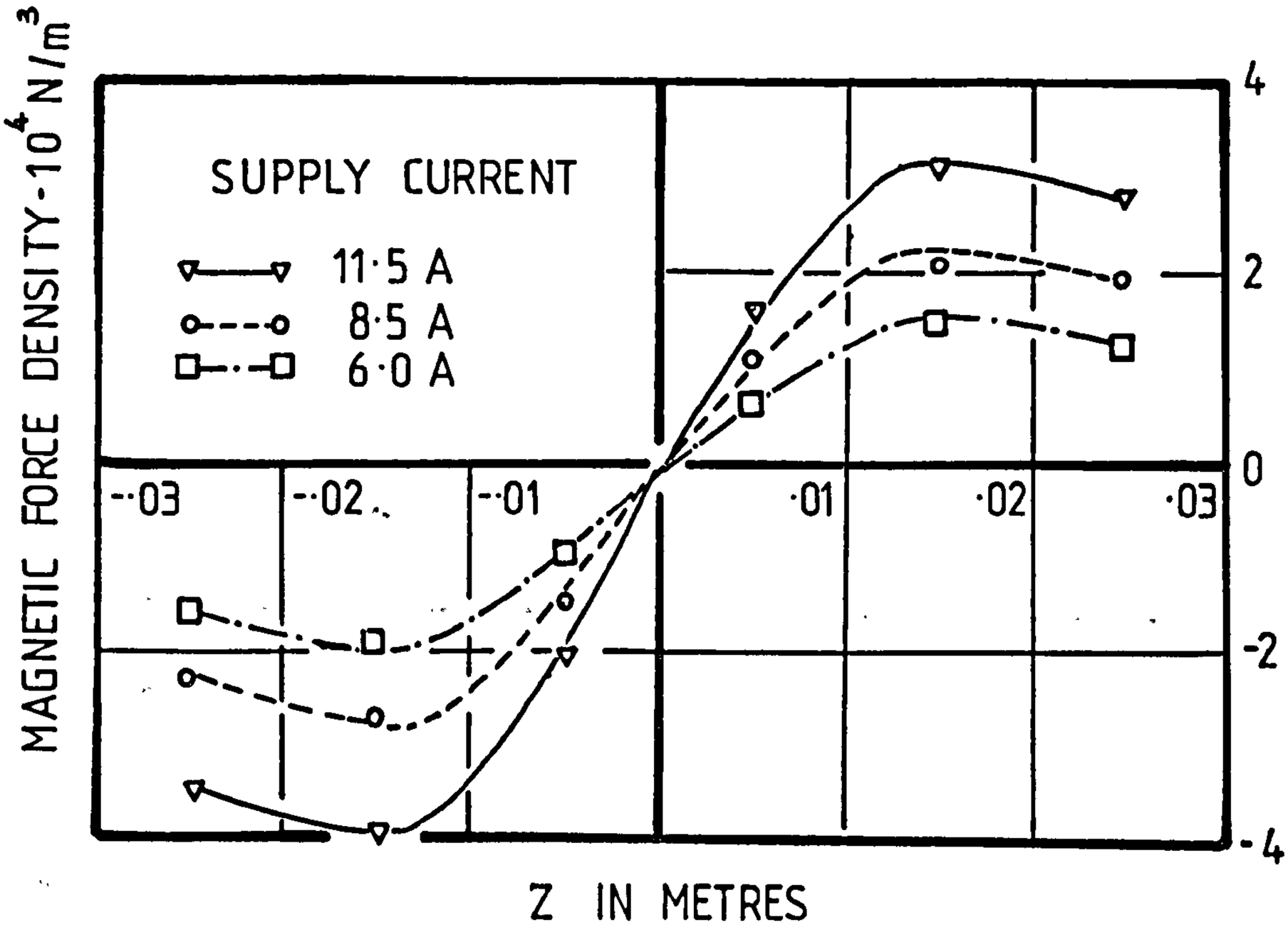

FIG. 3.25. VARIATION OF MAGNETIC FORCE DENSITY WITH Z - LINEAR CONFIGURATION - FLUID CONTAINS 6·4% BY VOLUME MO-2035 IN PARAFFIN.

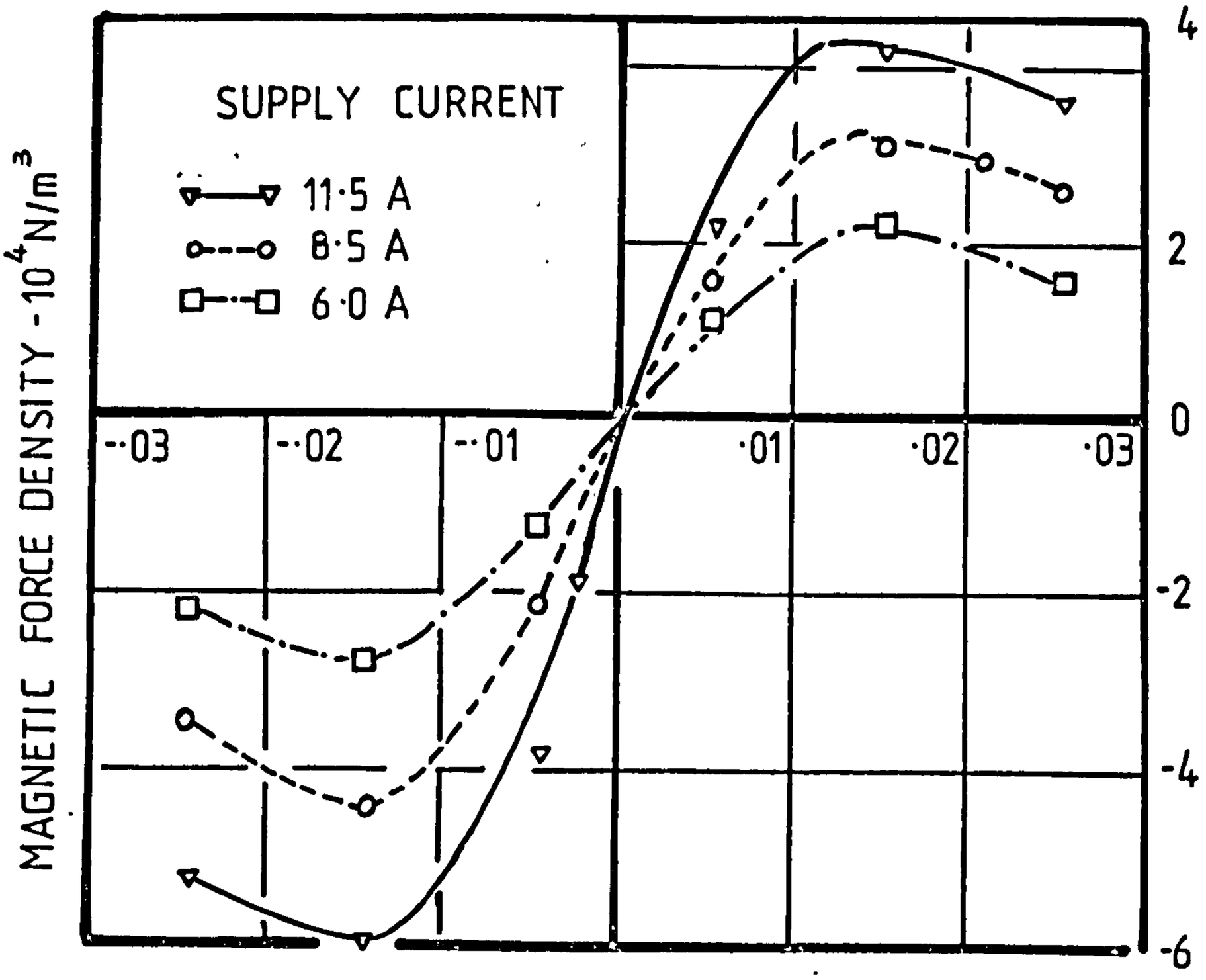

FIG. 3.26. VARIATION OF MAGNETIC FORCE DENSITY WITH Z - LINEAR CONFIGURATION - FLUID CONTAINS 9·85% BY VOLUME MO-2035 IN PARAFFIN.

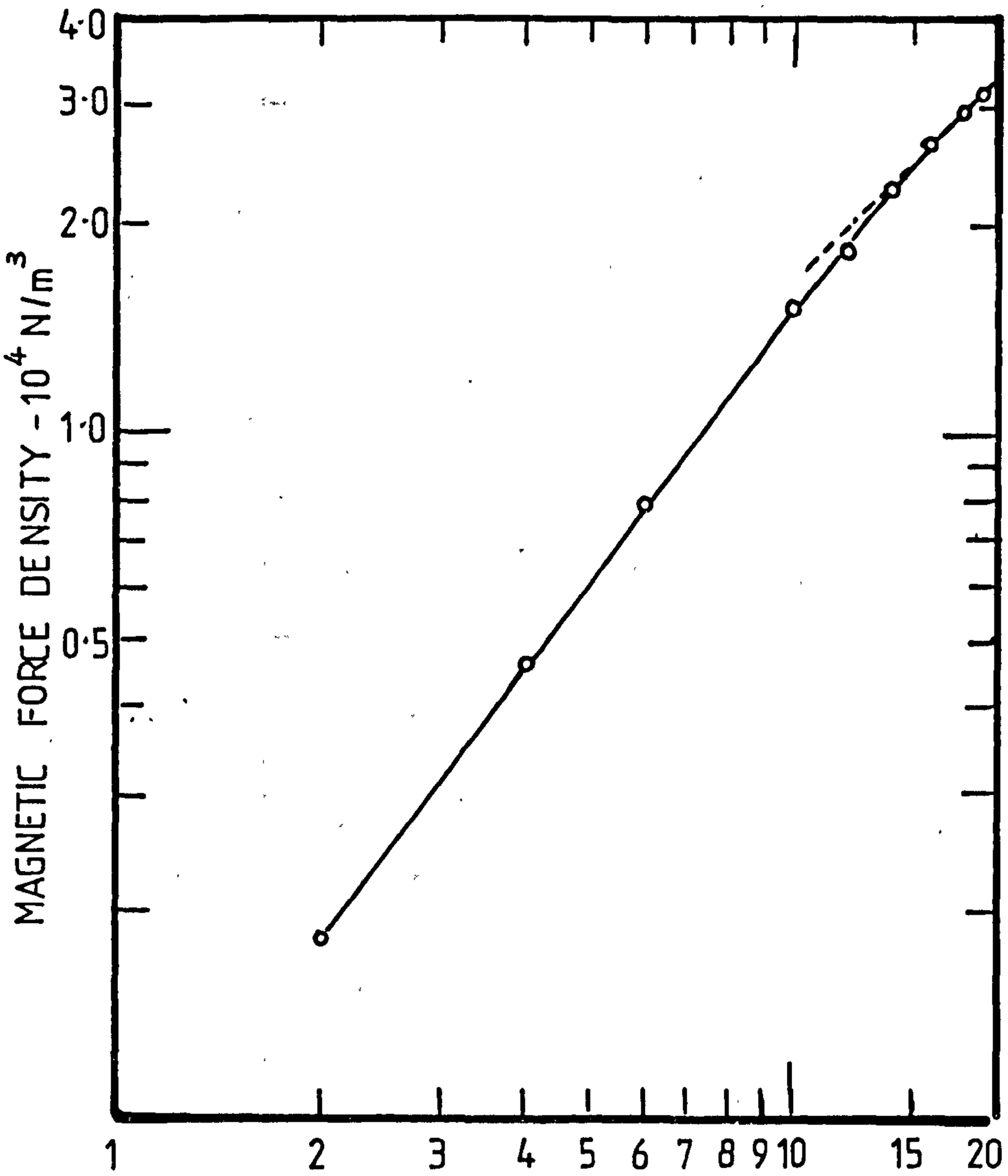

FIG. 3.27. VARIATION OF MAGNETIC FORCE DENSITY WITH SUPPLY CURRENT FOR COLLOIDAL SUSPENSION FERROFLUID - Z = 0·06 m

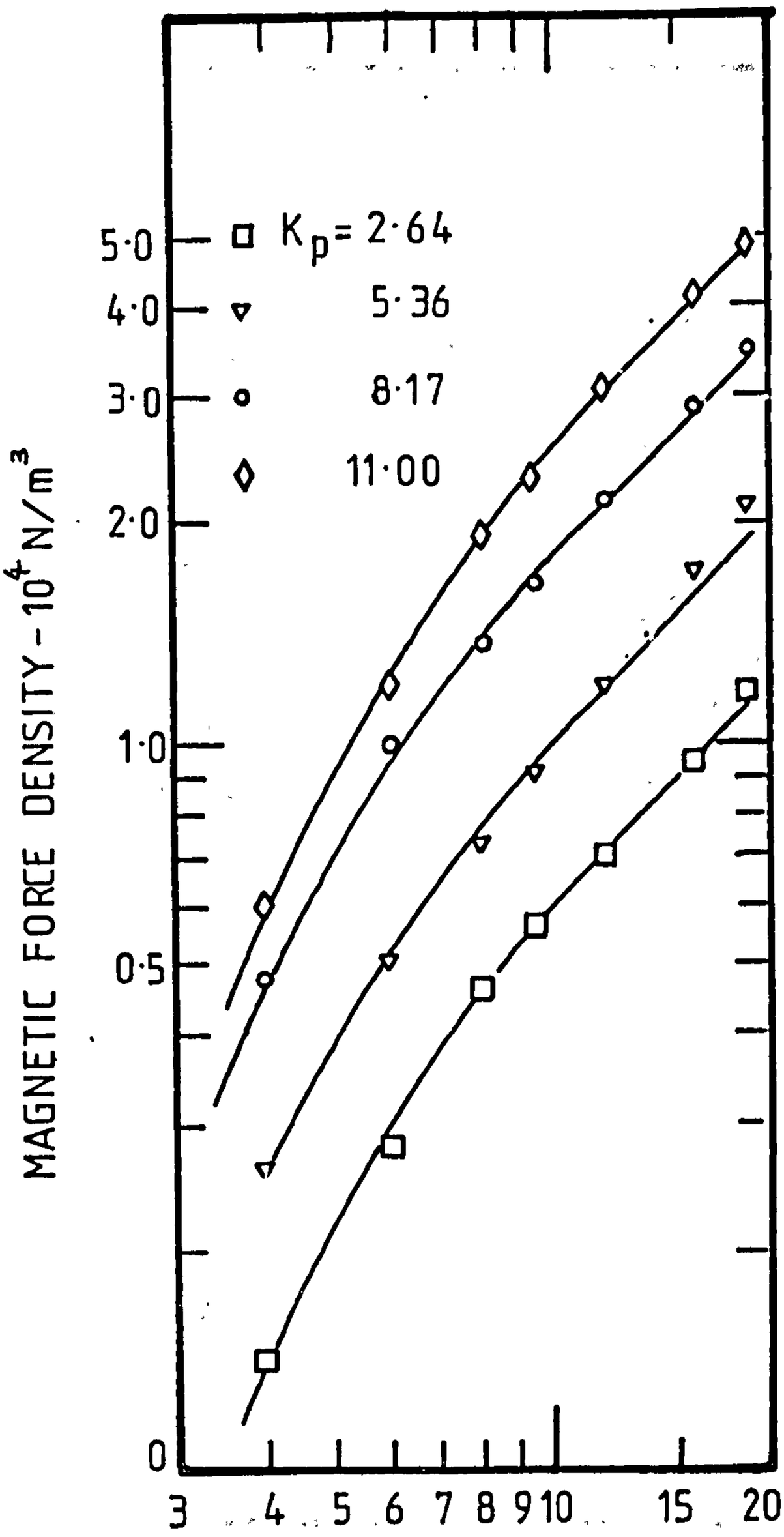

FIG. 3.28. VARIATION OF MAGNETIC FORCE DENSITY WITH SUPPLY CURRENT FOR MO-2035 FLUIDS - Z = 0·04m.

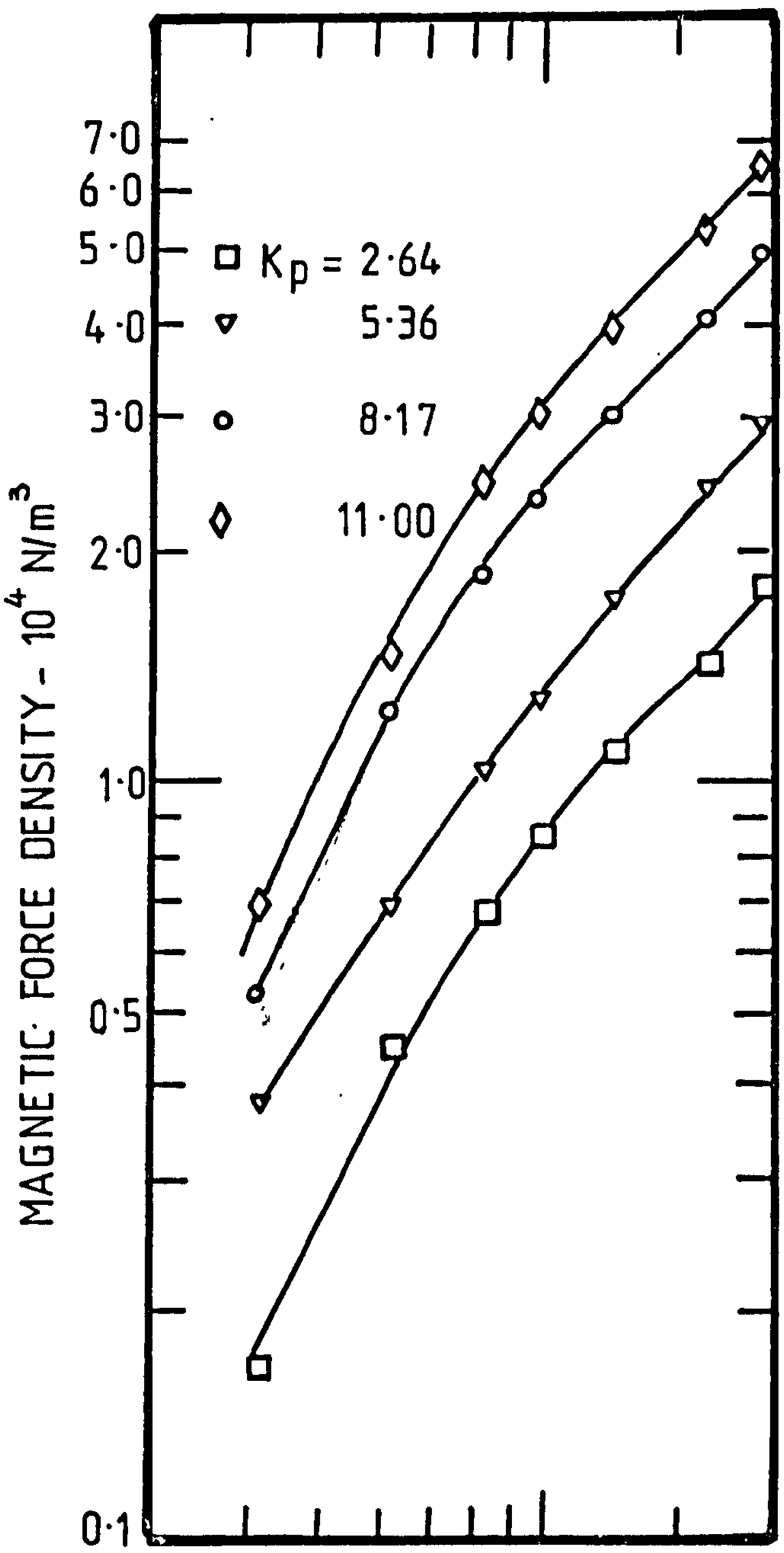

FIG. 3.29. VARIATION OF MAGNETIC FORCE DENSITY WITH SUPPLY CURRENT FOR MO 2035 FLUIDS - Z = 0·06 m.

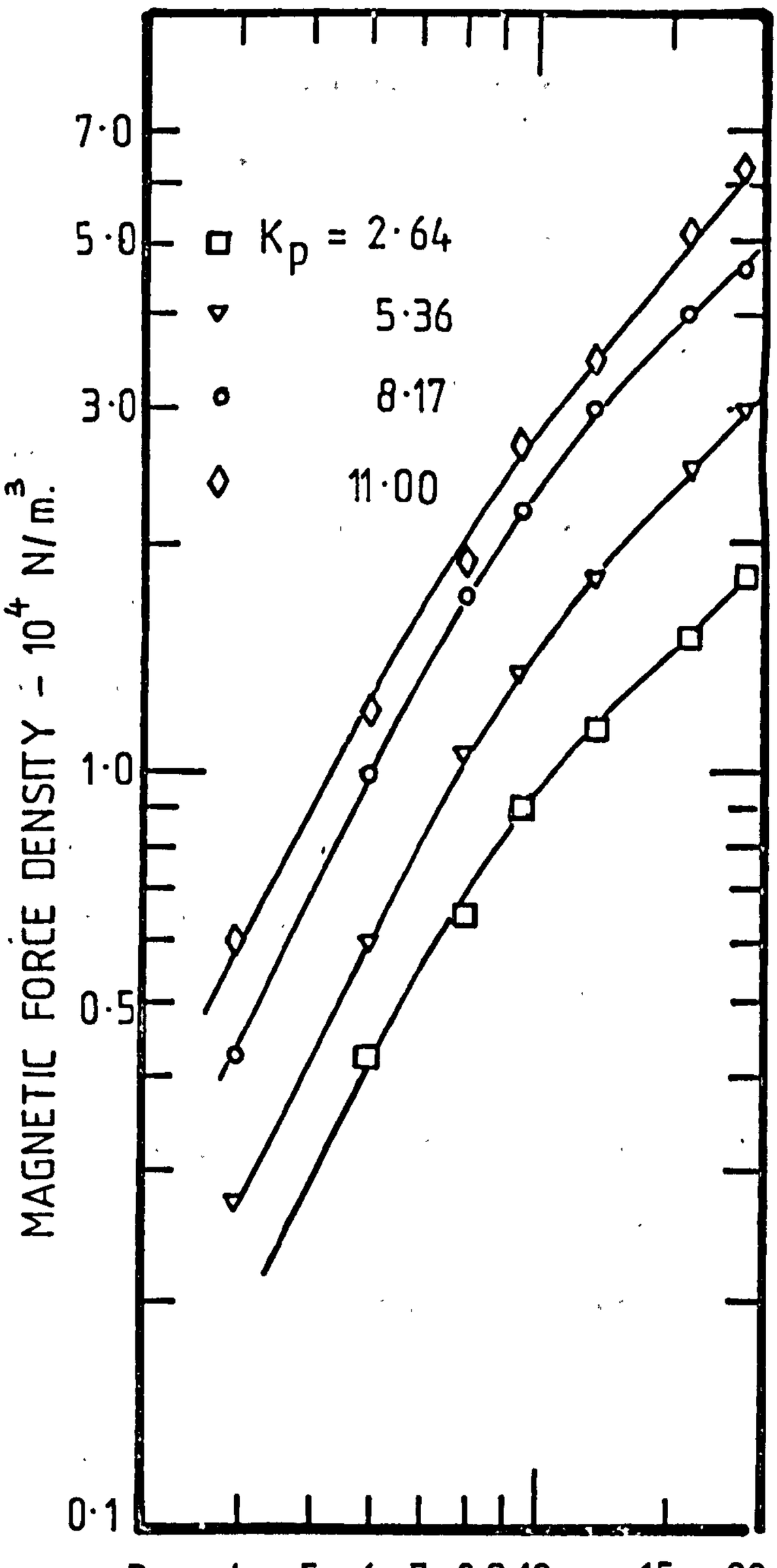

FIG. 3.30. VARIATION OF MAGNETIC FORCE DENSITY WITH SUPPLY CURRENT FOR MO-2035 FLUIDS - Z = 0·07 m.

The second region must be where the fluid is saturated and hence the magnetization in this region is the saturation magnetization of the fluid. Thus the magnetic force density is expected to be proportional to the current as indicated by the unity slope on a log-log scale.

The exciting current at which the saturated region starts varies from curve to the other, but if the currents are referred to the corresponding field strengths, it is found that the saturation starts at about 4 to 5 x 10^5 A/m.

3.4.2 Assessment of the approximate fluid magnetization curve from force measurements.

At the flux-densities which are likely to be produced in the stator bore (0.18 T) saturation of the stator iron should not occur (in any reasonably designed stator). Since the fluid permeability (relative) is of the order of 1 to 2 only nearly all of the stator mmf will be expended in driving flux through the fluid. Therefore the field intensity in the fluid, H, is proportional to the exciting current.

From the values of ρ_m and knowing the relationship between H (and $\frac{\partial H}{\partial z}$) and exciting current from Figs. 3.19 and 3.20, equations 3.2.8 and 3.2.9 can be used to obtain values of χ and $\mu_o M_{sat.}$ These values can again be used to predict magnetization curves and saturation levels for the fluids. They can be compared with curves obtained by direct magnetic measurement in section 1. Some comparisons are made in figures 1.11 to 1.18 and it will be seen that the agreement is very reasonable.

It was found that the estimated values of saturation magnetization of a fluid varied slightly from one set of measurements to the other within about 5%. As an approximation, the average values were considered. The values were 0.01, 0.017, 0.027 and 0.039 Tesla for the fluids of volume concentrations of Pfizer material in paraffin of 2.64, 5.36, 8.17 and 11% respectively. If these values of saturation magnetization are referred to 100% volume concentration

they give values of 0.38, 0.31, 0.33 and 0.353 Tesla respectively. These figures are comparable with 0.35 Tesla by Pfizer for this material and the greatest error between them and the values measured more directly in section 1 is about 7%, and as expected occurs for the lowest volume concentration.

The susceptibility value, χ, of the unsaturated fluids were found to be 0.192, 0.352, 0.51 and 0.664 respectively for volume concentrations listed above. These values are also roughly proportional to the volume concentrations, and $\frac{K_p}{\chi} \simeq .15$. It is shown in Appendix 2 that

$$\chi = \mu_f - 1 \simeq \frac{K_p}{K_z},$$

therefore the expected value of K_z is $\simeq .15$ and from Fig.3.3 this corresponds to an aspect ratio of $\frac{a}{b} = 2.2$ which supports the acicular shape claimed by the supplier.

Similar agreements with the measurements of χ and M_{sat} in section 1 were obtained for the magnetite, ferrosilicon and the colloidal suspension fluid.

The above was also the case for the results of the tests on the 140 mm diameter stator, a sample of which is shown in Fig.3.16.

3.4.3 Variation of magnetic force with the volume concentration of the magnetic material in fluids.

Fig.3.2 shows that for a spherical body an almost linear relationship exists between X and $\mu_e - 1$, i.e. , at least from $0 \leq \chi \leq 5$. Since χ is expected to be proportional to packing factor, as was verified in section 1, the magnetic force density can be expected to be proportional to volume packing factor (as long as χ is not very large). Plots of magnetic force density ρ_m against volume packing factor, K_p, are shown in Fig.3.31, and are indeed substantially linear.

3.4.4 Comparison between the various magnetic materials used in the investigation.

The highest values of K_p was on the basis that non-magnetized fluid was almost solid at the highest value of K_p selected for each particular material.

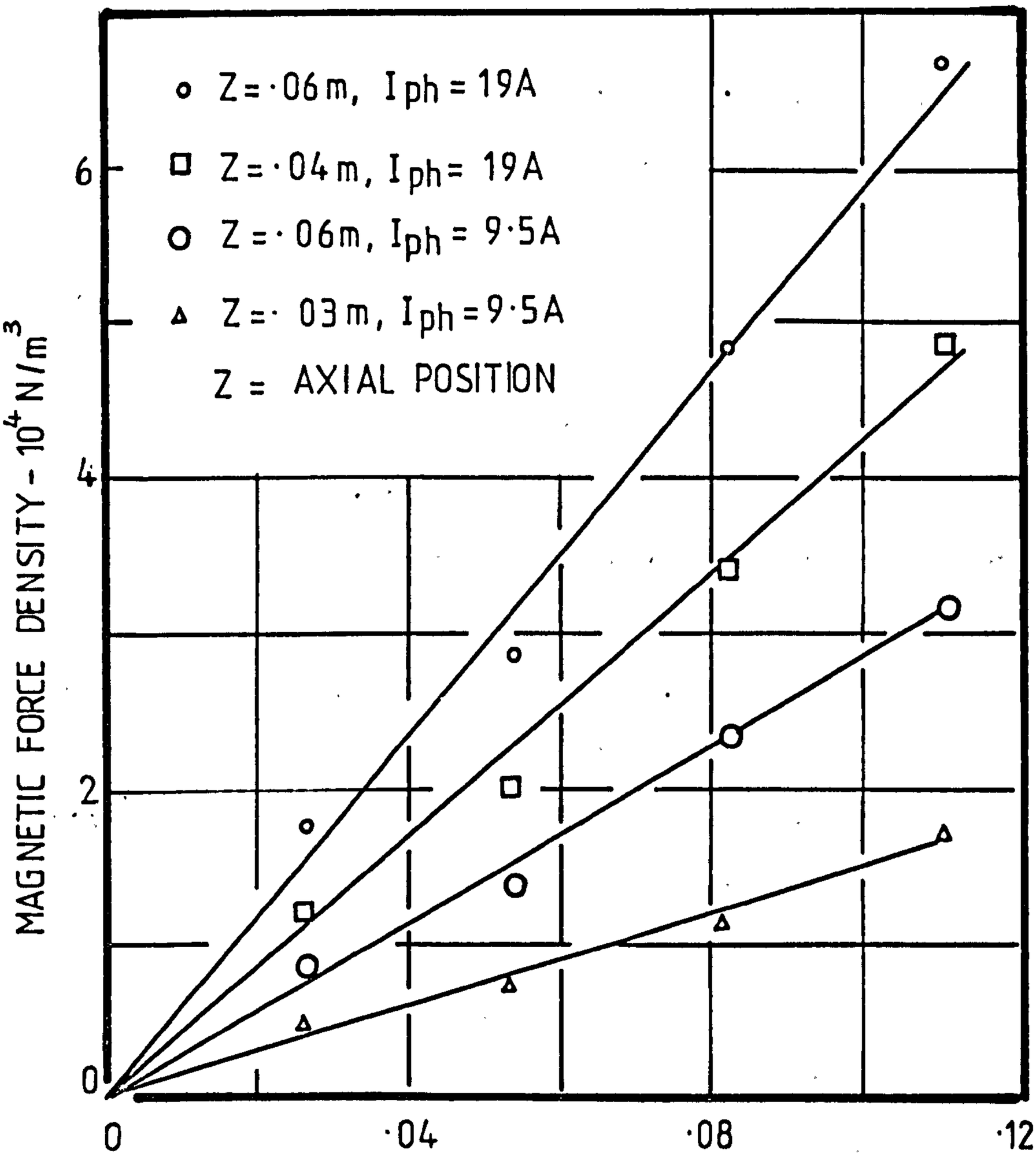

FIG. 3.31. EFFECT OF VOLUMETRIC LOADING OF MAGNETIC MATERIAL IN FLUID UPON THE MAGNETIC FORCE DENSITY - THE 118 mm DIAMETER TWO POLE STATOR.

If for the highest volume concentrations used in the tests, the non-magnetized densities of the MO-2035, magnetite and ferrosilicon fluids were added to the magnetic force densities, we get 7.8×10^4, 11.74×10^4 and 7.74×10^4 N/m^3 respectively. These densities divided by the volume loadings of the fluids are 700×10^4, 535×10^4 and 1200×10^4 N/m^3 respectively. This means that ferrosilicon fluid is the best followed by the MO-2035 fluid and then by the magnetite fluid, at least from the point of a higher ratio of force density to volume loading.

3.4.5 Influence of frequency upon the magnetic force.

As expected the variable frequency tests indicated that the magnetic force does not vary very much with frequency. Sample results are shown in Fig.3.11. The slight variations with frequency, generally less than 6%, are believed to be due to experimental error which is not more than 6%.

3.4.6 Influence of body shape upon the magnetic force.

The results of Fig.3.12 do not indicate any clear difference between the two shapes of bodies. This can be explained by referring to equation 3.2.6 and Fig.3.3. The merit factor $|X|$ which is a measure of the force for a given field gradient, for $\mu_e = 1.664$, which is the permeability of the investigated fluid, varies from 0.721, ($K_z = .2$) to 0.766, ($K_z = .333$), $K_z = 0.2$, corresponding to the prolate spheroid and $K_z = 0.333$ for a spherical body. This means that there is only a difference of 5.8% in X which might be masked by experimental error. Another factor is that the assumption behind the theory that the variation in stored energy density through the volume of the body is small is even less reasonable than for the case of the sphere.

3.4.7 Effect of varying the length of the 2-pole stator upon the field gradient.

Some of the results of varying the stack length of the steel stampings, keeping the diameter fixed, are shown in Fig.3.22. As the stack length becomes

shorter, the two end-regions begin to overlap leading to a weaker field in the middle of the stack. The longer the length of iron, the longer the region over which the field is uniform. As far as the magnetic separation process is concerned this is an inactive zone since the field gradient in it, and hence the magnetic force is zero.

As the stator power loss is proportional to the length of winding, which increases as the stack length increases, the smaller the length the better from the point of minimum power dissipation.

Assuming that the field intensity is to be high enough to saturate the particles (this is a practical requirement for high-densities) a large value of field gradient per unit length of conductor is required. However, since the kinetic energy of the material to be separated is also an important factor, it would be unwise to have too low a value of H_{max}, and thus of L, since the peak energy that can be 'absorbed' is proportional to this. For both the 'normal' and the Gramme-ring winding a value of L/D of about 0.3 would seem to be reasonable.

Direct comparison between the two windings is not at all straightforward since the Gramme-ring winding length increases with the radial depth of the stator and due to the leakage flux from the external curved surfaces of the stator which result with this winding this dimension must be much greater than for the 'normal' winding. It is felt that in a practical system it will offer no real advantage over the 'normal' winding and will possibly be worse.

3.4.8 Effect of varying the stator diameter upon the field gradient.

If the length to diameter ratio is kept constant then the field gradient at any particular value of Z/D should not vary from a stator to another. Fig.3.23 which verifies this is a plot of the ratio H/H_{max} against Z/D for two stators. One of them was one of the stators used in Fig.3.22 with length 0.103 m and diameter 0.066 m with the 'normal' single coil winding. The other was a

conventional 2-pole 3-phase stator winding of length 0.133 m and diameter 0.085 m.

From the above $\frac{\partial H}{\partial (Z/D)}$ must be constant for any fixed value of Z/D.

But, $\frac{\partial H}{\partial (Z/D)} = D \frac{\partial H}{\partial Z}$

$\therefore \frac{\partial H}{\partial Z} \propto \frac{1}{D}$

Similarly $\frac{\partial H^2}{\partial (Z/D)}$ is constant, and since

$$\frac{\partial H^2}{\partial (Z/D)} = D \frac{\partial H^2}{\partial Z} = D \times 2H \frac{\partial H}{\partial Z}$$

$$\therefore H \frac{\partial H}{\partial Z} \propto \frac{1}{D}$$

Thus for a high value of $H \frac{\partial H}{\partial Z}$ (unsataturated case) and for a given H_{max}, we need a small value of D, the smallest consistent with the required throughput. This applies also to the saturated case, where $\frac{\partial H}{\partial Z}$ is the important quantity. However, if the dynamics of the bodies to be separated must be considered, L and D may have to be larger.

3.4.9 The linear arrangement.

Measurement of field intensity over a wide range of currents indicated that there was negligible saturation of the stator iron. On the other hand, the plots of magnetic force density against stator current shown in Fig.3.32 indicate that the fluid was saturated, since the relationship between the two is linear and not a square law as would apply in the unsaturated case. The smallest field strength in the measurement area was about 6×10^4 A/m, which can be seen from results of section 1 to be greater than that necessary to saturate the basic magnetic oxide.

The results suggest that a linear arrangement for variable density separation is possible provided that a means is achieved of preventing the magnetic

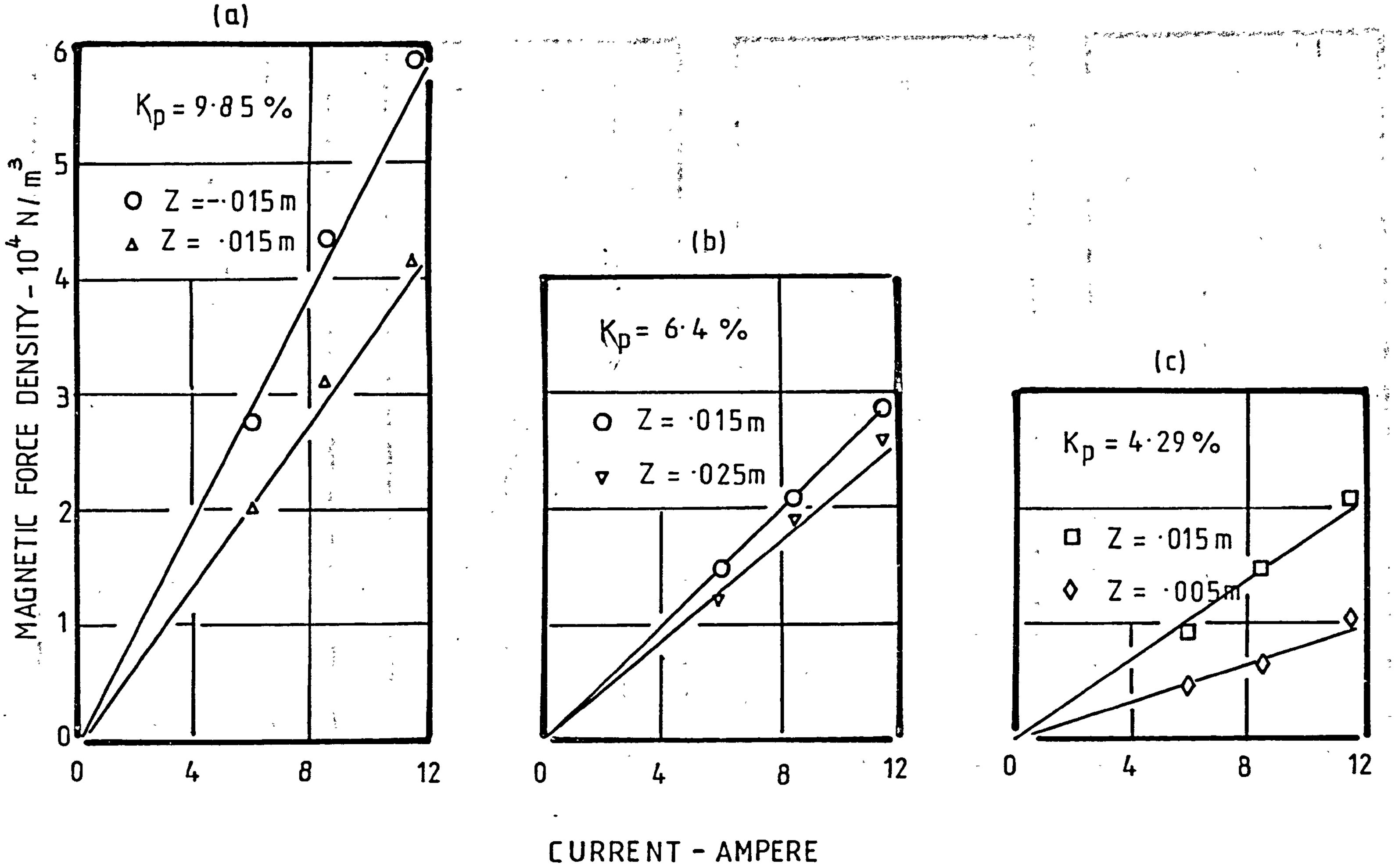

FIG. 3.32. EFFECT OF EXCITATION UPON MAGNETIC FORCE DENSITY - LINEAR CONFIGURATION

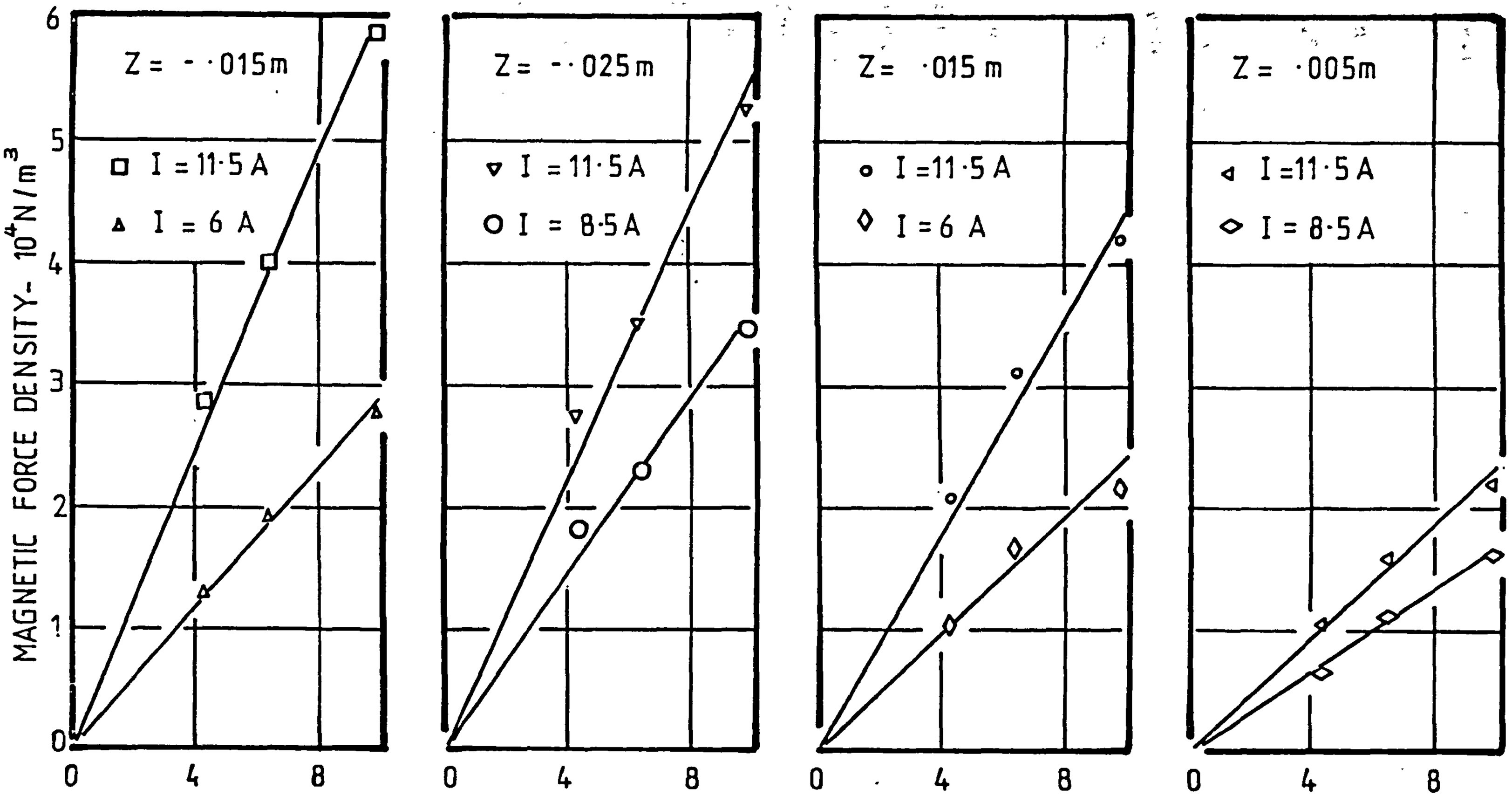

FIG. 3.33. EFFECT OF VOLUME PACKING FACTOR UPON MAGNETIC FORCE DENSITY-LINEAR CONFIGURATION

particles in the region midway between the two faces from flocculating.

The graph of magnetic force density against percentage volume of MO-2035 in paraffin, shown in Fig.3.33, again indicates a linear relationship.

3.5 Analytic study of the magnetic force in the cylindrical configuration.

Curves of measured values of the radial magnetic field intensity along the axis of the two-pole machines are shown in Figs. 3.19 and 3.20. Off axis values for the four-pole machine are shown in Fig.3.34. They indicate an almost cosinusoidal variation and in Appendix 4 is an analysis of the three-dimensional field distribution based on the assumption that the variation is of the form Cos γz where z is the distance along the axis from the middle of the machine. Since the m.m.f. is periodic around the stator surface, the field components can be expected to vary in the same periodic manner. Thus, knowing the basic form of variation with respect to z and θ an estimate of the possible form of the field distribution can be made by applying Maxwell's equations.The solution should be reasonably correct for r less than the radius R_b of the stator bore, and for γz less than π, i.e. for most of the area of interest.

It can be seen from Appendix 4 that the magnetic energy density, E_m, as well as the magnetic force densities in the axial and radial directions, ρ_{mz} and ρ_{mr} respectively, are given by:

$$E_m = \tfrac{1}{2}\,\mu_o\,\mu_f\,A^2 \left\{ \left[\frac{I_{p+1}^2(\gamma r) + I_{p-1}^2(\gamma r) + 2I_p^2(\gamma r)}{2} \right] + \left[\frac{I_{p+1}^2(\gamma r) + I_{p-1}^2(\gamma r) - 2\,I_p^2(\gamma r)}{2} \right] \cos(2\gamma z) \right\}$$

$$+ \quad \text{time varying components.} \qquad \ldots\ldots \qquad \text{A4.19}$$

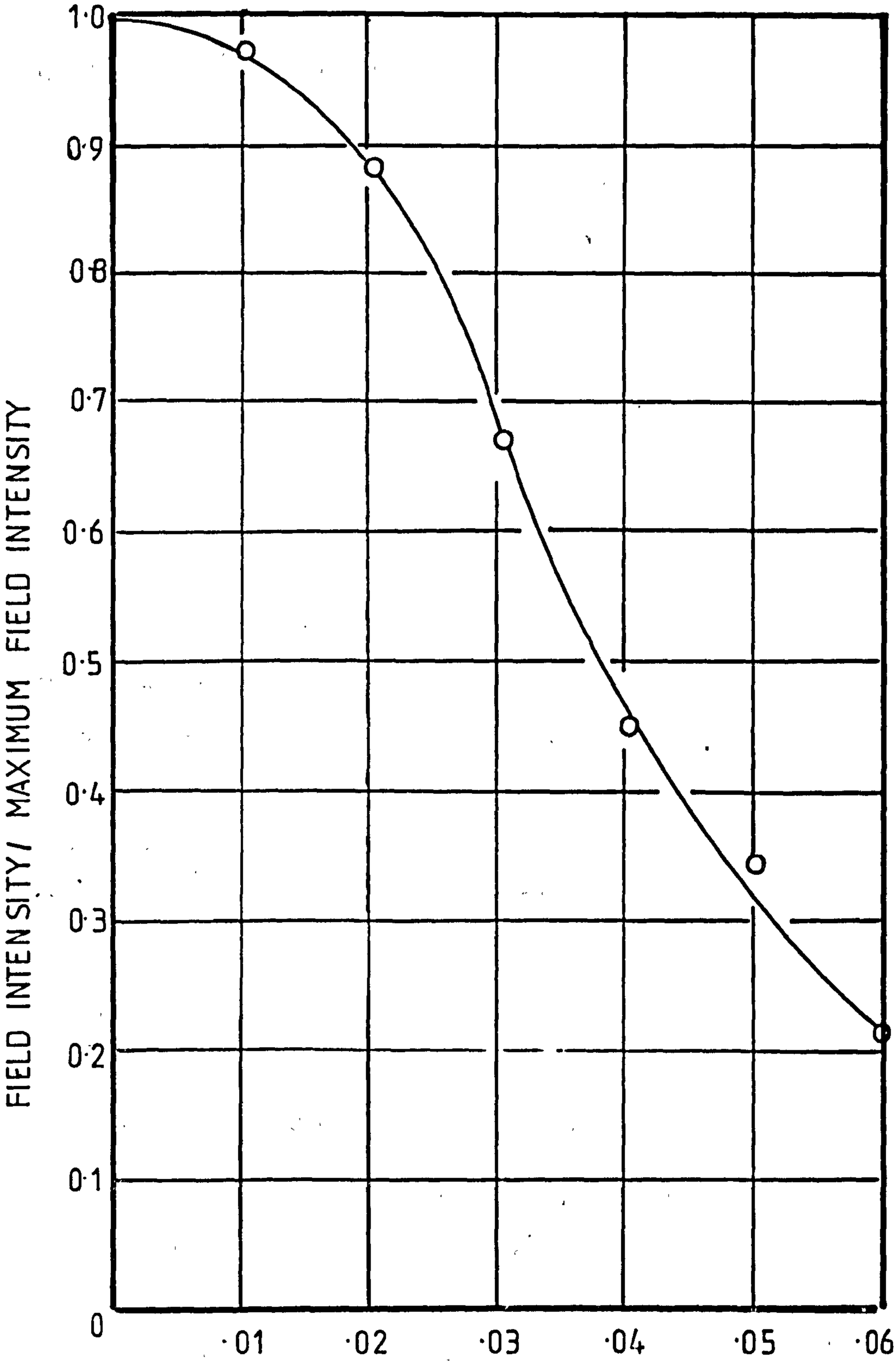

FIG. 3.34. VARIATION OF FIELD INTENSITY WITH OFF AXIS POSITIONS OF FOUR POLE STATOR. r=.035 m

$$\rho_{mz} = \tfrac{1}{2}\ \mu_o\ \mu_f\ K\ A^2\ \gamma\ \Big[I_{p+1}^2\ (\gamma r) + I_{p-1}^2\ (\gamma r) - 2 I_p^{\,2}\ (\gamma r) \Big]\ \sin(2\gamma z) \qquad \ldots\ldots \qquad \text{A4.20}$$

$$\text{and}\quad \rho_{mr} = \tfrac{1}{2}\ \mu_o\ \mu_f\ K\ A^2\ \gamma\ \Big\{ \Big[\frac{-2(p+1)}{\gamma r}\ I_{p+1}^2\ (\gamma r) + \frac{2(p-1)}{\gamma r}\ I_{p-1}^2\ (\gamma r) \Big]\ \cos^2(\gamma z) + 2\ I_p\ (\gamma r)\ \Big[I_{p+1}\ (\gamma r) + I_{p-1}\ (\gamma r) \Big] \Big\} \qquad \ldots\ldots \qquad \text{A4.21}$$

where K is a constant governed by the shape of the body.

The winding power loss is obviously an important parameter, and since the latter is very dependent upon J_{max}, this has been chosen as a basis of comparison.

Plots of $\dfrac{2\ \rho_{mz}}{K\ \mu_o\ \mu_f\ J_{max}^{\,2}\ \gamma}$ and $\dfrac{2\ \rho_{mr}}{K\ \mu_o\ \mu_f\ J_{max}^{\,2}\ \gamma}$

are shown in Figs. 3.37 to 3.40 for various values of p, γr and γz. The results shown are restricted to the two and four-pole cases only - those for higher pole numbers are similar to those for 4-poles. Contours of constant energy density, $\dfrac{2\ E_m}{\mu_o\ \mu_f\ J_{max}^{\,2}}$, are shown in Figs. 3.35 and 3.36. Magnetic forces will tend to act along lines at right angles to these contours, except near the stator surface where 'dipole image' forces tend to be large.

Fig.3.36 illustrates the case of a multipolar (other than 2-pole) a.c. stator which produces zero field in the middle, thus rendering the central core unavailable for the separation process.

The variations of the axial force densities with the radial and axial positions are shown in Figs. 3.37 and 3.38. It will be seen that ρ_{mz} is little affected by r in the case of 2-pole, but there is a substantial variation with

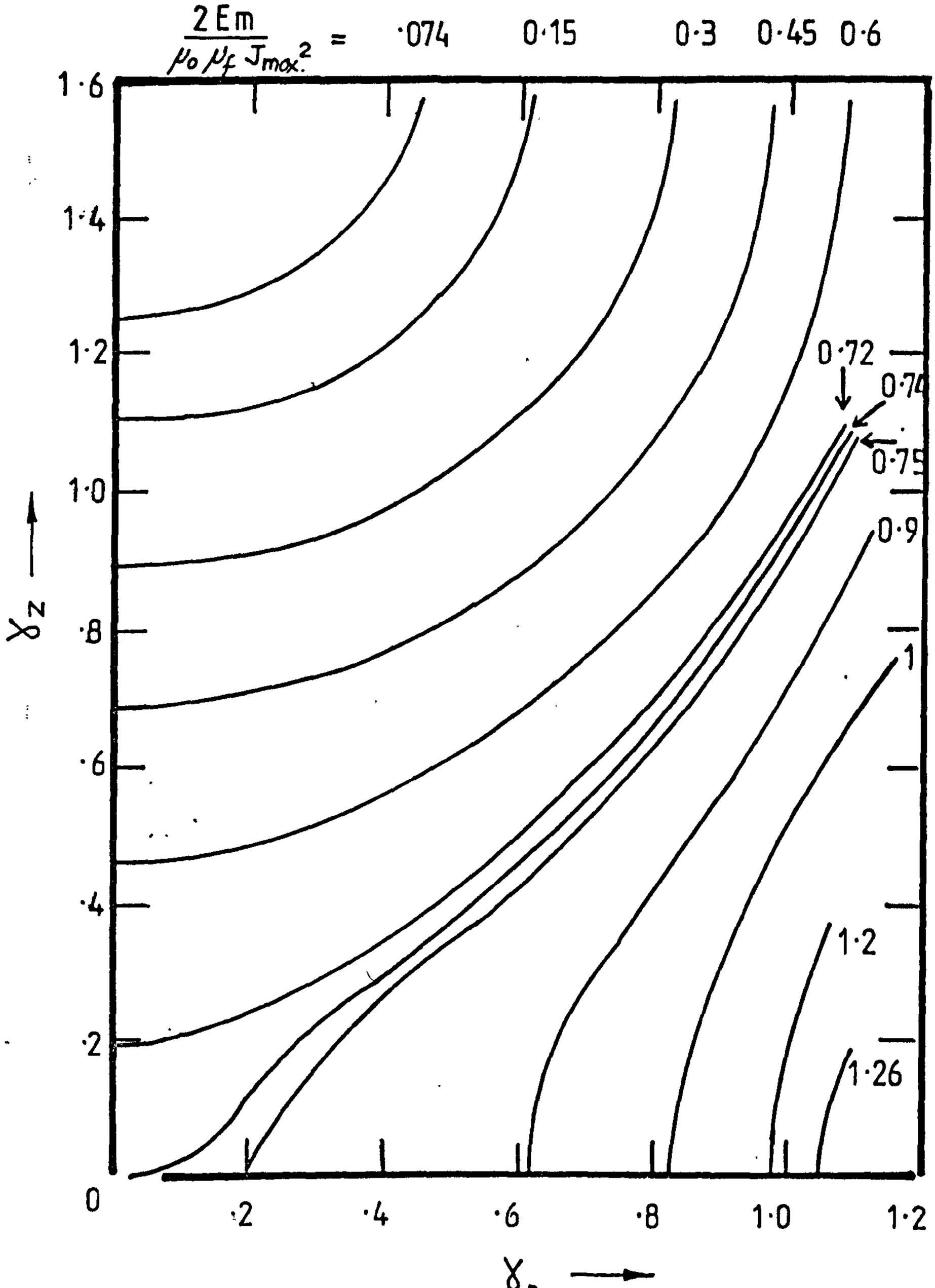

FIG. 3.35. CONTOURS OF $\frac{2E_m}{\mu_o \mu_f J^2_{max.}}$, 2-POLE CASE

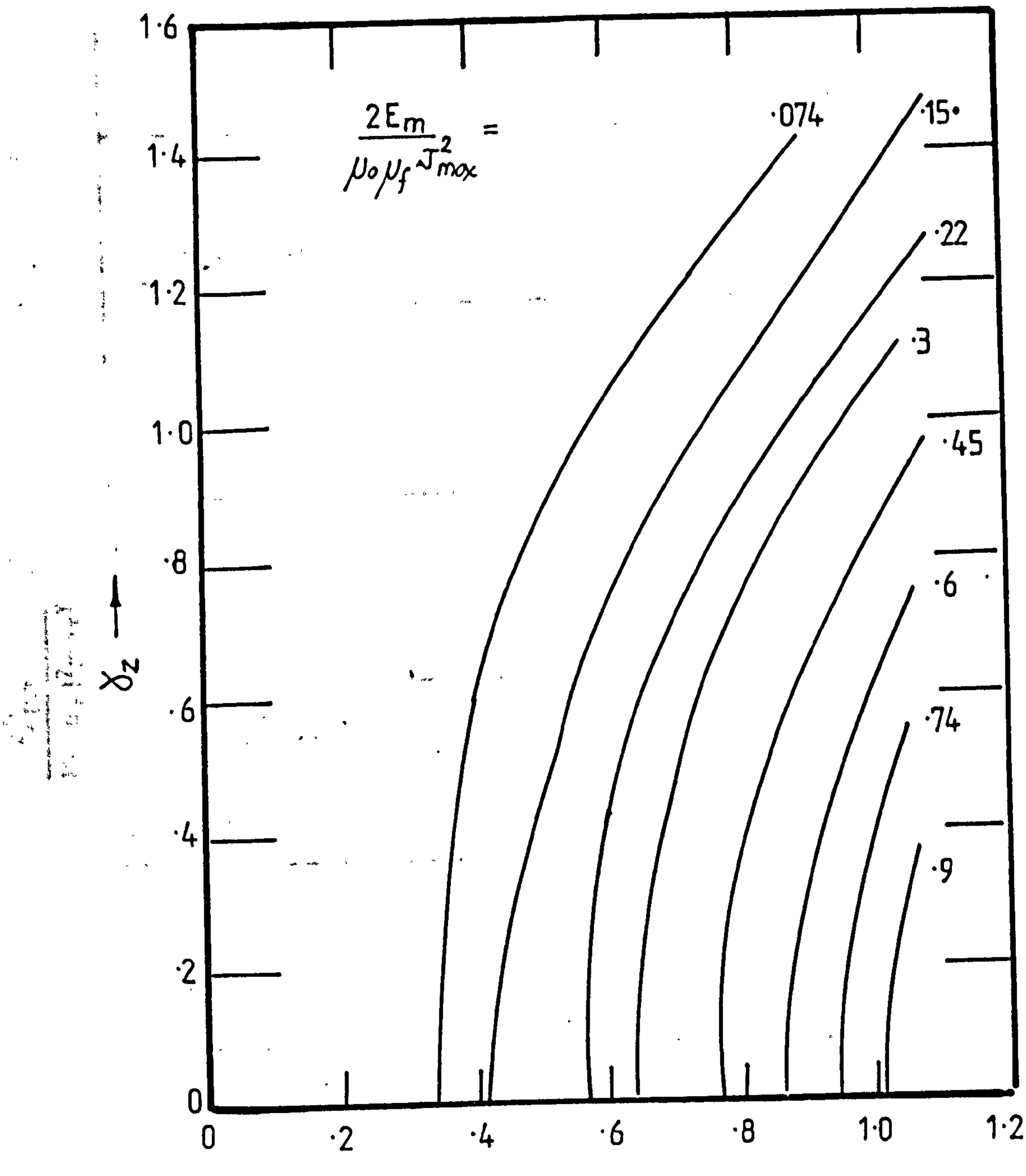

FIG. 3.36. CONTOURS OF $\frac{2E_m}{\mu_0 \mu_f J_{max}^2}$, 4 - POLE CASE

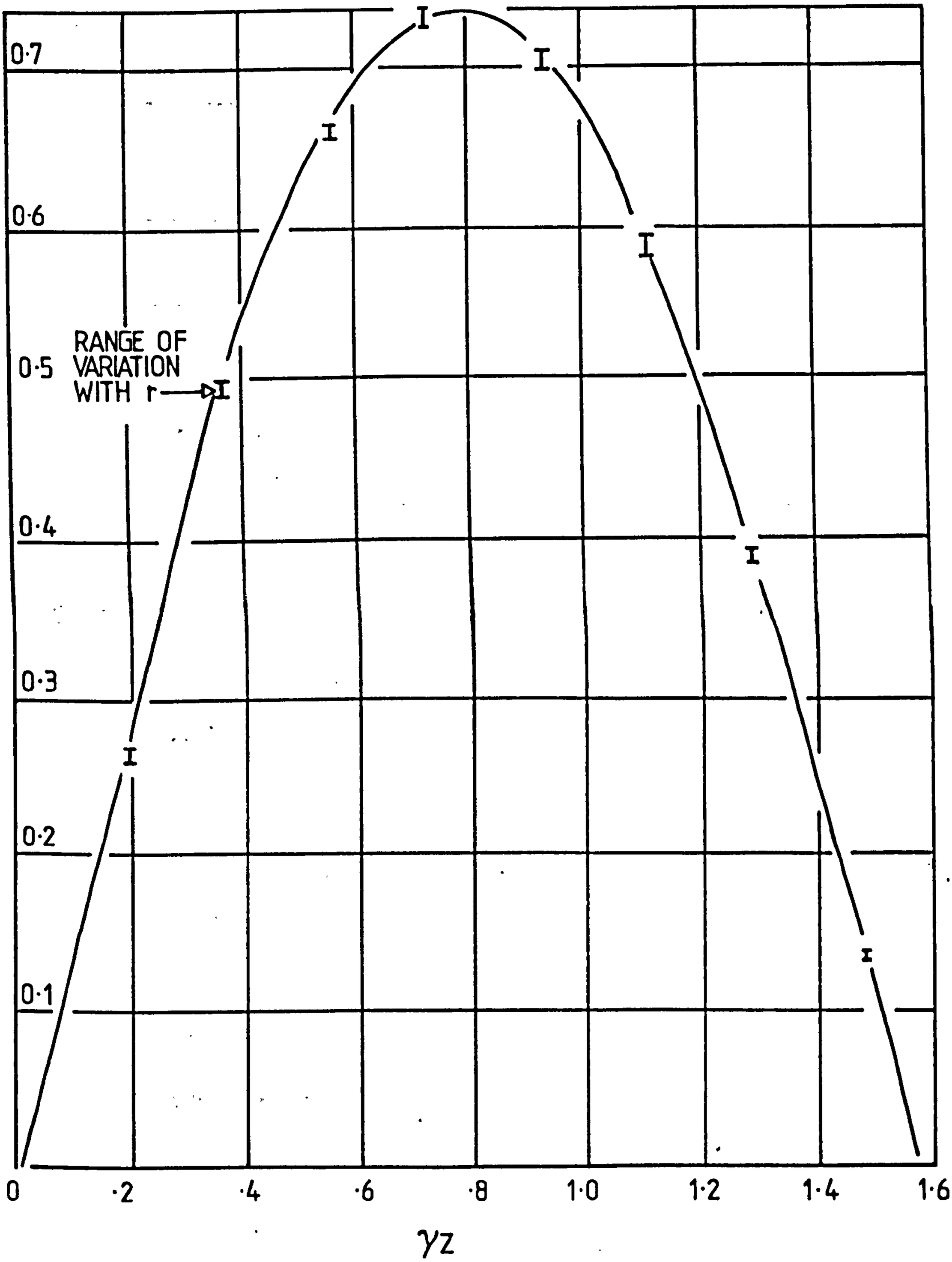

FIG.3.37 VARIATION OF AXTIAL FORCE DENSITY, ρ_{mz}, WITH AXIAL POSITION, z, 2-POLE CASE.

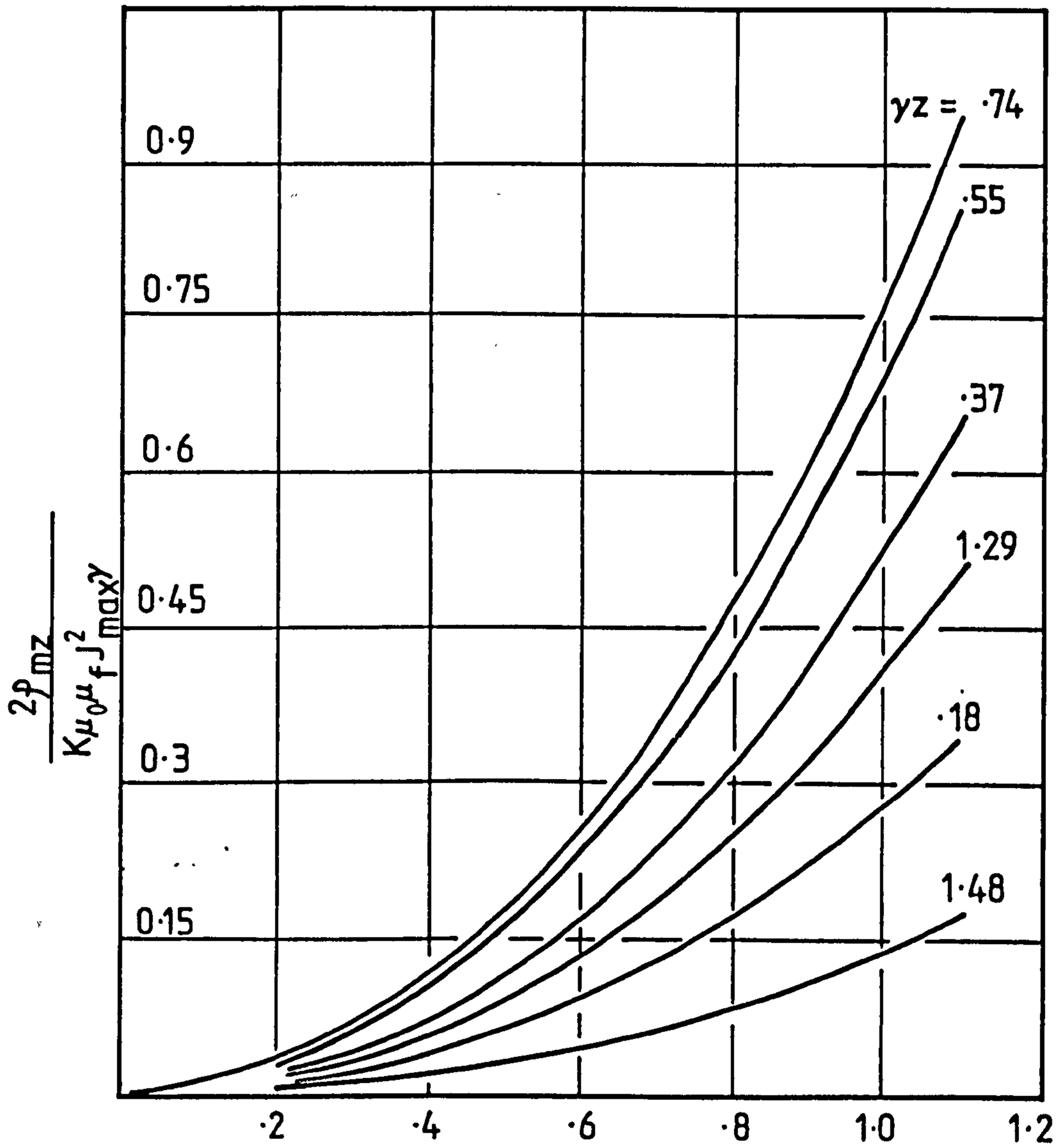

FIG.3·38 VARIATION OF AXIAL FORCE DENSITY, p_{mz} WITH RADIUS, r, 4-POLE CASE

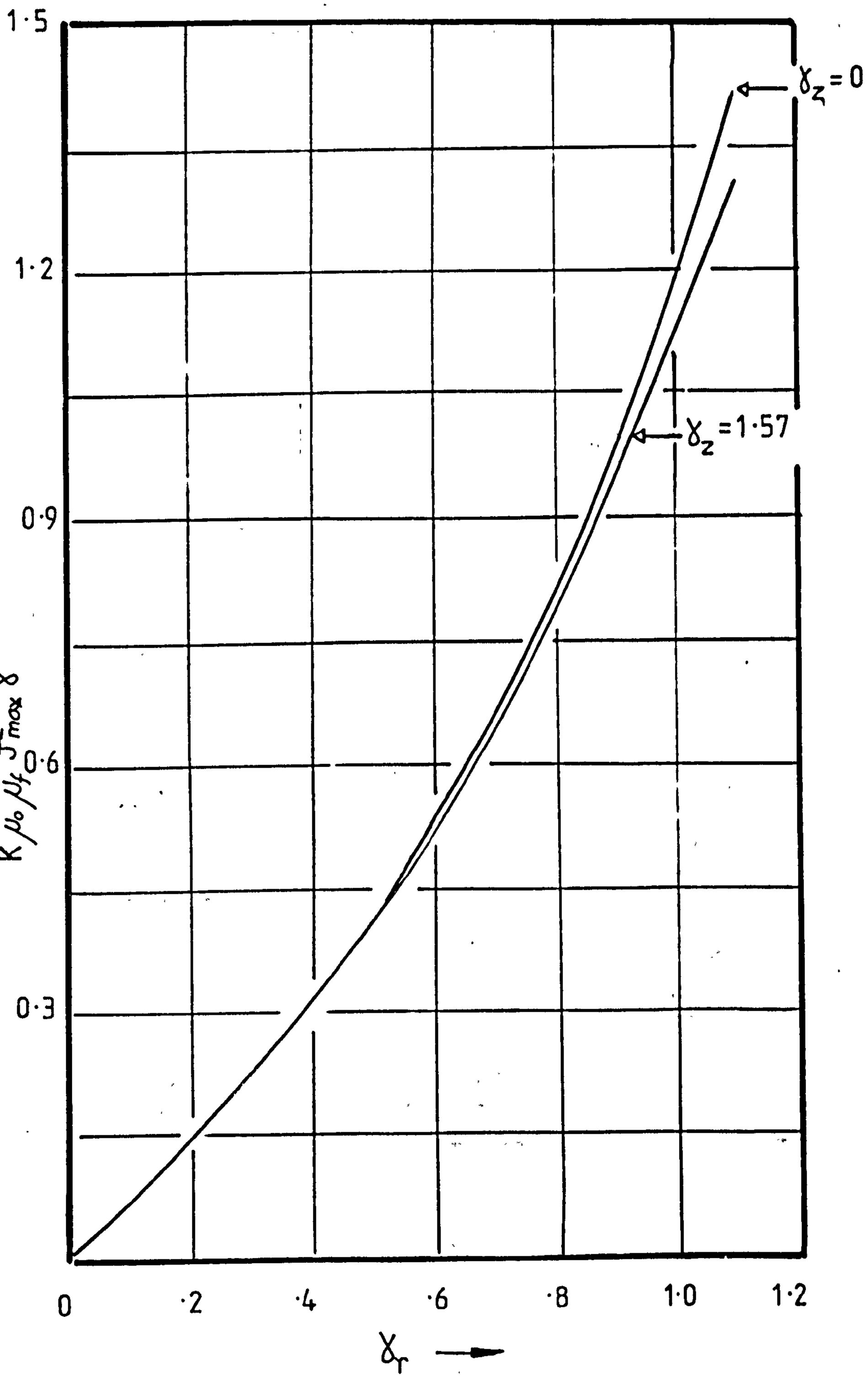

FIG. 3.39. VARIATION OF RADIAL FORCE DENSITY, f_{mr}, WITH RADIUS , r , 2-POLE CASE.

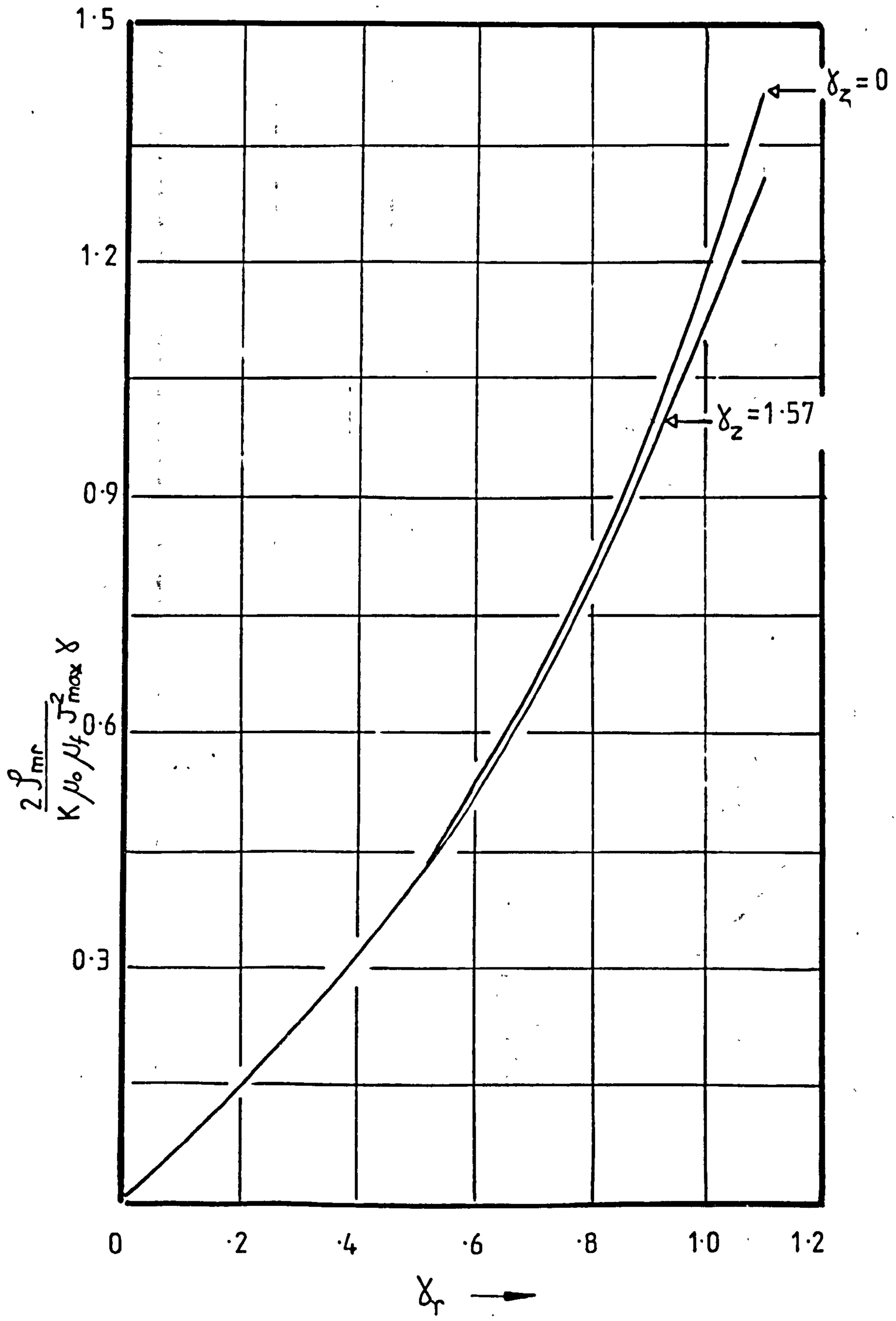

FIG. 3.39. VARIATION OF RADIAL FORCE DENSITY, ρ_{mr}, WITH RADIUS , r , 2-POLE CASE.

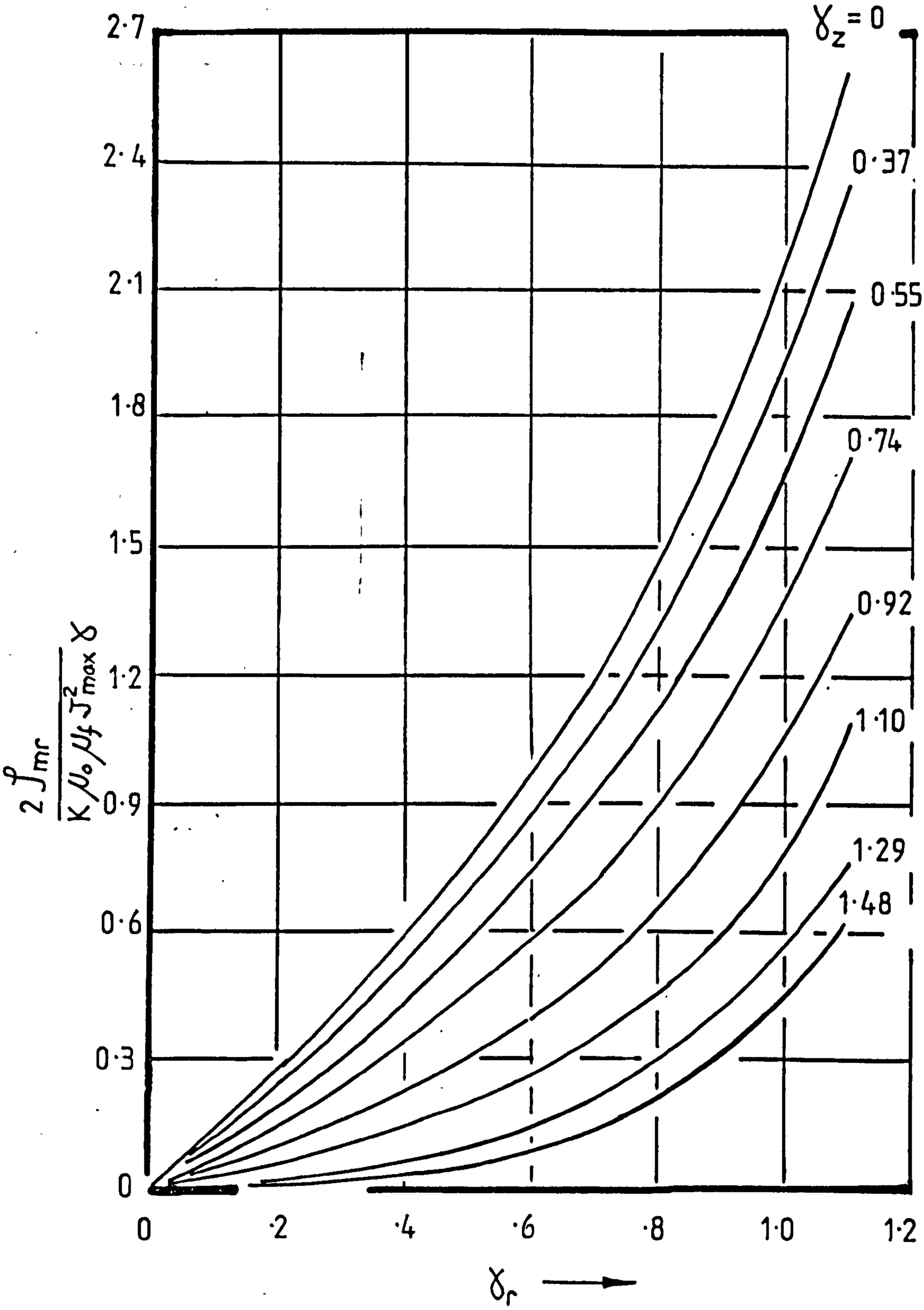

FIG. 3.40. VARIATION OF RADIAL FORCE DENSITY, f_{mr}, WITH RADIUS, r, 4 - POLE CASE.

r in the 4-pole case. This does suggest that a separation process utilizing the axial forces is more practical with a two-pole than a four-pole winding. On the other hand, the higher radial forces for the four-pole winding suggests that this is better should radial separation be required. The fact that the four-pole stators produce constant radial field gradient, see Appendix 6, support their use, in preference to higher pole numbers, for radial separation.

3.6 Discussion of Potential Practical Systems for the Separation Process.

3.6.1 Introduction.

The process of separation can be achieved by making use of axial or radial forces, possibly produced by conventional a.c. stators. In the first one no substantial variation of the field intensity in the radial direction is required so that all the throughput material encounters the same effective fluid density at any fixed axial position. The two-pole stators provide this requirement since Fig.3.37 shows no substantial variation of ρ_{mz} with r. As stated earlier, the four-pole stator is suitable for a separation process utilizing radial force.

3.6.2 Axial separator.

Fig.3.41 shows a schematic diagram of a bench scale equipment designed as a demonstration model. The beaker contains a fluid of 8% by volume of magnetite in water using 10% solution of sodium silicate as a surfactant. The height of the surface of the fluid as well as the excitation current of the 118 mm diameter two-pole stator was adjusted so that the light material, which was Felspar of S.G.2.6, could float and it was brought towards the outer region under the effect of the fluid rotation where it was collected on the top grid upon switching off the current. In a practical system the floating material should be skimmed off the top of the fluid for the process to be continuous. The heavy material, which was Galena of S.G.7.5, sank and was collected on the bottom grid.

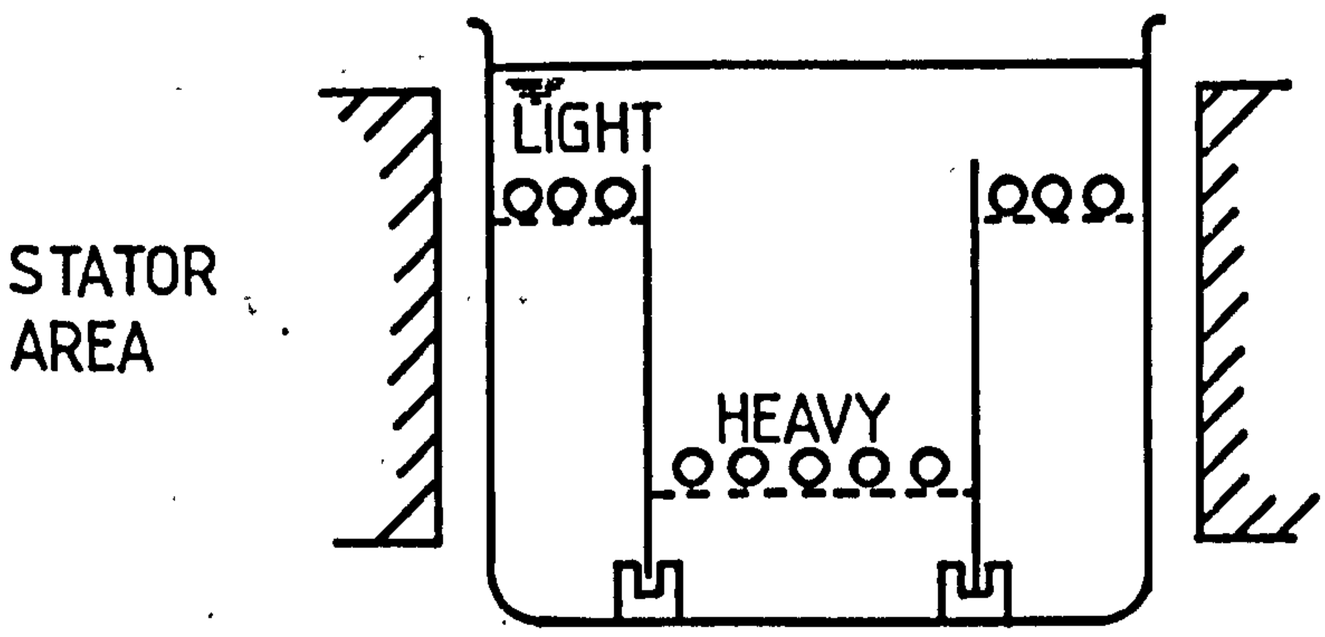

FIG 3.41 AXIAL SEPARATOR ARRANGEMENT

3.6.3 Radial separator.

The axial separator utilizes the non-uniform field region at the end of the two-pole stator to produce the required axial field gradient. On the other hand the radial separator utilizes the 'uniform' field region, where there is much less variation in the field with axial position, and avoids the end region where there is such variation. The radial separator relies on the constant radial field gradient in that uniform region produced by a four-pole cylindrical configuration. The radial acceleration of the material is dependent on its density and therefore distance separation can be achieved.

The kinematic equations of motion for a moving body in a ferrofluid under the effect of gravity and constant radial field gradient are dealt with in Appendix 5 and they are given by:

$$\frac{d^2z}{dt^2} = g - \frac{b}{m}\frac{dz}{dt} \qquad \ldots\ldots \qquad \text{A5.2}$$

and $$\frac{d^2r}{dt^2} = \frac{\mu_o M_{sat} A}{\rho_b} - \frac{b}{m}\frac{dr}{dt} \qquad \ldots\ldots \qquad \text{A5.3}$$

If we use the transform $r = x.\frac{\mu_o M_{sat} A}{\rho_b g}$ equation A5.3 becomes the same as A5.2 and the general solution is given by

$$z = \frac{m}{b} gt + \left[\left(\frac{m}{b}\right)^2 g - \left(\frac{m}{b}\right) V_o\right](e^{-bt/m} - 1)$$

taking $z = 0$ at $t = 0$, the instant at which the body hits the fluid surface.

Therefore we expect a straight line trajectory if the initial velocities $\dot{x}_o$ and $\dot{z}_o$ are zero. Fig.3.42.a is a plot of calculated trajectories for four spheres, each of radius 5 mm but of different densities, deposited with zero initial velocities in a fluid of M_{sat} = .011 T and η = 0.004 MKS units. The separation region is the central zone of a 4-pole stator of 0.12 m diameter, which produces an almost constant radial field gradient of 79.6 x 10^5 A/m^2. However, if

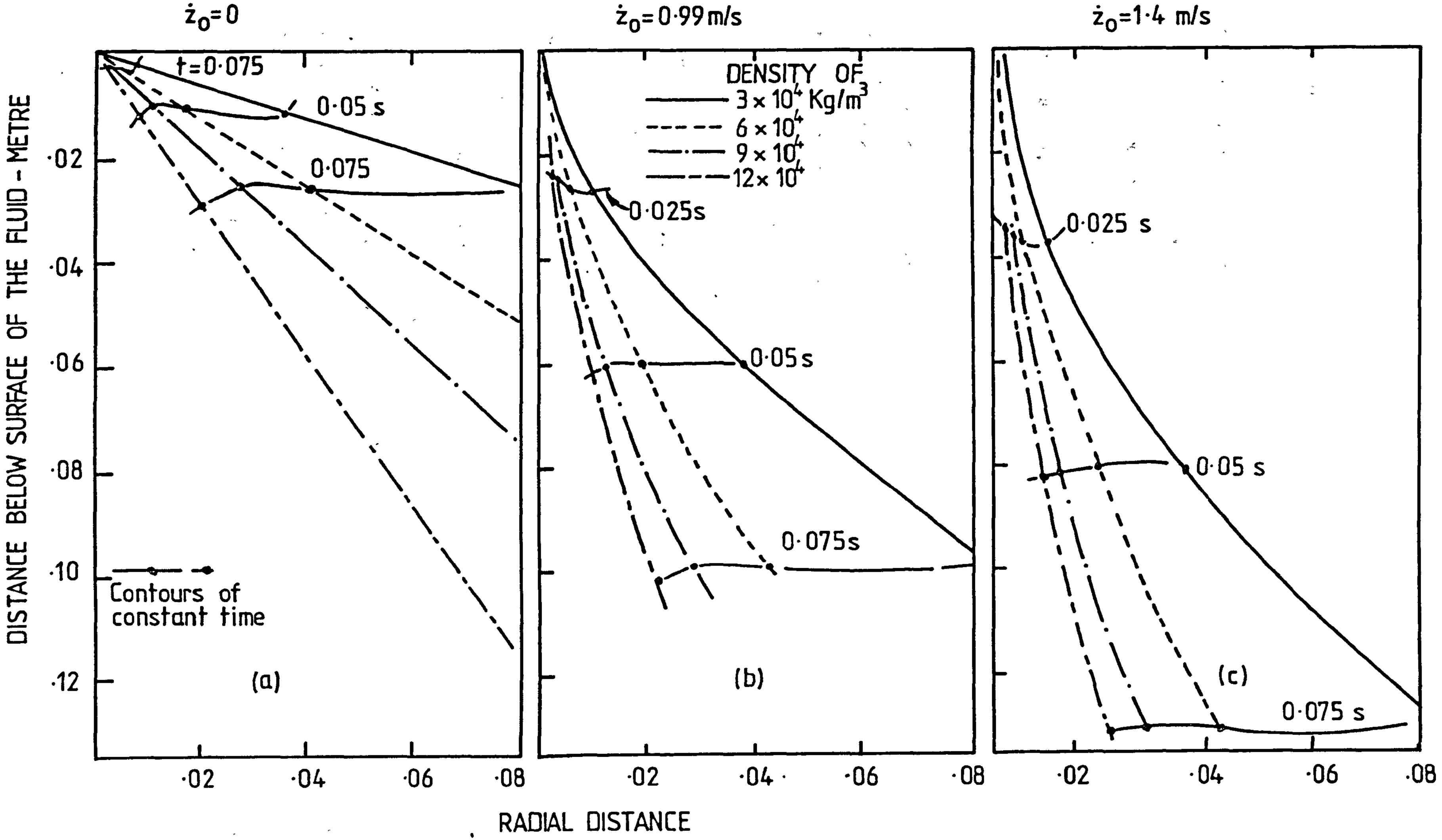

FIG. 3.42 POSSIBLE TRAJECTORIES FOR RADIAL SEPARATION

the motion of the body before it hit the fluid surface was perfectly vertical there will be an initial velocity $\dot{z}_o$ but $\dot{x}_o$ will be zero. But if the previous motion was not perfectly vertical $\dot{x}_o$ will exist and upset the separation process if all bodies do not have the same value of $\dot{x}_o$. Fig.3.42.b and 3.42.c give the expected trajectories for $\dot{z}_o$ equal to 0.99 and 1.4 m/s respectively and $\dot{x}_o = 0$. The length of time of separation process was assumed to be 0.075 S. Fortunately, the effect of the viscous force over even double this length of time and for a fluid viscosity as high as 0.016 MKS was found to be negligible compared to both the gravity and magnetic forces. This is a desirable feature from the point of view of the separation process since it allows the use of a longer stack length and a smaller value of current density. For the same radial separation of material the power consumption can thus be reduced.

The intention was to use fluids of low concentration, and thus of low viscosity, so that the throughput could be high and for the fluids to be easily handled outside the magnetic region. On trial,however, the low concentration fluids gave rise to a strong swirling acting in the fluid which upset the above pleasant theory. Attempts to stop the fluid swirl by reducing the frequency and by putting radial fins inside the beaker were unsuccessful.

3.7 Conclusions.

The theoretical expressions for the magnetic force exerted on a body situated in a ferrofluid and experiencing a magnetic field gradient has been verified by experiments. These have been used to estimate the values of the susceptibility and of the saturation magnetization of the fluids. For the Pfizer powder, type MO-2035, the projected value of saturation moment, $\mu_o M_{sat}$, for 100% volume loading agrees very well with that given by Pfizer for the solid material.

The magnetic force has been shown to be proportional to the volume loading of the ferrofluid and, for a given shape, to the volume of the immersed body,

irrespective of saturation. In the unsaturated case the force is proportional to the magnetic energy - density gradient (in space) but with saturation the force (increment) is proportional to the field gradient. Due to a mistake the effect of body shape was not investigated for the unsaturated case - the 'unsaturated' fluid later turned out to have been saturated. However, that saturated case is the more important in a practical separation application, and here the force is independent of body shape - a very desirable situation.

As expected, the magnetic force is independent of frequency, at least at frequencies of practical interest.

The force measurements have been extended to cover water-based fluids, using sodium silicate as the surfactant. Magnetite and ferrosilicon have also been used in addition to the Pfizer powder. As expected the change of carrier-fluid caused no change in the magnetic properties of the fluid, and there has been no sign of the fluid deteriorating with time. The highest total effective density measured, for the water-based magnetic fluid of volume loading 21%, was 11.7×10^4 $N.m^{-3}$.

No comparison, for cylindrical arrangements, between computed and experimental curves of magnetic force has been attempted. The computed curves have shed light on some important facts such as the very slight variation of axial forces with radial positions for the same axial level. They have also served to indicate higher radial forces in the case of multipolar machines other than the 2-pole.

The disadvantage of the linear arrangement is that there is some tendency for the magnetic particles in the middle to flocculate and the effective viscosity becomes large. On the other hand, the traverse of the fluid along the stator surface could be used as a means of transporting the light material away from the charging area.

The theoretical study of radial separation, centred upon 4-pole stators, gave very promising predictions of body trajectories. The swirl of the fluid due to the magnetic field, neglected in the predictions, produced relatively, large centrifugal forces which opposed separation and this system appears to be impractical.

The experiments with the 2-pole stator, relying upon axial separation, indicate that the swirling action is advantageous, in that the float material can be carried away from the 'feed' region. With a short axial length of stator, to keep the supply power and stored energy low, the system appears promising, but further evaluation is needed. Viability will also depend upon the economics of each practical separation application.

SECTION 4.

GENERAL CONCLUSIONS

It has been shown to be relatively straightforward to predict the magnetic properties of fluids from those of the parent magnetic material, and predicted and measured values of effective magnetic density for the mineral separation application have agreed fairly closely.

The dynamic performance of the fluids in rotating fields has been much more intransigent however. The torque mechanism is complicated in case of these primitive fluids where there is a wide range of particle sizes. There is the possibility of both saliency and hysteresis components being present, and at some instant some particles could be synchronized and exerting saliency torques, while others are slipping and exerting an average torque due to hysteresis. In each case the average torque generated must be equal to the torque demanded by the fluid, but with possible particle to particle random impacts and interference of eddies due to the adjacent particles the load torque is almost impossible to estimate. The mechanism of torque transfer through the fluid to the container is still not understood particularly in view of the fact that reverse rotation of the fluid did not seem to affect this torque appreciably. The torque per unit volume is small and this appears to be an inevitable feature. In any case there appears to be little promise of practical application of the fluid in either the pump or motor application.

Turning to the variable density application it is obvious that from the economic point of view one would want to use the largest possible size of particles in order to minimize the grinding time and hence the cost. However, if the particles are too large they tend to flocculate. It would appear that

the particle size of just under about 5 micron is a reasonable compromise.

The reactive Volt-Amperes, not measured in section 3, is large due to the large air gaps in the system. By reducing the supply frequency the reactive Volt-Ampere could be reduced, and it seems that one could use a frequency as low as, say, 12 Hz without severely increasing the possibility of flocculation. Alternatively the reactive Volt-Amperes could be got rid of completely by the use of rotating electromagnets excited by d.c. current. However a system to rotate such a bulk of steel poles would be cumbersome and possibly difficult to maintain.

It might help to increase $\frac{\partial H}{\partial z}$ by shaping the field by additional pole pieces. However, the latter introduces reverse rotation vectors which may cause agglomeration of the particles.

Most of the thermal energy is a loss as far as the separation process is concerned and so should be kept as small as possible. It seems that by reducing the frequency to about 12 Hz this loss could be kept down without significantly increasing the possibility of agglomeration.

The variable density application seems to be very promising, and further work is being carried out. It has not yet been shown that the method is completely practical but a prototype separator is being developed to determine this.

SECTION 5.

RECOMMENDATION FOR FURTHER WORK

The technique of using primitive ferrofluids as variable density fluids in mineral separation seems to be of practical potential. The maximum achieved density so far, i.e. 11.7×10^4 $N.m^{-3}$, could be increased by a proper design and construction of a water-cooled stator. The stack length should be selected on the basis of the present work to optimise the $\frac{\partial H}{\partial Z}$ levels for a given power. Investigation should be carried out at the higher driving force levels to attempt to minimize the volume loading of the ferrofluid (in order to reduce the viscosity). The effect of viscosity upon throughput will also need to be determined. The proposed axial separator ought to be modified in order to achieve continuous separation process. One idea is to pump the light material mixed with the fluid to the top of the separation zone and then collect the float and sink materials on separate meshes. The fluid can be recirculated to the mixing area.

Further investigation of the linear arrangement for a magnetic separator is also recommended. Belatedly it now seems that the traverse of the fluid along the stator surfaces could be used as a means of transporting the light material away from the charging area.

It is likely that superimposed d.c. fields may affect the shape and direction of the resultant forces and may possibly increase them. Their effects ought to be investigated.

Another area of possible future investigations is the study of medium recovery systems, i.e. the use of low a.c. fields to maintain fluid flow outside the separator zone and the recovery of the magnetic material after washing the separated minerals, simply by possible sedimentation. This method suggests the use of relatively coarse particles to give a short sedimentation time.

REFERENCES

1. LAITHWAITE, E.R.: 'The mysterious rolling cylinder', Electrical Review, 26 January, 1968.

2. BROWN, R. and HORSNELL, T.S.: 'The wrong way round', Electrical Review, 14 February, 1969.

3. MOSKOWITZ, R. and ROSENSWEIG, R.E.: 'Nonmechanical torque-driven flow of a ferromagnetic fluid by an electromagnetic fluid', Applied physics letters, 15 November, 1967, Vol.11, (10), pp.301-303.

4. RABINOW, J.: 'Magnetic fluid clutch', NBS Tech.News Bull., 1948, vol.32, (5), pp.54-60.

5. BROWN, R., BIRCH, T.S. and McCORMICK, M.: 'A Ferrofluid motor', EM70 Conference, University of Dundee, July, 1970.

6. BROWN, R.: 'Travelling magnetic waves in electrical machines described by rotating vectors', Proc.I.E.E., June, 1969, vol.116, (6), pp.1011-1013.

7. RAPELL, S.S. : 'Low viscosity magnetic fluid obtained by colloidal suspension of magnetic particles', U.S. Pat.3,215,572, Nov.2, 1965.

8. ROSENSWEIG, R.E. and NESTOR, J.W. and TIMMINS, R.S.: 'Ferrohydrodynamic fluids for direct conversion of heat energy', A.I.Ch.E. - I.Chem.E. Symposium series No. 5, 1965 (London: Instn. Chem.Engrs.).

9. REIMERS, G.W. and KHALAFALLA, S.E.: 'Dispersing antiferromagnetic Precursors to prepare magnetic fluids', Report of investigations 7702, United States Department of the Interior, Bureau of Mines.

10. REIMERS, G.W. and KHALAFALLA, S.E.: 'Preparing magnetic fluids by a peptizing method', Technical progress report 59, United States Department of the Interior, Bureau of Mines.

11. OPPEGARD, A.L. and others: 'Magnetic properties of single-domain iron, and iron-cobalt prepared by Borohydride reduction', Journal of applied physics, 1961, supplement to Vol.32, (3), pp.184S-185S.

12. BROWN, R., BIRCH, T.S. and McCORMICK, M.: 'A Magnetoviscous valve', EM70 Conference, University of Dundee, July, 1970.

13. NEURINGER, J.L. and ROSENSWEIG, R.E.: 'Ferrohydrodynamics', The physics of fluids, 1964, Vol.7, (12), pp.1927-1937.

14. ROSENSWEIG, R.E.: 'Magnetic fluids', International Science and Technology, July, 1966, pp.48-56.

15. YULISH, J. : 'Unusual devices developed for high seas oil cleaning', Chem.Eng., August, 1971, Vol.78, (18), pp.60-64.

16. BEAN, C.P. : 'Hysteresis loops of mixtures of ferromagnetic micropowders', Journal of applied physics, November, 1955, Vol.26, (11), pp.1381-1383.

17. MIYAIRI, S. and KATAOKA, T. : 'A basic equivalent circuit of the hysteresis motor', Japan J.I.E.E., 1965, Vol.85,pp.41-50.

18. LAMB, H. : Hydrodynamics, 6th ed. (Dover Publications, New York, N.Y., 1945), pp.589.

19. HUGHES, W.F., and GAYLORD, E.W. : Basic equations of Engineering Science, (Schaum Publishing Company, New York, N.Y., 1964), pp.44.

20. DELESSE, A. : 'Sur le pouvoir magnetique des mineraux et des roches', Annales des mines, 1848, Vol.14, pp.429-486.

21. BERG, G.A.: 'Notes on the dielectric separation of mineral grains', Jour. Sed. Petrology, 1936, Vol.6, pp.23-27.

22. CROOK, T. : 'The electrostatic separation of minerals', Mineral Mag., 1909, Vol.15, pp.260-264.

23. KITTEL, C. : Introduction to solid state physics, 3rd ed. (John Wiley, New York, 1967), pp.432-490.

24. GRAETZ : Handbuch der electrizitat und des magnetismus (Barth, 1920), pp.357.

26. OSBORN, J.A. : 'Demagnetizing factors of the general ellipsoid', Physical review, June, 1945, Vol.67, (11) and (12), pp.351-357.

27. Plonsey, R. and COLLIN, R.E. : 'Principles and applications of electromagnetic fields', (McGraw-Hill Book Company, Inc., New York, Toronto and London, 1961), pp.142-143.

28. GOPINATH, A. : 'An investigation into the uses of magnetic fields to accelerate Ferromagnetic particles', Ph.D. Thesis, 1965, University of Sheffield.

29. CLARK, D.A.R. : 'Materials & Structures', (Blackie & Son Limited, London and Glawgow, 1960), pp.134-135.

30. FITZGERALD,A.E. and KINGSLEY, C. JR. : 'Electric Machinery', (McGraw-Hill Book Company, Inc., Tokyo, Second International Student Edition), pp.112.

APPENDIX 1.

DERIVATION OF THE EXPRESSION FOR A SPHERICAL DIPOLE

Sphere Placed in Uniform Magnetic Field.

This derivation follows closely upon that for a dielectric sphere in an electric field by Plonsey and Collin[27]..

If ϕ is a scalar potential, then

$$\text{at } r \leq R_s, \quad \phi_i = - H_o\, r\, P_1^{\,o} (\cos\theta) + \sum_{o}^{\infty} a_m\, r^m\, P_m^{\,o} (\text{Cos}\ \theta)$$

..... A.1.1

and at $r \geq R_s$

$$\phi_e = - H_o\, r\, P_1^{\,o} (\cos\theta) + \sum_{o}^{\infty} b_m\, r^{-(m+1)}\, P_m^{\,o} (\cos\theta) \qquad \text{.....} \qquad \text{A.1.2}$$

where $P_m^{\,o}$ is a Legendre Polynomial and m is an integer.

At $r = R_s$, $\phi_i = \phi_e$

$$\therefore \quad a_m R_s^m = b_m R_s^{-(m+1)} \qquad \text{.....} \qquad \text{A.1.3}$$

Also, $B_{r_{(i)}} = B_{r_{(e)}}$, i.e.

$$\mu_i \frac{\partial \phi_i}{\partial r} = \mu_e \frac{\partial \phi_e}{\partial r}$$

$$\therefore \quad \mu_i \{(-H_o + a_1) P_1^{\,o} \text{Cos}\ \theta + m \sum_{o}^{\infty} a_m R_s^{m-1} P_m^{\,o} \text{Cos}\ \theta\}$$

$$= \mu_e \{(-H_o - 2 b_1 R_s^{3}) P_1^{\,o} \cos\theta - (m+1) \sum_{o}^{\infty} b_m R_s^{-(m+2)} P_m^{\,o} \text{Cos}\ \theta\}, \ m \neq 1$$

where μ_i and μ_e are the permeabilities inside and outside the sphere.

Equating the coefficients of $P_1^{\,o}$ (Cos θ) on both sides

$$\mu_i (- H_o + a_1) = \mu_e (- H_o - 2 b_1 R_s^{-3}) \qquad \text{.....} \qquad \text{A.1.4}$$

Similarly, equating coefficients of P_m^o (Cos θ),

$$\mu_i \, m \, a_m \, R_s^{m-1} = - \mu_e \, (m + 1) \, b_m \, R_s^{-(m+2)}, \quad m \neq 1 \qquad \text{..... A.1.5}$$

From A.1.4, $$\frac{\mu_i}{\mu_e} = \frac{- H_o - 2 \, b_1 \, R_s^{-3}}{- H_o + a_1} \qquad \text{..... A.1.6}$$

Putting m = 1 in equation A.1.3

$$\therefore \; a_1 = b_1 \, R_s^{-3} \qquad \text{..... ..... A.1.7}$$

substituting from equation A.1.7 into equation A.1.6

$$\frac{\mu_i}{\mu_e} = \frac{- H_o - 2 \, a_1}{- H_o + a_1}$$

$$\therefore \; a_1 = \frac{\mu_i - \mu_e}{\mu_i + 2 \, \mu_e} \, H_o \qquad \text{..... A.1.8}$$

From equations A.1.7 and A.1.8

$$b_1 = \frac{\mu_i - \mu_e}{\mu_i + 2 \, \mu_e} \, H_o \, R_s^3 \qquad \text{..... A.1.9}$$

From equation A.1.5, with m = 0

$$a_o = b_o = 0 \qquad \text{..... A.1.10}$$

and from equations A.1.3 and A.1.5

$$a_m = b_m = 0, \quad m \neq 1 \qquad \text{..... A.1.11}$$

Substituting from A.1.8 into A.1.1, and from A.1.9 into A.1.2

$$\phi_i = - H_o \, r \, P_1^o (\cos \theta) + a_1 \, r \, P_1^o (\cos \theta)$$

$$= - H_o \, r \, P_1^o (\cos \theta) + \left(\frac{\mu_i - \mu_e}{\mu_i + 2 \, \mu_e} \right) H_o \, . \, r \, P_1^o (\cos \theta)$$

$$= \left(\frac{-3\mu_e}{\mu_i + 2\mu_e} \right) r P_1^{o}(\cos\theta) \cdot H_o , \qquad r \leq R_s \quad \ldots\ldots \text{A.1.12}$$

and $\phi_e = -H_o r P_1^{o}(\cos\theta) + \left(\frac{\mu_i - \mu_e}{\mu_i + 2\mu_o} \right) H_o \frac{R_s^3}{r^2} P_1^{o}(\cos\theta)$

$$= \left[-r + \frac{\mu_i - \mu_e}{\mu_i + 2\mu_e} \cdot \frac{R_s^3}{r^2} \right] P_1^{o}(\cos\theta) \cdot H_o , \quad r \geq R_s \quad \ldots\ldots \text{A.1.13}$$

Thus inside the sphere, the field is in the z-direction and

$$H_z = \frac{3\mu_e}{\mu_i + 2\mu_e} \cdot H_o \quad \ldots\ldots \text{A.1.14}$$

Outside the sphere, the field caused by its presence is the same as would be produced by a magnetic dipole of strength m_b, where

$$\bar{m}_b = 4\pi R_s^3 \frac{\mu_i - \mu_e}{\mu_i + 2\mu_e} \cdot \bar{H}_o \quad \ldots\ldots \text{A.1.15}$$

For the more general case of an Ellipsoid[26] (with a principal axis aligned with the field)

$$\bar{m}_b = \frac{(\text{volume of body}) \cdot (\mu_i - \mu_e)}{K_z \left[\mu_i + (1/K_z - 1)\ \mu_e \right]} \bar{H}_o \quad \ldots\ldots \text{A.1.16}$$

where K_z is a depolarizing factor depending upon the aspect ratio. For a sphere $K_z = 1/3$.

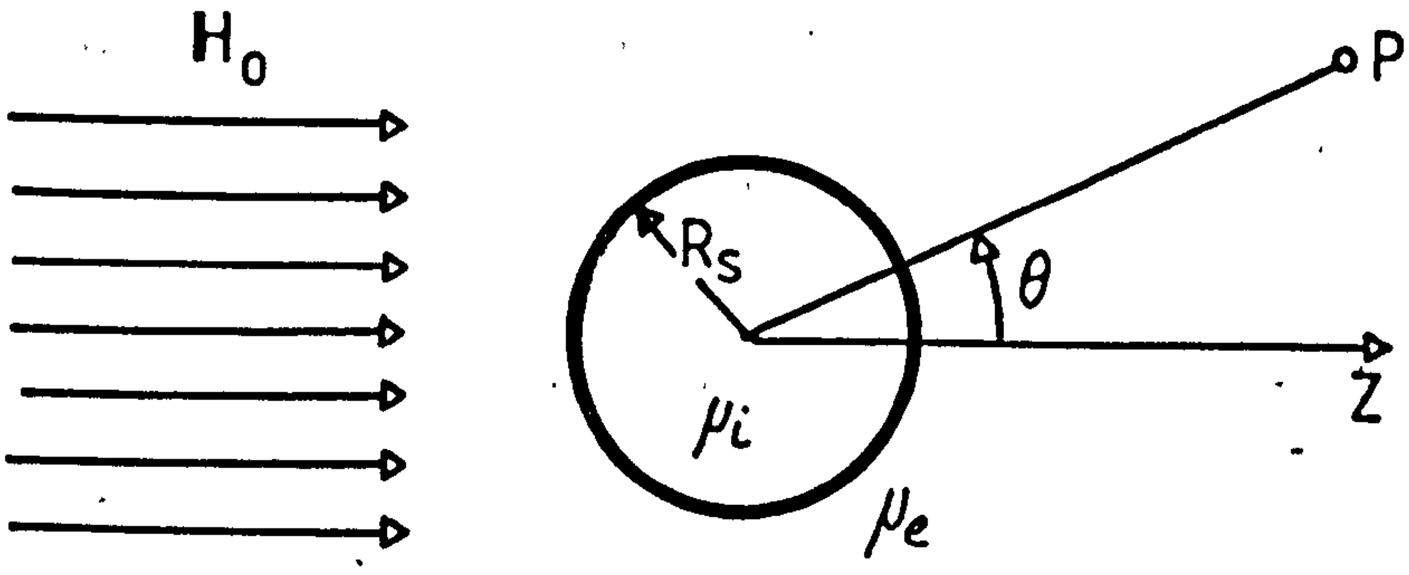

FIG. A.1.1 FOR EQUATIONS 1& 2 OF APPENDIX 1

APPENDIX 2.

ESTIMATION OF THE PERMEABILITY OF A FERROFLUID

Consider an array of particles of magnetic material of permeability μ_p situated in a uniform magnetic field H_o, Fig.A.2.1. Assume that each particle has a dipole moment m.

We wish to replace this array by a macroscopically equivalent continuous medium having a permeability μ_f. If a sphere of volume 1/N is removed from this equivalent medium, where N is the number of particles per unit volume, then it can be shown (see equation A.1.14), that the field within the spherical hole will be uniform and of magnitude H_L where

$$H_L = \frac{3\,\mu_f}{1+2\mu_f} \cdot H_o \qquad \ldots\ldots \qquad A.2.1$$

If a single particle was now placed in the spherical hole then (if the particle is small compared to the hole, i.e. if the packing density is small), from equation A.1.15; the dipole moment m produced by the localised field, H_L, could be given by:

$$m = \text{particle volume.} \frac{(\mu_p - 1) \cdot H_L}{K_z\left[\mu_p + (1/K_z - 1)\right]} \qquad \ldots\ldots \qquad A.2.2$$

where K_z is the demagnetizing factor of the magnetic particle, which depends upon its aspect ratio.

Thus $\mu_o M$ for the equivalent continuum is given by:

$$\mu_o M = \mu_o m N = \mu_o \cdot \text{particle volume} \cdot N. \frac{(\mu_p - 1) H_L}{K_z\left[\mu_p + (1/K_z - 1)\right]}$$

$$\therefore \quad \mu_o M = \mu_o K_p \cdot \frac{(\mu_p - 1)}{K_z\left[\mu_p + (1/K_z - 1)\right]} \cdot \frac{3\,\mu_f}{1 + 2\,\mu_f} \cdot H_o \qquad \ldots\ldots \qquad A.2.3$$

where K_p is the volume loading of the magnetic material in the continuous medium = volume of a particle . N

$$\text{But} \quad \mu_f - 1 = \frac{\mu_o M}{\mu_o H_o}$$

$$\therefore \mu_f - 1 = K_p \frac{(\mu_p - 1)}{K_z\left[\mu_p + (1/K_z - 1)\right]} \cdot \frac{3\,\mu_f}{1 + 2\,\mu_f}$$

$$\therefore (\mu_f - 1)(1 + 2\,\mu_f) = \frac{3K_p}{K_z} \cdot \frac{(\mu_p - 1)}{\mu_p + (1/K_z - 1)} \cdot \mu_f$$

$$\text{or} \quad 2\,\mu_f^2 - \mu_f\left[1 + \frac{3K_p}{K_z} \cdot \frac{(\mu_p - 1)}{\mu_p + (1/K_z - 1)}\right] - 1 = 0$$

$$\text{i.e.} \quad 2\,\mu_f^2 - \mu_f\left[1 + \beta\right] - 1 = 0$$

$$\text{where} \quad \beta = \frac{3K_p}{K_z} \cdot \frac{(\mu_p - 1)}{\mu_p + (1/K_z - 1)}$$

If $(1 + \beta)^2 << 8$ i.e. $2\beta << 9$

Then this approximation yields to an error approaches 10.7% when β approaches 2.

$$\therefore \mu_f \simeq \frac{1 + \beta \pm 3\,(1 + \beta/9)}{4}$$

$$= 1 + \frac{\beta}{3} \quad \text{or} \quad \frac{\beta}{6} - 0.5$$

The later is not acceptable since $\mu_f > 1$

$$\therefore \mu_f \simeq 1 + \frac{K_p}{K_z} \cdot \frac{(\mu_p - 1)}{\mu_p + (1/K_z - 1)} \qquad \ldots\ldots \quad \text{A.2.4}$$

If μ_p is large

$$\mu_f \simeq 1 + \frac{K_p}{K_z} \qquad \ldots\ldots \quad \text{A.2.5}$$

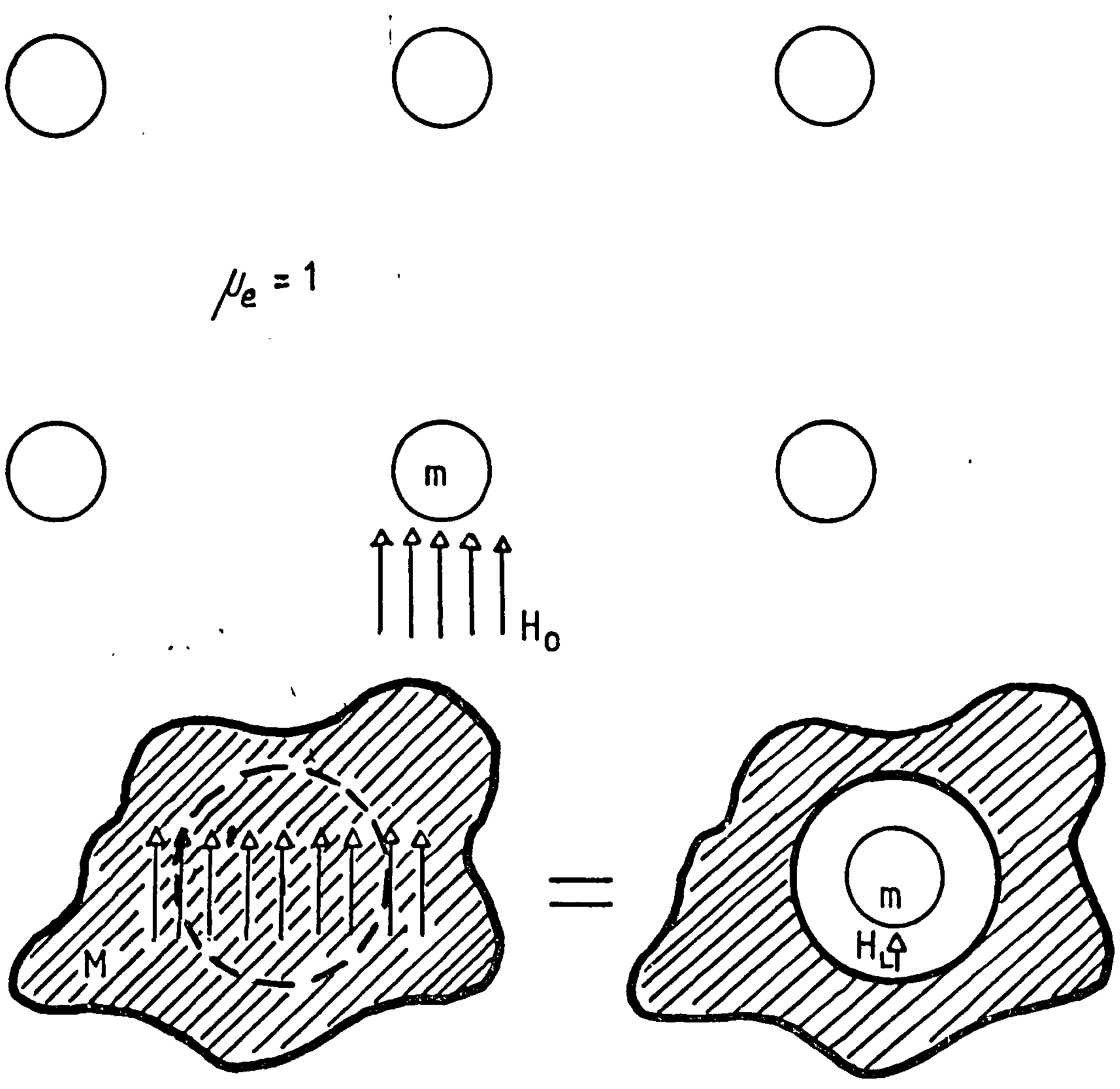

FIG A.2.1

APPENDIX 3.

DESIGN OF THE TORQUE REACTION TUBE

Assume that the shear stress, f_s, is uniform over the wall thickness, t. Now this shear stress has a moment about the axis of the tube which resists the reaction torque, T, therefore

$$f_s = \frac{T}{2 \pi r^2 t}$$

where r is the radius of the tube.

Any shear stress, f_s, is equivalent to a tensile stress, f_t, and a compressive one[29], f_c, each of half the magnitude of f_s. The tensile, or compressive strain ϕ is related to f_c by:

$$\phi = \frac{f_c}{C}$$

where C is the modulus of rigidity.

$$\therefore \quad \phi = \frac{T}{4 \pi r^2 t \, . \, C}$$

Consider T to be 0.1 N.m, $C = 2.75 \times 10^{10}$ N/m^2 for duralumin. Select $r = 5.08 \times 10^{-3}$ m and $t = 6.35 \times 10^{-4}$ m

$$\therefore \quad \phi \simeq 20 \text{ microstrain}$$

The mass suspended from the tube was that of the dynamometer, about ½ Kg. Therefore the tensile stress is 2.42×10^5 N/m^2 which is permissible. Since the tube cross-section is under tension, the length of the tube was not restricted. A length of .038 m was chosen.

APPENDIX 4.

DERIVATION OF THE EXPRESSION OF THE MAGNETIC FORCE IN THE CYLINDRICAL CONFIGURATION

Applying Maxwell's equations and assuming periodic variations with respect to z and θ, the field components for a machine having p pairs of poles are given by:-

$$H_r = \left[A_1 I_{p+1}(\gamma r) + A_2 I_{p-1}(\gamma r) + B_1 K_{p+1}(\gamma r) + B_2 K_{p-1}(\gamma r)\right] e^{j\gamma z} e^{j(\omega t - p\theta)} \quad \ldots\ldots \quad A.4.1$$

$$H_\theta = j\left[A_1 I_{p+1}(\gamma r) - A_2 I_{p-1}(\gamma r) + B_1 K_{p+1}(\gamma r) - B_2 K_{p-1}(\gamma r)\right] e^{j\gamma z} e^{j(\omega t - p\theta)} \quad \ldots\ldots \quad A.4.2$$

$$H_z = \left[C I_p(\gamma r) + D K_p(\gamma r)\right] e^{j\gamma z} e^{j(\omega t - p\theta)} \quad \ldots\ldots \quad A.4.3$$

where H_r, H_θ and H_z are the radial, tangential and axial components of the magnetic field, and r, θ and z the coordinates of the point at which these components occur.

$I_{p+1}(\gamma r)$ and $K_{p+1}(\gamma r)$ are modified Bessel functions of the first and second kind respectively, and are of order P + 1.

A_1, A_2, B_1, B_2, C and D are constants.

Since the field must be finite at r = 0, then we must have the

$$B_1 = B_2 = D = 0 \quad \ldots\ldots \quad A.4.4$$

i.e.

$$H_r = \left[A_1 I_{p+1}(\gamma r) + A_2 I_{p-1}(\gamma r)\right] e^{j\gamma z} \cos(\omega t - p\theta) \quad \ldots\ldots \quad A.4.5$$

$$H_\theta = -\left[A_1 I_{p+1}(\gamma r) - A_2 I_{p-1}(\gamma r)\right] e^{j\gamma z} \sin(\omega t - p\theta) \quad \ldots\ldots \quad A.4.6$$

$$H_z = C I_p(\gamma r) e^{j\gamma z} \cos(\omega t - p\theta) \quad \ldots\ldots \quad A.4.7$$

Now these three components must satisfy the appropriate divergence relationship, which if the material is isotropic can be $\nabla.H = 0$.

Applying this condition and making use of the relationship

$$r \frac{\partial I_n(\partial r)}{\partial r} = n I_n(\gamma r) + \gamma r I_{n+1}(\gamma r)$$

$$= - n I_n(\gamma r) + \gamma r I_{n-1}(\gamma r) \quad \ldots\ldots\ldots \quad A.4.8$$

it can be shown that

$$C = j (A_1 + A_2) \quad \ldots\ldots\ldots \quad A.4.9$$

and equation A.4.7 becomes:

$$H_z = j (A_1 + A_2) I_p(\gamma r) . e^{j\gamma z} \cos(\omega t - p\theta) \quad \ldots\ldots\ldots \quad A.4.10$$

Taking the real part of $e^{j\gamma z}$ of the right hand sides of equations A.4.5, A.4.6 and A.4.10 yields

$$H_r = \left[A_1 I_{p+1}(\gamma r) + A_2 I_{p-1}(\gamma r)\right] \cos\gamma z \cos(\omega t - p\theta) \quad \ldots\ldots \quad A.4.11$$

$$H_\theta = - \left[A_1 I_{p+1}(\gamma r) - A_2 I_{p-1}(\gamma r)\right] \cos\gamma z \sin(\omega t - p\theta) \quad \ldots\ldots \quad A.4.12$$

$$H_z = - (A_1 + A_2) I_p(\gamma r) . \sin\gamma z \cos(\omega t - p\theta) \quad \ldots\ldots\ldots \quad A.4.13$$

Equations A.4.11 to A.4.13 satisfy Maxwell's equation $\nabla XH = 0$ in a non-conducting region if

$$A_1 = A_2 = A \quad \text{say} \quad A.4.14$$

Thus the field can be represented by:-

$$H_r = A \left[I_{p+1}(\gamma r) + I_{p-1}(\gamma r)\right] \cos\gamma z \cos(\omega t - p\theta) \quad \ldots\ldots\ldots \quad A.4.15$$

$$H_\theta = - A \left[I_{p+1}(\gamma r) - I_{p-1}(\gamma r)\right] \cos\gamma z \sin(\omega t - p\theta) \quad \ldots\ldots \quad A.4.16$$

$$H_z = - 2 A I_p(\gamma r) \sin\gamma z \cos(\omega t - p\theta) \quad \ldots\ldots\ldots \quad A.4.17$$

In an anisotropic medium, the magnetic energy density E_m at any point in this magnetic field is proportional to H^2, i.e.

$$E_m = \tfrac{1}{2}\ \mu_f\ \mu_o\ (H_r^2 + H_\theta^2 + H_z^2) \qquad \ldots\ldots \qquad A.4.18$$

where μ_f is the permeability of the medium.

This yields:

$$E_m = \tfrac{1}{2}\ \mu_f\ \mu_o\ A^2 \Bigg\{ \left[\frac{I_{p+1}^2(\gamma r) + I_{p-1}^2(\gamma r) + 2\ I_p^{\,2}(\gamma r)}{2}\right] + \left[\frac{I_{p+1}^2(\gamma r) + I_{p-1}^2(\gamma r) - 2\ I_p^{\,2}(\gamma r)}{2}\right] \cos(2\gamma z) \Bigg\}$$

$$+\ 2\ I_{p+1}(\gamma r)\ .\ I_{p-1}(\gamma r).\cos^2 \gamma z.\cos\ 2(\omega t - p\theta)$$

$$+\ 2\ I_p^{\,2}(\gamma r)\ .\ \sin^2 \gamma z.\cos\ 2(\omega t - p\theta) \qquad \ldots\ldots\ldots \qquad A.4.19$$

If the region is occupied by a magnetic fluid the magnetic force density encountered by a non-magnetic (non-conducting) body placed in it (assuming the body dimensions to be small compared to $2\pi/\gamma$) will, as before, be proportional to the energy density gradient,

i.e. $\rho_{mz} = -\ K \dfrac{\partial E_m}{\partial z}$ where K is a constant governed by the body shape.

From equation A.4.19 the average magnetic force density will be given by:-

$$\rho_{mz} = \tfrac{1}{2}\ \mu_f\ \mu_o\ K\ A^2\ \gamma \left[I_{p+1}^2(\gamma r) + I_{p-1}^2(\gamma r) - 2\ I_p^{\,2}(\gamma r) \right] \sin 2\gamma z \qquad \ldots\ldots \qquad A.4.20$$

Similar arguements will apply in the radial direction and the average magnetic force density, ρ_{mr} is given by:-

$$\rho_{mr} = - K \frac{\partial E_m}{\partial r}$$

$$= \tfrac{1}{2} \mu_f \mu_o K A^2 \gamma \left\{ \left[\frac{-2 (P + 1)}{\gamma r} I^2_{p+1} (\gamma r) + \frac{2 (P - 1)}{\gamma r} I^2_{p-1} (\gamma r) \right] . \cos^2 \gamma z + \right.$$

$$\left. 2 I_p (\gamma r) . \left[I_{p+1} (\gamma r) + I_{p-1} (\gamma r) \right] \right\} \quad \ldots\ldots\ldots \quad A.4.21$$

There are no non-time varying components of force in the θ direction, i.e. the average value of $\rho_{m\theta}$ is equal to zero.

Evaluation of the constant A.

An approximate relationship between the stator m.m.f. and the constant A can be obtained as follows:-

Assume a linear current density, J_z in a current sheet at the stator surface, as in Fig.A.4.1, such that

$$J_z = J_{max} \cos \gamma z . \sin (\omega t - p\theta) \quad \ldots\ldots\ldots \quad A.4.22$$

Consider the line integral of both H_θ and J_z along the closed curve ABCD in Fig.A.4.1

$$\therefore \int_{\theta_1}^{\theta_2} J_z . R_b . d\theta = \oint_{ABCD} H_\theta . d\ell \quad \ldots\ldots\ldots \quad A.4.23$$

Assuming the permeability of the stator iron to be high the m.m.f. expended in it can be neglected, as can be the m.m.f.'s along the elemental lengths AB and CD

$$\therefore \int_{\theta_1}^{\theta_2} J_z . R_b . d\theta = \int_{\theta_1}^{\theta_2} H_\theta . R_b . d\theta \quad \ldots\ldots\ldots \quad A.4.24$$

$$\therefore \quad J_z = H_\theta \qquad \ldots\ldots \qquad \text{A.4.25}$$

From equations A.4.16, A.4.22 and A.4.25

$$\therefore A = - \frac{J_{max}}{I_{p+1}(\gamma R_b) - I_{p-1}(\gamma R_b)} \qquad \ldots\ldots \qquad \text{A.4.26}$$

Relationship between J_{max} and the stator m.m.f.

J_{max} can be related to the stator winding m.m.f., but since the latter does not vary with z (at least along the length of the stator stack) whereas J_{max} is defined at z = 0 there is a discrepancy in the analysis here. Nevertheless the error involved in relating J_{max} to the peak stator m.m.f. should not be too great it is believed.

The peak fundamental component of the m.m.f. per phase, F_p, is given by[30]:-

$$F_p = \frac{4}{\pi} K_w \frac{N}{(2p)} I_a$$

where N is the number of series turns per phase, K_w the winding factor, p the number of pairs of poles and I_a the phase current.

For 3 phases, the resultant peak m.m.f., F, is given by $F = \frac{3}{2} F_p$

$$= \frac{3}{\pi} K_w \frac{N}{p} I_a$$

$$\text{But } F = \int_0^{\pi/2p} J_{max} \cos p\theta \cdot R_b \cdot d\theta = \frac{J_{max} \cdot R_b}{p}$$

where R_b is the bore radius, therefore

$$J_{max} = \frac{3}{\pi} K_w N \cdot I_a \cdot \frac{1}{R_b} \qquad \ldots\ldots \qquad \text{A.4.27}$$

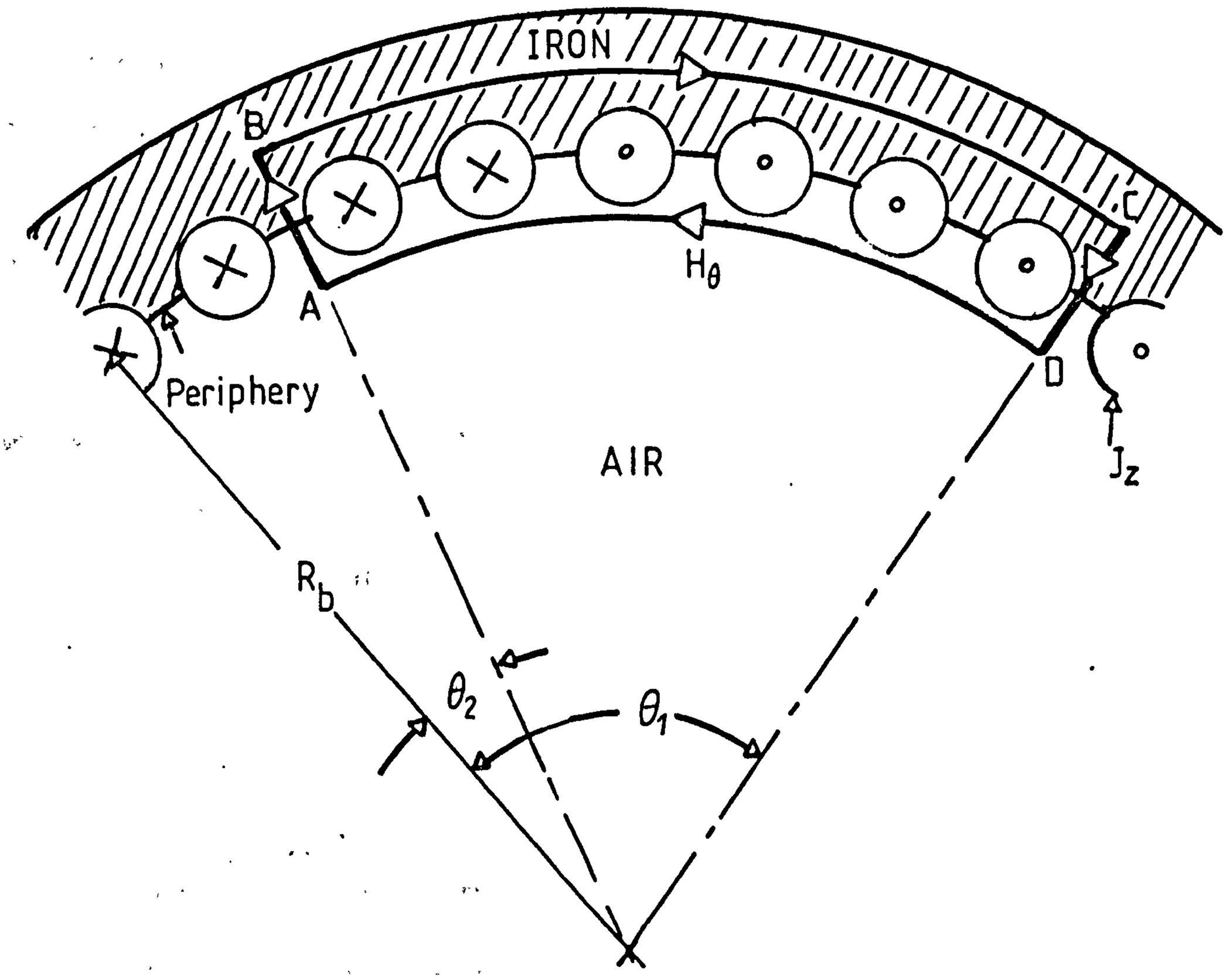

FIG. A.4.1

APPENDIX 5.

ANALYSIS OF SEPARATION BY RADIAL MAGNETIC FORCE

The body moves vertically under gravity and radially under constant field gradient.

The viscous force acts on a spherical body of radius 'a' moving in a fluid of viscosity η is given by Stoke's law as

$$F_v = -6\pi\eta a v = -bv \quad \ldots\ldots \quad A.5.1$$

where v is the velocity of the body, and b is the Stoke's coefficient.

Combining the magnitude of the frictional force with the gravitational force, $F_g = mg$, one obtains

$$mg - bv_z = m\frac{dv_z}{dt}$$

$$\text{or} \quad \frac{d^2z}{dt^2} = g - \frac{b}{m}\frac{dz}{dt} \quad \ldots\ldots \quad A.5.2$$

where m is the mass of the body and $v_z = \frac{dz}{dt}$.

In the radial direction there will be a magnetic force in the radial direction, F_r, which if the fluid is saturated, from equation 3.2.9, will be given by:

$$F_r = \mu_o M_{sat} . A. V$$

where V is the volume of the body and A is the field gradient.

The equation of motion in the radial direction will be given by:

$$F_r - b\frac{dr}{dt} = m\frac{d^2r}{dt^2}$$

$$\text{or} \quad \frac{d^2r}{dt^2} = \frac{\mu_o M_{sat} A}{\rho_b} - \frac{b}{m}\frac{dr}{dt} \quad \ldots\ldots \quad A.5.3$$

where ρ_b is the density of the body.

APPENDIX 6.

THE FIELD PRODUCED BY AN INFINITE LONG 4-POLE STATOR

If a stator with p pairs of poles is infinitely long there will be no variation in the axial direction and the field solution is given by:

$$H_r = A\, r^{(p-1)} \cos(\omega t - p\theta)$$

$$H_\theta = A\, r^{(p-1)} \sin(\omega t - p\theta)$$

$$\therefore \quad H = \sqrt{H_r^{\,2} + H_\theta^{\,2}} = A\, r^{(p-1)}$$

For the case of a four-pole stator, i.e. p = 2

$$H = A\, r$$

$$\text{i.e.} \quad \frac{dH}{dr} = A = \text{constant.}$$